2015

Magnetic Susceptibility of North American Ordovician Epicontinental Seas: Spatial Variability and Sandbian-Katian Boundary Correlation

Thomas J. Schramm
Louisiana State University and Agricultural and Mechanical College, tschra2@tigers.lsu.edu

MAGNETIC SUSCEPTIBILITY OF NORTH AMERICAN ORDOVICIAN EPICONTINENTAL SEAS: SPATIAL VARIABILITY AND SANDBIAN-KATIAN BOUNDARY CORRELATION

A Dissertation

Submitted to the Graduate Faculty of the
Louisiana State University and
Agricultural and Mechanical College
in partial fulfillment of the
requirements for the degree of
Doctor of Philosophy

in

The Department of Geology

by
Thomas J. Schramm
B.S., S.U.N.Y. New Paltz, 2009
M.S., University of Cincinnati, 2011
May 2015

For the Great Stratigraphers

ACKNOWLEDGEMENTS

The completion of this project would not be possible without the help of many people. First, I think my advisor and committee for guiding me throughout this project. The fieldwork for this project would not have been possible without lodging provided by Rebecca Freeman, C.J. Hartwell, and James Thomka. I would like to thank Gordon Baird, Alex Bartholomew, Carlton Brett, Benjamin Dattilo, Jesse Carlucci, Dan Goldman, Warren Huff, and Steve Westrop for their insight into this project, stratigraphy, discussion, and phone calls while in the field. James Thomka, Evan Krekelar, Brooks Ellwood and Sue Ellwood provided assistance in the field: Amber Ellwood and Abigail Heath provided assistance in the lab. I would also like to thank Dr. Hanor, Kathryn Denommee, and Crawford White for assistance in constructing figures. This project would not have been possible without the love and encouragement of my parents. I've found completion of this degree to be, at times, discouraging and arduous and thank all of those who encouraged me to continue through this. I would like to thank Hunter's Run Gun Club, Alliance Auto Paint and Supply, and The Chimes of Highland Road.

I would like to thank the LSU Geology Department for financial support as a TA, and scholarship funding from Encana, Devon Energy, the New Orleans Geological Society, Adam Sturlese Memorial Scholarship and the Mary Jo Klosterman Fellowship. Partial funding of field research was provided by the Robey Clark endowed professorship.

PREFACE

Correlating shelf to basin sequences remains one of the most persistent problems in the study of stratigraphy. The difficulty of correlating synchronous horizons across depositional facies has puzzled geologists since the origination of this branch of geology. The naming and description of lithographic units and their correlation represents the first step in stratigraphy. 'What's in a name?' He who names it owns it for eternity, and so much of stratigraphy owes to this principle. The name of a stratigraphic unit assigns a type locality to it and pairs a physical location to this lithology. As geologic environments, or facies, change spatially at any given point in time application of these locality defined names describing lithofacies become limited.

A second aspect of stratigraphy does not represent the naming of formations or units, but instead attempts to solve a series of problems, or issues within Earth's history. These could include, global climate, tectonic, faunal origination, biodiversity, and mass extinctions. The assessment of all of these problems is contingent on the accurate comparison of coeval units and their chronologies. Simply put, without the accurate correlation of stratigraphic units it is not possible to accurately access these 'second level' issues. Stratigraphic correlation, the identification of synchrounous horizons, and their correlation both regionally, and globally, is critical to accessing these issues.

These physical, stratal problems, based around the correlation of rock based units represent some of the oldest unsolved geologic problems, and many have yet to be solved. In constructing a dissertation, my goal was to solve the biggest, baddest, remaining unsolved rock-based stratigraphic problems. Many geologists are no longer concerned with the assessment of

these insular stratigraphic problems, even though, they are the foundation upon which the geologic timescale, and our knowledge of Earth History has been composed.

The Ordovician System has specifically been chosen for the purpose of this investigation because it largely remains understudied. The Ordovician as a system (Lapworth, 1871) represents the final named geologic system in Earth history. Due to poor biostratigraphic resolution and provinciality of faunas its chronostratigraphy remains one of the least understood. A lack of correlatable units generally plagues Ordovician stratigraphy. The level of correlation to access these events within Ordovician strata occurs below the resolution of biostratigraphy, and thus will remain controversial. Simply, higher levels of biostratigraphic resolution within other systems better permit assessment of such problems. In order to solve these correlation issues a somewhat unorthodox study using magnetic susceptibility (χ) based correlation has been conducted.

TABLE OF CONTENTS

ABSTRACT

Magnetic susceptibility (χ) has gained increased usage as a stratigraphic correlation tool. This project evaluates the utility of χ as a correlation tool, including its shortcomings, and attempts its integration with other datasets. The Upper Ordovician of eastern North America represent the stratigraphic interval in which these experiments were conducted. 4566 samples were collected for the purposes of this study, and χ was measured on 3345 of the samples. This project includes three major facets, 1) the spatial variability of χ, 2) correlation of Sandbian-Katian boundary interval strata in eastern North America using χ, and 3) utility of χ for interpreting stratigraphic sequences.

1) Testing the spatial variability of χ was conducted by sampling a single isochronous Upper Ordovician limestone horizon across the lateral extent of the Cincinnati Arch. A small but predictable decrease in χ values with increased distance from the clastic sediment source was documented. These observations match the hypotheses of the Episodic Starvation model of sedimentation on the Cincinnati Arch. Facies changes in proximal positions of the basin, and interbedding of muddy carbonates with shales, result in the deterioration of the χ signature, and correlation becomes increasingly difficult using this method. Based upon this, correlation using χ profiles is most suited for distal portions of basins.

2) Application of the χ technique has been used for correlation of the Sandbian-Katian boundary interval in eastern North America. A series of correlation hypotheses have been proposed but a unique correlation has not been found. Due to a series of unconformities, and biostratigraphic discrepancies it has not been possible to find a datum to hang χ profiles upon. The leading hypothesis is that deepening strata of the Logana-Napanee interval correlates to the lower wackestone unit of the Viola Springs Formation, and upper Womble Shale.

3) In order to incorporate χ datasets into sequence stratigraphic analyses a series of χ samples have been collected across sequence stratigraphic surfaces of know interpretation. Large shifts to lower measured χ values at some sequence boundaries and shifts to higher χ values at most flooding surfaces may be used to aid in sequence stratigraphic interpretation.

CHAPTER 1
TESTING THE SPATIAL VARIABILITY OF MAGENTEIC SUSCEPTIBILITY (χ) IN ORDOVICIAN EPICONTINENTAL SEAS

ABSTRACT

Magnetic susceptibility (χ) is a physical property of a material indicating the strength of its transient magnetism when in the presence of an induced magnetic field. χ has gained increased use as a correlation proxy for stratigraphic units on both a regional and global level. Early research suggests that χ in lithified sediments is constant spatially at one point in time, but these studies have been hindered by small geographic coverage and unknown basin geometries. In order to address whether or not χ changes along distal to proximal transects in ancient strata, a single synchronous Ordovician (basal Maysvillian) horizon, the "Z-bed" and overlying "2 foot shale," spanning the lateral extent of the Cincinnati Arch, was sampled and its χ measured. This paper expands upon previous research and evaluates the uses of χ as a correlation method, evaluating its utility, applications, and shortcomings. As χ is a physical property, it is predicted that as physical or lithologic changes occur throughout a stratum, changes in χ should be observed. The Storm Winnowing and Episodic Starvation models of limestone bed formation are evaluated in relation to the horizon sampled in this single bed study, yielding testable predictions of basin-wide χ values. This investigation demonstrates a small but predictable decrease in χ values in association with increased distance from the sediment source and supports predictions of the Episodic Starvation Model during the time of "Z-bed" deposition on the Upper Ordovician Cincinnati Arch.

KEYWORDS

Magnetic Susceptibility, Episodic Starvation Model, Cincinnati Arch, Katian

INTRODCUTION

Low-field bulk mass-specific magnetic susceptibility (χ) measurements indicate the strength of a material's transient magnetism in the presence of an inducing magnetic field (Ellwood *et al*., 2000). How susceptible a material is to becoming magnetized is a distinct property different from remanent magnetism, which is responsible for the magnetic polarity, declination and inclination of rocks. These two measurements are very different for the same samples (Ellwood *et al*., 2006). χ in marine strata is dominantly controlled by detrital/eolian paramagnetic and/or ferrimagnetic grains contained in samples. Diamagnetic materials ($-\chi$), such as calcite and quartz, are the dominant mineral components of marine sediments, but their very low $-\chi$ values have little effect on total χ (Ellwood *et al*., 2000; 2013; Febo, 2007). The smaller percentage of detrital/eolian components controlling susceptibility values can be used as an independent proxy of climate (Weedon and Jenkyns, 1999). Used in a vertical succession, χ provides an independent dataset to adjust and evaluate the stratigraphic position of successions to improve their correlation, and can be used to establish χ zones to correlate stratigraphic sections with high precision, even when biostratigraphic discrepancies or small unconformities are known to occur (Ellwood *et al*., 2007).

The measurement of χ in stratigraphic sequences provides a useful tool for the regional and global correlation of strata (Crick *et al*., 1997). Early research demonstrated that χ remains relatively stable and constant spatially, once marine sediments have undergone diagenesis and lithification. Some of this early work was based in part on the examination of samples from a single discrete Devonian bed in Morocco, sampled at ~100 m intervals over a km, and tracing the bed to another sampling locality 25 km away. Multiple other experiments and observations have

also been reported (Crick *et al.*, 1997, Ellwood *et al.*, 1999; 2000, 2007, 2013). The relationship of the stratigraphic sections relative to depositional strike, however, is unclear. While use of χ has gained increased acceptance in stratigraphic research it is unknown how variations in χ values change on an onshore-offshore gradient in ancient strata. Does magnetic susceptibility change in a predictable manner on an onshore-offshore gradient, and if so how? A small but predictable decrease in χ values is anticipated with increased distance from the clastic sediment source.

χ Spatial Distribution

In order to address the spatial variability of χ, it is the intent of this work to measure χ values from a single synchronous horizon across the lateral extent of the Cincinnati Arch for which the paleo-depositional strike is known (Miller *et al.*, 2001). Whalen and Day (2010) used χ values to examine the spatial variability of Devonian sediments in a series of outcrops in Canada, however, their study does not address how χ changes basinally at one specific time. Similarly, magnetic susceptibility of Upper Devonian subtidal-intertidal carbonate microfacies demonstrate higher values for proximal facies (da Silva and Boulvain, 2006). These observations, however, occur in vertical successions of multiple sections and not a single synchronous time-frame.

Previously, Sachs and Ellwood (1988) and Ellwood *et al*., (2006) examined the spatial variation in anhysteretic remanent magnetism (ARM) and χ for modern surface sediments in the Argentine Basin in the western South Atlantic Ocean, and for the whole Gulf of Mexico basin, respectively, as well as the redistribution of χ throughout the basin, they attribute χ variations to sediment sources and pathways as well as distribution of sediment via longshore currents and

nepheloid flows. This study examines the spatial variability of χ within the US mid-continent Ordovician epicontinental sea to test for constancy or change in χ and provide further models for sedimentation, cycle propagation, and sediment distribution on the Cincinnati Arch.

Cincinnatian χ

χ has been applied previously in correlation and interpretation of Upper Ordovician stratigraphic sequences of the Cincinnati Arch (Ellwood *et al*., 2007; 2012; Schramm, 2011; Brett *et al*., 2012), where Ellwood *et al*. (2007) showed that clay deposition was the dominant χ driver within Kope Formation strata. In the Ellwood *et* al., (2007) study, bed-for-bed correlation was made using this technique, for stratigraphic sections lying within close proximity to each other. A series of Milankovitch peaks have been recognized within a Kope composite section, and based on this work, it has been possible to assign an age duration of approximately 2 million years to the Kope composite section (Ellwood et al, 2012). Schramm (2011) and Brett *et al*., (2012) later used this technique, integrated with sequence stratigraphy, to aid in the physical correlation of Maysvillian Stage strata across the Cincinnati Arch. They recognized similar cycles within these successions, with the exception of less mud.

Regional Setting

A very high-resolution stratigraphic framework for Late Ordovician (Katian) strata of the Cincinnati Arch provides the basis for this study (Holland, 1993; Jennette and Pryor, 1993; Holland and Patzkowsky, 1996; Holland *et* al., 1997; Brett and Algeo, 2001, Holland *et al*., 2001; Schramm, 2011; etc.). It has been well established that individual time-correlative horizons (beds) are traceable across the lateral extent of the Cincinnati Arch. These strata comprise the North American (NA) standard Late Ordovician time-rock unit, the Cincinnatian

Series, which in turn is divided into the lower, Edenian Stage; middle, Maysvillian Stage; and upper, Richmondian Stage (Figure 1.1). Type-Cincinnatian strata of the southeastern Indiana, southwestern Ohio, and northern Kentucky region have received considerable paleoecological

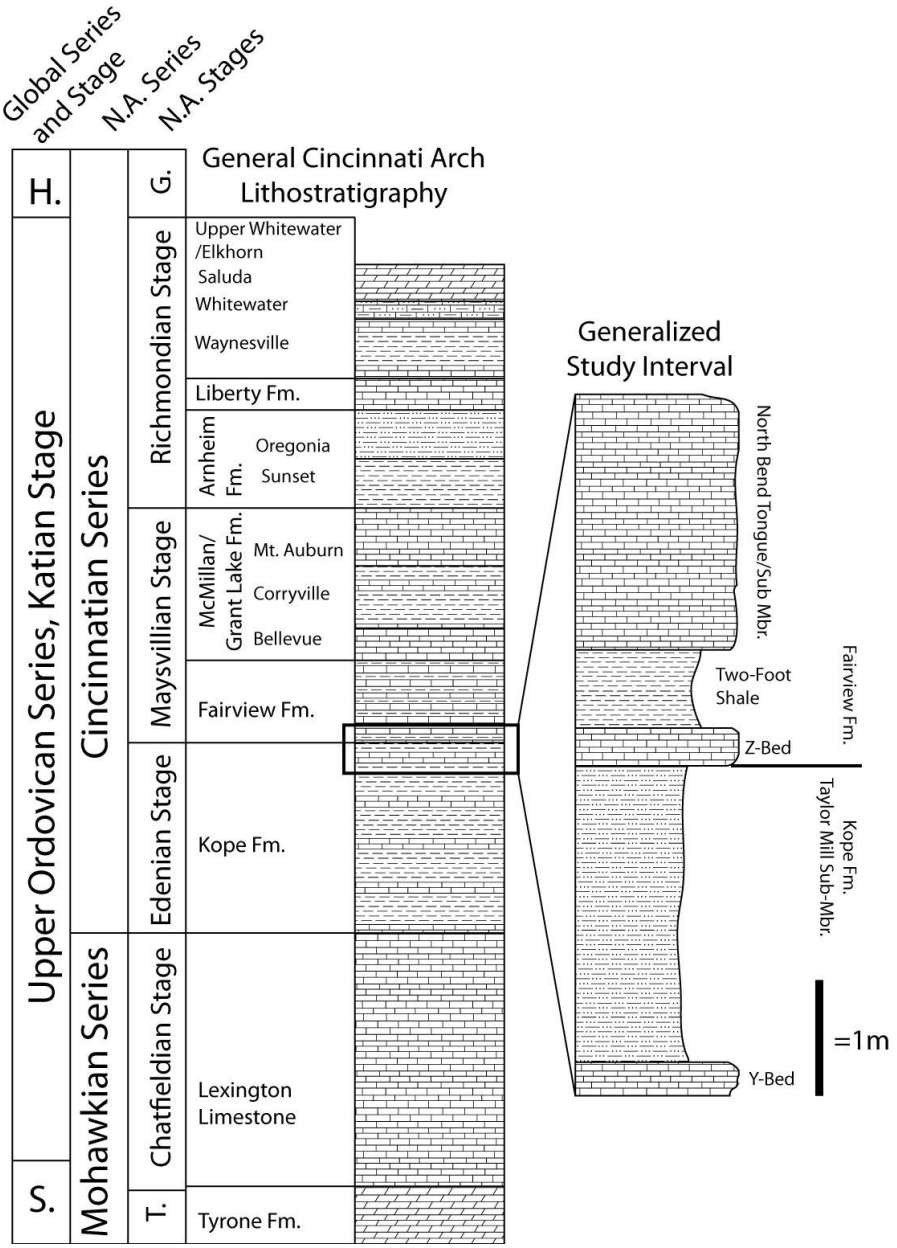

Figure 1.1 Generalized stratigraphic column showing, Global Series and Stages (S. Sandbian, H. Hirnantian); North American Ordovician Series; North American Ordivician Stages (T. Turinian, G. Gammachian); Lithostratigraphy of the Cincinnati Arch; and the high resolution study interval.

research, specifically relating to faunal gradient analysis, mainly within the Edenian, Kope Formation and lowest Maysvillian strata (Holland *et al*., 2001; Miller *et al*., 2001; Webber, 2002; etc.). Such strata were deposited in shallow epicontinental seas, on a northwestwardly dipping ramp (Miller *et al.*, 2001). Based upon the use of photoautotropic microendoliths, Vogel and Brett (2009) have inferred water depths similar to the estimates for deposition of Cincinnatian strata, by Holland and Patzkowsky (1996), as being deposited average and deep storm wave base (~30-50 m water depth), for the deposition of Kope Formation strata. The large number of well-preserved Ordovician exposures facilitates testing χ variability across this region along a distal-to-proximal transect.

The Ordovician strata of the Cincinnati Arch were deposited at the interface between siliciclastic deposition and carbonate sedimentation. Active Taconic tectonism (Vermontian Phase) during the Chatfieldian and Edenian Stages (Figure 1.1) resulted in the formation of widespread mountains along the eastern North American continental margin. This Taconic Hinterland was the source of detrital sediment (Quinland and Beaumont, 1984; Bretsky 1970, Keith 1989, Ettensohn 1991, Pope *et al*., 1997, Ettensohn et al. 2002). Flysch-phase sediments filled much of the Taconic Foreland Basin, while carbonate production occurred on cratonic shelves/platforms (Galena, Lexington, Trenton). Distal Cincinnatian sections are near the southwest-northeast trending Sebree Trough (Figure 1.2a), and in general, water depths shallowed south of present day Cincinnati approaching the proto-Nashville Dome. Autochthonous shelly carbonates are present in shallow regions, and interfinger with allochthonous Taconian-derived clastic sediments, resulting in mixed carbonate-clastic deposition.

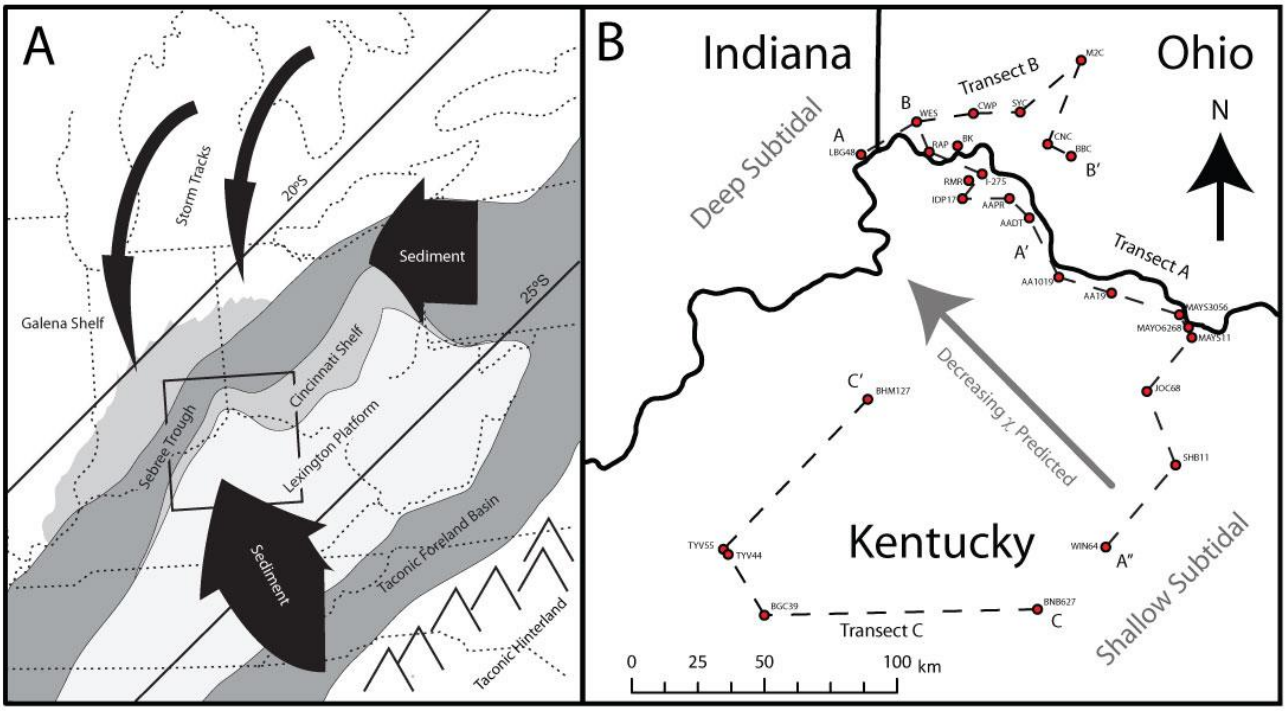

Figure 1.2 A.) Regional paleogeographic map (Modified from Dattilo *et al*., 2012) showing the study area, storm tracks, and possible sediment transport routes. B.) Location map showing 27 "Z-Bed" sampling localities in red. Abbreviations of locations are given. Gray letters indicated paleoenvironments, and predictions of decreasing χ in a basin-ward direction. Three transects appear on this diagram and are shown on the correlation diagrams.

Given the close proximity of outcrops and high degree of stratigraphic resolution, the Cincinnati Arch represents one of the few regions in which χ spatial variability of a single temporal horizon may be evaluated. Furthermore, Kentucky is the only state that has been entirely geologically mapped at a 1:24,000 scale (Weir *et al*., 1984; etc.). The specific sampling horizon is at the mapped Kope (Edenian) -Fairview (Maysvillian) formation boundary interval (Figure1.1), and this allows rapid identification of potential sampling localities. The specific meter-scale cycle to be sampled is composed of the "Z-Bed" and overlying "2 foot shale" of Brett and Algeo, (2001; Bed-40 of Holland *et al*., 1997: Figure 1.3). This horizon and overlying mudstone hemicycle have been chosen due to their ease of recognition by early workers, who

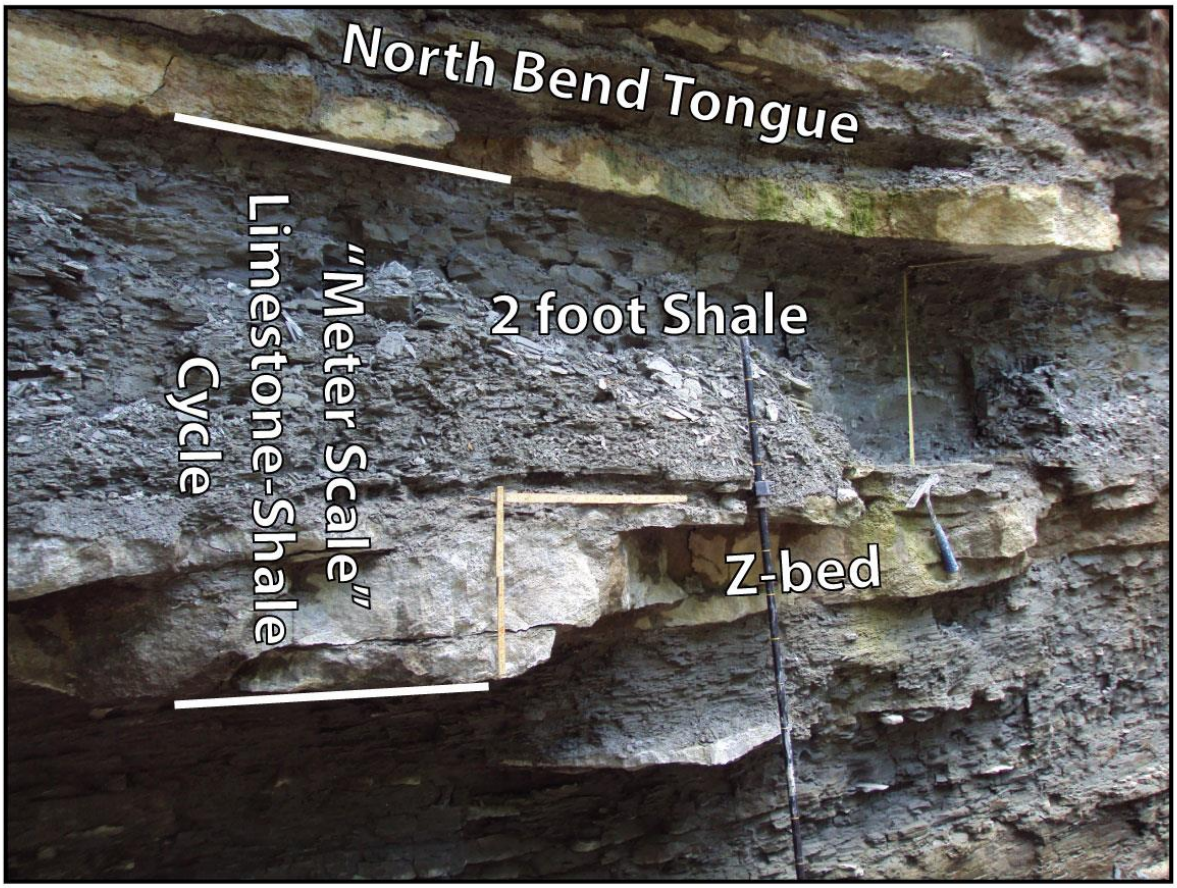

Figure 1.3 Outcrop photograph of study interval Rapid Run, Ohio. Hammer and Jacob Staff for scale. Note "Z-Bed" composed of multiple condensed limestone beds in downramp positions, and overlying "buttery" "2 foot shale".

placed the physical boundary of the Fairview Formation, Mt. Hope Member, and NA Maysvillian Stage at the base of the "Z-Bed" (Nickles, 1902; Bassler, 1906; Fenneman, 1916). Schramm (2011) recognized that the "Z-Bed" regionally oversteps truncated strata of the Taylor Mill submember (of the Kope formation) and equivalent-Garrard Formation and thus, the base of this bed has been identified as a 3rd order sequence boundary. A precise physical correlation of this bed is of paramount importance to the results of this experiment: faunal epiboles are used here to confirm the position of this bed. Elements of the Maysvillian fauna enter at this horizon

and provide a useful biostratigraphic marker (Caster, 1963). An attempt is made here to demonstrate the effects of χ on an onshore-offshore gradient using the "Z-Bed" to represent a single coeval limestone horizon. Sampling the overlying "2 foot shale" may allow additional insight into the formation of meter-scale cycles, and associated "regressive" hemicycle. A result of this study is that the "Z-Bed" actually represents a bedset and is composed of multiple limestone interbeds. These interbeds are agglomerated together into a single bed in the downramp portions of the basin, and classic Cincinnatian type area, but when traced into the upramp portions of the basin may be separated by shale partings. This "Z-bed", or "Z-bedset" will be referred to as the "Z-bed" throughout the remainder of this paper.

Meter-Scale Cycles and Depositional Models

Limestone-mudstone alternations represent a common motif of typical Cincinnatian strata. While thickness of these low order-high frequency cycles may vary, such cycles are often referred to as meter-scale cycles (Tobin, 1982; Jennette and Pryor; Holland *et al*., 1997; Holland *et al*, 2001; Miller *et al*., 2001; Webber, 2002; Brett *et al*., 2003, 2008; Dattilo, *et al*., 2008; Schramm, 2011; Brett *et al*., 2012; Dattilo *et al*., 2012; etc.). Such cycles are commonly represented by a carbonate (pack-grainstone) hemicycle, and a coarsening upward mudstone-siltstone hemicycle, which together may be interpreted as 5^{th}-6^{th} order (~100-20k: Vail *et al*., 1991) depositional cycles/stratigraphic sequences (Schramm, 2011; Brett *et al*., 2003; 2012), or 'parasequences.' The time-series work of Ellwood *et* al., (2007; 2012) indicated that such cycles may be long-term climate driven Milankovitch cycles, verifying initial speculations of Jennette and Pryor (1993).

A series of divergent hypotheses have been proposed concerning the genesis of these cycles. It has been suggested that Cincinnatian shell-beds represent tempestites, or "storm cycles" formed by the accumulation of shells/bioclasts into limestone horizons and removal of fine-grained sediments/muds from an undifferentiated shelly-mudstone source. This represents the primary under-pinning of the "Storm Winnowing" or "Tempestite Proximality" models of shell bed formation (Kreisa and Bambach, 1982; Aigner, 1985). While very similar, the primary difference between these models is that in the storm-winnowing model, storms winnow the subtidal seafloor to create shell beds (Kreisa, 1981), while in the tempestite proximality model, - sea-level fluctuations modulate the position of wave base, and thus, the degree of storm winnowing, to produce sedimentary cycles (Aigner, 1985). While these models have been widely cited (Miller *et al*., 1997; Holland *et al*., 1997; Miller *et al*., 2001; Drummond and Sheets, 2001) for the formation of meter-scale cycles, Holland *et al* (2001), and Webber (2002) did not recognize significant differences in water-depth, based upon the faunal differences between the limestone and mudstone portion of these cycles. Thus, it has been suggested that the degree of storm winnowing may result from climatic cycles or variations in storm intensity, as opposed to eustatic sea-level variations. In contrast to this, when traced into the peritidal facies alternations between marine limestone and mud-cracked strata, there is clear evidence of sea-level variation during meter scale cycles (Schramm, 2011).

An alternative depositional model for shell-bed deposition has been termed the "Episodic Starvation Model" (Brett *et* al., 2008; Dattilo *et al*., 2008; 2012). This model suggests that shell-beds form via the accumulation of autochthonous shells over long time periods, with some degree of further concentration by winnowing, and that shell-bed growth was halted by sudden influxes of blanketing mud (obrution deposits).

The Storm Winnowing Model predicts that carbonate shell-beds should be increasingly condensed in upramp positions due to the removal of muds by wave-associated winnowing. Muds transported into downramp positions result in downramp splaying, thin shell beds interbedded with increasingly thick mud deposits downramp (Figure 1.4A). In contrast, small-scale cycles preserve many features of larger, high-order (low frequency) cycles, including sharp basal

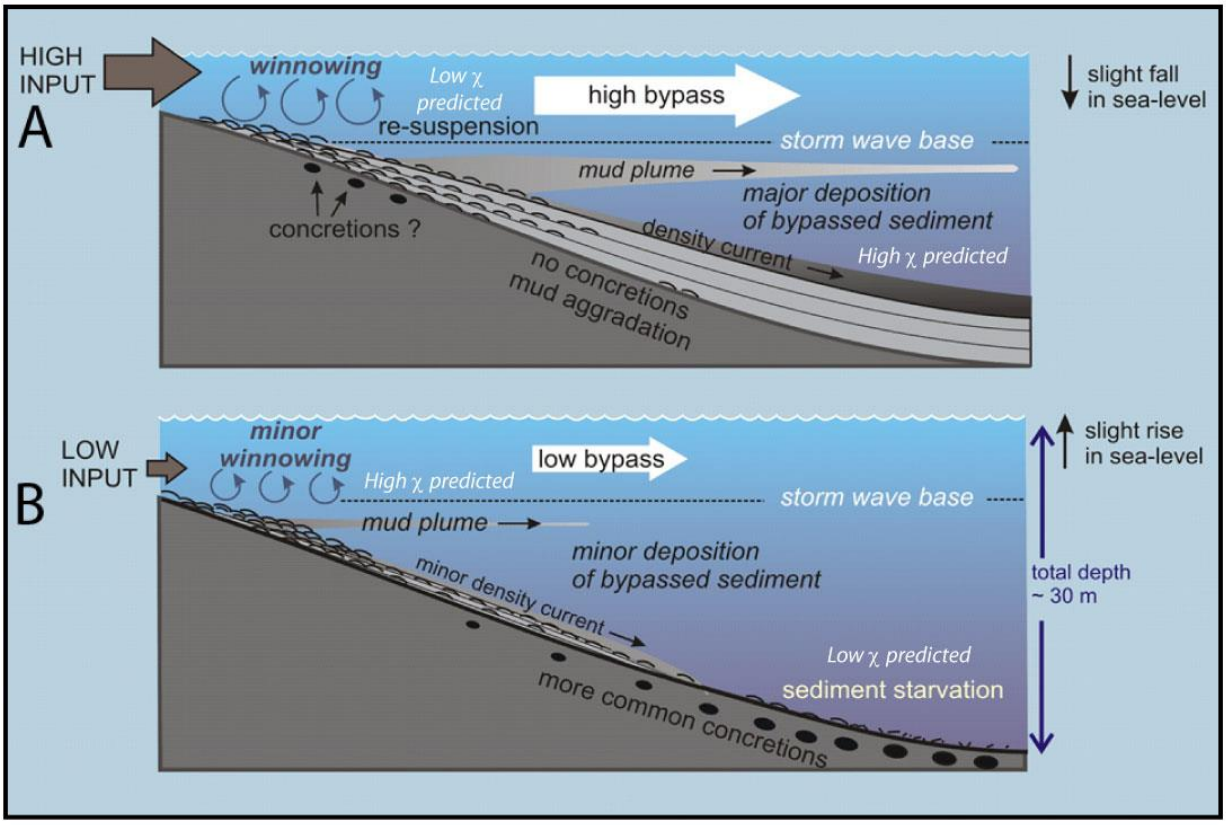

Figure 1.4 A.) Storm Winnowing and B.) Episodic Starvation models modified from Brett *et al*., (2008, 2012). Ellwood *et al*., (2007) determined that clay content drives χ in the Ordovician Kope Formation Thus, physical properties driving limestone bed formation on the Cincinnati Arch should have a predictable effect on χ values on a distal to proximal transect. Two models of shell bed genesis and χ predictions are given. A.) Storm Winnowing Model: If winnowing by storms influences shell bed development, higher χ values should be expected in down-ramp positions were thick muddy-carbonate deposits would occur. B.) Episodic Starvation Model: If shell beds represent time-condensed amalgamations of autochthonous sediment lower χ values

should be expected in down-ramp positions where sediment starved phosphatic shell beds would be found.

sequence boundaries, carbonate transgressive systems tract deposits, highstand mudstone deposits, and silty falling stage deposits (Brett *et al*., 2012). Such cycles may more simply be interpreted as transgressive-regressive (T-R) cyles (Dattilo *et al*., 2012). According to the episodic starvation model, small-scale rises in base-level (transgression) result in increased accommodation in upramp positions, in which argillaceous sediments may be sequestered. The resulting siliciclastic mud-free, sediment starved basin is associated with autochthonous carbonate development and condensed, phosphatic deposits downramp. Thus, shell beds should splay upramp, thicken, and interbed with muds (Figure 1.4B). This transgressive model of shell bed formation, largely matches the predictions of the episodic starvation model (Brett *et al*., 2008; 2012; Dattilo *et al*., 2008; 2012).

PREDICTIONS/HYPOTHESES

Ellwood *et al*., (2007) identified clay as the dominant driver of χ in Kope Formation strata, and the episodic starvation model (Dattilo *et al.* 2012) makes specific predictions about the distribution of clay. If interbedding of shelly carbonate and mudstone units occurs in upramp positions, then χ values are predicted to be more variable in vertical successions, in upramp positions. Similarly, if mudstone interbeds thin or decrease in a downramp position, and carbonates grow in the absence of siliciclastic sediment input, then χ is predicted to remain more constant in vertical successions.

If carbonates beds form in downramp positions because of sediment starvation and low amounts of bypassed sediment input, then values are predicted to be relatively low. If

argillaceous sediments are trapped in upramp positions, then χ in those beds is predicted to be high.

Rapid sulfate-reduction by sulfate reducing bacterial organisms in the marine system is known to decrease χ values downward in modern marine sediments (Karlin and Levi, 1983; 1985), as a result of reduction of magnetite to paramagnetic mineral phases such as pyrite of siderite. Condensed Cincinnatian limestone beds formed by an amalgamation of shells (Dattilo *et al*., 2012) may be expected to have a low χ values, as the zone of sulfate reduction remains stagnant for a long interval of time (Brett *et al*., 2008). Conversely, mudstones, commonly representing obrution deposits are expected to yield higher measured χ values.

METHODS

A meticulous search was conducted for all accessible, well exposed sections of the "Z-Bed"–"2 foot shale" interval where correlations are firmly established (Brett and Algeo, 2001). This search revealed some previous misidentifications/correlations in the literature, and finally resulted in 27 sections, of the Kope-Fairview formation boundary interval, that were examined for this study. These extend across the lateral extent of the Cincinnati Arch. Each section was cleaned in order reduce sample contamination and remove weathered material (Ellwood *et al*., 2013). 771 samples were collected through the "Z-Bed" – "2 foot shale" interval, with resolution of 5 cm, for all but four sections, which were collected at 10 cm resolution. Lithology, where exposed, was measured at the cm scale in order to reduce the possibility of miscorrelation. Additionally, to reduce the possibility of miscorrelation and contamination, subsurface samples/cores were not used in this study. Incorporation of drilling fluids into pore-spaces may alter χ values and thus, cores were not sampled.

Collected samples were broken into approximately pebble-sized pieces to reduce the anisotropy of magnetic susceptibility in these samples. Approximately 10 grams of sample were measured for χ using the Williams Magnetic Susceptibility Bridge, a balanced coil induction system located in the Rock Magnetism Laboratory at LSU. The bridge is calibrated relative to mass (Ellwood *et al*., 1999). The mean of three sample measurements was used for determining χ of the measured sample. Measurements taken on the LSU magnetic susceptibility bridge reach down into the 10^{-10} and 10^{-11} m^3/kg range in addition to recording some negative χ values.

Stratigraphic sections were drafted and χ was plotted relative to sampling position. Lithology-based correlations of measured sections were made based upon known lithologic correlation, allowing χ to be independently interpreted (Figure 1.5 and 1.6). Sections were hung upon the top of the "Z-Bed", as this abrupt shift in lithology, in this meter scale cycle indicates a basin- wide change in sedimentation and represents an approximately synchronous surface. It is argued here that hanging sections upon this surface resulted in the most realistic stratal geometry. "Z-Bed" χ values were selected from slightly below the top of the "Z-Bed", as well as in the lower "2 foot shale". These data-points are indicated with yellow stars on the correlation diagram (Figure 1.5 and 1.6) were then plotted relative to sample locality using Surfer. The Kriging algorithm was used to construct contours of these values, and these data were plotted spatially (Figure 1.7 and 1.8).

To evaluate the magnetic mineralogy within the "Z-Bed" and "2 foot shale", four samples were taken from near the top of the "Z-Bed" and from within the "2 foot shale", and the thermomagnetic susceptibility was measured using the KLY-3S Kappa bridge in the Rock Magnetism Laboratory at LSU. These data are reported in Figure 1.9.

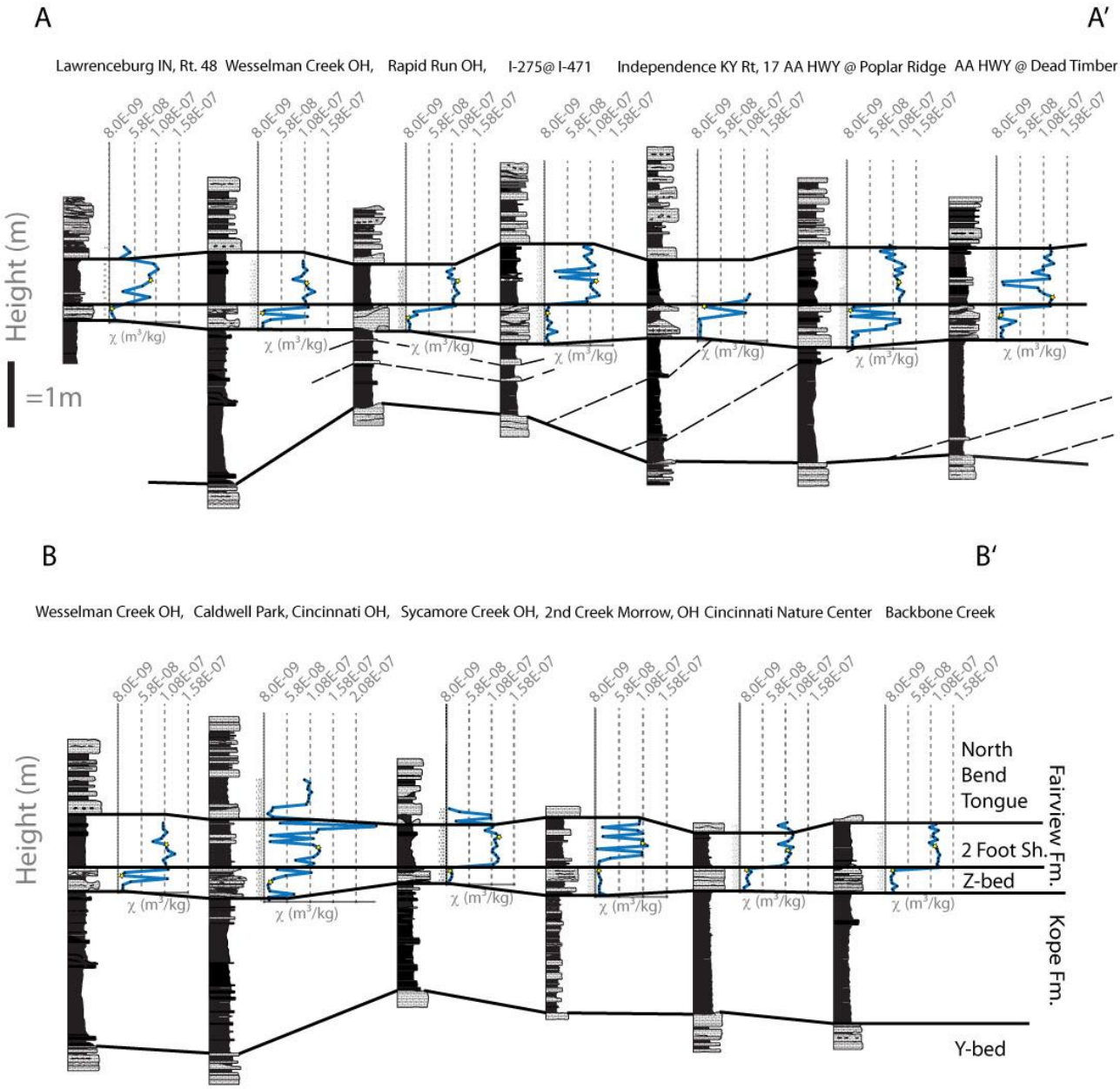

Figure 1.5 Lithologic correlation diagram showing horizons studied and the surrounding strata used to bracket this interval. Litholoigic based correlations are hung upon the top of the "Z-Bed", representing a synchronous time horizon in order to independently evaluate χ. χ measurements shown relative to lithology are shown with a blue line and individual data points indicated with a small black dot. Yellow stars near the top of the "Z-Bed" and in the "2 foot shale" indicate data points shown on the contour maps of χ values. Thick black lines indicate established lithologic correlations. Thin dashed black lines in the Y to Z bed interval indicate a possible correlation of inter-beds demonstrating a clinoformal morphology. Note physical

changes in "Z-Bed" thickness and mud interbeds in proximal portions of the basin. Transects A, B, and C and outcrop localities of these appear on the location map, (Figure 1.2).

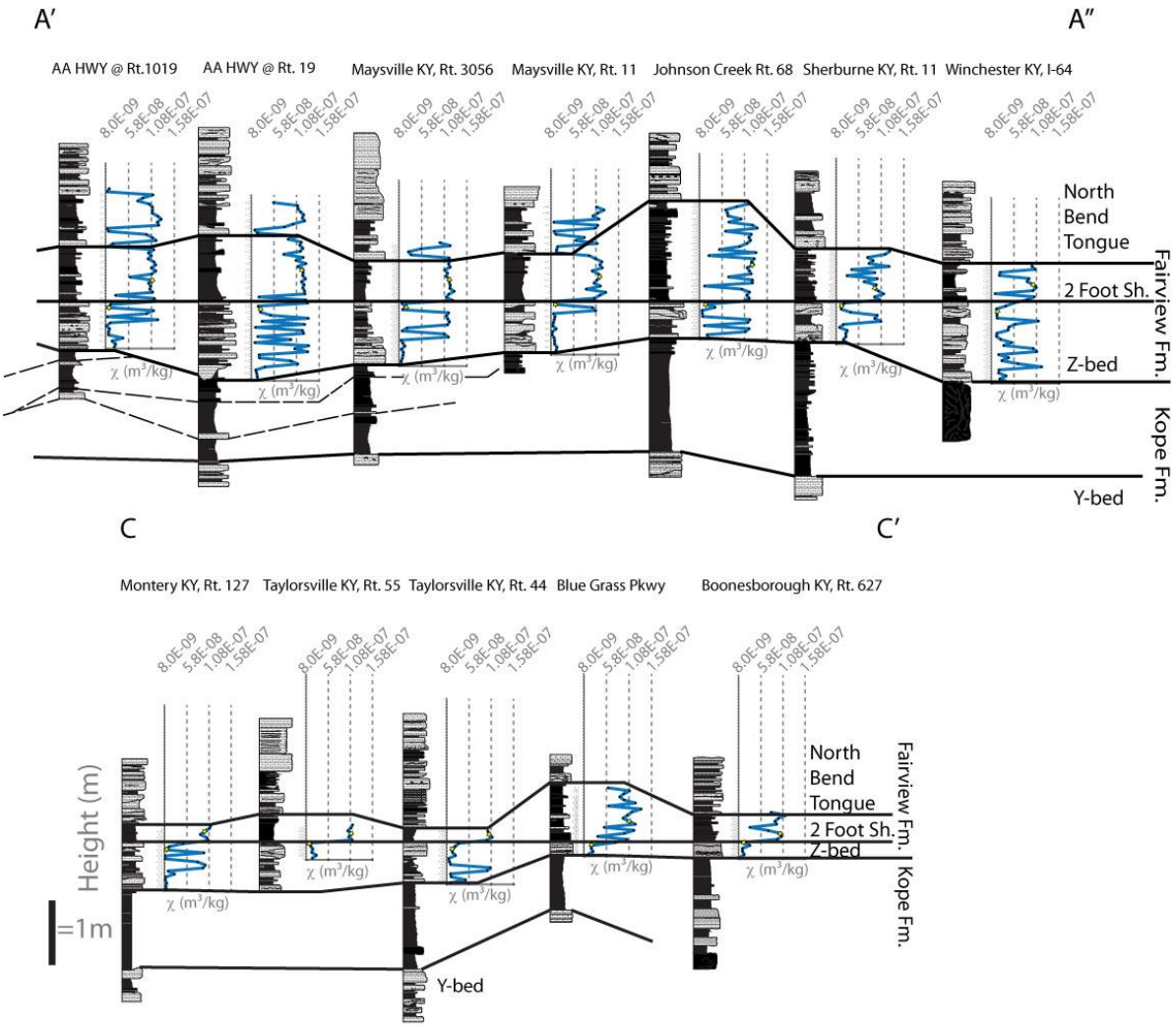

Figure 1.6 Continued Correlation Diagram from Figure 1.5.

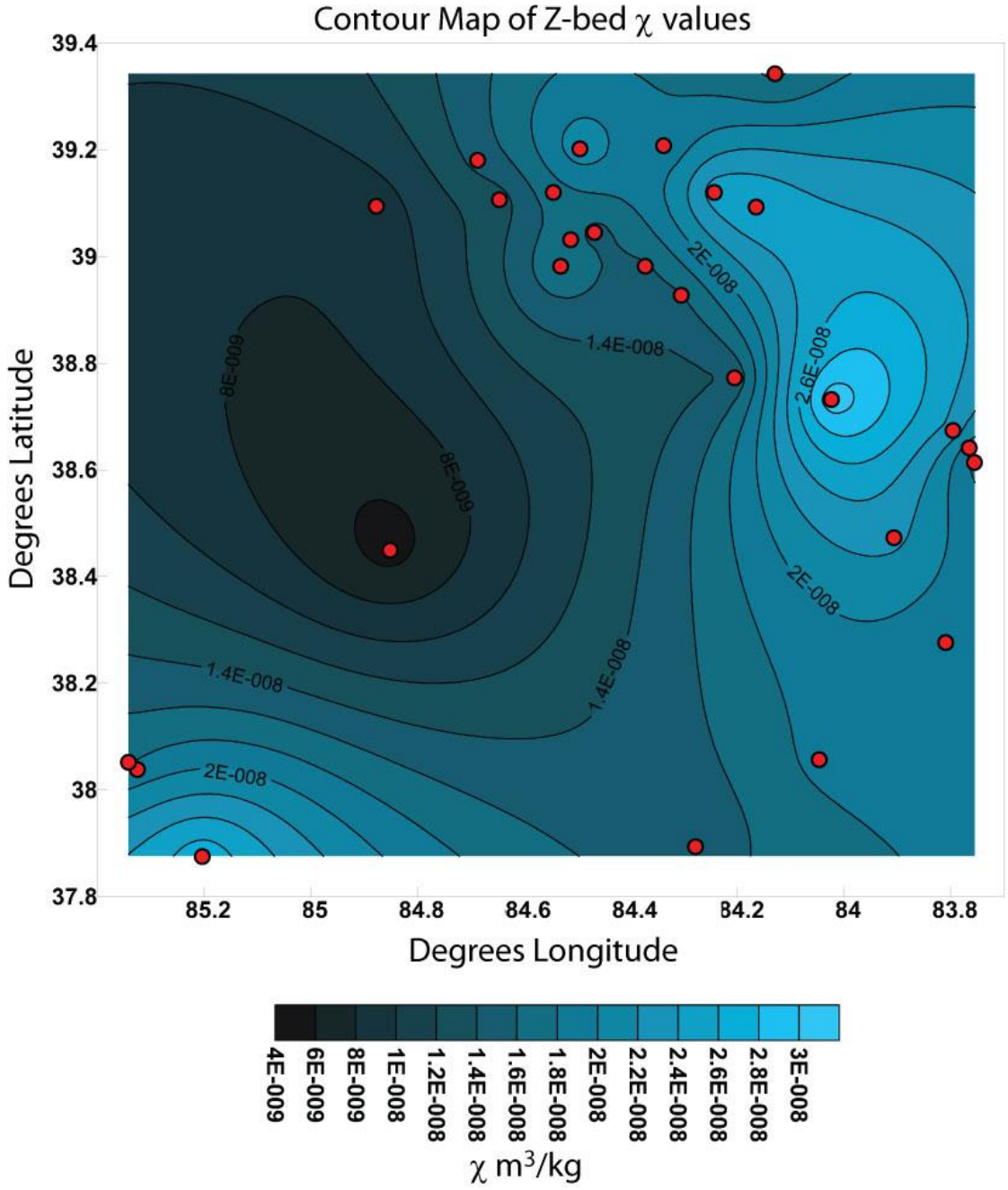

Figure 1.7 Contour map of χ values selected from the top of the "Z-Bed", indicated in the correlation diagram in Figures. 1.5 and 1.6, with stars, made using the Kriging algorithm with Surfer software. Darker colors indicate lower χ values. Axes indicate Latitude and Longitude location indicated with red dots. This indicated that χ values are not constant spatially but have a small yet predictable decrease in values in the distal portions of the basin.

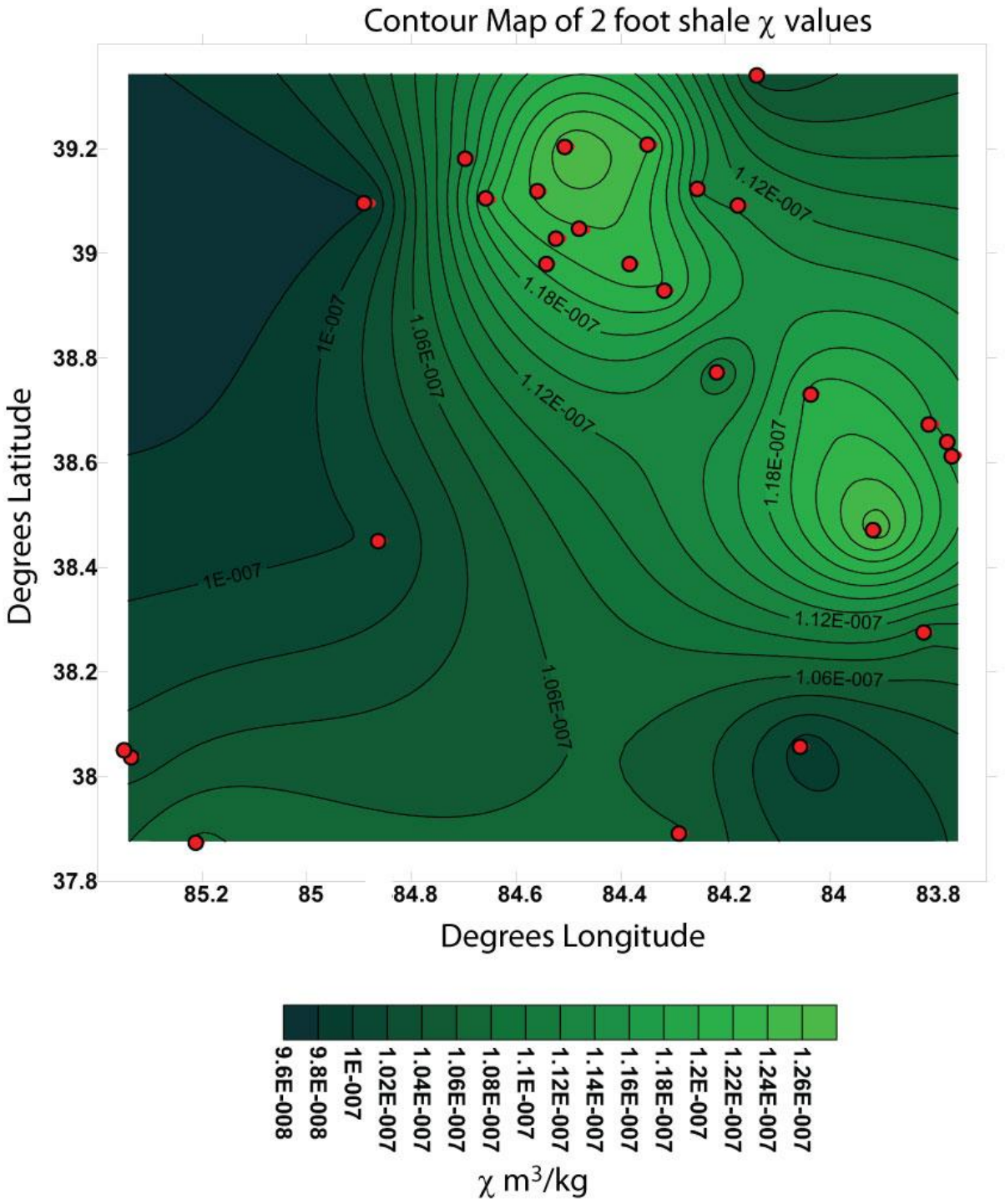

Figure 1.8 Contour map of χ values selected from the "2 foot shale", indicated in the correlation diagram in Figures 1.5 and 1.6, with stars, made using the Kriging algorithm with Surfer software. Darker colors indicate lower χ values. Axes indicate Latitude and Longitude, location indicated with red dots. "2 foot shale" values show a decrease in the downramp direction. They display a wider range of values than their "Z-Bed" counterparts and values are somewhat more scattered.

RESULTS

Sample Measurement values

χ values for the top of the "Z-Bed" χ values range from 1×10^{-8} to 3×10^{-8} m^3/kg, and in the most distal sampling localities in the upper 10^{-9} m^3/kg exponent range. "2 foot shale" χ values are somewhat higher and appear in the range from 9×10^{-8} to 1.3×10^{-7} m^3/kg. These values are well within the normal range of marine values (Ellwood *et al*., 2013). Standard deviation of samples measured in this study generally appears in the 10^{-10} exponent range: standard deviation values are typically two orders of magnitude lower than the individual sample measurements. Likewise, the resolution of the contour maps of χ values (Figures 1.7 and 1.8) does not exceed the range of instrumentation error.

Lithology Driven Values

A strong correlation exits between the lithology of Cincinnatian samples and χ values. Limestone sample values in this study are typically "low", but well within the range of typical marine χ values (Ellwood *et al*., 2011), while mudstone sample values for χ are consistently higher than limestone values. This matches the observations of Ellwood *et al*., (2007) that Kope Formation χ values are driven by clay content. The "Z-Bed" physically splays from one condensed bed downramp into multiple limestone beds interbedded with shale in more proximal settings and may more accurately be characterized as a bedset instead of a single bed. A mean from the entire "Z-Bed" thickness was calculated from each sampling locality (Table 1.1). This did not show as much variation spatially as within a single horizon at the top of the "Z-Bed"set and likely represents a time-averaging of this bed reflecting a homogenization of limestone and interbedded shale lithologies, as opposed to a single synchronous horizon.

Table 1.1

Section	Top "Z-Bed" χ	Top "Z-Bed" χ Standard Deviation	Total "Z-Bed" Thickness χ Mean	"2 foot shale" χ
Lawrenceburg, IN	1.13E-08	5.00E-10	1.513E-08 N=3	9.76E-08
Wesselman Creek	1.62E-08	5.79E-10	3.425E-08 N=7	1.12E-07
Rapid Run	1.28E-08	4.68E-10	2.66E-08 N=8	1.21E-07
Bald Knob	1.67E-08	9.53E-10	1.502E-08 N=3	NA
I 275@ I 471	1.39E-08	6.20E-10	1.689E-08 N=14	1.21E-07
Independence, KY	2.08E-08	5.76E-10	3.086E-08 N=6	NA
Reidlin-Mason Road	1.75E-08	1.00E-09	1.800E-08 N=6	NA
AA @ Poplar Ridge	1.64E-08	1.56E-10	5.212E-08 N=14	1.23E-07
AA @ Dead Timber	1.67E-08	3.95E-10	2.250E-08 N=11	1.24E-07
AA @ Rt 1019	1.30E-08	5.77E-10	3.804E-08 N=15	1.10E-07
AA @ Rt 19	2.85E-08	4.63E-10	6.267E-08 N=25	1.23E-07
Maysville, KY 3056	2.32E-08	3.41E-10	4.935E-08 N=21	1.19E-07
Maysville, KY Rt 62-68	1.82E-08	1.30E-10	4.673E-08 N=19	1.21E-07
Maysville, KY Rt 11	1.58E-08	3.35E-10	2.536E-08 N=18	1.17E-07
Johnson Creek	2.19E-08	2.47E-10	5.341E-08 C=12	1.28E-07
Sherburne, KY	2.02E-08	4.14E-10	4.222E-08 N=14	1.08E-07
Winchester, KY	2.11E-08	5.83E-10	4.665E-08 N=27	9.70E-08
Caldwell Park	2.22E-08	3.64E-10	3.807E-08 N=11	1.26E-07
Sycamore Creek	1.61E-08	5.92E-10	1.688E-08 N=6	1.25E-07
2nd Creek	1.55E-08	4.41E-10	1.806E-08 N=10	1.05E-07
Cincinnati Nature Center	2.42E-08	3.83E-10	2.450E-08 N=8	1.12E-07

Section	Top "Z-Bed" χ	Top "Z-Bed" χ Standard Deviation	Total "Z-Bed" Thickness χ Mean	"2 foot shale" χ
Backbone Creek	2.26E-08	4.66E-10	2.439E-08 N=8	1.17E-07
Montery, KY	8.96E-09	2.02E-10	3.533E-08 N=16	9.91E-08
Taylorsville KY, Rt. 55	1.55E-08	5.38E-10	2.169E-08 N=6	1.03E-07
Taylorsville KY, Rt 44	1.88E-08	4.44E-10	3.395E-08 N=14	1.04E-07
Blue Grass Pkwy	2.41E-08	7.64E-10	3.406E-08 N=5	1.08E-07
Boonesborough, KY	1.80E-08	2.91E-10	1.931E-08 N=6	1.03E-07

Episodic Starvation

Limestone beds are observed to thicken upramp, splay open into multiple beds that are interbedded with mudstones, and increasingly demonstrate a more argillaceous character. In downramp positions, beds are thin, condensed, amalgamated phosphatic grainstones with rare concretions occurring beneath them. These physical changes match the predictions of the Episodic Starvation Model of shell bed formation. Likewise, decreased χ values are observed in distal portions of the basin, matching the predictions associated with this model.

Spatial Change in χ values

Small but predictable changes in "Z-Bed" χ values appears to occur with increased distance from sediment source. Proximal portions of the basin generally record somewhat higher χ values, while distal portions of the basin record lower χ values. This result matches predictions of decreasing χ values for limestones with increased distance from the siliciclastic sediment source and refutes the predictions of increased χ values downramp if these shell beds were formed by increased storm winnowing. Instead, these lower values in distal positions

indicate a sediment starved basin. High χ values in proximal positions indicate argillaceous sediments filling increased upramp accommodation.

Thermomagnetic susceptibility

Thermomagnetic susceptibility measurements taken on the LSU kappabridge indicate very low values and a paramagnetic signature for both "Z-Bed" and "2 foot shale" samples at low temperature, with essentially no ferrimagnetic components (Figure 1.9). "Z-Bed" values are very low with one sample being diamagnetic. Two foot shale samples are still very low but initial values are approximately and order of magnitutude higher than the "Z-bed" values. Breakdown effects indicate that "Z-Bed" and "2 foot shale" samples of the Cincinnati Arch have not been heated over ~250 degree °C. Conodont Alteration Index of the study area is less than 1.5; when used as geothermometer (Epstein *et al*., 1977) this indicates heating of 50°-90° and supports the kappabridge results. The significance of this is that samples used in this study have no observed alteration affects due to heating. The "Z-Bed" and "2 foot shale" samples analyzed using this technique show similar results within each individual bed, respectively. This method produces a similar result in terms of mass based χ measurements, downramp "Z-Bed" samples (WES 0.25) display lower thermomagnetic susceptibility magnitudes than their upramp counterparts. Furthermore, "2 foot shale" samples display higher magnitudes than the "Z-Bed" samples. Magnetic breakdown effects at greater than 400 degrees °C (Figure 1.9) support the conclusions of Ellwood *et al*., (2007) indicating illite concentration as driving χ values. Some siderite or ankerite may also influence these thermomagnetic susceptibility values (Ellwood *et al*., 1986; 1989).

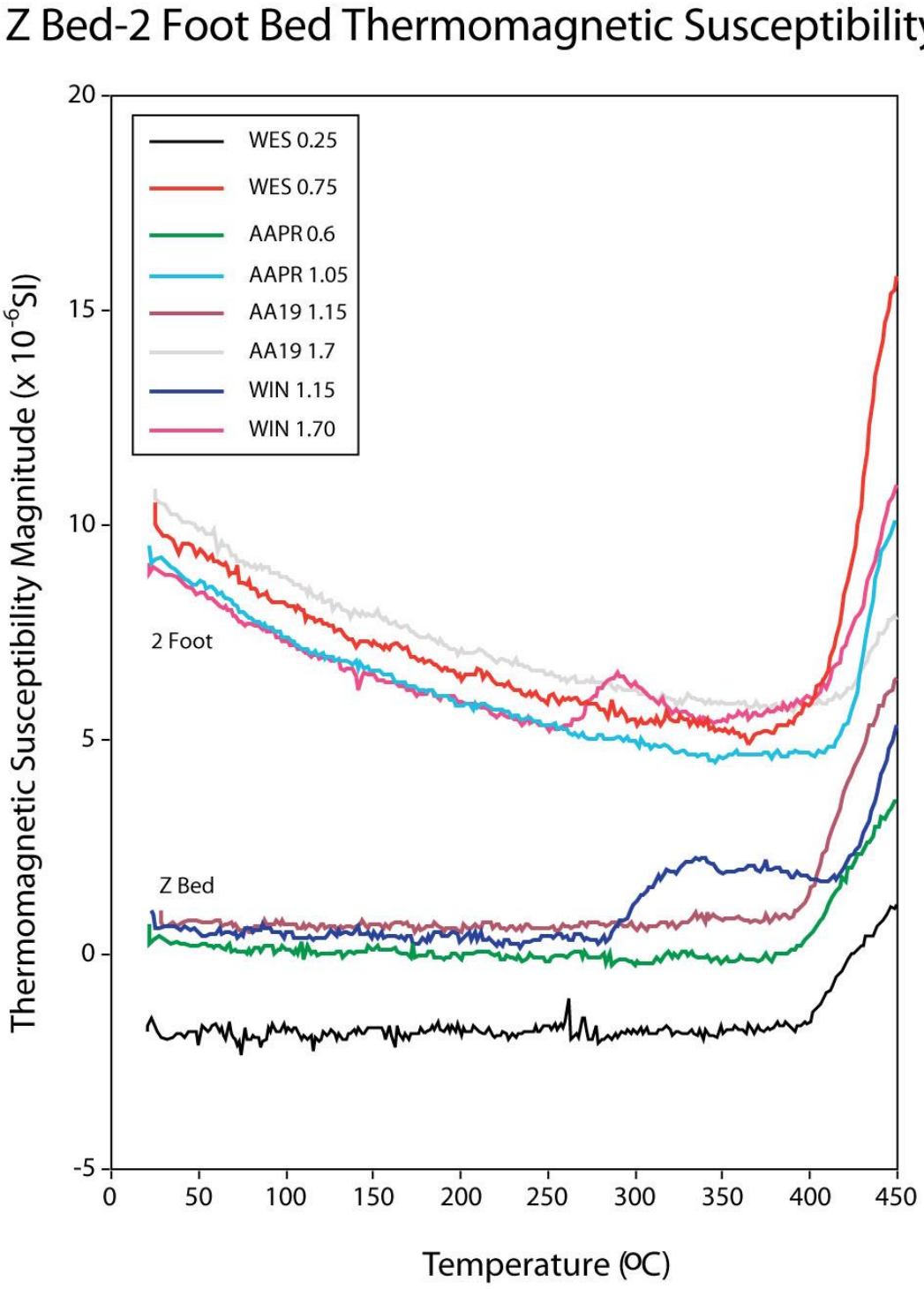

Figure 1.9 Thermomagnetic susceptibility of typical "Z-Bed" and "2 foot shale" samples. Samples display a paramagnetic signature at room temperature. (WES, Wesselman Creek; AAPR, AA Highway at Poplar Ridge; AA19, AA Highway at Rt. 19; WIN, Winchester KY, I-64).

Small amounts of dolomite associated with voids, rip-up clasts and reworking of shells has been reported in Cincinnatian strata (Dattilo pers com. 2014; Freeman *et al*., 2013; Freeman *et al*., 2012). It is suggested that these occurrences may actually represent ankerite, or ferroan dolomite and contribute to Cincinnatian χ values in time-rich horizons such as the "Z-Bed" and the horizons they studied.

DISCUSSION

Correlation Potential

A sharp offset from low to high χ values exists at the "Z-Bed"– "2 foot shale" contact in distal portions of the basin (Figure 1.5 and 1.6) . This represents a basin-wide change in sediment source that may be associated with climatic oscillations, which in turn produced fluctuations in weathering and sediment input. In more proximal portions of the basin, this signal appears to break down. As the "Z-Bed" physically thickens, splaying into multiple limestone beds inter-bedded with mudstones, χ values appear more variable. Similarly, as the "2 foot shale" becomes interbedded with increasing numbers of siltstones and thin-packstones, and generally becomes more calcareous in proximal positions, the average χ increases in variability. These features can be observed at the Johnson Creek, Sherburne, and Winchester sections (Figure 1.6). Because these "Z-Bed" and "2 foot shale" units have variable χ lithology, in proximal positions the ability to distinguish the two units from each other diminishes when using χ curves. Therefore, correlation applications using χ are best suited to distal portions of basins and not proximal positions. Likewise, regardless of correlation proxy used, correlating in near-shore environments remains difficult. Stratigraphic studies utilizing this correlation method may be better suited to facies below storm wave base.

Stratal Geometry and Sequence Stratigraphic Implications

An erosional morphology exists at the base of the "Z-Bed" and a broad-scale or scour-like feature is present at its base. The base of the bed oversteps underlying strata and is interpreted to represent a sequence boundary. Beds from within the "Y-bed" to "Z-Bed" silty shale interval are removed by this hiatus, and easily recognizable beds appearing in multiple sections also appear to lap-out onto the top of the "Y-bed" in a downramp direction. This indicates that this interval is progradational and represents a falling stage deposit, while the "Z-Bed" and "2 foot shale" may be aggradational. A return to carbonate deposition at the base of the North Bend submember (Schramm, 2011), represents retrogradation. This brackets the "Z-Bed"– "2 foot shale" interval as a Lowstand Systems Tract. The clinoformal morphology found within the Y to "Z-Bed" interval has not been previously observed within Cincinnatian strata. While the widespread traceability of shell beds matches the predictions of Brett *et al*. (2008), this clinoformal morphology is also consistent with sequence stratigraphic models.

"Z-Bed" Trough

A prominent feature present in Figure 1.6 is a NW-SE trending contour containing low χ values shown in dark blue-black. Here, lower values are shown in black and higher values are shown in blue. Samples collected along Rt. 127 in Montery, Kentucky, and Lawrenceburg, Indiana displayed the lowest measured χ values, falling into the 9×10^{-9} exponent range. While these localities only occupy two points on the map (Figure 1.7) they both contained multiple measured χ values in this low range. This indicates that these do not represent spurious values.

We suggest a broad correlation between water depth, or proximality and χ values. In the case of Kope limestone bundles, putatively formed during transgressions, higher χ values occur

in apparently more proximal localities, closer to shoreline, with higher concentrations of argillaceous sediment, and lower χ values occur in more distal localities with increased sediment condensation. In general, χ values do decrease downramp from shalier and shallower facies in the SE to more condensed sections to the NW. However, features indicated on this map appear to be more complex than a progressive, northwest decrease in χ values, as lower values occur also in the few localities that define the NW-SE "trough" on Figure 1.7. Similarly, the original paleotopography may be more complex than a simple northwestwardly dipping Cincinnatian ramp; the ramp may have included subtle saddles, plateaus, and other topographic features (see Miller et al., 2001). It is speculated that the interval of low χ values in the center of the map may represent an embayment of the Sebree Trough (Kolata *et al*., 2001), a NE/SW trending area of deeper water occurring to the north of Cincinnati (Figure 1.2). Here Kope Formation strata interfinger with distal lithologies of the Utica Shale in the subsurface representing condensed downramp deposits.

While this prominent feature on Figure 1.7 is perpendicular to the main NE/SW trend attributed to the Sebree Trough it may represent an embayment of that trough. Such a feature may have permitted an avenue for sediment redistribution in Ordovician seas. The low amount of data only permits the preliminary suggestion of such a feature and does not unequivocally demonstrate it. While, this is an intriguing scenario we must be careful not to over interpret these data, as this feature occurs in an area with poor sampling density. Additionally, this apparent feature may be a result of the contouring algorithm used. Unfortunately, outcrop distribution does not permit further sampling in areas occupying the Jessamine Dome as the pertinent beds are erosionally removed everywhere over the crest of the dome.

Short Comings

It was not possible to distinguish if χ for "Z-Bed" samples in distal portions of the basin is driven by very low concentrations of terrigenous detrital mater, or if aeolian dust in the marine realm is driving these values. While the Cincinnati Arch provides an area where such an investigation is possible, this study is limited by the extent of the Kope–Fairview formation boundary outcrop belt. Erosional removal of these beds at the center of the Jessamine Dome, limit the extent to where this study can be conducted. Further limitations include a lack of knowledge of traceable horizons in the Appalachian Basin. Consequently, bed-by-bed correlation from the Cincinnati Arch to the Martinsburg Foreland Basin does not exist, thus this study was not able to sample all the way to the sediment source. The majority of this study is limited to the classic Cincinnatian outcrop belt, generally, between Maysville, Kentucky, and Lawrenceburg, Indiana. Thus, when analyzing the contour maps of "Z-Bed" values, sample localities on the periphery of this study are less well defined. Interpretations of these maps should be limited to the highest sampling density in the northeast area of the map (Figure 1.7).

Additionally, high-resolution correlations within the "Z-Bed" remain tentative. Points were chosen slightly below the top of this bed as this is assumed to represent the most time-synchronous horizon, but minor errors in correlation are possible. Furthermore, while the point slightly below the top of the "Z-Bed" is interpreted to be isochronous, some degree of time averaging may be present. If this limestone hemicycle represents half of a twenty thousand year precessional cycle, then a minimum of ten thousand year resolution can be assumed. These short durations are insignificant relative to geologic time.

While the results of this study do indicate that χ is not spatially constant, this investigation is limited to one basin at one point in time. Other basins during other time periods may yield similar, or widely varying results. Furthermore, the sequence stratigraphic interval or lowstand systems tract, within which this experiment was conducted, may yield different physical properties and χ values than other systems tracts in which retrogradation, or progradation may occur. The aggradational stacking pattern produced during a stillstand does, however, provide a somewhat idealized time of investigation in which the paleo shoreline is not migrating.

CONCLUSIONS

In Cincinnatian strata, a small but predictable decrease in χ and in variability occurs with increased distance from the detrital sediment source. Similar trends of high χ values decreasing away from the past have been observed in the modern Argentine Basin (Sachs and Ellwood, 1988). These values appear to be the result of the changing physical properties of the study interval lithology throughout the Cincinnatian basin. As χ is a physical property of the rock, spatial variability is expected, and has been demonstrated for Cincinnatian strata. Physical observations of the "Z-Bed" match the predictions of the Episodic Starvation Model of shell bed formation. Correlation using χ is best applied in distal portions of basins. Changes in lithology, represented by interbedding of limestone and shale, may obscure large trends used to correlate, if based solely on χ curve matching. The erosional morphology and regional truncation of strata - below the base of the "Z-Bed" match the predictions of Schramm (2011), this surface represents a sequence boundary.

REFERENCES

Aigner, T. 1985. Storm Depositional Systems: Dynamic Stratigraphy in Modern and Ancient Shallow Marine Sequences: Lecture Notes in the Earth Sciences 3. Springer-Verlag, Berlin.

Bassler, R.S., 1906. A study of the James types of Ordovician and Silurian Bryozoa. Proceedings of the U.S. National Museum, V. 30 No. 1442.

Bretsky, P. 1970. Upper Ordovician Ecology of the Central Appalachians. Peabody Museum of Natural History, Bulletin 34, Yale University

Brett, C.E. and Algeo, T.J., 2001. Stratigraphy of the Upper Ordovician Kope Formation in its Type Area, Northern Kentucky, Including a Revised Nomenclature. *in*: T.J. Algeo and C.E. Brett., eds. Sequence, Cycle, and Event Stratigraphy of Upper Ordovician and Silurian Strata of the Cincinnati Arch Region.

Brett, C.E., Algeo, T.J., McLaughlin, P.I. 2003. Use of event beds and sedimentary cycles in high-resolution stratigraphic correlation of lithologically repetitive successions. In Harries, P.J., ed. High-Resolution Approaches in Stratigraphic Paleontology. Kluwer Academic Publishers, Netherlands, pp. 315-350.

Brett, C.E., McLaughlin, P.I., and Baird, G.C., 2007. Eo-Ulrichian to Neo-Ulrichian views: The renaissance of "layer-cake stratigraphy". Stratigraphy, vol. 4, nos. 2/3 p201-215.

Brett, C.E., Kirchner, B.T., Tsujita, C.J., Dattilo, B.F., 2008. Sedimentary Dynamics in a Mixed Siliciclastic-Carbonate System: The Kope Formation (Upper Ordovician), Southwest Ohio and Northern Kentucky: Implications for Shell Beds Genesis in Mudrocks, in: Holmden, C., Pratt, B.R. (Eds.), Dynamics of Epeiric Seas: Sedimentological, Paleontological and Geochemical Perspectives, Geological Association of Canada, Special Paper 48. Geological Association of Canada, p. 406.

Brett, C.E., Schramm, T.J., Dattilo, B.F., Marshall, N.T. 2012, Upper Ordovician Strata of Southern Ohio-Indiana: Shales, Shell Beds, Storms, Sediment Starvation, and Cycles. 2012 GSA North-Central Section Meeting Fieldtrip 405 Guidebook. 80 p.

Caster, K.E., Dalvé, E.A., and Pope, J.K. , 1961. Elementary guide to the fossils and strata of the Ordovician in the vicinity of Cincinnati, Ohio: Cincinnati Museum of Natural History, 47 p.

Crick, R.E., Ellwood, B.B., El Hassani, A., Feist, R., and Hladil, J., 1997. MagnetoSusceptibility event and cyclostratigraphy (MSEC) of the Eifelian-Givetian GSSP and associated boundary sequences in North Africa and Europe, Episodes 20, 167-175.

Da Silva, A.C., Boulvain, F. 2006. Upper Devonian carbonate platform correlations and sea level variations recorded in magnetic susceptibility. Palaeogeography, Palaeoclimatology, Palaeoecology, V. 240 p. 373-388

Dattilo, B.F., Brett, C.E., Tsujita, C.J., Fairhurst, R., 2008. Sediment supply vs. storm winnowing in the development of muddy and shelly interbeds from the Upper Ordovician of the Cincinnati region, USA. Canadian Journal of Earth Sciences 45, 243-265.

Dattilo, B.F., Brett, C.E., Schramm, T.J., 2012, Tempestites in a teapot? Condensation-generated shell beds in the Upper Ordovician, Cincinnati Arch, USA, Palaeogeography, Palaeoclimatology, Palaeoecology, doi:10.1016/j.palaeo.2012.04.012 V. 367-368 p. 44-62

Drummond, C., Sheets, H. 2001. Taphonomic reworking and stratal organization of tempestite deposition: Ordovician Kope Formation, Northern Kentucky, U.S.A. Journal of Sedimentary Research 71: 621-627.

Ellwood, B.B., Balsam, W., Burkart, B., 1986. Anomalous Magnetic Properties in Rocks Containing the Mineral Siderite: Paleomagnetic Implications. Journal of Geophysical Research, V. 91. P 12,779-12,790.

Ellwood, B.B., Burkart, B., Rajeshwar, K., Darwin, R.L., Neeley, R.A., McCall, A.B., Long, G.J., Buhl, M.L., Hickcox, C.W., 1989. Are the Iron Carbonate Minerals, Anekerite and Ferroan Dolomite, Like Siderite, Important in Paleomagnetism? Journal of Geophysical Research, V. 94 P 7321-7331.

Ellwood, B.B., Crick, R.E., El Hassani, A., 1999. The Magneto-Susceptibility Event and Cyclostratigraphic (MSEC) Method used in Geological Correlation of Devonian Rocks from Anti-Atlas Morocco. AAPG Bulletin, V. 83, No. 7

Ellwood, B.B., Crick, R.E., El Hassani, A., Benoist, S. and Young, R., 2000. MagnetoSusceptibility Event and Cyclostratigraphy (MSEC) in Marine Rocks and the Question of Detrital input versus Carbonate Productivity, Geology, 28, 135-1138.

Ellwood, B.B., Balsam, W.L., Roberts, H.H., 2006. Gulf of Mexico Sediment Sources and Sediment Transport Trends from Magnetic Susceptibility Measurements of Surface Samples. Marine Geology 230, 237-248.

Ellwood, B.B., Brett, C.E., and MacDonald, W.D., 2007. Magnetostratigraphy susceptibility of the Upper Ordovician Kope Formation, northern Kentucky. Palaeontology, Palaeoclimatology, Palaeoecology 243. 42-54.

Ellwood, B.B., Tomkin, J.H., El Hassani, A., Bultynck, P., Brett, C.E., Schindler, E., Feist, R., Bartholomew, A.J. 2011. A climate-driven model and development of a floating point time scale for the entire Middle Devonian Givetian Stage: A test using magnetostratigraphy susceptibility as a climate proxy. Palaeogeography, Palaeoclimatology, Palaeoecology. V. 304. P. 85-95.

Ellwood, B.B., Brett, C.E., Tomkin, J.H., MacDonald, W.D., 2012. Visual identification and quantification of Milankovitch climate cycles in outcrop: an example from the Upper Ordovician Kope Formation, northern Kentucky, in: Herrero-Bervera, E., Jovane, L. (Eds.), Magnetostratigraphy: Not only a dating tool. The Geological Society of London Special Publication, London.

Ellwood, B.B., Wang, W.H., Tomkin, J.H., Ratcliffe, K.T., El Hassani, A., Wright, A.M. 2013. Testing high resolution magnetic susceptibility and gamma radiation methods in the Cenomanian-Turonian (Upper Cretaceous) GSSP and near-by coeval section. Palaeogeography, Paaeoclimatology, Palaeoecology 378. 75-90.

Ettensohn, F.R., 1991. Flexural interpretation of relationships between Ordovician tectonism and stratigraphic sequences, central and southern Appalachians, U.S.A.; *in:* Advances in Ordovician Geology, C.R. Barnes and S.H. William (ed.), Geological Survey of Cananda, Paper 90-9, p. 213-224

Ettensohn, F.R., Hohman, J.C., Kulp, M.A., Rast, N. 2002. Evidence and implications of possible far-field responses to the Taconian Orogeny:Middle-Late Ordovician Lexington Platform and SeBree Trough, east-central United States. Southeastern Geology 41: 1-36.

Epstein, A.G., Epstein, J.B., Harris, L.D., 1977. Conodont Color Alteration-an Index to Organic Metamorphism. Geological Survey Professional Paper 995.

Fenneman, N.M., 1916. Geology of Cincinnati and Vicinity. Geological Survey of Ohio. Fourth Series Bulletin 19.

Freeman, R.L., Dattilo, B.F., Morse, A., Blair, M., Utesch, B.A., Felton, S., Pojeta, J. 2012 The Brachiopod Trap: What their oldest (Upper Ordovician, Ohio) failed escape burrows tell us about the evolution of burrowing in Linguids. Geological Society of America Abstracts with Programs.

Freeman, R.L., Dattilo, B.F., Morse, A. Blair, M., Felton, S., Pojeta, J. 2013. The "Curse of Rafinequina:" Negative Taphonomic Feedback Exerted by Strophomenid Shells on Storm-Buried Lingulids in the Cincinnatian Series (Katian, Ordovician) of Ohio. Palaios 28. 359-372.

Holland, S.M. 1993. Sequence stratigraphy of a carbonate-clastic ramp: The Cincinnatian Series (Upper Ordovician) in its type area. Geological Society of America Bulletin, 105. 306-322.

Holland, S.M., Miller, A.I., Dattilo, B.F., Meyer, D.L., Diekmeyer, S.L., 1997. Cycle anatomy and variability in the storm-dominated type Cincinnatian (Upper Ordovician): Coming to grips with cycle delineation and genesis. Journal Of Geology 105, 135-152.

Holland, S.M., Miller, A.I., Meyer, D.L., Dattilo, B.F., 2001. The detection and importance of subtle biofacies within a single lithofacies: The Upper Ordovician Kope Formation of the Cincinnati, Ohio region. Palaios 16, 205-217.

Holland, S.M., and Patzkowsky, M.E. 1996. Sequence stratigraphy and long-term paleoceanographic change in the Middle and Upper Ordovician of the eastern United States. Geological Society of America Special Papers. 306. P. 117-129.

Jennette, D.C., Pryor, W.A., 1993. Cyclic alternation of proximal and distal storm facies: Kope and Fairview Formations (Upper Ordovician), Ohio and Kentucky. Journal of Sedimentary Petrology 73, 306-319.

Karlin, R., Levi, S. 1983. Diagenesis of magnetic minerals in recent hemipelagic sediments. Nature 303, 327-330.

Karlin, R., Levi, S. 1985. Geochemical and sedimentological control of the magnetic properties of hemipelagic sediments. Journal of Geophysical Research 90. 10373-10392.

Keith, B.D., 1988. Regional facies of the Upper Ordovician series of eastern North America. In: Keith, B.D. (Ed.), The Trenton Group (Upper Ordovician Series) of eastern North America: Deposition, Diagenesis, and Petroleum. American Association of Petroleum Geologists Studies in Geology, vol. 39, pp. 1– 16.

Kolata, D.R., Huff, W.M., and Bergström, S.M. 2001. The Ordovician Sebree Trough: An oceanic passage to the Midcontinent United States. GSA Bulletin, V. 113, p. 1067-1078

Kreisa, R.D., 1981a. Storm-generated sedimentary structures in subtidal marine facies with examples from the Middle and Upper Ordovician of southwestern Virgina. Journal of Sedimentary Petrology 51: 823-848.

Kreisa, R.D., 1981b. Origin of stratification in a Paleozoic epicontinental sea: the Cincinnatian Series. Geological Society of America Abstracts with Programs 13: 491.

Kreisa, R.D., Bambach, R.K., 1982. The Role of Storm Processes in Generating Shell Beds in Paleozoic Shelf Environments. In Einsele, G., Seilacher, A. (Eds.), Cyclic and Event Stratification. Springer-Verlag, Berlin, p. 200-207.

Miller, A.I., Holland, S.M., Dattilo, B.F., Meyer, D.L. 1997. Stratigraphic resolution and perceptions of cycle architecture: Variations in meter-scale cyclicity in the type Cincinnatian Series. Journal of Geology 105: 737–743.

Miller, A.I., Holland, S.M., Meyer, D.L., Dattilo, B.F., 2001. The use of faunal gradient analysis for intraregional correlation and assessment of changes in sea-floor topography in the type Cincinnatian. Journal Of Geology 109, 603-613.

Nickles, J.M., 1902. The Geology of Cincinnati, Journal of the Cincinnati Society of Natural History, V 20. No.2, Article 3.

Pope M.C., Read, F.J. Bambach R. and Hofmann, H.J., 1997. Late Middle to Late Ordovician seismites of Kentucky, southwest Ohio and Virginia: Sedimentary recorders of earthquakes in the Appalachian basin. Geological Society of America Bulletin 1997; 109; 489-503.

Quinland, G.M., Beaumont, C. 1984. Appalachian thrusting, lithospheric flexure, and the Paleozoic stratigraphy of the eastern interior of North America. Canadian Journal of Earth Sciences, v. 21, p. 973-996.

Sachs, S.D., Ellwood, B.B. 1988. Controls on magnetic grain-size variations and concentration in the Argentine Basin, South Atlantic Ocean. Deep-Sea Research V. 35. No. 6. p. 929-942.

Schramm, T.J., 2011. Sequence stratigraphy of the Late Ordovician (Katian), Maysvillian Stage of the Cincinnati Arch, Indiana, Kentucky, and Ohio, U.S.A., Department of Geology. University of Cincinnati, Cincinnati, Ohio, p. 215

Schramm, T.J., Brett, C.E., Dattilo, B.F., Ellwood, B.B. 2012. Ordovician Strata of the Type North American Maysvillian Stage. *in* Brett, C.E., Cramer, B.D., and Gerkie, T.L. (*eds*) Middle Paleozoic Sequence Stratigraphy and Paleontology of the Cincinnati Arch: Part 1 Central Kentucky and Southern Ohio. International Geoscience Programme (IGCP) Project 591 Fieldtrip Guidebook. p. 113-119.

Schramm, T.J., Brett, C.E., Dattilo, B.F. 2012. Stop 1. Rte. 11 Roadcuts, Maysville Kentucky: The Type Maysvillian. *in* Brett, C.E., Cramer, B.D., and Gerkie, T.L. (*eds*) Middle Paleozoic Sequence Stratigraphy and Paleontology of the Cincinnati Arch: Part 1 Central Kentucky and Southern Ohio. International Geoscience Programme (IGCP) Project 591 Fieldtrip Guidebook. p. 126-139.

Tobin, R.C., 1982. A model for cyclic deposition in the Cincinnatian Series of southwestern Ohio, northern Kentucky, and southeastern Indiana. University of Cincinnati, Cincinnati, Ohio, p. 483.

Vail, P.R., Audemard, F., Bowman, S.A., Eisner, P.N., Perez-Cruz, C. 1991. The stratigraphic signatures of tectonics, eustasy and sedimentology-an overview. *In* Einsele, G., Ricken, W., and Seilacher, A., eds. Cycles and Events in Stratigraphy. Springer-Verlag, p. 617-659.

Vogel, K., Brett, C.E., 2009. Record of microendoliths in different facies of the Upper Ordovician in the Cincinnati Arch region USA: The early history of light-related microendolithic zonation. Palaeogeography, Palaeoclimatology, Palaeoecology 281, 1-24.

Webber, A.J., 2002. High-resolution faunal gradient analysis and an assessment of the causes of meter-scale cyclicity in the type cincinnatian series (Upper Ordovician). Palaios 17, 545-555.

Weedon, G.P., Jenkyns, H.C., 1999. Cyclostratigraphy and the Early Jurassic time scale: data from the Belemnite Marls, Dorset, southern England. Bull. Geol. Soc. Am., 111, 1823-1840.

Weir, G.W., W.L. Peterson, and Swadley, W.C. 1984, Lithostratigraphy of Upper Ordovician strata exposed in Kentucky. U.S. Geological Survey Professional Paper 1151-E.

Whalen, M.T., Day, J.E. 2010. Cross-basin variations in magnetic susceptibility influenced by changing sea level, paleogeography, and paleoclimate: Upper Devonian, Western Canada sedimentary basin. Journal of Sedimentary Research. V. 80, 1109-1127.

CHAPTER 2
MAGNETIC SUSCEPTIBILITY - BASED DISSOCIATION OF SANDBIAN-KATIAN BOUNDARY STRATA IN EASTERN NORTH AMERICA: A CONUNDRUM

ABSTRACT

An investigation of the newly defined Sandbian-Katian boundary has been conducted across Eastern North America. Magnetic susceptibility integrated in a sequence stratigraphic context has been used to in an attempt to correlate this boundary. Areas of investigation include, the New York Trenton Platform; Kentucky Jessamine Dome; Virginia Taconic Foreland Basin; Oklahoma, Arbuckle Mountains, and Oklahoma Ouachita Mountains. Due to a series of unconformities, biostratigraphic enigmas, and chemostratigraphic correlation discrepancies it has not been possible to establish a correlation of a precise datum necessary to compare equivalent magnetic susceptibility profiles, and thus pinpoint the Sandbian-Katian boundary in stratigraphic sections other than the GSSP. High resolution correlation within K-bentonite bearing strata of the Black River Group, however, has been possible due to magnetic susceptibility based investigations, including the recognition of minor un-named ashes. Hypotheses concerning lithostratigraphic, and sequence stratigraphic correlation of lower Chatfieldian (Trentonian) strata are presented here. The leading hypothesis is that Logana-Napanee strata represent a correlative widespread deepening. This event is also associated with graptolitic wackestones of the lower Viola Springs Formation, and graptolitc mudstones of the upper Womble Shale. An alternative hypothesis exists that Watertown Formation may represent a shelf perched systems tract, and more time may be absent at the M4-M5 boundary. Due to biostratigraphic discrepancies within this interval it has not been possible to precisely resolve Sandbian-Katian boundary placement across North America. These represent long standing problems within

Ordovician stratigraphy, and when applying new abiotic correlation techniques dependent upon biostratigraphic correlation it is not fully possible to exploit the use of these non-biostratiraphic methods.

INTRODUCTION

Precise physical correlation of North American (Orodovician) Turinian-Chatfieldian Stage strata within the widespread Black River-Trenton Group interval remains controversial. K-bentonites provide a powerful correlation tool. However, their application is limited by spatial distribution of ash falls, or absence via unconformities in some localities (Kolata *et al*., 2001). Those that have proven most useful are the "Big Bentonites" (Deicke and Millbrig) within the Black River Group, but application is more limited within Trenton Group strata (Kolata *et al.,* 1996). Moreover, some K-bentonite correlations remain speculative, and lack geochemical evidence.

A widespread unconformity, the M4-M5 sequence boundary of Holland and Patzkowsky (1996, etc.) - provides a useful marker to divide Black River and Trenton Group strata, but widespread erosion associated with this surface also may have removed critical portions of the record in many localities, obscuring internal correlations. Biostratigraphic correlation is limited by poor temporal resolution, provinciality of key taxa, facies limitations owing to paleoecological preference, and an absence of key taxa, especially graptolites, in most facies (Finney 2005; Störch pers comm. 2012). $\delta^{13}C$ isotopic excursions have been used to constrain lower Trenton sequences, yet the precise internal physical subdivisions of these strata remain ambiguous (Young *et al*., 2005).

As a result of these problems, precise physical placement of the recently defined Sandbian-Katian boundary is problematic within all North American sections, with the exception of the Katian Global Boundary Stratotype Section and Point (GSSP) at Blackknob Ridge, Oklahoma (Goldman *et al*., 2007). Graptolites used to define the boundary are not commonly found in carbonate platform successions typical of much of North America at this time (Finney *et* al., 2005). Provincialism of conodont faunas further hinders correlation across North America (Sweet, 1984). In order to meaningfully apply global stage boundaries to classic North American successions, high-resolution regional correlation of Late Ordovician strata is required. Magnetic susceptibility (χ) of strata provides a potential non-biostratigraphic, lithology/facies independent, correlation tool.

Integration of outcrop-based sequence stratigraphic interpretations, high-resolution χ, biostratigraphy, and geochemical datasets into a temporal framework may permit evaluation of critical issues in Earth history. However, in order to address these issues, correlation of the Sandbian-Katian boundary from the GSSP into classic North American Ordovician successions in the Midwest and New York State is necessary. Furthermore, correlation within lower Trentonian strata is required. Linking together lower Trenton strata of different regions permits investigation of critical issues such as the timing of the Taconian (Vermontian) tectonism, climatic change, and Ordovician biodiversification (Webby *et* al., 2004) in a temporal context, as well as precisely defining the position of the Sandbian-Katian boundary in North American sections other than the GSSP.

A magnetic susceptibility (χ) based investigation of strata spanning the Sandbian-Katian boundary in Eastern North America has not yielded a unique correlation solution for this interval. Factors associated with this include both widespread major unconformities in this

interval, and multiple small unrecognized discontinuities and diastems; discrepancies associated with correlation of minor ashes within lower Trenton strata; and correlations based upon curve-matching of $\delta^{13}C$ isotopic excursions have insufficient temporal resolution. The high resolution required for stage boundary correlation within the eastern North American Upper Ordovician Series is less than the level of biostratigraphic zonation, and thus remains controversial. A lack of correlatable datums between regions investigated within this study does not facilitate a unique correlation solution upon which χ profiles can be hung. While individual classic Upper Ordovician regions each have received a high degree of study, correlation among these disparate regions remains difficult.

BACKGROUND

Ordovician Timescale

A series of regional subdivisions of Ordovician Strata have resulted in a high degree of local stratigraphic resolution (Figure 2.1). However, global correlation of Ordovician strata remains problematic. Associated with this is the need to standardize use of the term, 'Upper Ordovician.' While, the British system (Fortey *et al*., 1995; 2000) has historically provided a standard for the Ordovician System, correlation of its series boundaries to those in North America and elsewhere is problematic, mainly as a result of provinciality of biostratigraphically significant faunas (Finney, 2005). Using British regional subdivisions, the base of the Upper Ordovician has recently been placed at the base of the Caradoc Series. The base of the Upper Ordovician had historically been placed at the base of the North American Cincinnatian Series (Newbury, 1873; Sweet and Bergström, 1971). Thus, the newly proposed definition lowers the Middle-Upper Ordovician boundary by nearly 7 million years (Figure 2.1). The base of the

Upper Ordovician Series as approved by the ISOS (Webbey, 1998), has been placed at the base of the *Nemagraptus gracilis* Biozone, based upon graptolite work of Finney (1986). To allow a standard for which geologists globally can communicate using equivalent terms, the Upper Ordovician Series, Sandbian Stage GSSP was proposed by Bergström *et al*., (2000) and ratified in 2005; this led to the development of a new Ordovician Timescale (Finney, 2005). The Upper Ordovician Series is divided into three Global Stages, these being the Sandbian, Katian, and Hirnantian Stages (Bergström *et al.*, 2006a). North American, Mohawkian Series strata, formerly considered Middle Ordovician now belong to the Upper Ordovician Global Series and the Sandbian Stage, leading to discrepancies when applying new changes to the Ordovician timescale to previous literature.

Sandbian-Katian Boundary

The GSSP marking the base of the Katian Stage was proposed at Black Knob Ridge, Oklahoma (Finney, 2005), and later ratified in 2006 (Bergström *et al*., 2006a). The stage boundary is placed at the FAD of the graptolite *Diplacanthograptus caudatus*, and occurs 4 meters above the base of the Big Fork Chert (Goldman *et al*., 2007). While many sections spanning this boundary exist across North America, FAD occurrences of *D. caudatus*, which is constant with respect to a succession of first appearance of graptolite taxa, are limited to one or two other sections globally. "Correlation of Upper Ordovician strata above the *Climacograputs bicornis* Zone is one of the longstanding problems in Ordovician graptolite biostratigraphy" (Goldman *et al*., 2007). Thus, identification of the approximate position of the boundary based on non-biostratigraphic criteria, or abiotic methods, is necessary in most localities. Bedded chert and mudstone facies occurring at the GSSP are unlike the carbonate platform deposits typical of much of North America, and yield graptolites not typically found in these shallow facies.

Conodont and chitinozoan biostratigraphy of the GSSP section also does not permit precise correlation across North America. A series of K-bentonites have been found in the GSSP section; however, geochemical analysis has not, as yet, allowed positive correlation to other widely studied ash beds in eastern North America (Leslie *et al*., 2008).

North American Ordovician Timescale

A change from using British Series (Fortey, 2000) as the Ordovician standard to the new Ordovician Timescale (Finney, 2005), has resulted in increased stratigraphic resolution by increasing from two, to now three (global) stages within the Upper Ordovician Series (Figure 2.1). This level of stratigraphic resolution, however, is still low in comparison to other

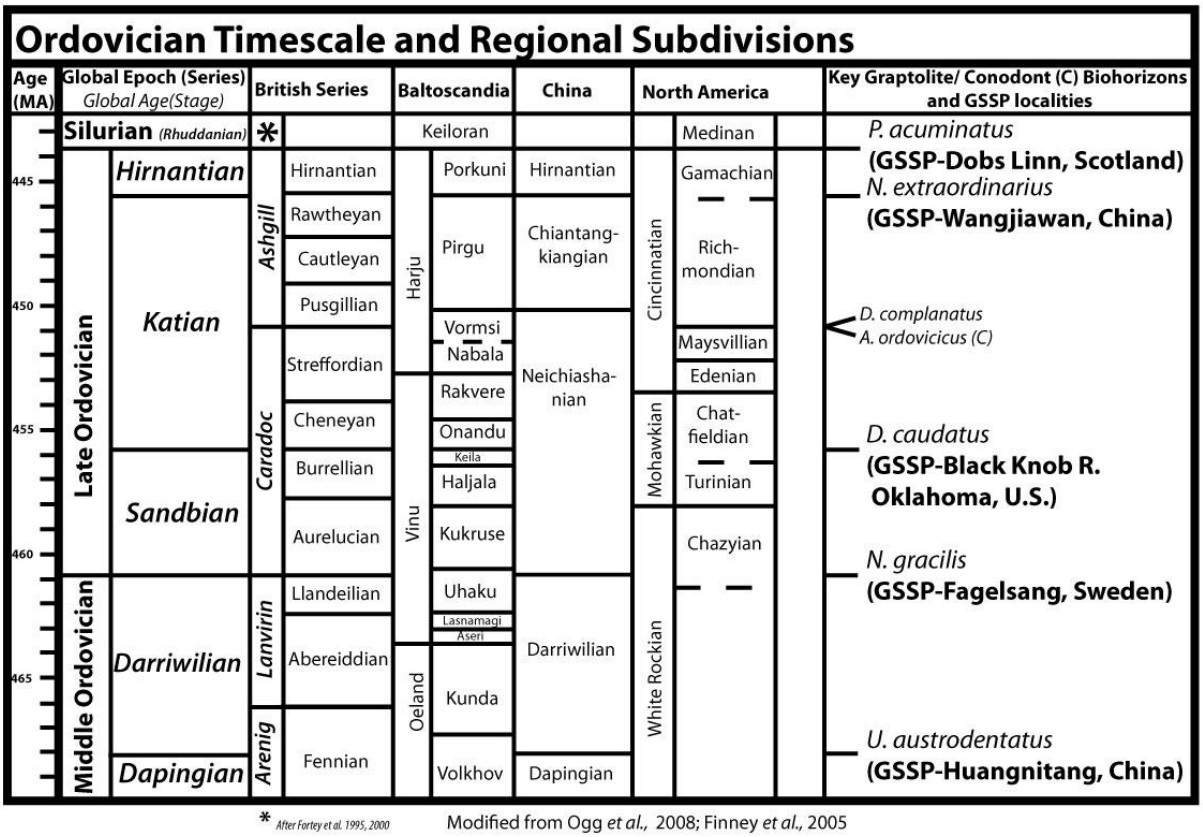

Figure 2.1 Ordovician Timescale showing global and regional subdivisions including series and stages. Modified from Ogg *et al*., 2008

geological systems, such as the Silurian. As a result, classic North American (NA) series and stages may be used to facilitate higher temporal precision when correlating classic sequences. The Upper Ordovician Series, as presently defined, contains portions of the NA upper Whiterockian, Mohawkian, and Cincinnatian Series. The basal Sandbian Stage includes strata formerly assigned to the NA Chazyan and subsequent to the Whiterockian, in part, and Mohawkian Series, in northeastern New York based upon conodont correlations (Hall *et al*., 1986). The type NA Mohawkian Series, defined in the Mohawk Valley region of New York State occurs at the base of the Black River Group and also contains the Trenton Group. Multiple systems exist for dividing Mohawkian strata into stages, a recent one divides (older) Turinian Stage strata (most of the Black River Group) from the younger Chatfieldian Stage with the boundary placed at the the Millbrig K-Bentonite. Problems associated with a definition that is based upon an ashfall include its absence, or truncation via unconformities in some localities. The Chatfieldian interval was previously subdivided into a different set of stages in the New York-Ontario Mohawkian type-area. Here the Rocklandian, Kirkfieldian, and Shermanian Stages were named from former formations, which were later upgraded to stages (Kay, 1968). These stages were based upon brachiopods, echinoderms, and ash beds and their application is spatially limited. The global Sandbian-Katian boundary occurs within the lower Chatfieldian Stage, and lies near the former Rocklandian-Kirkfieldian boundary.

The NA Cincinnatian Series comprises strata that overlie the Trenton Group, and is further subdivided into four NA Stages: the Edenian, Maysvillian, Richmondian, and Gamachian. The lower three stages were named for exposures on the Cincinnati Arch, while the Gamachian (Schuchert and Twenhofel, 1910) consists of the remaining Ordovician strata not found in the Richmond type area. The Gamachian Stage is approximately coincident with the

Hirnatian Global Stage (Chen, 2006), and named for strata in the Ellis Bay region of Anticosti Island, Canada.

The current study is largely restricted to the Sandbian-Katian boundary interval, and an attempt to establish these international units in eastern North America. However, application of NA Ordovician subdivisions may provide increased stratigraphic resolution, and thus their boundaries are also considered herein (Figure 2.1). These data should be incorporated in new timescale developments.

Regions Studied

A multitude of outcrops spanning the Sandbian-Katian boundary interval exist within North America, but only well studied outcrops in regions containing historically recognized Ordovician exposures have been sampled for the purposes of this study. Four disparate regions representing classic Upper Ordovician successions, compose the study area for this research. These include a) the New York Mohawk Valley Trenton Group, b) the Kentucky Jessamine Dome Lexington Limestone, c) the Taconic Foreland Basin, and d) the Oklahoma Ouachita and Arbuckle uplifts (Figure 2.2).

New York Trenton

Classically studied Upper Ordovician stratigraphic successions in New York's Mohawk Valley compose the North American standard Mohawkian Series, consisting of the widespread Black River and Trenton Groups (Figure 2.1). These units were formerly regarded as Middle Ordovician, but due to recent changes in the Ordovician Timescale (Finney, 2005) are now assigned to the Upper Ordovician Series. Black River Group fenestral micrites are overlain by fossiliferous, phosphatic pack-grainstones of the Trenton Group.

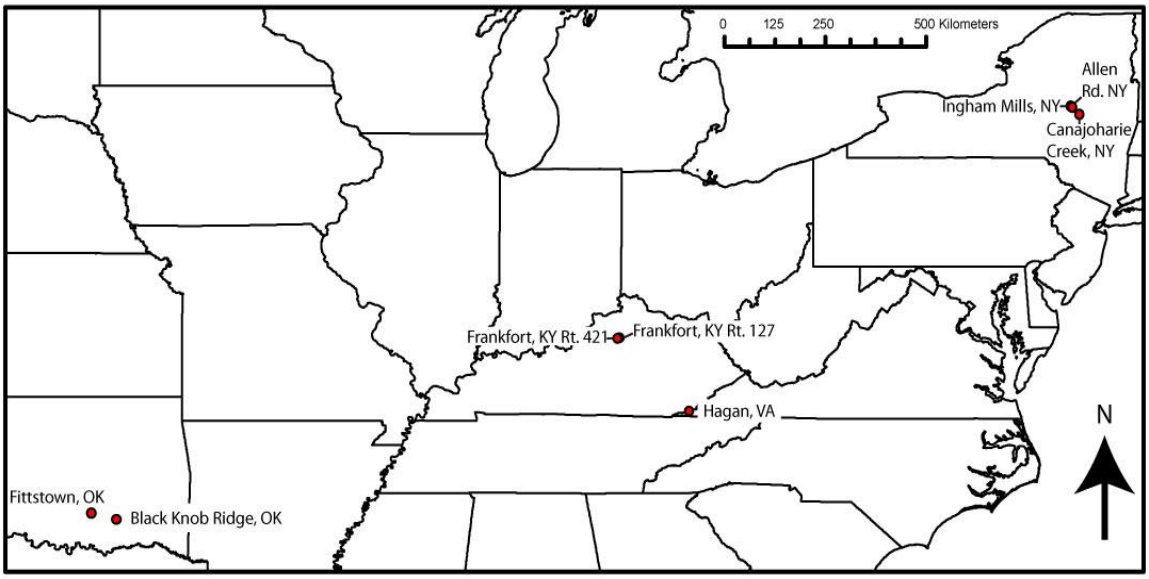

Figure 2.2 Map of Sandbian-Katian Stage boundary interval outcrop localities. Eastern United States.

These limestones deposited on the Trenton Platform are laterally equivalent to deeper, shale-rich basinal sediments of the Utica Formation Flat Creek Member (Goldman et al., 1994), and the onlap of Utica shales onto Trenton carbonates is diachronous. Establishing high resolution correlations between adjacent units with ample stratigraphic exposure remains difficult (Baird and Brett, 2002). Furthermore, a series of fault-blocks result in local facies variations within Trenton strata (Hay and Cisne, 1988; Jacobi and Mitchell, 2002). However, this is the standard to which all North American "Mohawkian" age units are compared.

Originally named by Vanuxem (1838), the Trenton Group has received a high degree of study with many of the formations and stages, named and correlated into Ontario by Marshall Kay (1931; 1937; 1943; 1968). This name was used as a time-rock unit by Dana (1862), and is used widely to designate strata of equivalent age in eastern North America, especially within the subsurface. The type-locality of this unit at Trenton Falls is currently inaccessible, further complicating incorporation of previous works into current research.

The lower Trenton strata are classically subdivided into the Selby, Napanee, Kings Falls, and Sugar River formations (Kay 1937; 1931; 1968), and include the units within the current study. The overlying Denley Formation (Kay 1943; 1968; Brett and Baird, 2002) and its members, Poland, and Russia, are largely above the Sandbian-Katian boundary study interval. In much of northwestern New York State the Trenton Group is underlain by massive, bioturbated mollusk rich carbonates of the Watertown Formation, traditionally assigned to the Black River Group. Due to widespread truncation at its base, Cornell and Brett (2000) and Brett *et al* (2004) assigned the Watertown Formation to the same depositional sequence as the Trenton Limestone, thus they postulated that these units are genetically related.

Kentucky Lexington

The Lexington Platform occupying the Jessamine Dome, represents a paleotopographic high upon which shallow marine carbonates were deposited during the Sandbian and Katian Stages. Shallow marine dolomitic and fenestral carbonates of the High Bridge Group, Tyrone Formation (Miller, 1905) represents Black River Formation equivalent strata. These outcrops are largely restricted to the Kentucky River Valley (Cressman and Noger, 1976). The Lexington Limestone (Campbell, 1898) occupying the Inner Bluegrass region of Kentucky overlies the Tyrone Formation Excellent exposures of this unit are common on roadcuts in the Lexington-Frankfort capital region (McLaughlin, *et al*., 2008). The Lexington Limestone is largely composed of phosphatic, skeletal pack-grainstones (Cressman, 1973) and is associated with general tectonic quiescence within the midcontinent.

Appalachian Basin

The peripheral foreland basin associated with the Taconic Orogeny is sometimesreferred to as the Taconic foreland basin, or in some cases Martinsburg foreland basin. The basin is filled with flysch sediment, largely shales, from the Taconic hinterland, the basin is largely filled with shales. The Martinsburg Formation spanning from New York through Tennessee occupies hundreds of meters thickness, or more. The Martinsburg Formation in Pennsylvania to West Virginia has been divided into three members: Bushkill, Ramseyburg, and Penn Argyl, approximately equivalent to the Chatfieldian (Trenton,) Edenian (Kope-Utica formations.), and lower Maysvillian (Fairview Formation), respectively (Drake and Epstein 1967). Shallow water equivalents include shell rich siltstones and sandstones, of the Reedsville Formation in Pennsylvania. Progradation of the Queenston delta is also recorded in the transition from the Martinsburg to Juniata Formations. Crustal shortening in this region, both syndepositional, and from later Appalachian mountain building, results in a series of different thrust-sheets through this region: facies found on different thrust sheets may vary.

Samples taken from the Hagan, Virginia. locality are from the Eggleston (Black River equivilent) strata, which are overlain by carbonate grainstones referred to as Trenton. In places this Eggleston interval, containing large K-bentonites overlies, the Moccasin Formation, which represents deltaic clastics and red-beds from the Blountian Tectophase. Elsewhere, the Moccasin Formation includes these same large K-bentonite beds (Brett pers comm. 2012).

Oklahoma Ordovician

Ordovician strata in Oklahoma have been studied for more than 100 years (Ulrich, 1911). Exposures occur in two general regions, the Arbuckle and Ouachita mountains. Strata of the

Ouachita mountians are allochthonous and represent basinal sediments thrust into their present position during the Carboniferous Ouachita Orogeny. Ordovician strata of the Arbuckle Mountains represent autochthonous carbonate platform deposits, containing the Bromide and Viola Spring Formations (Amsden and Sweet, 1983). Conversely, the stratigraphy of the nearby Ouachitas preserves deep basinal sediment of the Womble Shale and Big Fork Chert (Finney, 1986). Furthermore, these regions contain highly refined graptolite zonations (Decker, 1933; Finney, 1986; Goldman *et al*., 2007; and others). Most importantly this represents one of the few regions in which graptolites are found within carbonate strata, allowing the comparison of shelf and basinal successions. Diverse conodont faunas contain both North Atlantic and Midcontinental Faunal Province elements and are used as part of Sweet's graphically correlated sections (Sweet, 1983, 1984, 1985). Possible K-bentonites have been recognized in the Oklahoma study area (Decker, 1933; Goldman *et al.*, 2007; Leslie *et al.*, 2008) and may eventually allow correlation to other North American Ordovician ashes (Kolata *et al*., 1996; Sell, 2010).

Taconic Orogeny

Ordovician tectonism may be associated with a change from widespread carbonate bank facies to more diverse platform and basinal facies due to crustal downwarping. The Taconic Orogeny, driving the collision of the Taconic Island Arc with Laurentia, resulted in the formation high mountains in eastern North America and a peripheral foreland basin (Quinland and Beaumont, 1984; Ettensohn, 1991). A deep basin (foredeep) associated with this mountain building event was filled by siliciclastic sediments derived from the advancing Taconic Mountains. A decline in Laurentian tectonism during the middle-late Katian Stage (Maysvillian-Richmondian NA Stages; Figure 2.1), and high erosion rates associated with monsoonal

climates, resulted in the overfilling of the Taconic Foreland Basin, caused by progradation of nonmarine clastic sediments of the Queenston Delta.

The Taconic Orogeny occurred in two phases, the earlier Blountian tectophase was coincident with the Darriwilian-Sandbian stage boundary and associated with deposition of the Athens Shale and coarse clastics of the overlying Sevier-Tellico formations. The onset of tectonism was diachronous and was largely restricted to the Southern Appalachian region (Grubb and Finney, 1995; Finney *et al*., 1996). The younger Vermontian tectophase occurred throughout the central and northern Appalachian area began in late Turinian Time and continued through Chatfieldian and Edenian time. Deposition of basinal sediments during the Vermontian tectophase occurred diachronously throughout the Taconic Foreland Basin.

GICE

The use of carbon isotopes in stratigraphic successions provides an additional abiotic tool for widespread correlation of strata. Since the discovery of a carbon isotopic excursion in the Guttenburg Member of the Decorah Formation, Iowa (Hatch *et al.*, 1987), chemostratigraphic research in the Upper Ordovician has been ongoing (Ludvigson *et al.,* 2004; Saltzman *et al.*, 2003; Ainssar *et al.*, 2004; Young *et al.*, 2005; 2008; etc.). This first $\delta^{13}C$ excursion has been named the Guttenberg Carbon Isotope Excursion (GICE), and a later $\delta^{13}C$ excursion in the Hirnantian Stage has been termed the Hirnantian Carbon Isotope Excursion (HICE) (Saltzman and Young, 2005; Bergström *et al.*, 2006b; 2011; etc.). The GICE occurs approximately coincident with the Sandbian-Katian Stage boundary, within the North American, Chatfeldian Stage (Figure 2.1). In North America widespread bentonites (Deicke and Millbrig) occur

directly below the GICE providing dated, and instantaneously deposited marker horizonss throughout eastern North America (Bergström *et al.,* 2004; Kolata *et al.,* 1996; etc.).

While the GICE has been used for bracketing the Sandbian-Katian boundary interval (Young *et al.,* 2008), it has not been used to precisely locate the boundary in sections other than the GSSP. This is largely a result of the use of conodont biostratigraphy to locate the GICE interval in shallow carbonate facies. The low resolution of conodont-based correlation does not permit precise boundary identification (Goldman, pers comm. 2014). Curve matching of $\delta^{13}C$ excursions may not represent the GICE and instead could represent Kope, or Waynesville excursions (Bergström *et* al., 2010) in strata without adequate biostratigraphic/temporal resolution.

K-Bentonites

A series of bentonite beds in the Black River Group, and equivalent strata are spatially widespread across eastern North America. These K-bentonites, particularly the Deicke and Millbrig, have been located in a number of regions, and have been extensively researched (Haynes, 1994; Kolata *et al*., 1996), and represent some of the largest recorded ashes worldwide (Bergström *et al*., 2004). While these 'big' bentonites are commonly used for correlation, the surfaces on which they are deposited commonly show indications of hiatuses, such as hardgrounds, intense burrowing or phosphatic clasts, and are referred to as "Drowning Unconformites" by Kolata *et al*. (2001). They thus may represent time condensed horizons in which these ash beds are concentrated by default during periods of sediment starvation. A series of other large ash beds, the Ocoonita and Hockett are found below the Deicke K-bentonite, and likely are deposited on the same type of stratigraphic surfaces: they typically have a similar

spacing to the distance between the Deicke and Millbrig K-bentonites. Such deposits may be confused for one another in the field if not carefully studied. Thinner and other regionally less persistent ashes have not received the same level of research, and are typically un-named. The presence of these ashes beneath the M4/M5 sequence boundary limits the correlation potential of these ashes because it is not possible to extend datasets above this sequence boundary, as the amount time missing is unknown.

Smaller un-named K-bentonites in the Black River Group and other small ashes in the Trenton Group require further research if they are to be used as effective correlation tools. Specifically, the identification of the Dickeyville K-bentonite could be used to bracket the Sandbian-Katian boundary interval, but it is presently limited to the Mississippi Valley (Kolata *et al*., 1998). Sell (2010) attempts to correlate many Chatfieldian K-bentonites, but several are located much higher stratigraphically than the boundary interval.

Sell (2010) correlated a series of Upper Ordovician ashes across eastern North America and supports the finding of Mitchell *et al*., (2004), Several, of these ashes, however, are well above Sandbian-Katian boundary interval, and correlations of many of the ashes recognized in the current study were not attempted. The Sell (2010) paper supports the findings here that poor biostratigraphic resolution and a series of internal unconformities obfuscate long distance correlation. His findings that ashes within the Womble Shale at Black Knob Ridge are not the Deicke and Millbrig K-bentonites also support the findings presented here. Based upon lithologic evidence of these ash beds, here it is suggested that the ash beds at Black Knob Ridge are the same as Decker's clay bed (1933), found at the Fittstown locality, and represent small ashes within lower Trenton Strata.

METHODS

Five stratigraphic successions within the Sandbian-Katian boundary interval have been sampled across eastern North America. These include localities at Ingham Mills New York, Frankfort Kentucky, Hagan Virginia, Fittstown Oklahoma, and Black Knob Ridge Oklahoma (Figure 2.2). Samples through vertical successions were collected at high resolution, 5cm for all but the Lexington Limestone strata outside of the Sandbian-Katian boundary interval collected at a 10 cm interval. Outcrops were meticulously cleaned to reduce sample contamination, and the lithology was measured at a cm scale. Samples were broken into approximately pebble-sized pieces to reduce anisotropy, and approximately 10 grams of sample were measured for χ in the Williams Magnetic Susceptibility bridge at LSU, a balanced-coil induction system. The bridge is calibrated relative to mass (Ellwood *et al*., 1999). The mean of three sample measurements was used for determining χ of the measured sample. A total of 2,241 samples were collected and measured for this study. (See chapter one for further background on χ).

χ values for samples are plotted relative to their stratigraphic position, and data points are indicated with a small circle and connected by a fine or dashed line. These data have been smoothed using splines typically shown in blue (Ellwood *et al*., 1999).

Stratigraphy of Localities Sampled

Ingham Mills, New York

Outcrops at Ingham Mills, New York along East Canada Creek expose Beekmantown, Black River, and Trenton age strata (Figure 2.3). In many classic Trenton localities lower Trenton strata are not exposed. Strata of the Selby and Napanee formations are absent or cut out

at many Mohawk Valley locations; however, due to increasing proximity to the sediment source and thus, basin center, these units occur at Ingham Mills. These horizons are overlain by the Kings Falls and Sugar River formations. A series of 287 samples have been collected through the Lowville, Watertown, Selby, Napanee, Kings Falls, and Sugar River interval. These strata are exposed below the base of a dam of a hydro-electric power plant, and thus access is limited.

Additional exposures along Schnell/Allen Road in the nearby town of Oppenheim, New York allow the creation of a composite section based upon the recognition of a prominent marker horizon in the Sugar River Formation. Originally sections continued along East Canada Creek through the base of the Dolgeville Formation and Utica (Indian Castle) Shale, and were formerly recognized by Cushing (1909) along the then undammed creek. These are now under water. An erosional unconformity between the Lowville and Watertown formations was recognized as the M4-M5 sequence boundary (Holland and Patzkowsky, 1996), by Cornell (2008) and Brett *et al*., (2004). The overlying Selby Formation has traditionally been regarded as the base of the Trenton Group. While this unit is absent throughout much of the Mohawk Valley, a thin remnant, including a mineralized and burrowed top is present at Ingham Mills. A nearly complete section of the Napanee Formation is present here and is composed of dark brown calcareous shales interbedded with calcilutites and marls, in addition to the presence of the brachiopod *Triplecia* and a diverse trilobite fauna. The M5A-M5B sequence boundary is found at the base of the overlying Kings Falls Formation (Brett *et al*., 2004). This calcareous grainstone unit contains large, cobble to boulder sized gneiss and granite clasts at its base, indicating a major interval of uplift and erosion during a period of sea level lowstand.

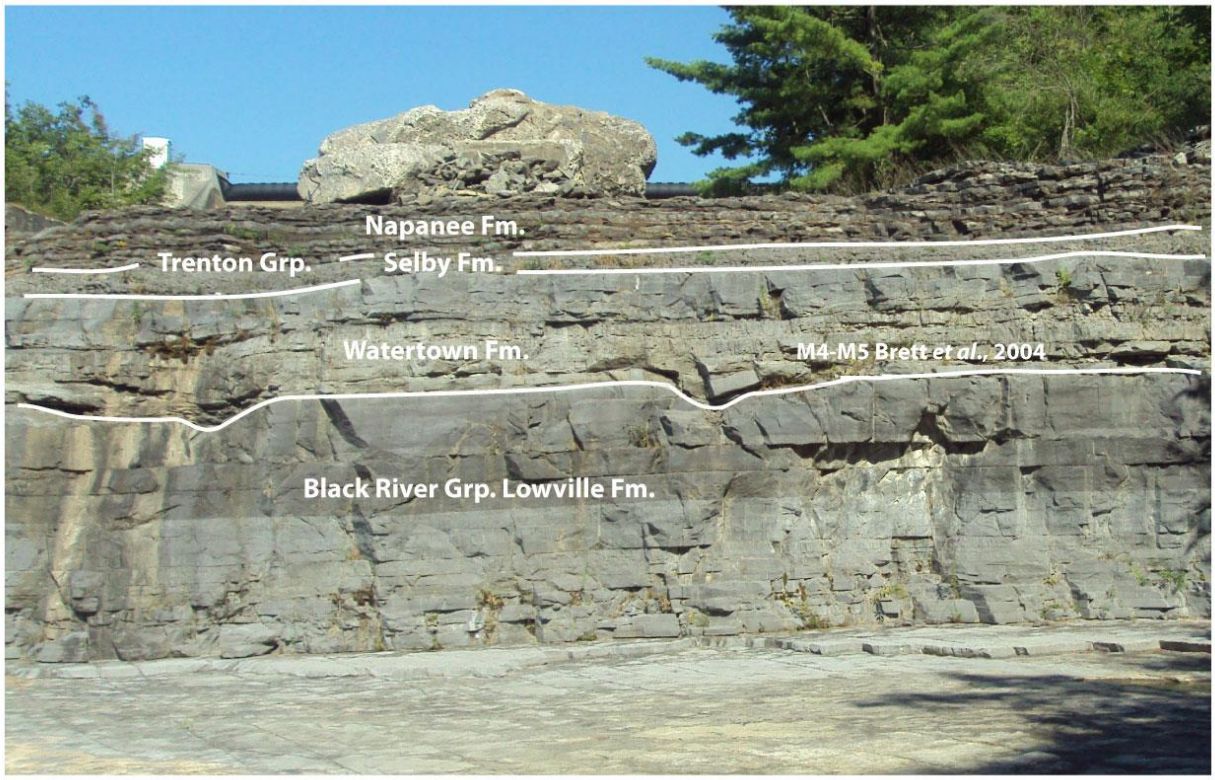

Figure 2.3 Outcrop photo of Black River and lower Trenton Group strata at Ingham Mills, New York.

Another depositional hiatus, probably associated with a flooding surface, is present at the top of the Kings Falls Formation at the contact with the overlying Sugar River Formation. This unit consists largely of compact, wavy pack- and grainstones interbedded with thin shales and thick grainstone ledges, typically with very abundant *Prasopora* bryozoan colonies.

Frankfort, Kentucky

Excellently preserved exposures of Upper Ordovician strata are present in Frankfort, Kentucky (Figure 2.4), the state capital city. Outcrops along Rt. 127 compose a significant portion of a continuous section through the upper Tyrone Formation and Lexington Limestone (Cressman, 1973; Cressman and Noger; 1976). This composite section begins at the base of the nearby Cove Springs Quarry in the upper Tyrone Formation, extending through the Deicke K-

bentonite and up to an unnamed middle bentonite. This unnamed bentonite has been traced approximately 150 meters away to a large roadcut along Rt. 127. About 1 meter above this bed is the unconformable basal contact of the Lexington Limestone on the Tyrone Fm, representing the M4/M5 sequence boundary of Holland and Patzkowsky (1996). The Millbrig K-bentonite is absent at this locality, where it was erosionally removed at the sequence boundary, although it is present in nearby localities such as Shakerton, Kentucky (Kolata *et al*., 1996).

The outcrop of Lexington Limestone begins at the base of the Curdsville Member, and is composed of compact echinoderm grainstones. A faunal epibole of rare *Cryptolithus* trilobites is found here. The Curdsville Member is a three-part unit composed of lower limestone, a middle shaly submember with deformed calcisiltites termed the Capitol metabentonite (submember), and a thinner upper limestone interval. An ash referred to as the Capitol K-bentonite (Conkin and Dasari, 1986) can sometimes be found within the middle shaly unit. The Curdsville Member is overlain by interbedded shales and marls of the Logana Member. The Logana Member too, is a three part unit but instead is composed of interbedded shales and marls, with thin shell beds packed with the brachiopod *Dalmanella*, and contains a middle compact grainstone unit. The Logana is sharply overlain by the Grier Member with basal ledge-forming beds composed of compact pack-grainstones: this contact represents the M5A-M5B sequence boundary (Brett *et al*., 2004). Wavy bedded, shaly packstones and thin grainstones of the lower Grier Member are overlain by the Macedonia Bed, a thin shale and calcisiltite rich interval closely resembling the Logana facies, and the grainstone dominated Perryville Member. The M6 sequence boundary was originally placed at the base of the Brannon Member., which, however, records a strong deepening or flooding surface.

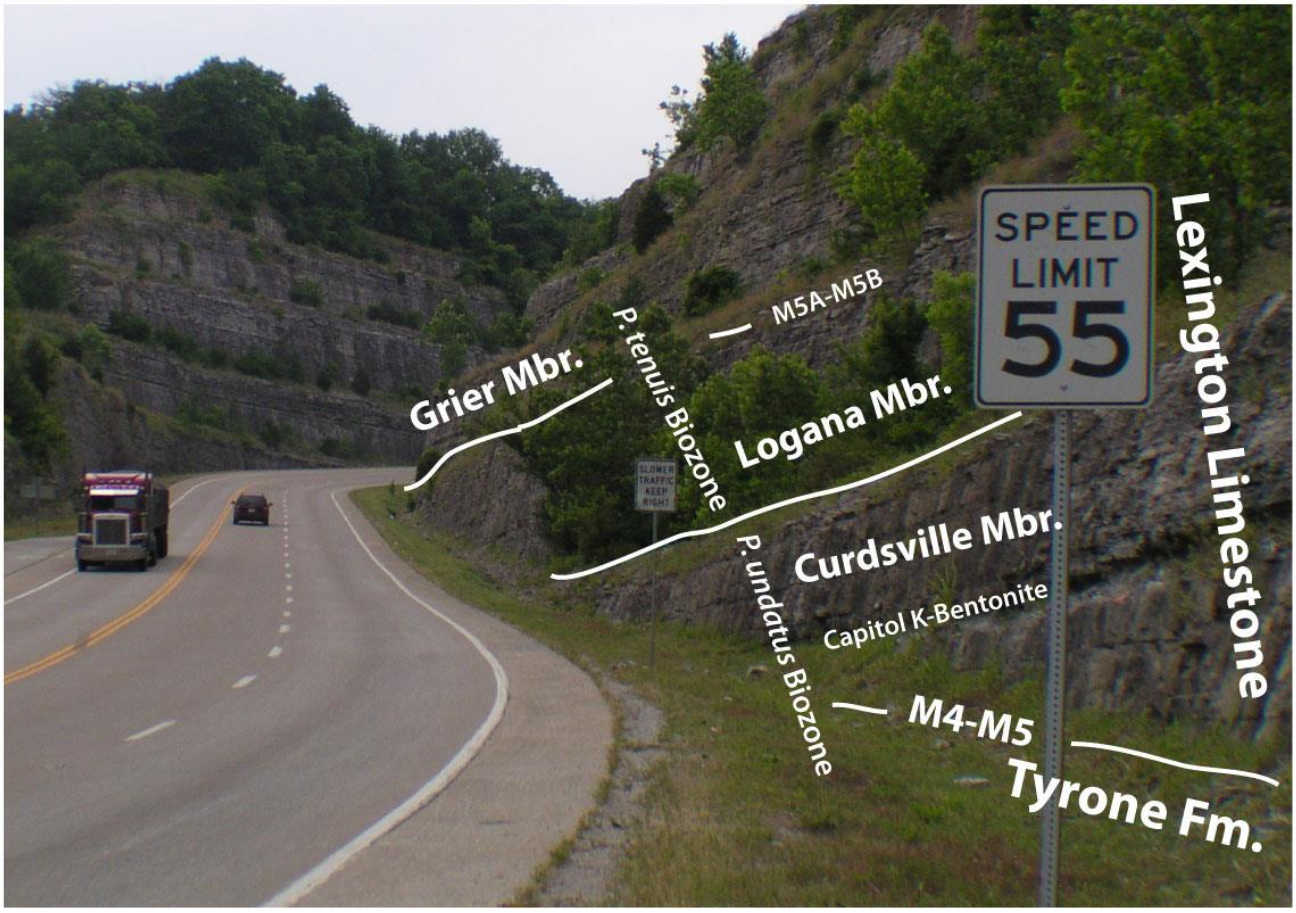

Figure 2.4 Outcrop photography of Frankfort, Kentucky roadcut along Rt. 127.

The Brannon Member comprises dark gray, sparsely fossiliferous shale and laminated calcicsiltite with spectacularly developed soft sediment deformed zones interpreted as seismites. The Brannon Member grades upward into thinly laminated phosphatic calcarenites (fine grained grainstones) referred to by informally McLaughlin et al. (2004) as the Donerail member, which is in turn, overlain unconformably by the commonly massive Sulphur Well Member grainstones and rudstones and more shaly, highly fossiliferous and commonly stromatoporoid-bearing Stamping Ground members. Samples have been collected through the basal Stamping Ground Member. A $\delta^{13}C$ profile for this outcrop through the Sandbian-Katian boundary interval

provides another abiotic correlation data set and makes this outcrop significant (Young *et al*., 2005).

Hagan, Virginia

A continuous exposure of Lower Ordovician through Devonian strata exists along a railroad switchback in Hagan, Virginia (Figure 2.5). Thick K-bentonites present at this locality have been traced throughout much of eastern North America and received considerable study (Kolata *et al*., 1996; 1998; Sell; 2010). The Sandbian-Katian boundary interval occurs within the upper Black River-equivalent Eggleston Formation or the immediately overlying lower Trenton Formation. Most importantly, sedimentation at this outcrop was fairly continuous, and Eggleston facies strata are found below and above the Millbrig K-bentonite here (Kolata *et al*., 2001). A series of 13 K-bentonites have been recognized in this area from nearby Rose Hill, VA (Miller and Brosge, 1954; Miller and Fuller, 1954). They have been designated with the letter "R", and have been correlated to other localities (Kolata *et al*., 1996; 1998).

The time-correlative Logana facies has been here termed Hermitage Member (of the lower Trenton Fm), a term extrapolated from the Nashville Dome (Huffman, 1945), and presumably includes the Sandbian-Katian boundary interval exposed here. A $\delta^{13}C$ profile has been measured through the Eggleston and Trenton formations for this succession (Young *et al*., 2005). Conodont studies of the outcrop did not reveal the precise level of the *P. undatus-P. tenuis* Zone boundary (Leslie, 1995; Bergström *et al*., 1988). Samples have been collected at this outcrop from the Deicke K-Bentonite upward to the base of the Trenton Formation. Due to limited access to this locality it was not possible to continue sampling the Sandbian-Katian boundary interval in the lower Trenton Formation.

Figure 2.5 Eggleston Formation outcrop along railroad switchback at Hagan, Virginia showing key K-bentonites and the M4-M5 boundary.

These samples do, however, occur in the interval of the Eggleston Formation with abundant K-bentonites and provide a control from which correlations of these known ashes can be made to other locations. A series of smaller un-named ash beds recognized in the Eggleston Formation, R8 and R9 (Miller and Fuller, 1954; Miller and Brosge, 1954), provide potentially powerful, high-resolution correlation tools. Furthermore, correlation of other large ashes, Hockett and Ocoonita, to the High Bridge Group of Kentucky may be possible (Kolata *et al*., 1998; Schramm; this study).

Above the base of the Trenton at Hagan Virginia, a pack to grainstone unit exists that occupies the position of the Curdsville Member of Kentucky. While this unit is somewhat thicker than its counterpart in Kentucky, the two bear a striking resemblance to one another. It is

suggested here that the Curdsville Member represents a condensed grainstone on the Nashville Dome, and the Hermitage above it, as in the same named unit in the Nashville Dome, is a Logana/Napanee equivalent. The base of this "Curdsville" unit represents the M4/M5 sequence boundary.

Black Knob Ridge, Oklahoma

Most sections spanning the Sandbian-Katian boundary in eastern North America are composed of platform carbonates. Conversely, sections in the Ouachita Mountains and the Martinsburg foreland basin are composed of basinal shales and thin cherts. The Sandbian-Katian boundary GSSP at Black Knob Ridge, Oklahoma (Figure 2.6) is composed of graptolitic shales and interbedded cherty mudstone deposits (Goldman, *et al*., 2007). The base of the Katian Stage is placed at the FAD occurrence of *Diplacanthograptus caudatus*, and occurs 4 meters above the base of the Big Fork Chert. This marks the *Climacograputs bicornis* Zone-*Diplacanthograptus caudatus* Zone boundary. Finney (1986) suggested that very little time is missing at the upper Womble Shale-Big Fork Chert contact and correlated this to the Bromide-Viola Springs Formation contact at nearby Fittstown, Oklahoma, which is recognized as the M4-M5 sequence boundary (Finney, 2005; Young *et al*., 2007). K-bentonites in the Womble Shale have been speculated to be the Deicke and Millbrig K-bentonites (Goldman *et al*., 2007; Leslie *et al*., 2008), however, this remains inconclusive, and these ash beds are not firmly correlated (Leslie *et al*., 2008; Sell, 2010). However, Sell et al., (2013) give ages of these bentonites (453.98 ± 0.33 and 453.16 ± 0.24 MA) permissive of their correlation with the Deicke and Millbrig, respectively.

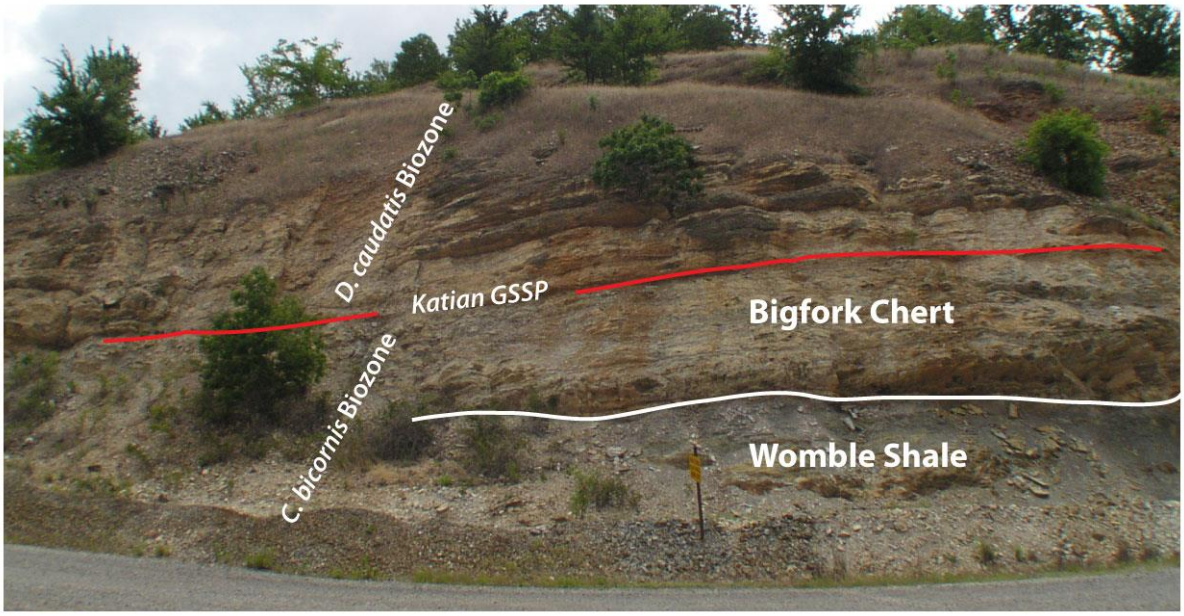

Figure 2.6 Outcrop photograph of Katian Stage GSSP at Black Knob Ridge, Atoka, Oklahoma showing lithostratigraphic units, and graptolite zones.

A positive $\delta^{13}C_{org}$ excursion exists within organic rich beds (high TOC) throughout the Sandbian-Katian boundary interval at Black Knob Ridge (Goldman *et al*., 2007). While this excursion may represent the GICE, direct comparison of $\delta^{13}C_{org}$ and $\delta^{13}C_{carbonate}$ are not possible. 270 samples have been collected from this outcrop at a 5cm sampling interval. The high TOC at this outcrop may be associated with biogenic gases moving through fractures within the system (Ellwood pers comm. 2012). Furthermore, coatings of the mineral jarosite are common from this location and may affect χ measurements.

Fittstown, Oklahoma

Outcrops along Rt. 99 in Fittstown, Oklahoma display stratigraphically complete and well-exposed sections of the Bromide and Viola Springs formations. This represents one of the most complete sections of the Bromide-Viola Springs contact, in which the lower Viola Springs wackestones contain *Climacograptus bicornis* Zone graptolites, typically not found in other

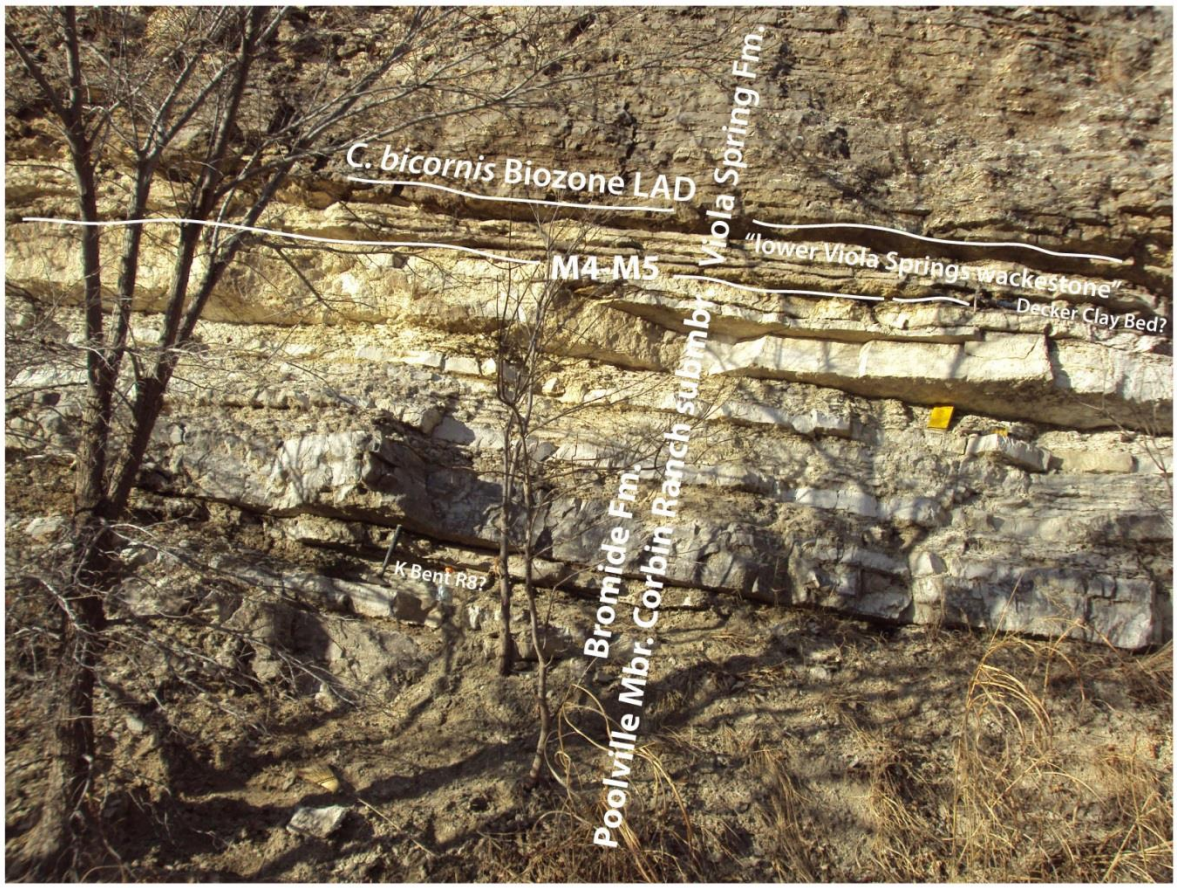

Figure 2.7 Outcrop photograph of the Bromide-Viola Springs Formation contact at Fittstown Oklahoma Rt. showing the *C. bicornis* last appearance datum, M4-M5 boundary, and possible R8 and 'Decker Clay Bed' K-Bentonites.

Viola Springs age sections. Thus, as the most nearby outcrop to Black Knob Ridge, this outcrop has been chosen as the auxialliary stratotype (Goldman *et al*., 2007).

Two prominent erosional recesses occur in the Bromide Formation at the Fittstown, Oklahoma outcrop have been confirmed as K-bentonites (Leslie *et al*., 2008); although, their correlation to other well known ash beds in Eastern North America remains uncertain. Geochemical analysis of these ashes provides insufficient evidence of their identification (Leslie *et al*., 2008). While, these beds occur within the same biozone as "Big-Bentonites" (Millbrig and Deicke), a positive identification has not been provided, although would be desired by stratigraphers. Based upon biostratigraphic correlations Young *et al*., (2008) suggest the

presence of the Deicke ash within this section based upon biostratigraphic correlations, which Rosenau *et al*., (2012), expands further upon claiming the presence of both the Deicke and Millbrig ash within this section. While seemingly insignificant, the repercussions of imprecise stratigraphic correlation within these intervals may diminish statements of geochemical correlation and events within this interval. These possible ash horizons occur within the *Climacograptus bicornis* Zone, and share an approximate stratigraphic age with the Deicke and Millbrig; however, their correlation remains speculative. Furthermore, in order to evaluate such events accurate correlation based upon a series of time-correlative horizons is required. Sell (2010) investigated the geochemistry of these ash horizons and does not suggest that they represent the Deicke and Millbrig K-bentonites. The present study recognizes these two erosional recesses as well as seven other possible ash beds in the Corbin Ranch Submember, and offers possible correlations of this interval.

Young *et al*., (2005) interpreted the Bromide-Viola Springs Formation contact as the M4-M5 boundary of Holland and Patzkowsky (1996). A $\delta^{13}C$ profile of this section provides another correlation tool, and shows a strong positive excursion, assumed to be the GICE, found high within this section. However, the correlation of this excursion to the GICE has been questioned (Westrop *et al.,* 2012). Instead, it may represent a later positive $\delta^{13}C$ excursion such as the Kope excursion (Bergström *et* al., 2010).

χ OBSERVATIONS

Ingham Mills, New York

A χ profile of the Sandbian-Katian boundary interval at Ingham Mills, N.Y. displays multiple levels of cyclicity (Figure 2.8). A series of high frequency cycles are present,

interpreted to represent Milankovich effects (Shakleton *et al*., 1999). Broader cycles indicated by the splined χ values, may represent long-term sea-level oscillations (Crick *et al*., 1997; Ellwood *et al*., 1999). Black River Group strata display higher χ values than the overlying Trenton Group. This change to lower χ values occurs at the Watertown-Selby formation contact, and at the Selby-Napanee formations contact. These prominent shifts in χ values provide further evidence for suspected unconformities at these surfaces. The Napanee Formation displays well-developed internal high-frequency cyclicity (Figure 2.8). An unconformity at the base of the Kings Falls Formation results in a slight offset to lower χ values, which rise slightly throughout the unit, whereas in the Sugar River Formation χ values gradually become lower.

Frankfort, Kentucky

Although taken through a continuous section without any biostratigraphic or physical evidence of unconformities, a series of large offsets in χ values are present in the Frankfort Kentucky, Lexington Limestone interval (Figure 2.9). The Tyrone Formation generally displays low χ values. A series of higher χ values within this interval are coincident with the position of K-bentonites within the section. While an unconformity is known to exist within this section, and the upper Tyrone Formation strata and the Millbrig K-bentonite are erosionally truncated at the base of the Lexington Limestone (Kolata *et al*., 1996), little offset in χ values is present. χ values in the Curdsville Member rise slightly, with the highest χ values occurring in the Capitol submember where the Capitol K-Bentonite is present. Values then decrease, returning to similar magnitudes as those found at the base of the Curdsville Member. While the Curdsville-Logana Member contact is somewhat gradational, there is a sharp offset to higher χ values at this contact, which generally represents a flooding surface. The Logana Member displays well developed internal cycles.

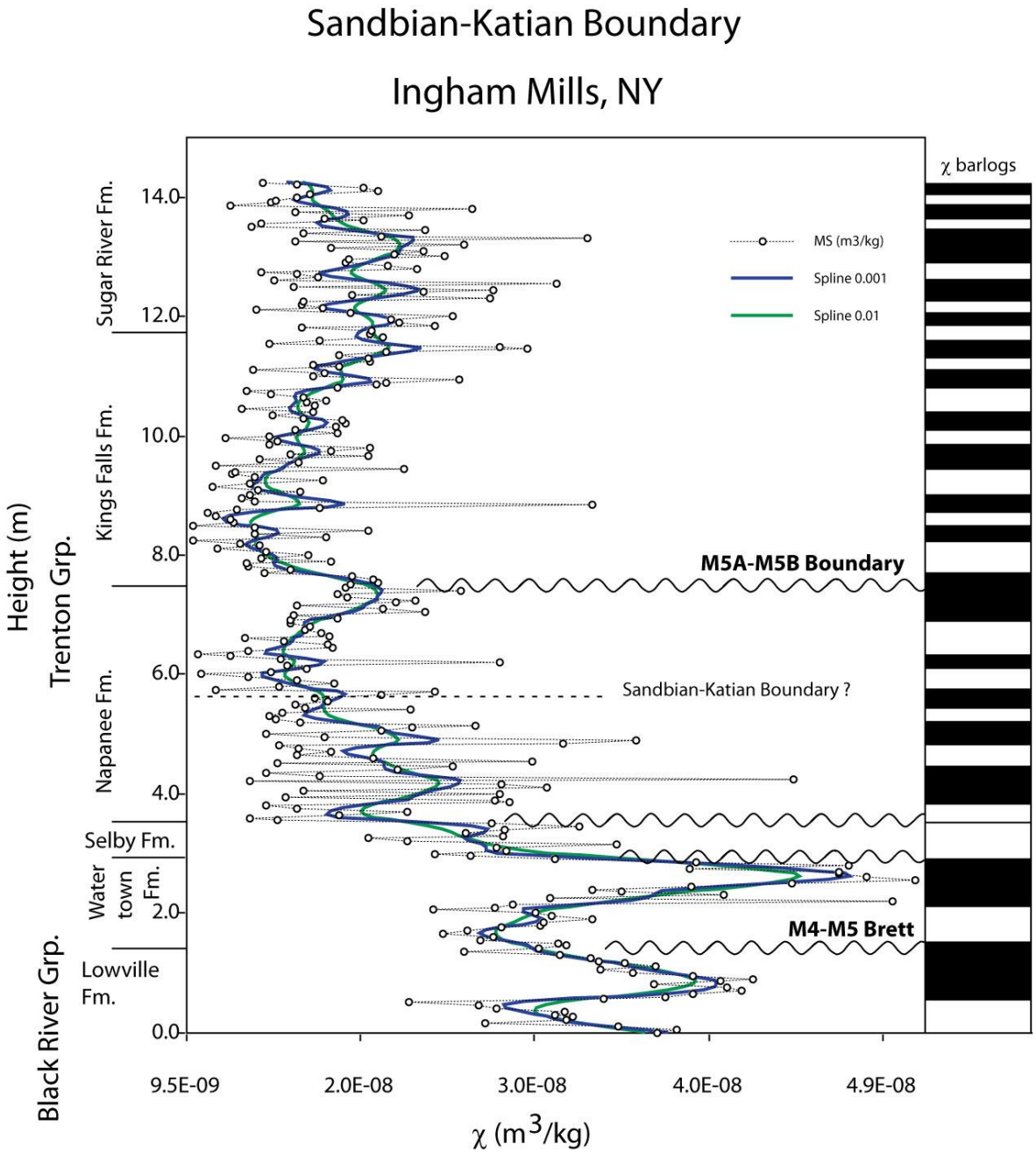

Figure 2.8 Magnetic susceptibility (χ) profile of Black River and Trenton Group stratigraphy at Ingham Mill, NewYork. showing lithostratigraphic units, unconformities, sequence boundaries and barlogs. Black Lines with white dots indicate χ data and blue and green lines are smoothed using splines. χ bar-logs indicated by black and white bars on the right side of the graph represent the inflection point of high and low χ values indicated by the blue splined line and may be used to aid in high resolution correlation.

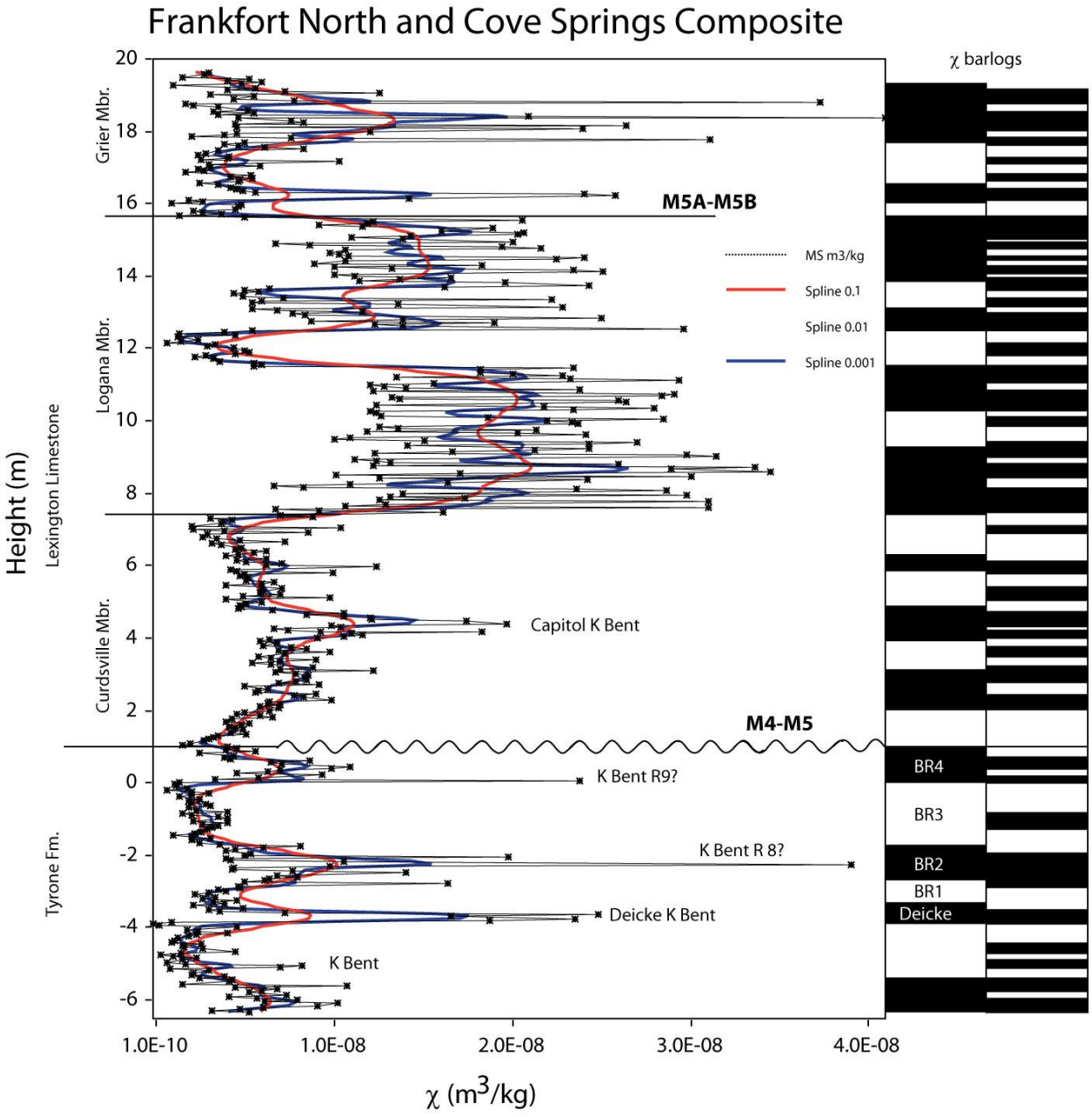

Figure 2.9 Magnetic susceptibility (χ) profile of Tyrone and Lexington Formation stratigraphy at Frankfort, Kentucky. showing lithostratigraphic units, unconformities, sequence boundaries and barlogs. Black Lines with black stars indicate χ datapoints and blue and red lines are smoothed using splines. χ bar-logs indicated by black and white bars on the right side of the graph represent the inflection point of high and low χ values indicated by the blue splined line and may be used to aid in high resolution correlation.

Middle Logana grainstones display a sharp shift to lower χ values. A return to facies similar to those of the lower Logana facies in the upper interval is followed by another sharp offset to higher χ values. A sharp shift from higher to lower χ values occurs at the base of the Grier Member, marking the M5A-M5B sequence boundary (Brett *et al*., 2004), this too may be somewhat hiatal in nature.

Hagan, Virginia

Expanded stratigraphic sections of the Eggleston Formation at Hagan, Virginia display multiple χ cyclicities (Figure 2.10). In additional to showing broad changes between lower and higher χ values, high frequency χ cycles overlap these trends. Samples from thick ashes in this section have not been omitted from χ profiles and generally correspond with normal or somewhat higher χ values. The lack of abrupt shifts in χ values indicates complete sedimentation during the time of Eggleston Formation deposition.

Black Knob Ridge

χ profiles of the Katian GSSP at Black Knob Ridge, Oklahoma (Figure 2.11) display a prominent shift from high χ values in the Womble Shale to lower χ values in the Bigfork Chert. While high frequency χ cycles are found in the Bigfork Chert, the underlying Womble Shale displays a more uniform, longer-term change from lower to higher and back to low χ values. Bigfork Chert samples do not display broad changes. Samples with high χ values in the Bigfork Chert are typically representative of thin ashes found within the section. A prominent ash found within the Womble shale, however, does not display higher χ values, and this may reflect low amounts of weathering of these thin horizons (Ellwood *et al*., 2013), or initial low χ values known for some ash beds such as the Devonian Tioga K-bentonite (Ellwood pers comm 2013).

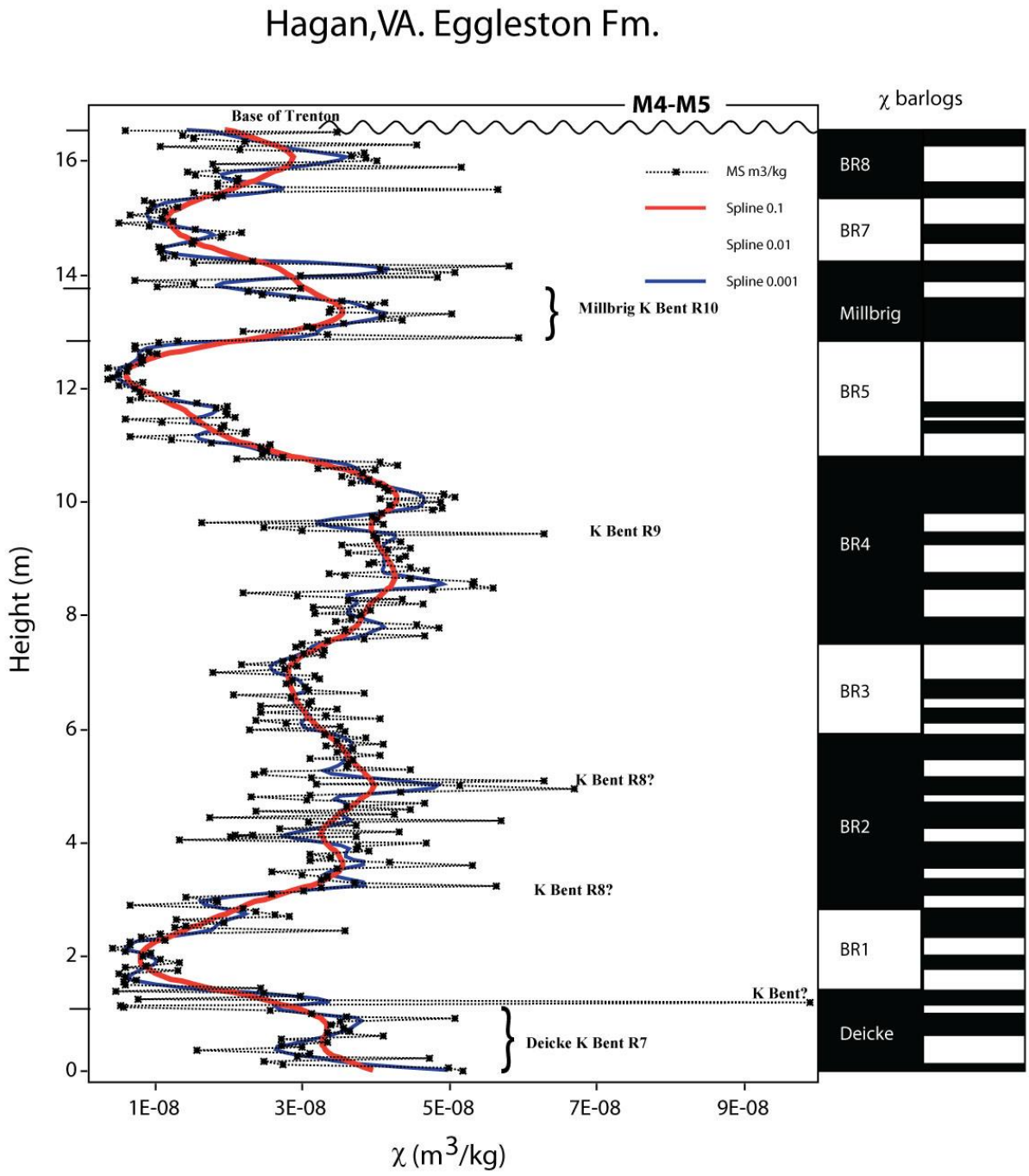

Figure 2.10 Magnetic susceptibility (χ) profile of Eggleston Formation and base of Trenton Group stratigraphy at Hagan, Virginia showing unconformities, sequence boundaries, K-bentonites and barlogs. Black Lines with black stars indicate χ data points and blue and green lines are smoothed using splines. χ bar-logs indicated by black and white bars on the right side of the graph represent the inflection point of high and low χ values indicated by the blue splined line and may be used to aid in high resolution correlation.

Fittstown, Oklahoma

The auxilliary Katian stratotype at Fittstown, Oklahoma (Figure 2.12) displays a much different looking χ profile than does the nearby GSSP. The section displays high-frequency χ cycles. The Corbin Ranch submember of the Bromide Formation displays alternations between low and high χ values. These may reflect erosional shaly recesses and possible ashes in the section interbedded with micrites. A sharp single data-point occurs at a possible ash identified previously as the Decker clay bed, at the Bromide-Viola Spring Formation contact. Otherwise, there is no large shift in χ values at this clearly unconformable contact. χ values range from higher to slightly lower, and then increase in value to a possible hiatus in the Viola Springs Formation χ values then decrease in the upper portion of the section.

DISCUSSION

Owing to a lack of correlatable datums between these disparate regions it has not been possible to develop a unique correlation solution for Sandbian-Katian boundary placement in eastern North America. However, it has been possible to hang χ datasets as isochronous markers by using K-bentonite beds to achieve a higher level of resolution than previously recorded.

Internal correlation within lower Trenton sequences remains controversial in eastern North America (Figure 2.13). Brett *et al*., (2004) present sequence stratigraphy based correlations between classic sequences of the New York Trenton, and Kentucky Lexington Platforms. Mitchell *et al*., (2004) offer different correlations of the Watertown and Selby formations of New York and Tyrone Formation, and Curdsville Member of the Lexington Limestone in Kentucky, based upon disputed K-bentonite correlations.

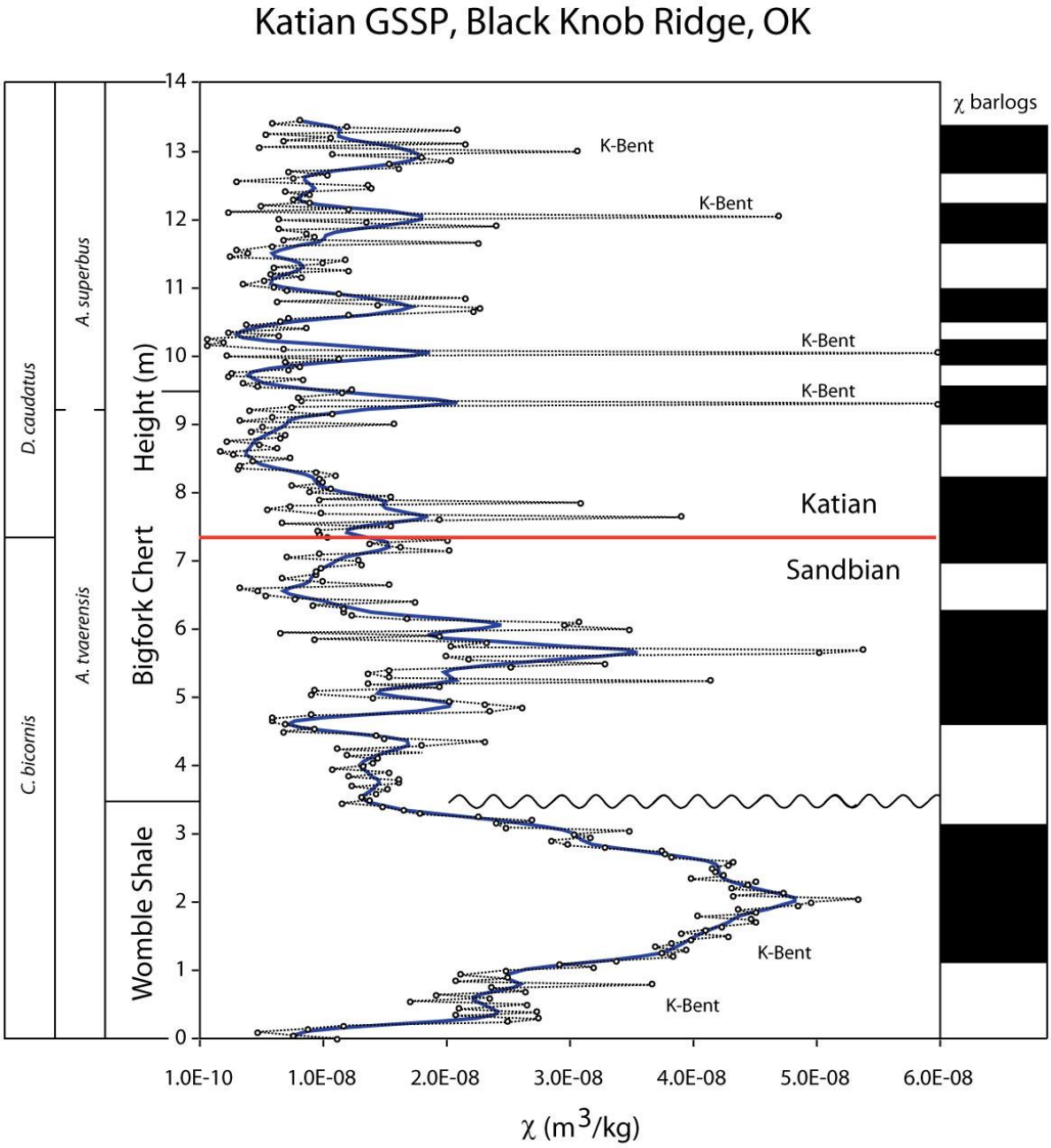

Figure 2.11 Magnetic susceptibility (χ) profile of Womble Shale and Bigfork Chert stratigraphy at the Katian, GSSP Black Knob Ridge, Oklahoma, showing unconformities, biostratigraphy, K-bentonites and barlogs. Black Lines with white dots indicate χ data points and blue lines are smoothed using splines. χ bar-logs indicated by black and white bars on the right side of the graph represent the inflection point of high and low χ values indicated by the blue splined line and may be used to aid in high resolution correlation.

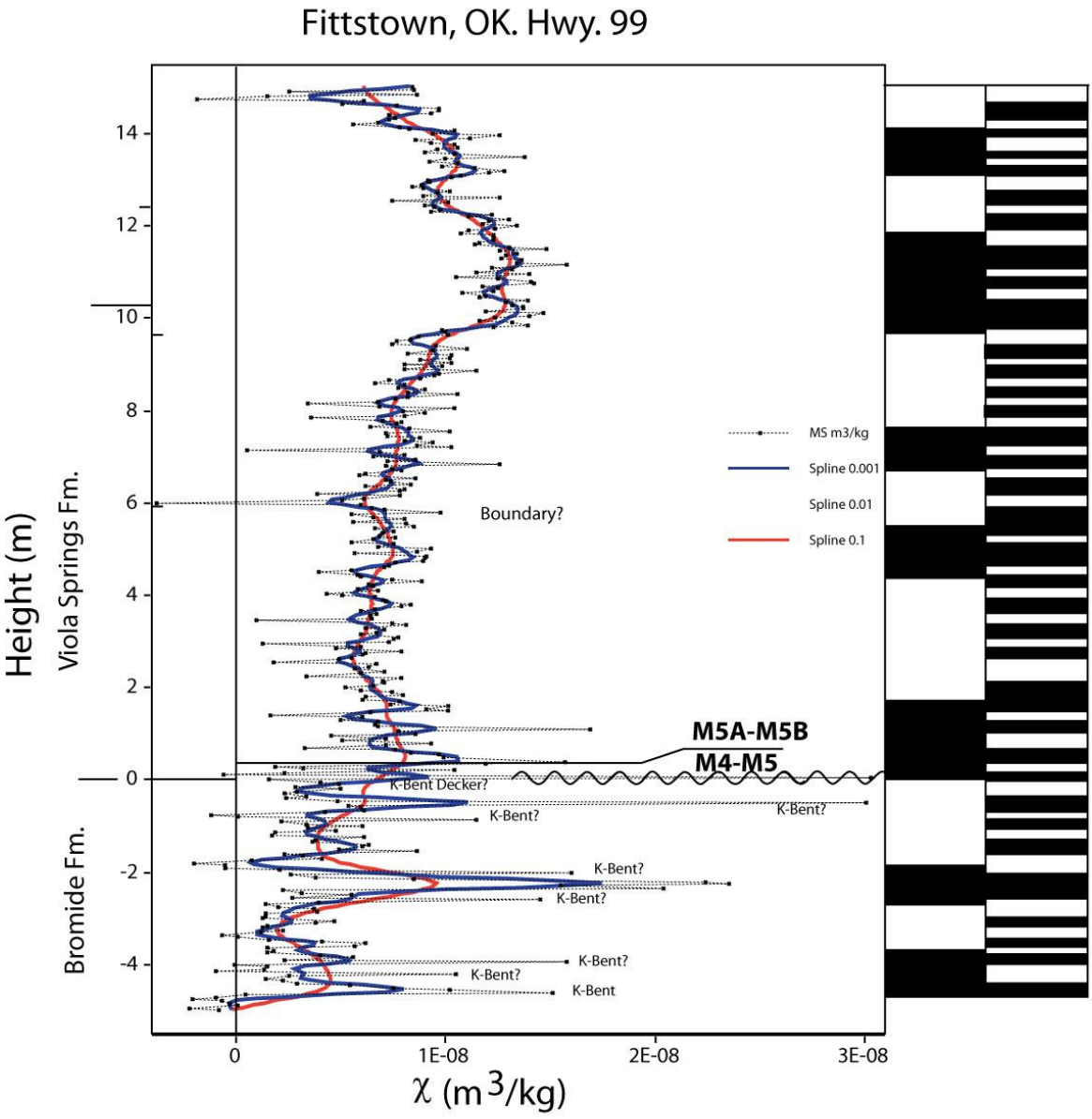

Figure 2.12 Magnetic susceptibility (χ) profile of Bromide and Viola Springs Formation stratigraphy at the alternate stratotype at Fittstown, Oklahoma, showing unconformities, K-bentonites and barlogs. Black Lines with white dots indicate χ data points and blue lines are smoothed using splines. χ bar-logs indicated by black and white bars on the right side of the graph represent the inflection point of high and low χ values indicated by the blue splined line and may be used to aid in high-resolution correlation.

Both research groups place the Napanee Formation and Logana Member as approximate equivalents, but disagree on the precise timing of their bounding surfaces. Thus, they have independently established that the Curdsville-Logana as Rocklandian, in contrast to most

previous workers (e.g., Cressman, 1973), who considered the Curdsville to be Kirkfieldian on the basis of echinoderm faunas, which closely resemble those of the Bobcaygeon (formerly Kirkfield) Formation in Ontario. Barta *et al*., (2007) identify the positive $\delta^{13}C$ excursion within the Napanee and Logana formations as the GICE, and infer correlation of the Napanee-Logana. They also regard the basal contacts of these units as equivalent, yet suggest that the upper surface of these units is not precisely correlative. This surface corresponds to Brett *et al's.,* (2004) M5A-M5B sequence boundary at the base of the Kings Falls Formation (New York) and of the Grier Member (Kentucky) and it is likely that this unconformity has eroded to different levels in different portions of the basin. Likewise, the documentation of a similar positive $\delta^{13}C$ excursion in the Hermitage Formation of Tennessee indicates that it is also coeval with very similar facies of the Logana in Kentucky. These new high resolution correlations of the Logana-Napanee-Hermitage strata in these disparate regions should faciliate the comparison of coeval faunas, climatology, and tectonic events surrounding the Sandbian-Katian boundary in classic Upper Ordovician sections.

It is suspected that Sandbian-Katian boundary placement occurs within the Napanee (New York) Logana (Kentucky) Hermitage (Tennessee) interval within eastern North America: a widespread deepening interval. The Napanee-Logana-Hermitage interval consists of a rhythmically interbedded shale-limestone succession, which Brett *et al*., (2012) recognized this as an interval of "time specific facies." If global boundary-defining graptolite diversification occured within

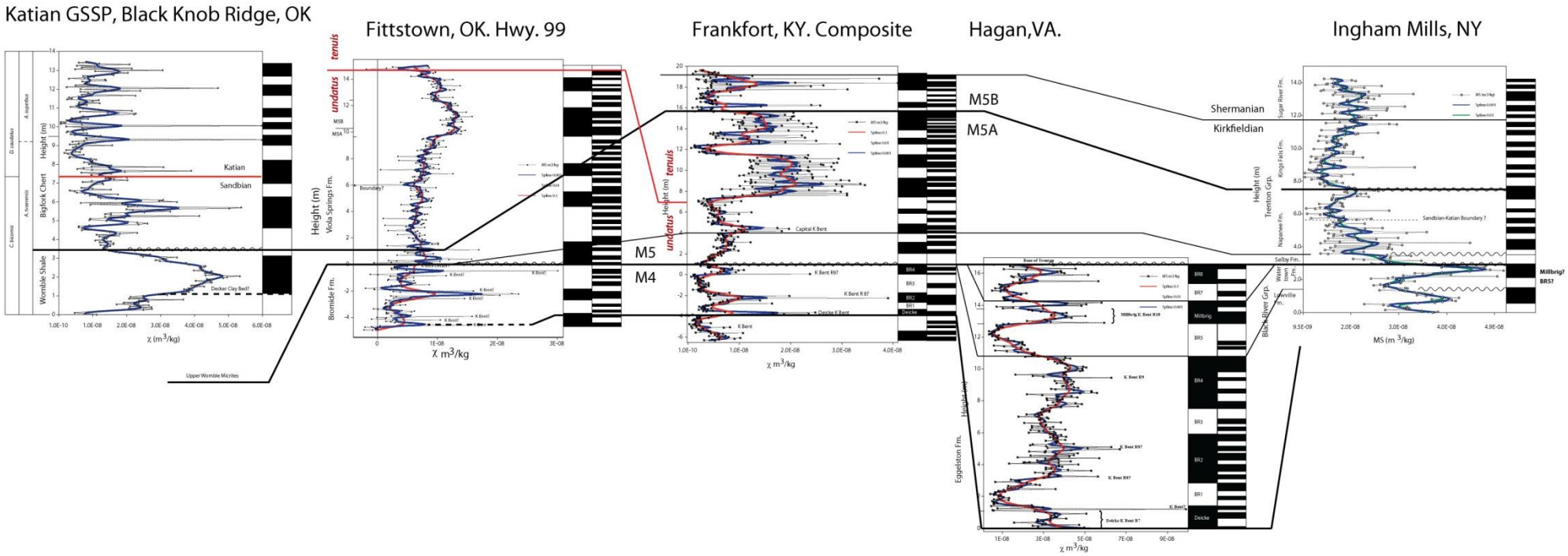

Figure 2.13 Correlation Diagram of Sandbian-Katian magnetic susceptibility (χ) profiles in Eastern North America. Correlations hung on M4-M5 sequence boundary from literature (Finney 1986; unit correlations based on sequence stratigraphic surfaces are crosscut by diachronous conodont zonation shown in red.

this deepening interval, then this deepening event may not be solely tectonically induced, but instead eustatic in nature.

Diachronous Conodont and Graptolite Zonation

The *P. undatus- P. tenuis* conodont Zone boundary appears to be diachronous relative to sequence stratigraphic-based correlations at some locations in eastern North America. The *P. tenuis* Zone boundary is approximately coincident with the Sandbian-Katian boundary in eastern North America. At the classic Cincinnati Arch section, in Frankfort, Kentucky, the *P. tenuis* Zone boundary occurs at 5.75m above the base of the Lexington Limestone, in the uppermost Curdsville Member, and near the transitional contact with the overlying Logana Mbr, (Young *et al*., 2005; Sweet, 1979). In the Fittstown, Oklahoma roadcut, the conodont composite reference section, the basal *P. tenuis* boundary has been located ~14.5m above the base of the Viola Springs Formation (Young *et al*., 2005; Sweet, 1983, 1984), based upon conodont graphic correlation. However, this zonal boundary occurs within a covered interval within the section. Additionally, the nominal conodont *P. tenuis,* has not been found, rather, the boundary has been based upon elements resembling this taxon. The highest *Climacograptus bicornis* Zone graptolites are found at 0.85 meters above the base of the Viola Springs Formation (Goldman *et al*., 2007), this limiting the Sandbian-Katian boundary to within this lower Viola Springs wackestone interval, or unconformably at its upper surface. Moreover, Goldman reports the occurrence of late forms of *C.bicornis* at this level, indicating that this position is near the top of the *C. bicornis* Zone. Carlucci *et al*., (2014) identify this lower meter of graptolitic wackestone of the lower Viola Springs Formation at Fittstown as a distinct, highly condensed fourth-order cycle, and displays graptolitic sediments recording anomalously deep offshore environments relative to the strata bounding it. Such correlations would place the unit lying above the

graptolitic wackestone unit as Grier Member equivalent, and the sharp contact between this unit as possibly the M5A-M5B sequence boundary of Brett et al. (2004). Both sequence stratigraphic, and biostratigraphic correlations are assumed to be synchronous, or at least semi-synchronous. Biostratigraphically based correlations do admit some degree of diachroneity associated with the lowest observed occurrence of diagnostic taxa. We suspect that the basal *P. tenuis* Zone boundary, as presently recognized at Fittstown has approximately half a fourth-order cycle diachroneity (~200k years) between the lowest observed occurrence in Kentucky relative to Oklahoma.

Finney (1986) reports the graptolite *Diplacanthograptus spiniferus* within the Fittstown section at approximately 33 meters above the base of the Viola Springs Formation The lowest observed occurrence of *D. spiniferus* in Oklahoma is younger than the *D. spiniferous* Zone and may be indicative of older ages (Goldman *et* al., 2007; pers comm. 2014). However, his still may make the $\delta^{13}C$ excursion at Fittstown (Young *et al*., 2005) outside of the stratigraphic interval for the GICE.

Ash Bed Based χ Black Riveran Correlation

While, it has not been possible to further resolve boundary correlation within lower tTrenton strata, an unexpected outcome of this study is very high resolution χ-based correlation of upper Black Riveran (Turinian or upper Sandbian) strata across North America. Using known "Big Bentonite" correlations it has been possible to resolve the correlation of smaller less persistent K-Bentonites within this interval. Based upon distinct magnetic properties of known ash beds it has been possible to recognize these horizons in sections in which identification has been problematic in the past. Furthermore, intracratonic correlations within this interval occur at

a much higher resolution that previously recognized in the past, based upon “Big Bentonite”, or biostratigraphic correlations alone (Figure 2.13).

Correlating from thick and stratigraphically complete sections in Hagan, Virginia, at the border of the Taconic Foreland Basin, to sections on the Lexington Platform, K-bentonite correlations have provided a datum upon which high-resolution χ-based correlations can be based. Identification of the Deicke K-Bentonite in both of these sections (Kolata *et al*., 1996) has provided this background. Establishment of χ barlogs (Ellwood *et al*., 2007) in both of these sections has allowed the correlation of minor K-bentonites within these sections: specifically the correlation of K-bentonites R8 and R9, occurring between the Deicke and Millbrig ashes (Kolata *et al.,* 1996; 1998).

The Deicke K-bentonite has a unique lithologic composition and is easily distinguishable in the field by its pale green color (Huff, pers comm.). Thermomagnetic susceptibility measurements (see Chapter 1 for further details) indicate that the Deicke K-bentonite from reference sections in Kentucky and Hagan, Virginia also has a very distinctive signature (Figure 2.14). A nearly identical heating and breakdown signature of the Deicke K-bentonite was found within a sample taken from the upper prominent recess in the upper Pooleville Member (Corbin Ranch submember) of the Bromide Formation at Fittstown, Oklahoma (Ellwood pers. comm. 2014). This horizon at Fittstown, however, is not the clay recess identified by Rosenau *et al*., (2012) as the "Deicke K-bentonite". Hanging χ bar-logs based upon the thermomagnetic susceptibility identified Deicke ash bed reveals a very similar χ signature in the Corbin Ranch, at Fittstown Oklahoma, and to that around the Deicke K-bentonite in the Tyrone Formation at Frankfort Kentucky. This includes matching χ barlogs and identification of minor ashes within

the upper Bromide. Importantly, Millbrig K-bentonite has not been found within this section.

The minor “ash” directly above the base of the Viola Springs Formation, speculated

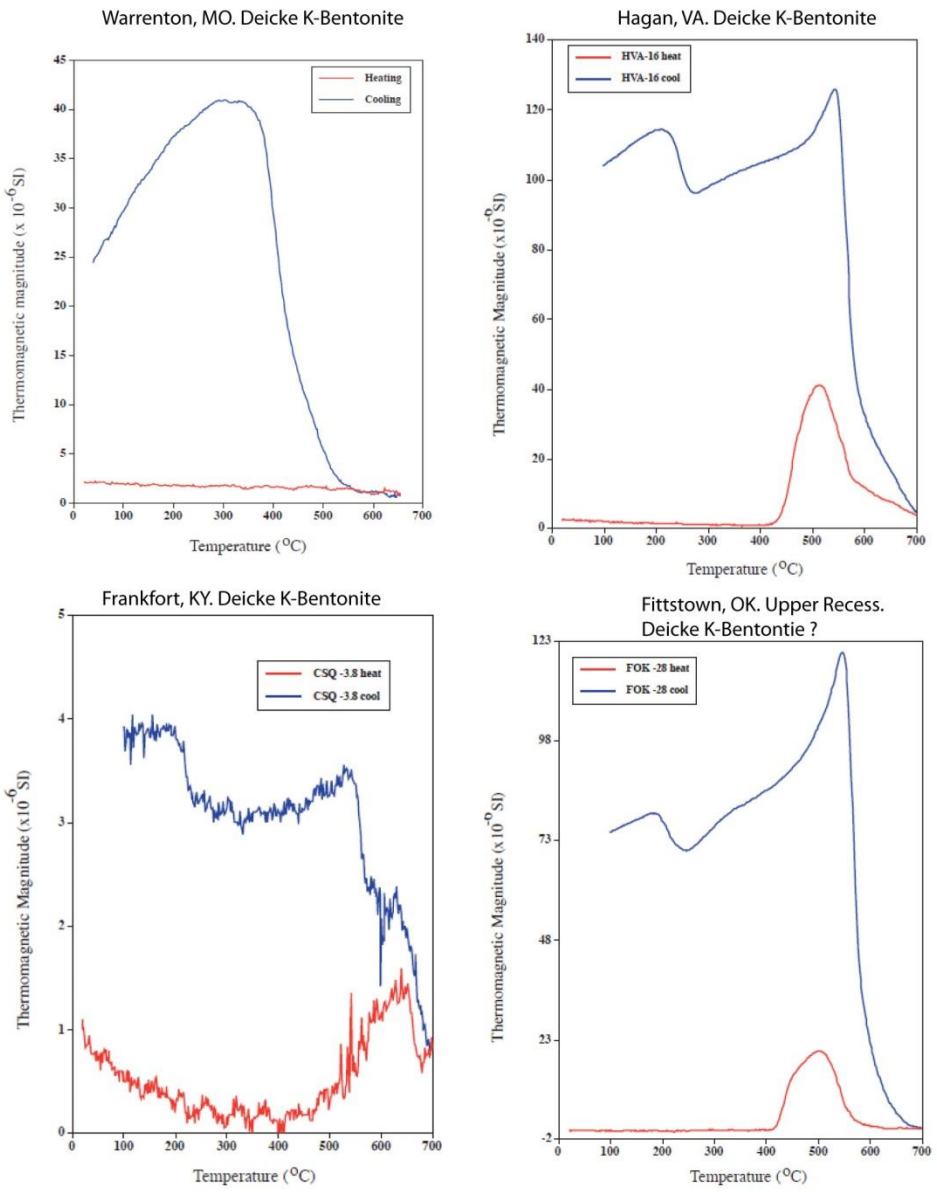

Figure 2.14 Thermomagnetic Susceptibility of Deicke K-bentonite samples from Warrenton, Missouri; Hagan, Virginia; Frankfort, Kentucky; and possible Deicke K-Bentonite at the ‘upper recess at Fittstown, Oklahoma. Blue Lines indicate cooling profiles and red lines indicate heating profiles. Similar heating and breakdown effects of the Fittstown, Oklahoma upper recess indicate the possibility of it being the Deicke K-bentonite.

to be Decker's "Clay Bed" might be considered to represent this horizon, because the relationship between the Millbrig K-bentonite and the basal Trenton remain unclear in the upper Mississippi Valley. However, the details of the χ data do not match. Moreover, a specimen of the trilobite *Flexicalymene* was collected immediately above this clay layer and that trilobite, thus far, is only known from Trenton and higher strata (S. Westrop, pers comm). This clay also occurs above a prominent erosional surface at the base of a thin basal lag bed which has previously been identified as the M4-M5 sequence boundary (Young *et al.*, 2007, etc.) All of this evidence strongly suggests that this clay bed is not the Millbrig K-bentonite, and that the latter may be cut out beneath the M4-M5 sequence boundary, as is in a number of other localities. Moreover, this "ash" is lithologically similar to the thick ash bed found near the base of the upper shale-rich interval of the Womble Formation at the Black Knob Ridge GSSP locality. Based upon lithologic evidence of these ash beds it is suggested here that the ashes at Black Knob Ridge are the same as Decker's clay bed (1933), found at the Fittstown locality, and represent small ashes within lower Trenton (Curdsville-Logana) strata. The findings of Sell (2010), indicates that both ash beds within the upper Womble Shale at Black Knob Ridge are distinct from the Deicke and Millbrig K-Bentontites , although subsequent work (Sell et al, 2013) suggests that they are similar in age to the latter.

While the upper recess of the Fittstown outcrop is suggested to be the Deicke K-Bentonite, other workers have previously suggested, that the lower recess was the Deicke K-Bentonite. Here it is postulated that the lower recess in the Fittstown outcrop instead represents one of the other "Big Bentonites" occurring below the Deicke ash bed, and is the Okoonita K-bentonite (Kolata *et al.*, 1996), which occurs at a similar spacing below the Deicke as stratigraphic thickness between the Deicke and Millbrig K-Bentonites at High Bridge, Kentucky.

Based on their similar size and appearance it is probable that they were confused at certain localities in the past. Additional sampling of outcrops yielding all of these ash beds would help to verify these speculations.

Correlation Hypothesis 1: Lower Viola Springs-Curdsville-Logana-Hermitage

The basal ~1 meter lower Viola Springs succession at Fittstown has long been recognized as a distinctive unit, but generally treated as simply lowest Chatfieldian strata without detailed attention to position with respect to; Millbrig K-bentonite and the basal Chatfieldian boundary; the M4-M5 sequence boundary; the conodont zonal boundary; and the base of the GICE carbon isotopic excursion. Here the evidence for the relative positioning of this unit is reviewed. Then, the case for three distinct scenarios that can be viewed as alternative hypotheses for correlation with other outcrop areas is presented, including the Katian stratotype section at Black Knob Ridge, and areas of the Cincinnati Arch, Appalachian Basin, and New York, which require further testing.

Based upon sequence stratigraphic evidence Brett (per comm. 2014) suggested that the wackestone-shale unit of the lower Viola Springs Formation is the unconformity bound equivalent of the Curdsville-Logana transgression on the Lexington Platform (Figure 2.15). Graptolites within the wackestone interval confirm its position within the upper *D. bicornis* Zone (Goldman *et al*., 2007), the biostratigraphic resolution of which limits it to either the upper Black River, or lowermost Trenton interval. Based upon these sequence stratigraphic interpretations, the GICE may be very condensed within the lower 0.85 m of the Viola Springs Formation, or cut out at the sharp contact with the overlying main unit of the Viola Springs, inferred to be the M5A-M5B sequence boundary. Incomplete sampling resolution may not capture this

unconformity-bound remnant of the GICE. The major positive $\delta^{13}C$ excursion within the lower 15 to 30 m of this section may not be the GICE, but instead may represent another younger excursion, such as the Kope excursion (Bergström *et* al., 2010). Based on this reinterpretation of the $\delta^{13}C$ profiles and conodont biostratigraphy, the Sandbian-Katian boundary, as well as the true GICE excursion would be hypothesized to be much lower in the section than previously indicated (Young *et al.*, 2007), and would either lie within the basal 0.85 m unit or be cut out by an unconformity at its top.

Similarly, a varying interpretation of the Black Knob Ridge, Katian GSSP exists based upon sequence stratigraphic evidence. This suggests that the Womble Shale-Bigfork Chert boundary is not the M4-M5 sequence boundary, but instead the M5A-M5B boundary. Such correlations would make the basal Bigfork Chert equivalent to the Grier Formation in Kentucky. Brett (pers. comm. 2014) makes this hypothesis based upon the distinctly shaly nature of the upper 3 m of the Womble Shale, suggesting that this is an anomalously deep water interval reflecting a major highstand, and indeed the same major deepening that is recorded in the lower Logana-Hermitage-Napanee successions. The strata assigned to the Womble Shale below this level appear much more micritic and less shaly. A channelized deposit below this upper fissile Womble Shale could represent the actual M4-M5 sequence boundary.

Finney (1986) suggested that the base of the Bigfork Chert and the base of the Viola Springs Formation at Fittstown are the same age. Based upon this biostratigraphic evidence this same surface may be represented by the basal grainstone of the lower Viola Springs wackestone unit at Fittstown, while the top of the 0.85 m wacketone would represent the M5A-MB sequence boundary. Both of these interpretations fall within the range of the current biostratigraphic zonation. Furthermore, the Decker Clay bed at Fittstown closely resembles the lithology of the

ash bed near the base of the upper Womble Shale unit at Black Knob Ridge. These may be the same ash, but this hypothesis requires further confirmation via geochemical analysis of these horizons. This hypothesis would also then suggest that despite its relatively distal facies the GSSP section is not condensed but has a high sediment accumulation rate relative to the Fittstown section. Slumping features and synsedimentary deformation in the Womble Shale and Big Fork Chert indicate rapid deposition of sediment on a slope.

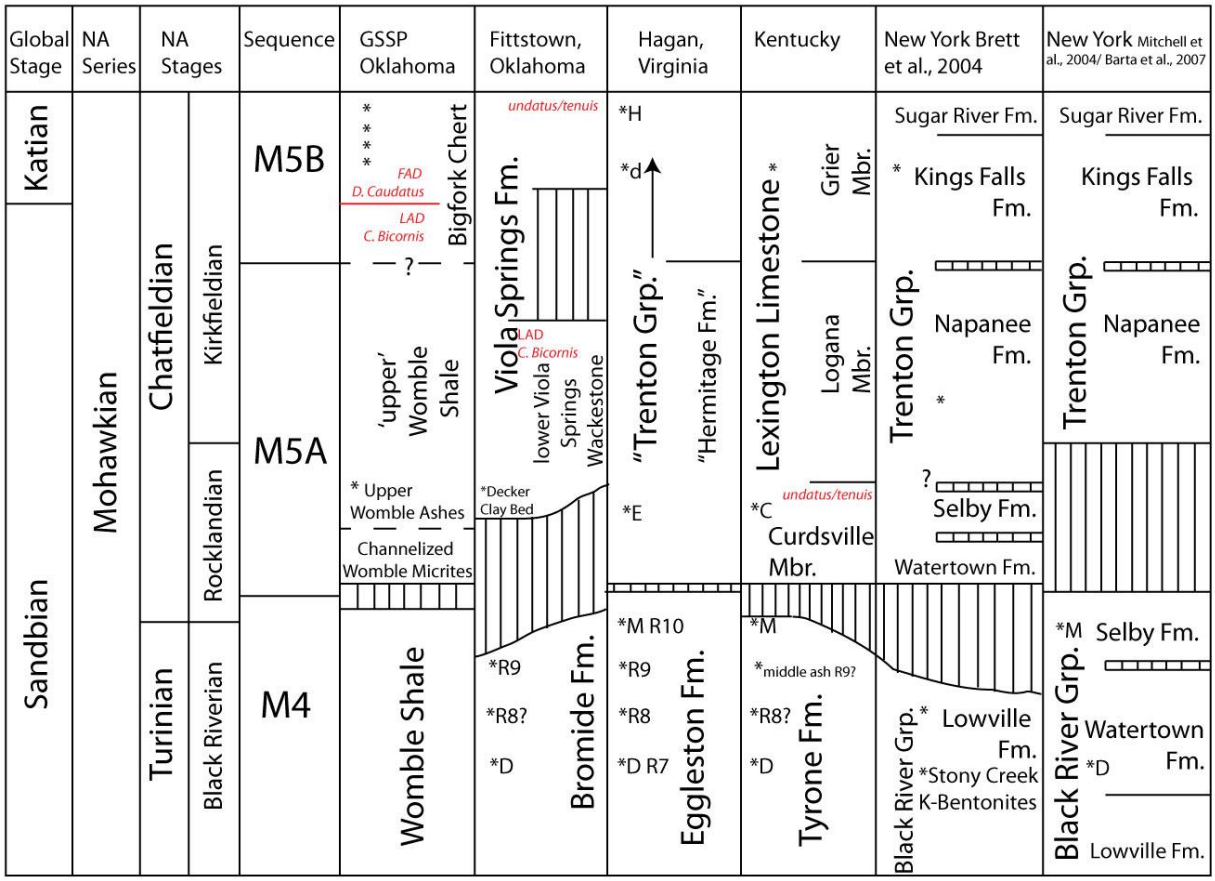

Figure 2.15 Wheeler Diagram showing correlation of Lithologic Units across North America. Vertical lines indicate unconformities, time indicated on the Y-axis is relative and does not represent unit thickness. * = K-Bentonites, M=Millbrig, D=Deicke, C= Capitol, E= Elkport, d= Dickeyville.

If the Viola Springs Formation rests on the M4-M5 sequence boundary, as previously inferred, the lower 0.85 m wackestone portion of the Viola Springs Formation could also be partially or entirely equivalent to the Curdsville Member in Kentucky, which occurs immediately

above the M4-M5 boundary there. If this is the case, the basal cm-thick grainstone may represent a highly condensed equivalent of the Curdsville Member, as it occurs in the Nashville area where it is represented by a thin grainstone that is generally less than 10 cm thick, with multiple hardgrounds occurring below the shaly Hermitage Member. Alternatively, this grainstone may represent only the lower subdivision of the Curdsville Member with most of the 0.80 m shaly wackestone representing the middle shaly Capitol submember of the Curdville Member in Kentucky. An upper, thin grainstone that fills scours in the upper part of the wackestone unit could either represent the upper Curdsville Member or possibly is the location of the M5A-M5B unconformity. The condensed transgressive, deepening upward pattern observed within the Curdsville Member, however, does not match the instantly deep facies recognized above the M4/M5 sequence boundary here. This either indicates this unconformity moved upwards into the lower Viola Springs (Trentonian) strata, or that the Curdsville and lower Viola Springs wackestone units are not equivalent. These deep wackestone facies are most likely equivalent to the Logana/Napanee formations and may include all or some of these formations.

Correlation Hypothesis 2: Watertown Shelf Perched Systems Tract

Kolata *et* al., (2001) report deepening upwards in post Millbrig "Black Riveran" strata below the M4-M5 sequence boundary. Observations of the Hagan, Virginia, post Millbrig Black Riveran Eggleston Formation strata reveal ~ 1 m of black petroliferous micritic deposits. Such a unit could represent a missing, minor sequence between the M4-M5 boundary and base of the Trenton Group, occurring as localized in pods. It is also possible that at least some post-Millbrig pre-Trenton Group strata represent a lowstand, or shelf perched systems tract of sequence M5, occurring as a pod-like unconformity bound unit. Posamentier and Vail (1988) recognized such

remnant shelf perched lowstand deposits. Additionally, similar shelf-perched shoreface deposits have been recognized by Van Wagoner *et al*., (1990). In such a case, the true M4-M5 sequence boundary would lie above the Millbrig K-bentonite, but below the surface generally identified as that boundary, which would instead represent a transgressive ravinement surface. In most areas the two surfaces would be combined as is common in so-called composite sequence boundaries.

In view of this "extra package" a more radical hypothesis is presented here that the lower Viola Springs wackestone unit at Fittstown, Oklahoma, is actually equivalent to these black petroliferous micritic horizons in the upper Eggleston Fm at Hagan Virginia, and lie below the M4-M5 sequence boundary. While somewhat obscure, an alternative correlation hypothesis is presented in which post Millbrig Black Riveran strata compose a "hanging systems tract" isolated shelf perched deposit, and thus is not present in all localities. The M4-M5 boundary results in the truncation of the Millbrig K-bentonite in places. In other places the basal Trenton Group strata (i.e., Curdsville Member in Shakterton, Kentucky) rest directly on the Millbrig K-bentonite. Further complicating this, basal Trenton Group strata in the Mississippi Valley, as presently defined, actually encompass the Millbrig K-bentonite. As this ash bed and the M4/M5 sequence boundary both represent isochronous surfaces, a correlation, or classification error exists. While strata above the Millbrig K-bentonite may be age equivalent to the basal Trenton Formation, pre Millbrig “Trentonian” strata must be "Black Riveran" in age . What is the position of the M4/M5 sequence boundary in relation to the post Millbrig-pre Trentonian strata regionally?

This leads to the question are these strata truly Trentonian, or strata of the post Millbrig (Black Riveran) transgression? Similarly, should post Millbrig strata be assigned to the Black River (M4), Trenton (M5), or does a pod-like, unknown sequence exist locally below this

widespread unconformity, which is missing at most localities. Kolata (2001) places a "drowning surface" at the base of the Millbrig K-bentonite which can be traced throughout the subsurface. Is this the true position of the M4/M5 sequence boundary, or does it lie somewhere below the Millbrig K-bentonite?

Brett *et al*., (2004) identify a major sequence boundary they regarded as coincident with the M4-M5 boundary at the base of the Watertown succession in New York. However, Mitchell *et al*., (2004) identify the Deicke K-bentonite within the Watertown Formation, and Barta *et al*., (2007) recognize the Millbrig K-Bentonite in or at the base of the Selby Formation strata in New York. If this is true, then the sharp contact at the base of the Watertown cannot be the M4-M5 sequence boundary, but must be an older surface within the Turinian, representing some sort of lowstand deposit. In this scenario the Decker clay bed in the lower wackestone unit of the Bromide Formation could represent the Millbrig K-bentonite.

If the grey "ash" (Decker Clay Bed) directly above the base of the Viola Springs Formation is the Millbrig Ash, the lower wackestone portion of the Viola Springs Formation could represent the equivalent of the Watertown/Selby Limestone. This graptolite bearing wackestone unit in the lower Viola Springs Formation seems anomalously deep relative to the surrounding strata, given that the Bromide Formation below displays fenestral micrites, while the overlying Viola Spring displays hummocks and swaley bedding and is shallow relative to the wackestone unit. The Black River-Eggleston Formation displays a deepening above the Millbrig K-bentonite, similar to the wackestone unit. Graptolites within the wackestone interval confirm its position within the *biocornis* Zone, the biostratigraphic resolution of which only limits it to the upper Black River, or lower Trenton interval.

Regional correlation of units suggests the Deicke and Millbrig K-bentonites may be part of two separate sequences. Kolata *et al*., (2001) recognizes each of the horizons on which these ash beds are deposited, as 'drowning surfaces' or 'drowning unconformities.' These may represent maximum flooding surfaces (Baum and Vail, 1988). In this case a sequence boundary would be placed between these two horizons, or the combined horizon would lie above unconformable strata. Kolata *et al*., (2001) recognizes sediment starvation in bored hardground surfaces of the Castlewood Formation occurring between these two ash beds in Missouri. Brett (pers comm. 2015) also reports sedimentary hiatuses within this interval. The Colvin Mountain Sandstone (Drahovzal and Neathery, 1971) in the Alabama Appalachians, occurring between these two ash beds (Haynes, 1994), may represent a lowstand deposit, referred to as the Blount Clastic Wedge. This lowstand, or possibly transgressive deposit occurring between these two units would further verify the possibility of post Millbrig-pre Trentonian strata existing as a separate 'hanging systems tract.'

χ Applications Summary

Ambiguous correlation solutions using χ profiles of the Sandbian-Katian boundary is not a result of the MSEC/χ method itself (Crick *et al*., 1997; Ellwood *et al*., 1999), but rather reliance of this method by hanging χ profiles on traditional, poorly resolved biostratigraphic zonations. This represents a major shortcoming in the χ method, as the correlation of orbitally tuned χ cycles is only possible if previous positive correlation exists. This level of stratigraphic refinement does not exist within the Upper Ordovician Series. A lack of correlatable units generally plagues the Ordovician System and its workers. While researchers may have detailed understanding of specific regions, establishing correlations between disparate regions remains difficult. Poor temporal resolution of traditional biostratigraphic methods does not constitute

high enough resolution to accurately access major events in Earth history, such as biodiversification, mass extinction events, tectonic events, and major changes in Earth climate.

CONCLUSIONS

The findings of this study suggest that a unique χ–based correlation solution for placement of the Sandbian-Katian boundary in the sections sampled does not exist. Complications due to biostratigraphic uncertainties, small hiatuses throughout the sampled interval, and unknown ash bed-based correlations, do not permit a single datum present in all localities sampled. While this study attempts to sample some key sections of this interval, with high biostratigraphic control and additional non-biostratigraphic datasets, sampling of additional sections of this interval containing identifiable ash beds and graptolite faunas is necessary. Carbonate shelf deposits may be plagued with unconformities, so deep flysch deposits of the Taconic Foreland basin are suggested for future sampling. Specifically, sections in Tumbling Run, VA, and Strasburg, PA, may provide suitable sections.

Differential erosion at the basal M4/M5 sequence boundary may result in a theoretical time bounding surface, however, some degree of diachroneity also may be associated with it. Using this surface as the lower datum for this study may then contain some degree of error. However, another suitable datum bracketing the Sandbian-Katian boundary above this unconformity has not been identified.

Correlation of some K-bentonites above the Sandbian-Katian boundary interval is now possible (Sell, 2010), although these ashes are not present in all sections. Several, of these ash beds, lie well above Sandbian-Katian boundary interval, and correlations of many of the ash beds recognized in the current study were not attempted. This paper supports the findings that poor

biostratigraphic resolution and a series of internal unconformities obfuscate long distance correlation.

These new correlations also suggest that the *undatus-tenuis* conondont zonal boundary may diachronous across North America. Moreover, the base of the *confluenes* Zone (the conodont zone above the *tenuis* Zone) also appears diachronous (Leslie *et* al., 1995) and appears too far above the study interval for reasonable sampling in anything but condensed sections. This is simply an artifact of poor biostratigraphic resolution within the Ordovician System relative to other Times and remains a persistent problem.

The level of correlation required to access these events within Ordovician strata occurs below the resolution of biostratigraphy, and thus will remain controversial. Simply, higher levels of biostratigraphic resolution within other systems better permit assessment of such problems. These other systems are easier to work on and the Ordovician System will continue to remain more poorly understood. Due to this lack of knowledge, continued Ordovician research, specifically developing precise chronologies, is necessary.

REFERENCES

Ainsaar, L., Meidla, T., Martma, T. 2004. The Middle Caradoc facies and faunal turnover in the Late Ordovician Baltoscandian palaeobasin: Palaeogeography, Palaeoclimatology, Palaeoecology, v. 210, p. 119-133.

Amsden, T.W., Sweet, W.C. 1983. Upper Bromide and Viola Group (Middle and Upper Ordovician) in Eastern Oklahoma.

Baird, G.C., Brett,C.E. 2002. Indian Castle Shale: Late synorogenic siliciclastic succession in an evolving Middle to Late Ordovician foreland basin, eastern New York. P 203-230. *In* C.E. Mitchell, Jacobi, R. (eds.), Taconic Convergence: Orogen, Foreland Basin and Craton. Physics and Chemistry of Earth. 27.

Barta, N.C., Berström, S.M., Saltzman, M.R., Schmitz, B. 2007. First Record of the Ordovician Guttenburg $\delta^{13}C$ Excursion (GICE) in New York State and Ontario: Local and Regional

Chronostratigraphic implications. Northeastern Geology and Envrionmental Sciences, v. 29, no. 4, p. 276-298.

Baum, G.R. and Vail, P.R. 1988. Sequence Stratigraphic concepts applied to Paleogene outcrop, gulf and atlantic basins. *In:* Sea Level Changes-and Integrate Approach, C.K. Wilgus, B.S. Hastings, C.G. St.C. Kendall, H.W. Posamentier, C.A.Ross, and J.C. Van Wagoner, Eds., pp. 309-327. SEPM Special Publication 42.

Bergström, S.M., Carnes, J.B., Hall, J.C., Kurapkat, W., O'Neil, B.E., 1988. Conodont biostratigraphy of some Middle Ordovician stratotypes in the Southern and Central Appalachians. New York State Museum Bulletin 462, 20-32.

Bergström, S.M., Finney, S.C., Chen, X., Pålsso, C., Zhi-hao, W. Grahn, Y. 2000. A proposed global boundary stratotype for the base of the Upper Series of the Ordovician System: The Fågelsång section, Scania, southern Sweden. Episodes, Vol. 23, no. 2. p. 102-109.

Bergström, S.M., Huff, W.D., Saltzman, M.R., Kolata, D.R., Leslie, S.A. 2004. The Greatest Volcanic Ash Falls in the Phanerozoic: Trans-Atlantic Relations of the Ordovician Millbrig and Kinnekulle K-Bentonites. The Sedimentary Record. Vol. 2, No. 4 p. 4-8.

Bergström, S.M., Finney, S.C., Chen, X., Goldman, D. Leslie, S.A. 2006a. Three new Ordovician global stage names. Lethaia. Vol. 39. p. 287-288

Bergström, S.M., Saltzman, M.M., Schmitz, B. 2006b. First record of the Hirnantian (Upper Ordovician) $\delta^{13}C$ excursion in the North American Midcontinent and its regional implications. Geology Mag. V. 143. No. 5. P. 657-678.

Bergström, S.M., Young, S., Schmitz, B. 2010. Katian (Upper Ordovician) $\delta^{13}C$ chemostratigraphy and sequence stratigraphy in the United States and Balto Scandia: A regional comparison. Palaeogeography, Palaeoclimatology, Paleoecology 296. 217-234.

Bergström, S.M., Kleffner, M., Schmitz, B., Cramer, B.D. 2011. Revision of the position of the Ordovician-Silurian boundary in southern Ontario: regional chronostratigraphic implications of $\delta^{13}C$ chemostratigraphy of the Manitouin Formation and associated strata. Canadian Journal of Earth Science. V. 48 p. 1447-1470.

Brett, C.E., Baird, G.C. 2002. Revised stratigraphy of the Trenton Group in the type area, central New York State: sedimentology, and tectonics of a Middle Ordovician shelf-to-basin succession. P. 231-263. *In* C.E. Mitchell, Jacobi, R. (eds.), Taconic Convergence: Orogen, Foreland Basin and Craton. Physics and Chemistry of Earth. 27.

Brett, C.E., McLaughlin, P.I., Cornell, S.R., Baird, G.C., 2004. Comparative sequence stratigraphy of two classic Upper Ordovician successions, Trenton Shelf (New York-Ontario) and Lexington Platform (Kentucky-Ohio): implications for eustasy and local tectonism in eastern Laurentia. Palaeogeography, Palaeoclimatology, Paleoecology 210. 295-329.

Brett, C.E., Schramm, T.J., Dattilo, B.F., Marshall, N.T. 2012, Upper Ordovician Strata of Southern Ohio-Indiana: Shales, Shell Beds, Storms, Sediment Starvation, and Cycles. 2012 GSA North-Central Section Meeting Fieldtrip 405 Guidebook. 80 p.

Campbell, M.R. 1898. Richmond folio, Kentucky. U.S. Geol. Surv., Geol. Atlas, folio No. 46.

Carlucci, J.R., Westrop, S.R., Brett, C.E., Burkhalter, R. 2014. Facies architecture and sequence stratigraphy of the Ordovician Bromide Formation (Oklahoma): a new perspective on a mixed carbonate-siliciclastic ramp. Facies.

Chen, X., Rong, J., Fan, J., Zhan, R., Mitchell, C.E., Harper, D.A.T., Melchin, M.J., Peng, P., Finney, S.C., Wang, X. 2006. The Global Boundary Stratotype Section and Point (GSSP) for the base of the Hirnantian Stage (the uppermost of the Ordovician System). Episodes. Vol. 29, no. 3. P. 183-196

Conkin, J.E., Desari, M.R. 1986. Capitol metabentonite in the Trenton Curdsville limestone of central Kentucky. University of Louisville notes in Paleontology and Stratigraphy. 14 p.

Cornell, S.R., Brett, C.E. 2000. K-Bentonite and sequence correlations of Upper Black River and lower Trenton Limestones from Lake Simcoe, southern Ontario Canada to Watertown, northern New York State. American Association for Petroleum Geologists Bulletin, vol. 84 (9): 1381.

Cornell, 2008 The Last Stand of the Great American Carbonate Bank: Tectonic Activation of the Upper Ordovician Passive Maring in Eastern North America. Dissertation. University of Cincinnati.

Crick, R.E., Ellwood, B.B., El Hassani, A., Feist, R., and Hladil, J., 1997. MagnetoSusceptibility event and cyclostratigraphy (MSEC) of the Eifelian-Givetian GSSP and associated boundary sequences in North Africa and Europe, Episodes 20, 167-175.

Cressman, E.R., 1973. Lithostratigraphy and depositional environments of the Lexington Limestone (Orodovician). U.S. Geological Survey Professional Paper 768. 59 p.

Cressman, E.R., Noger, M.C., 1976. Tidal-flat depositional environments in the High Bridge Group (Middle Ordovician) of central Kentucky. Report of Investigration-Kentucky Geological Survey 18.

Cushing, H.P. 1909. Geology of the Remsen Quadrangle: including Trenton Falls and vicinity in Oneida and Herkimer Counties. New York State Museum Bulletin, 19: 155-176.

Dana, J.D., Manual of Geology. 1862. New York. 1st ed. 1 800 p. Drake, A.A. Jr., and Epstein, J.B. 1967. The Martinsburg Formation (Middle and Upper Ordovician) in the Delaware Valley, Pennsylvania-New Jersey. U.S. Geological Survey Bulletin 1244-H, 16p.

Decker, C.E., Graptolites of the Sylan Shale of Oklahomas and Polk Creek Shale of Arkansas. Journal of Paleontology. V. 9. P. 697-708.

Drahovzal, J.A., Neathery, T.L., 1971. The Middle and Upper Ordovician of the Alabama Appalachian: Alabama Geological Society, Guidebook to the 9th Annual Field Trip, 229.

Ellwood, B.B., Crick, R.E., El Hassani, A., 1999. The Magneto-Susceptibility Event and Cyclostratigraphic (MSEC) Method used in Geological Correlation of Devonian Rocks from Anti-Atlas Morocco. AAPG Bulletin, V. 83, No. 7

Ellwood, B.B., Brett, C.E., and MacDonald, W.D., 2007. Magnetostratigraphy susceptibility of the Upper Ordovician Kope Formation, northern Kentucky. Palaeontology, Palaeoclimatology, Palaeoecology 243. 42-54.

Ellwood, B.B., Wang, W.H., Tomkin, J.H., Ratcliffe, K.T., El Hassani, A., Wright, A.M. 2013. Testing high resolution magnetic susceptibility and gamma radiation methods in the Cenomanian-Turonian (Upper Cretaceous) GSSP and near-by coeval section. Palaeogeography, Paaeoclimatology, Palaeoecology 378. 75-90.

Ettensohn, F.R., 1991. Flexural interpretation of relationships between Ordovician tectonism and stratigraphic sequences, central and southern Appalachians, U.S.A.; *in:* Advances in Ordovician Geology, C.R. Barnes and S.H. William (ed.), Geological Survey of Cananda, Paper 90-9, p. 213-224

Finney, S.C. 1986. Graptolite Biofacies and Correlation of Eustatic, Subsidence, and Tectonic Events in the Middle to Upper Ordovician of North America. Palaios v. 1 p. 435-461.

Finney, S.C., Grubb, B.J., Hatcher, R.D. Jr. 1996. Graphic Correlation of Middle Ordovician graptolite shale, southern Appalachians: An approach for examining the subsidence and migration of a Taconic foreland basin. GSA Bulletin. v. 108. no. 3. p. 355-371.

Finney, S.C., 2005. Global Series and Stages for the Ordovician System: A progress report. Geologica Acta. Vol. 3. No. 4. P. 309-316

Fortey, R.A., Harper, D.A.T, Ingham, J.K., Owen, A.W., Rushton, A.W.A. 1995. A revision of Ordovician series and stages from the historical type area. Geological Magazine, 132, 15-30.

Fortey, R.A., Harper, D.A.T., Inham, J.K., Owen, A.W., Parkes, M.A., Rushton, A.W.A., Woodcock, N.H. 2000. A revised correlation of Ordovician rocks in the British Isles. The Geologocial Society Special Report No. 24, 83 p.

Goldman, D., Leslie, S.A., Nõlvak, J., Young, S., Bergström, S.M., Huff, W.D. 2007. The Global Stratotype Section and Point (GSSP) for the base of the Katian Stage of the Uper Ordovician Series at Black Knob Ridge, Southeastern Oklahoma, USA. Episodes, Vol. 30. No. 4. P. 258-270.

Grubb, B.J., Finney, S.C. 1995. Graphic Correlation of Middle Ordovician Graptolite-Rich Shales, Southern Appalachians: Successful Application of the Technique to Apparently inadequate stratigraphic sections. *In:* Mann, K.O, Lane, H.R. Graphic Correlation. SEPM Special Publication No. 53.

Hall, J.C., Bergström, S.M., Schimdt, M.A. 1986. Conodont Biostratigraphy of the Middle Ordovician Chickamauga Group and related strata of the Alabama Appalachians. *In*

Benson, D.J., Stock, C.W. (Eds.) Depositional History of the Middle Ordovician of the Alabama Appalachians. 23rd Annual Field Trip Alabama Geological Society. p. 61-80.

Hatch, J.R., Jacobson, S.R., Witzke, B.J., Risatti, J.B., Anders, D.E., Watney, W.I., Newell, K.D., and Vuletich, A.K. 1987. Possible late Middle Ordovician organic carbon isotope excursion: evidence from Ordovician oils and hydrocarbon source rocks, mid-continent and east-central United States. American Association of Petroleum Geologist Bulletin, v. 71, p. 1342-1354.

Hay, B., J. Cisne, J.L. 1988. Deposition in the Oxygen-Deficient Taconic Foreland Basin, Late Ordovician, p. 387-416. *In* Keith, B. (ed.), The Trenton Group (Upper Ordovician Series) of Eastern North America. American Association of Petroleum Geologists Short Course, 29.

Haynes, J.T. 1994. The Ordovician Deicke and Millbrig K-Bentonite Beds of the Cincinnati Arch and the Southern Valley and Ridge Province. Geological Society of America Special Paper 290.

Holland, S.M., and Patzkowsky, M.E. 1996. Sequence stratigraphy and long-term paleoceanographic change in the Middle and Upper Ordovician of the eastern United States. Geological Society of America Special Papers. 306. P. 117-129.

Hohman, J.C., 1998. Depositional history of the upper Ordovician Trenton Limestone, Lexington Limestone, Maquoketa Shale and equivalent lithologic units in the Illinois Basin: an application of carbonate and mixed carbonate siliciclastic sequence stratigraphy. Indiana University, Bloomington, Indiana, p. 186.

Huffman, G.G. 1945. Middle Ordovician limestone from Lee County, Virginia to central Kentucky: Journal of Geology, v. 53. P. 145-174.

Jacobi, R.D., Mitchell, C.E., 2002. Geodynamical interpretation of a major unconformity in the Taconic Foredeep; slide scar or onlap unconformity? p. 169-201. *In* C.E. Mitchell, Jacobi, R. (eds.), Taconic Convergence: Orogen, Foreland Basin and Craton. Physics and Chemistry of Earth. 27.

Kay, G.M. 1931. Stratigraphy of the Ordovician Hounsfield Metabentonite. Journal of Geology, 39 (4). P 361-376.

Kay, G.M. 1937. Stratigraphy of the Trenton group. Geological Society of America Bulletin, 48 (2) p. 233-302.

Kay, G.M. 1943. Mohawkian Series on West Canada Creek, New York. American Journal of Science. 241 (10) p. 597-606.

Kay, G.M. 1968. Ordovician Formations in Northwestern New York. Le Naturaliste Canadien, 95: 373-1378.

Kolata, D.R., Huff, W.D., Berstrom, S.M. 1996. Ordovician K-bentonites of Eastern North America. Geological Society of America Special Paper 313. 84 p.

Kolata, D.R., Huff, W.D., Berstrom, S.M. 1998. Ordovician K-bentonites of Eastern North America. Geological Society of America Bulletin 110. p. 723-739

Kolata, D.R., Huff, W.M., and Bergström, S.M. 2001. The Ordovician Sebree Trough: An oceanic passage to the Midcontinent United States. GSA Bulletin, V. 113, p. 1067-1078

Leslie, S.A. 1995. Upper Middle Ordovician Conodont Biofacies and Lithofacies Distribution Patterns in Eastern North America and Northwestern Europe: Evaluations Using Deicke, Millbrig, and Kinnekulle K-bentonite beds as time planes. Ph.D. dissertation, The Ohio State University, Columbus, OH.

Leslie, S.A., Bergström, S.M., Huff, W.D. 2008. Ordovician K-bentonites discovered in Oklahoma. Oklahoma Geology Notes v. 68, N. 1 & 2. p. 4-14.

Ludvigson, G.A., Witzke, B.J., Gonzalez, L.A., Carpenter, S.J., Schneider, C.L., Hasiuk, F. 2004. Late Ordovician (Turinian-Chatfieldian) carbon isotope excursions and their stratigraphic and palaeoceanographic significance: Palaeogeography, Palaeoclimatology, Palaeoecology, v. 210, p. 187-214.

McLaughlin, P.I., Brett, C.E., Taha MchLaughlin, S.L., Cornell, S.R. 2004. High-resolution sequence stratigraphy of a mixed carbonate-siliciclastic, cratonic ramp (Upper Ordovician; Kentucky-Ohio, USA): insights into the relative influence of eustasy and tectonics through analysis of facies gradients. Palaeogeography, Palaeoclimatology, Palaeoecology, v. 210, p. 267-294.

McLaughlin, P.I., Brett, C.E., Taha McLaughlin, S.L., Holland, S.M. 2008. Upper Orodovician (Chatfieldian-Edenian) strata from central Kentucky to southern Ohio: Facies gradients, event beds and depositional sequences. *In*: McLauglin, P.I., Brett, C.E., Holland, S.M., Storrs, G.W. (eds.) Stratigraphic Renaissance in the Cincinnati Arch: Implications for Upper Ordovician Paleontology and Paleoecology. Cincinnati Museum Center Scientific Contributions No. 2.

Miller, A.M. 1905. Lead and Zinc-bearing rocks of central Kentucky, with notes on the mineral veins: Kentucky Geol. Survery, Bulletin, No. 2 35p.

Miller, R.L., Fuller, J.O. 1954. Geology and oil resources of the Rose Hill district: The enster area of the Cumberland overthrust block, Lee County, Virginia: Virginia Geological Survey Bulletin 71. 383 p.

Miller, R.L., and Brogse, W.P. 1954. Geology and oil resources of the Jonesville district, Lee County, Virginia: U.S. Geological Survey Bulletin 990. 240p.

Mitchell, C.E., Goldman, D., Delano, J.W., Samson, S.D., Bergström, S.M., 1994. Temporal and spatial distribution of biozones and facies relavie to geochemically correlated K-bentonites in the Middle Ordovician Taconic foredeep. Geology. v. 22 p. 715-717.

Mitchell, C.E., Adhya, S., Bergström, S.M., Joy, M.P, Delano, J.W., 2004. Discovery of the Ordovician Millbrig K-bentonite Bed in the Trenton Group of New York State:

implications for regional correlation and sequence stratigraphy in eastern North America. Palaeogeography, Palaeoclimatology, Paleoecology 210. 331-346.

Newberry, J.S. 1873. The general geological relations and structure of Ohio, IN Report of the Geological Survey of Ohio; Part I, Geology: Ohio Division of Geologocial Survey Report of Progress, 2nd Series, v. 1. p. 1-167.

Quinland, G.M., Beaumont, C. 1984. Appalachian thrusting, lithospheric flexure, and the Paleozoic stratigraphy of the eastern interior of North America. Canadian Journal of Earth Sciences, v. 21, p. 973-996.

Ogg, J.G., Ogg, G., Gradstein, F.M. 2008. The Concise Geologic Time Scale. Cambridge.

Posamentier, H.W., Vail, P.R. 1988. Eustatic controls on clastic deposition II – sequence and systems tract models. *In*: Wilgus, C.K., Hastings, B.S., Kendall, C.G. St. C., Posamentier, H.W., Ross, C.A., Van Wagoner, J.C. (eds.) Sea-Level Changes: An integrated approach.Society of Economic Paleontologists and Mineralogists Special Publications. 42. 125-154.

Rosenau, N.A., Herrmann, A.D., Leslie, S.A. 2012. Conodont apatite $\delta^{18}O$ values from a platform margin setting, Oklahoma, USA: Implications for initiation of Late Ordovician icehouse conditions. Palaeogeography, Palaeoclimatology, Palaeoecology, v. 315-316, p. 172-180

Saltzman, M.R., Berström, S.M., Huff, W.D., Kolata, D.R. 2003. Conodont and graptolite biostratigraphy of the Ordovician (Early Chatfieldian, middle Caradocian) δ13C excursion in North America and Baltoscandia: implications for the interpretation of the relations between the Millbrig and Kinnekulle K-bentonites. In Albanesi, G.L., Beresi, M.S., and Peralta, S.H. (eds.). Ordovician from the Andes: Proceedings of the 9th International Symposium on the Ordovician System: INSUGEO: Serie Correlación Geológica, v. 17, p. 137-142.

Saltzman, M.R., Young, S.A. 2005. Long-lived glaciation in the Late Ordovician? Isotopic and sequence-stratigraphic evidence from western Laurentia. Geology. V. 33. No. 2. P. 109-112.

Schuchert and Twenhofel. 1910. Geol Soc. Am. Bull., vol. 21. P. 700.

Sell, B.K. 2010. Apatite Trace Element Tephrochronology. Unpublished Dissertation. Syracuse University. 320 p.

Sell, B.K., Ainsaar, L., Leslie, S. 2013. Precise timing of the Late Ordovician (Sandbian) super-eruptions and associated environmental, biological, and climatological events. Journal of the Geological Society, London. V. 170. P. 771-714.

Shackleton, N.J., Crowhurst, S.J., Weedon, G.P., Laskar, J. 1999. Astronomical calibration of the Oligocene-Miocene time. Phil. Trans. R. Soc. Lond. A. 357. P. 1907-1929.

Sweet, W. C., Bergström, S.M. 1971. The American Upper Ordovician Standard: XIII A Revised Time-Stratigraphic Classification of North American Upper Middle and Upper Ordovician Rocks. GSA Bulletin

Sweet, W.C., 1979. Conodonts and conodont biostratigraphy of post-Tyrone Ordovician rocks of the Cincinnati region. United States Geological Survey Professional Paper 1066-G, 1-26.

Sweet, W.C. 1983. Conodont biostratigraphy of Fite Formation and Viola Group. Oklahoma Geological Survery Bulletin 132, 23-36.

Sweet, W.C., 1984. Graphic correlation of Middle and Upper Ordovician rocks, North American Midcontinent Province, USA. *In* D.L. Brunton, ed. Aspects of the Ordovician System: Palaeontological Contributions from the University of Oslo, 295. 23-35

Sweet, W.C. 1985. Conodonts; those fascinating little whatzits. Journal of Paleontology. 53(9) p 485-494.

Ulrich, E.O., 1911. Revision of the Paleozoic systems. Geological Society of Americ Bulleting. 22. P. 281-680.

Vanuxem, L., 1838. Second annual report of the geological survey of the third district of the State of New York. New York Geological Survey Annual Report, 2:253-286.

Van Wagoner, J.C., Mitchum, R.M., Campion, K.M., Rahmanian, V.D. 1990. Siliciclastic sequence stratigraphy in well logs, cores and outcrop. American Association of Petroleum Geologists, Methods in Exploration Series, 7.

Webby, B.D. 1998. Steps towards a global standard for the Ordovician stratigraphy. Newsletters on Stratigraphy. v. 36 p 1-33.

Webby, B.D., F. Paris, M.L. Droser, I.G. Percival, eds. 2004. The Great Ordovician Biodiversification Event. Critical Moments and Perspectives in Earth History and Paleobiology. Columbia University Press. New York, 483 p.

Westrop, S.R., Amati, L., Brett, C.E., Swisher, R.E., Carlucci, J.R 2012. When approaches collide: reconciling sequence stratigraphy, chemostratigraphy and biostratigraphy in the correlation of the Katian (Upper Ordovician) reference section, Central Oklahoma. Geological Society of America Annual Metting Abstracts with Program.

Young, S.A., Saltzman, M.R., Bergström, S.M. 2005. Upper Ordovician (Mohawkian) carbon isotope ($\delta^{13}C$) stratigraphy in eastern and central North America: Regional expression of a perturbation of a global carbon cycle. Palaeogeography, Palaeoclimatology, Palaeoecology, v. 222, p. 53-76.

Young, S.A., Saltzman, M.R., Bergström, S.M. Leslie, S.A., Chen, X. 2008. Paired $\delta^{13}C$carb and $\delta^{13}C$org records of Upper Ordovician (Sandbian-Katian) carbonates in North America and China: Implications for paleoceanographic change. Palaeogeography, Palaeoclimatology, Palaeoecology, v. 270, p. 168-178.

CHAPTER 3
MAGNETIC SUSCEPTIBILITY-BASED ANALYSIS OF SEQUENCE STRATIGRAPHIC PROFILES IN THE KATIAN STAGE OF EASTERN NORTH AMERICA: IS MAGNETIC SUSCEPTIBILITY A VIABLE TOOL FOR SEQUENCE STRATIGRAPHIC INTERPRETATION?

ABSTRACT

Early χ research suggests that χ in vertical successions responds to changes in base level. As χ in marine settings is driven by detrital input, the sedimentary response to changes in base-level will result in χ changes. Crick *et al.*, (1997) and Ellwood *et al.*, (1999) suggest a predicable χ response in relation to Transgressive-Regressive cycles. Changes in sea level, however, are not simply transgressive or regressive, and include different sequence stratigraphic surfaces, systems tracts, and stacking patterns (Catunaneu, 2006).

This preliminary investigation analyzes the relationship of magnetic susceptibility and sequence stratigraphy and sequence stratigraphic surfaces. While, the results of the investigation are incomplete it provides the basis for future studies. The investigation analyzes the use of χ to interpret stratigraphic sequences. Ordovician samples spanning the Sandbian-Katian boundary are analyzed relative to their sequence stratigraphic positions. A series of additional Ordovician, Silurian, and Devonian sections have been sampled for this future investigation and their analysis is pending. Sequence Boundaries and marine flooding surfaces have provided the most recognizable surfaces in χ profiles, represented by sharp offsets in χ values, however, these features are not ubiquitous.

INTRODUCTION

Sequence Stratigraphy is a branch of stratigraphy that analyzes the sedimentary response to changes in base level. This system seeks to establish a chronostratigraphic framework and

through its application allows predictions to be made concerning the sedimentary record (Catuneanu, 2006). This project analyses the utility of interpreting stratigraphic sequences based upon analysis of χ profiles. By measuring χ of outcrop collected samples across key sequence stratigraphic surfaces of known interpretation, the validity of analyzing stratigraphic sequences based upon χ profiles is evaluated.

Developing new and better correlation techniques is a continuing issue amongst stratigraphers. Correlation is fundamental to stratigraphy by allowing the comparison of coeval strata. While this task may seem mundane, correlation is the foundation upon which it is necessary to evaluate events in Earth History, large or small, in multiple locations. While χ–based correlations are used commonly in well-studied stratigraphic successions with high biostratigraphic resolution, application in more exploratory research remains limited. The present study, while still in its infancy, addresses how χ can be used to interpret successions, in order to provide a correlation/interpretation method for under-studied/controversial stratigraphic sequences. It has been shown (Chapter 2) that shallow marine systems in which hiatuses are present may not be ideal χ-based correlation. Similarly, the correlation potential of the χ profiles method decrease with increased proximity to shoreline (Chapter 1). Crick *et* al., (1997) and Ellwood *et al*., (1999) suggest limiting this application to pelagic sections. Thus, it is hoped to expand the use of χ in such shallow marine settings commonly preserved in Paleozoic strata through integration with other non-biostratigraphic means.

χ measurements taken across sequence stratigraphic surfaces and systems tracts from the Sandbian-Katian boundary interval provide the basis and control for this preliminary study. Additional samples for future examination have been collected from outcrops of multiple ages

with known sequence stratigraphic interpretation, and from literature (Holland and Patzkowsky, 1996; Ver Straeten, 2007; Brett *et* al., 2011; Schramm, 2011). These collections include samples from sequence boundaries, lowstand systems tracts, transgressive ravinement surfaces, transgressive systems tracts, maximum starvation/flooding surfaces, highstand systems tracts, forced regression surfaces, and falling stage systems tracts in Paleozoic mixed carbonate-siliciclastic systems.

BACKGROUND

Ellwood *et al*., (2010) demonstrated that sediment hiatuses/unconformities may result in large offsets in χ values when cyclic variations in χ are truncated. Furthermore removal of a χ cycle may also produce no significant offset. Is it possible, in turn, to recognize other sequence stratigraphic surfaces in a predictable manner within χ profiles? Due to base-level change, predictable sedimentological responses should occur. Based upon this premise, do changes in weathering and climate associated with changes in base-level, result in predictable changes in constituents responsible for χ values? Ellwood *et al*. (1999) suggest that χ changes can result from altering base/sea-level, and thus be affected by climate and therefore detrital sediment input.

Because χ is independent of gross lithology (limestone, shale, sandstone), χ values are controlled by variations in fine-grained detrital/eolian components. Ellwood *et al*., (2000; 2013; Febo, 2007) indicate that calcium carbonate content does not significantly control χ values. Thus, while predictions may be made about χ during certain stratigraphic intervals, these predictions are not based primarily on lithology, but rather on para-ferrimagnetic input. The sedimentary response associated with base level change should result in predictable variations.

These changes in χ values may result from changes in sediment provenance or source, and may be associated with different systems tracts, identified by sedimentary stacking patterns, such as aggradation, retrogradation, and progradation, and migration of delta lobes.

Sequence Boundaries

Sequence boundaries are placed at unconformities bracketing stratigraphic sequences, or their associated correlative conformities (Figure 3.1), and are associated with intervals of low sea-level, possible subaerial exposure, and karstification. Ellwood *et al.*, (2010) indicate that unconformities may result in large rapid/single point shifts in measured χ values relative to underlying beds based upon the missing portion of a cycle.

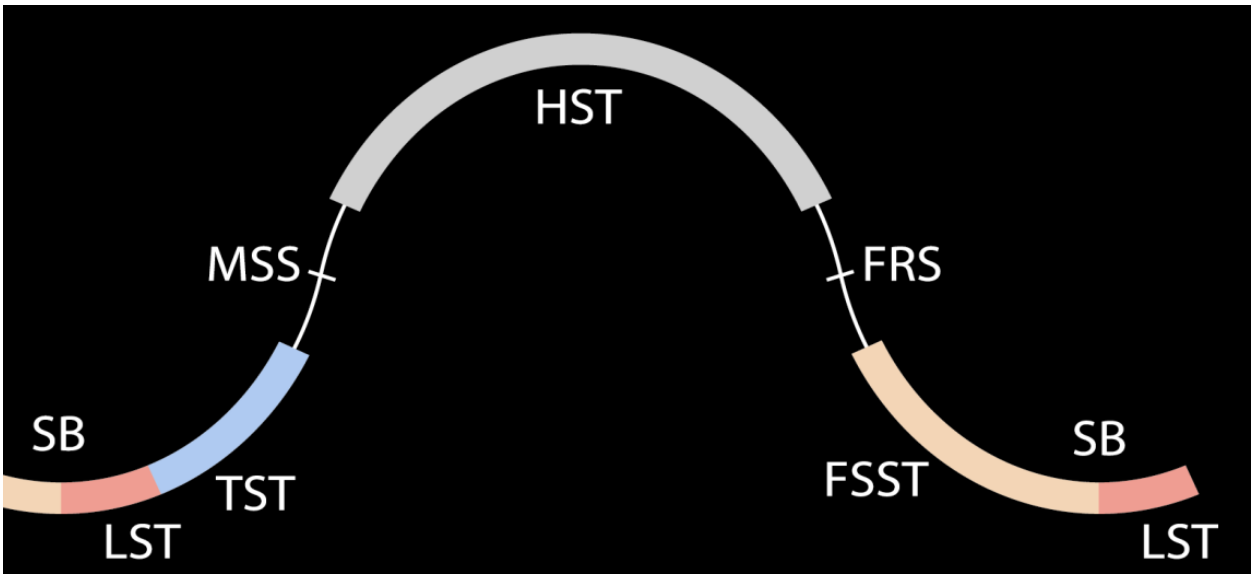

Figure 3.1 Idealized sea-level curve indicating key systems tracts and stratigraphic surfaces. SB (Sequence Boundary), LST (Lowstand Systems Tract), TST (Transgressive Systems Tract, MSS (Maximum Starvation Surface), HST (Highstand Systems Tract), FRS (Forced Regression Surface), FSST (Falling Stage Systems Tract). From McLaughlin, pers. comm.

However, for several reasons it is possible that little offset in χ values may occur, for example, if χ varies little throughout a cycle, or if erosions removes a complete cycle or cycles.

Preliminary evidence suggests that sequence boundaries with similar lithologies bordering them may or may not have offsets in measured χ values. Changes to lower χ values may be associated with low amounts of detrital sediment input during sea-level transgressions within the basin. It is suggested that some sequence boundaries may be recognizable in χ profiles. This work was designed to test this by sampling across several sequence boundaries (some containing different lithologies), and support these observations with published examples where possible.

Transgressive Systems Tracts

Transgressive systems tracts (Figure 3.1) are retrogradational deposits that occur during intervals of sea level rise in which the point of onlap moves in the landward direction (Van Wagoner *et al*., 1988; Posamentier *et al.,* 1988). Associated with developing accommodation, argillaceous sediments may be sequestered in nearshore/upramp settings. The offshore setting may thus, be starved of detrital sediments resulting in carbonate production and condensed deposits downramp.

Transgressive systems tracts in epicontinental seas are dominated by compact skeletal pack-grainstone deposits. These deposits generally display low measured χ values relative to overlying highstand deposits. This is largely attributed to low amounts of detrital sediment input in offshore areas. It is predicted that relatively low measured χ values will be found during transgressive systems tracts in downramp settings owing to nearshore (upramp) sequestering of sediments. Likewise, transgressive systems tract deposits may have higher measured values in upramp positions.

Maximum Flooding/ Starvation Surfaces

Maximum flooding, or starvation surfaces (Figure 3.1) represent condensation associated with base-level rise and changes from retrogradational to progradational stacking patterns, and are associated with deepening upwards (Van Wagoner *et al*., 1988; Posamentier *et al.*, 1988). They are interpreted to represent synchronous horizons. Such surfaces may become very condensed in basinal sections and be associated with phosphatic lag deposits, glauconite deposition, and reworked steinkerns (Baum and Vail, 1988). Such deposits mark the contact between the transgressive, and highstand systems tracts. Typical maximum starvation/flooding surfaces occur when carbonate shelf deposits are overlain by basinal shales. Rapid deepening in such sections may be the result of tectonism. The term 'drowning unconformity' may also be used to indicate the abrupt deepening and suppression of carbonate production recorded at this surface (Kolata *et al*., 2001). In sediment starved carbonate sections, phosphatic hardgrounds may be associated with such surfaces. Additionally, K-Bentonites, are frequently preserved at such horizons (Huff pers comm).

As basinal accommodation develops at its fastest rate at maximum starvation/flooding surfaces a change from sediment starved conditions to an input of detrital argillaceous deposits is predicted to occur. Associated with a large input of clay and terriginous derived para- and ferrimagnetic constituents into the system, measured χ values are expected to rise rapidly in the form of χ value shifts at such surfaces.

Highstand Systems Tracts

Progradational highstand systems tract deposits record intervals of normal regression (Figure 3.1). Associated with high amounts of basinal accommodation, these deposits are

dominated by fine-grained argillaceous material, or interbedded shales and limestones in epicontinental seas.

Due to the high input of clays, which are typically characterized by high χ values (Ellwood *et al*., 2007), highstands are predicted to have high χ values relative to the deposits they overlie. Due to decreasing accommodation in nearshore settings, it is predicted that a higher amount of paramagnetic or ferrimagnetic minerals will be deposited within the basin.

Forced Regression Surfaces

Regressive surfaces of marine erosion are associated with the rapid sea-level fall that brings the seafloor within storm to normal wave base (Figure 3.1). These often result in horizons with reworked concretions, erosive surfaces marked by course-grained materials sharply overlying finer-grained deposits. This is due to a high amount of sediment starvation prior to deposition of erosive falling-stage deposits, which may include incised channels, and time-rich accumulations or condensed shell-beds may develop by bypass and winnowing.

Falling Stage Systems Tracts

Falling stage systems tracts (Plint and Nummendal, 2000) are progradational intervals marked by actual base-level fall (forced regression; Figure 3.1). Exposure of upramp settings associated with base-level fall results in a high amount of course-grained detrital input being deposited in the marine realm. Rapid sediment accumulation, and earthquakes associated with a basinal shift in equilibrium point, often result in soft sediment deformation. Incised channels may form associated with basin incision. Tabular silty-carbonate deposits may form at this time.

Increased detrital components entering the marine realm may result in high χ values. Conversely, a high amount of diamagnetic quartz-rich (silt-sand sized) deposits may dominate falling stages and may buffer additional detrital components, and therefore reduce χ, perhaps by as much as 1/3 to 1/2 of an order of magnitude (Febo, 2007).

DISCUSSION

To test variations in χ, key sequence stratigraphic surfaces were sampled from Upper Ordovician successions in eastern North America (Figure 2.2). These include Sandbian-Katian Stage Boundary successions in New York, Virginia, Kentucky, and Oklahoma, as well as the Knox unconformity. Chapter 2 contains additional background information on these succesions and tectonic history. Sucessions spanning the onset of Taconian flooding at the basal Utica Shale have been sampled in eastern New York.

Shale High Value Paradigm

Argillaceous material is a driver of χ in the marine realm. A common misconception associated with χ research is that shales have high χ values and that limestones have low χ values. Limestones generally have low χ values, while shale χ values may be somewhat higher, and it is reasonable to predict that large limestone-shale contacts may result in an offset, or shift to higher χ values. This is not always the case. While there is some merit to this hypothesis, research through multiple experiments (Crick and Ellwood, 1997; Ellwood *et al*., 1999) has shown that limestone and shales in the marine system may have a similar range of χ values. Additionally, some limestones may have higher values than the shales surrounding them. χ samples from the Selby-Napanee Formation contact at Ingham Mills show a distinct change to lower values where burrowed hardground wackestones are overlain by calci-lutites interbedded

with shales (Figure 2.8). This deepening upwards may be associated with a marine flooding surface. A change from a retrogradational to a progradational stacking pattern in the deep basin should result in a compact wacke-packstone overlain by basinal shales at a sediment starved contact. Thus, a change from low to high χ values may be expected. The section at Ingham Mills displays the opposite trend; χ values of the overlying Napanee Formation are lower than limestones of the underlying Selby Formation It is likely that the sediment starved surface of the basal Napanee Formation may at Ingham Mills in fact be hiatal, and does not represent a typical flooding surface. A significant portion of the Selby Formation is likely missing as the unit thins considerably from its type locality in Canada (Brett *et al*., 2004). It is unclear if the basal Napanee Formation is precisely the same age as in Canada, as the section is progradational it may be slightly younger there if a clinoformal morphology exists, as it is located upramp of the Ingham Mills section.

M4-M5 Sequence Boundary

At hiatuses and unconformities, often represented by lithologic contacts, sharp shifts in measured χ values may be expected. This results from a portion of a cycle being cut out causing rapid change from low to high values, or vice versa. Furthermore, changing lithologic properties responsible for χ at lithologic contacts may be expected to result in a change in χ values. The M4-M5 sequence boundary is widely represented by a change from Black River Group shallow fenestral micrites and dolostones, to compact pack-grainstones of the Trenton Group across much of eastern North America (Holland and Patzkowsky, 1996). Deepening upwards occurs in the Trenton Group, and this juxtaposition of facies is basinwide. In accordance with this lithologic variation, a shift in values may be expected. However, a large shift in χ values has not

been observed at multiple locations where the position of the M4/M5 boundary is known. These include Hagan Virginia, and Frankfort Kentucky. In the case of the M4/M5 sequence boundary at Frankfort Kentucky a known truncation exists in which several cycles of Black River Group strata are missing (Figure 2.9). Similarly, the M4/M5 boundary at the Bromide-Viola Springs Formation contact does not display a large shift in χ values at the contact. There is, however, a single spurious datapoint at the boundary representing the stratigraphic position of a possible ash, but following this there is a return to typical χ values.

Some lower-order, high-frequency sequence boundaries, associated with 4^{th} order depositional cycles, display larger offsets in χ values than high-order, low frequency 3^{rd} order sequence boundaries. This has been prominent in the Frankfort Kentucky and Ingham Mills sections. It is suspected that these values are driven by lithologic variations, and may reflect differences between compact limestone, and argillaceous material. Ellwood *et al*., (2007) have linked χ values to clay content in the overlying Kope Formation. As these terrestrial components are derived from the same Taconic Hinterland source as observed for the Frankfort, Kentucky sections it is suspected the same would hold true there.

M5A-M5B Sequence Boundary

The M5A-M5B sequence boundary of Brett *et al*.,(2004) represents a 4^{th} order (~ 405 kyr) sequence boundary and does not show a consistent shift in χ values at the localities studied. This boundary at Ingham Mills, New York occurs at the Napanee-Kings Falls formations boundary (Figure 2.8). Here interbedded shales and lutites are overlain by an intraformational conglomerate at the sequence boundary, including large boulder-sized granite clasts. The Kings Falls Formation displays large ripple features and was likely deposited in a very shallow

environment. A large change in χ values at this contact, however, does not exist. χ values rise from 1 x 10^{-8} to 2 x 10^{-8} m^3/kg in the upper Napanee Formation and then fall from 2 x 10^{-8} back to 1 x 10^{-8} m^3/kg in the lower Kings Falls Formation (Figure 2.8). This slight increase in χ values may be associated with increased detrital sediment input at this unconformity. A large single point shift in χ values at this contact, however, has not been observed.

The M5A-M5B sequence boundary at Frankfort Kentucky, alternatively displays a large offset in values (Figure 2.9). This is represented by the Logana-Grier members contact. The Logana Member consists of interbedded shales and marls, and is sharply overlain by compact pack-grainstones of the Grier Member. χ values sharply change from approximately 2.5 x 10^{-8} to 1 x 10^{-9} m^3/kg at the contact.

This same boundary in the lower Viola Springs Formation at Fittstown Oklahoma, probably occurs at the boundary between condensed graptolitic wackestones and overlying cherty calcisiltites (Figure 2.12). The thin wackestones represent a thin remnant of cycle M5A, likely Napanee or Logana equivalent in this section. Very little offset in χ values is recorded at this contact.

A difference in χ offsets at this contact was not necessarily unexpected. As Ellwood *et al.*, (2010) predict missing portions of cycles could result in large or little to no offsets in χ values at sequence boundaries. While a significant portion of the M5A sequence may be missing at Fittstown, and cycles within it are almost certainly missing, the Napanee Formation and equivalent Logana Member are not expected to be missing cycles. The large offset in χ values at the Frankfort Kentucky section is not obscure: a similar trend at Ingham Mills would have been expected. Instead, the low χ values in the Napanee Formation, and the lower wackestone unit of

the Viola Springs Formation at Fittstown do not match general assumptionss of higher χ values during highstands. It is suspected that the interplay between autochonous carbonate development and clastic shale deposition, occurring within different portions of sequences, produces the large offset in χ values within sections on the Cincinnati Arch.

Knox Unconformity

The Knox Unconformity divides the Sauk and Tippecanoe cratonic sequences (Sloss, 1963). This represents a major lowstand deposit and the only 'Sloss-scale' sequence boundary analyzed in this preliminary portion of this study. Sections studied at Canajoharie Creek, New York, expose this sequence boundary at the Beekmantown Group (Knox equivalent) -Glens Falls (Trenton equivalent) contact (Figure 3.2). The equivilent horizon is exposed at Ingham Mills, New York, but due to powerplant-associated accessibility issues, sampling this contact has not been possible. Additionally, the Beekmantown-Black River formation contact has been sampled at Stony Creek, Middleville, New York. The Chuctanunda Member of the Tribes Hill Formation (Ulrich and Cushing, 1910; Fisher, 1954) of the Beekmantown Group is unconformably overlain by the Glens Falls Formation (Ruedemann, 1912) at Canajoharie Creek, New York. A sharp offset in χ values occurs at the Knox Unconformity (Figure 3.3). Values in the range of 2×10^{-8} to 3×10^{-8} m^3/kg in the Beekmantown Group rapidly shift to lower values in the 1×10^{-8} m^3/kg range at the basal Glens Falls Formation conctact, and then increase upward progressively. Four cycles are recognized within the χ profiles and correspond well to four low order-high frequency cycles recognizable in outcrop.

Sequence Boundaries

It appears that the sequence boundaries studied here generally display either little or no offset in χ values, or there is a shift to lower measured values. Schramm (2011), and Brett *et al*., (2012) recognized a sharp offset to lower χ values at the basal Bellevue Member unconformity on the Cincinnati Arch (Schramm, 2011; Schramm *et al*., 2012A; Brett *et al*., 2012).

Figure 3.2 Outcrop photograph of the Knox Unconformity at Canajoharie Creek New York were the Beekmantown Group in unconformably overlain by the Glens Falls Formation

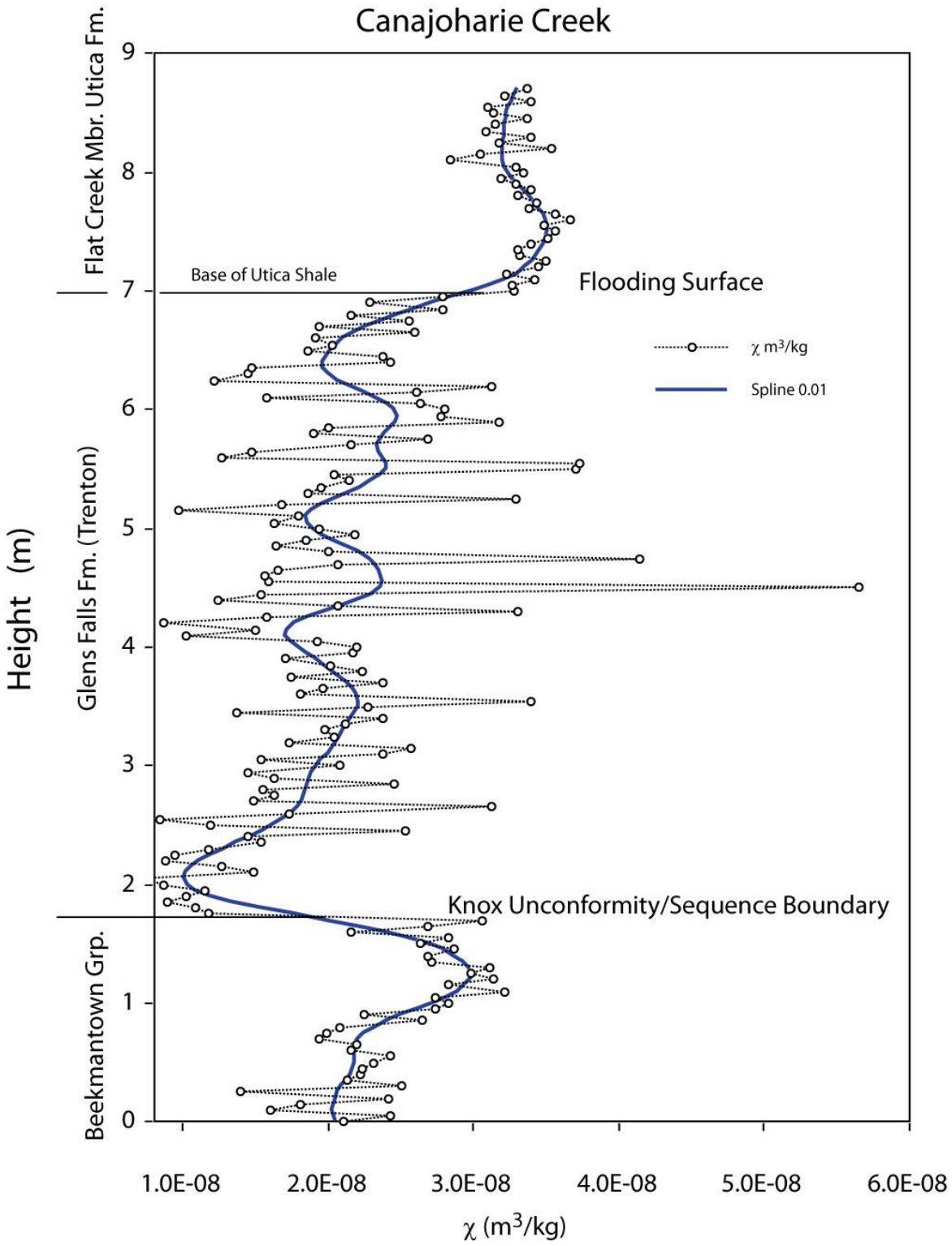

Figure 3.3 Magnetic Susceptibility (χ) profile of Beekmantown Group, Glens Falls Formation, and Utica Formation strata exposed at Canajoharie Creek New York.

This surface has been interpreted as a sequence boundary. Such surfaces generally have not yielded rapid shifts to higher χ values, in carbonate sections, and changes appear to represent aggradational, or retrogradational stacking patterns at these surfaces, resulting in low concentrations of detrital paramagnetic material being deposited in the basin at these times.

Lowstand Systems Tracts

Lowstand systems tracts are not widely represented in Ordovician epicontinential seas. Two lowstand systems tracts were sampled for the purposes of this study; the "Z-Bed" (see chapter 1), and the Watertown Limestone (Figure 2.8), based upon the sequence statigraphic interpretations of Brett *et al*., (2004). Both the "Z-Bed" and Watertown Limestone units begin with low χ values and then increase. These values then return to approximately original low χ values at the overlying transgressive ravinement surface. A similar pattern has been observed at the base of the Lawrenceburg submember of the Fairview Formation (Schramm, 2011; Schramm *et al*., 2012A; Brett *et al*., 2012) It is unclear whether this is simply a reflection of lowstand sytems tracts, or if this is the signal of low-order, high-frequency cycles, which compose the broader scale lowstand systems tracts. Despite the "Z-Bed" system being composed of compact grainstones overlain by shales, and the Watertown Limestone composed of fenestral micrites, and it is suspected that the higher χ values may indicate slight progradation in the form of increased deposition of paramagnetic components. Additionally, these aggradational patterns may vary relative to their location within the basin, and lowstand fans composed of course clastic deposits may be expected to yield higher χ values.

It would be advantageous to conduct further research on the χ of multiple lowstand systems tracts. These deposits are not readily preserved within Ordovician epicontinental seas,

where sequence boundaries are commonly combined with transgressive ravinement surfaces to represent, erosional-transgressive, or ET surfaces.

Base of Utica Shale

The onset of Taconian flooding is diachronous across New York State. This onset of flooding occurs earlier in eastern New York, than central New York. Localities in both eastern and central New York have been sampled for the purposes of this study. In eastern New York this represents the sharp contact of the Utica Shale on the Glens Falls Formation (Figure 3.4). The equivalent lithostratigraphic contact in central New York occurs at the Russia-Dolgeville Formation contact may be slightly younger. This contact was sampled at Allen/Schnell Road in Oppenheim New York (Figure 3.5). Baird and Brett (2002) further document the diachronous nature of the basal Utica Shale onlap. Additionally they recognize a series of synchronous horizons that cross-cut these facies variations. These include sequence stratigraphic surfaces, ash beds, faunal epiboles and other recognizable horizons. The ability to correlate shelf into basin sequences represents one of the most persistent problems within the science of stratigraphy. The study by Baird and Brett (2002), solving the Utica-Trenton problem represents the pinnacle of stratigraphic research in solving centuries old stratigraphic problems (Baird *et al*., 1992).

The contact of the Flat Creek Member of the Utica Formation (Goldman *et al*., 1994) contact onto the Glens Falls Formation at Canajoharie Creek represents a maximum flooding surface and a change from shelly carbonate shelf, to offshore shale facies. A slight offset to higher χ values occurs at this contact (Figure 3.3). Utica Shale χ values are consistently ~ 3.5 x 10^{-8} m^3/kg. More important is that χ values rise in the upper Glens Falls Formation and continue to rise in the lower Utica Shale. This may indicate deepening upwards in the upper Glens Falls

Formation with increased fine grain siliciclastic deposition, continuing upwards through the Utica Shale. This contact may be regarded as a drowning unconformity, maximum flooding surface, or downlap surface.

Figure 3.4 Outcrop photograph of the base of the Utica Shale at Canajoharie Creek New York. Here distal facies of the Flat Creek Member of the Utica Formation sharply overly the Glens Falls Formation at a marine flooding surface.

The same deepening at Allen Rd. in Oppenheim New York, is represented by the Sugar River Formation-Dolgeville Formation contact (Cushing, 1909; Baird and Brett, 2002). This section displays deepening upwards, beginning with compact grainstones fining upwards into argillaceous limestones with diverse trilobite faunas, distal *Cryptolithus* faunas in the Sugar River Formation, and continued deepening upwards into interbedded lutites and shales of the "Dolgeville Fm." (Figure 3.5). The basal Dolgeville Formation represents a marine flooding

Figure 3.5 Outcrop photograph of the Sugar River-Dolgeville formations contact at Allen Road, Oppenheim, New York.

surface and appears the same sequence stratigraphic contact as the base of the Flat Creek Member. At the base of the Dolgeville Formation there is a distinct shift to higher χ values at the onset of shale deposition (Figure 3.6). χ values rise from of 1×10^{-8} to 2×10^{-8} m^3/kg through the Sugar River Formation, and jump from about 2×10^{-8} to 4.5×10^{-8} m^3/kg at the basal Dolgeville contact at the onset of shale deposition. Values within the Dolgeville Formation

appear somewhat variable and lower values appear to correspond with lutite horzions. The values reach up to about 5.8 x 10^{-8} m^3/kg and then decrease to about 4.5 x 10^{-8} m^3/kg.

Four magnetic susceptibility cycles are recognized within the Trenton Group strata along Allen Rd., and values gradually rise throughout the formation. It is possible that the upper portions of the Trenton strata here may represent the transitional contact between the Sugar River and Poland members preserved in a different facies further to the west (Baird pers comm. 2012), while the *Cryptolithus* faunas preserved here may represent the equivalent of the City Brook Bed (Brett *et al*., 2004). The general trend in χ profiles between Allen Road and Canajoharie Creek is very similar. This may produce a false correlation between these localities. It is suggested that these χ values are facies dependent and record deepening upwards in both sections. Likewise, it is well understood that the Flat Creek Member strata are older than the Dolgeville Formation (Goldman *et al*., 1994).

Sections of the Trenton Group at Ingham Mills New York and those at Allen Rd. may be used to construct a composite Trenton section. Recognition of distinct grainstone ledges that occur in both sections suggests that there is a 35 cm overlap between these two sections. Additionally, the combined Trentonian thickness between the Ingham Mills and Allen Road localities, compares closely to measurements indicated in Cameron *et al*. (1972), and those of Smith *et al*., (2006), are approximately equivalent. Furthermore, the 'Abundant *Prasopora* colonies' (Smith *et al*., 2006) indicated the Sugar River Formation at Ingham Mills are not present until the last meter of Trenton strata at Allen Rd. The placement of formation boundaries at Ingham Mills indicated in Cameron *et al*. (1972), and Smith *et al*., (2006) is not coincident with observations presented here, suggesting a much thinner Kings Falls Formation and a thicker Sugar River Formation.

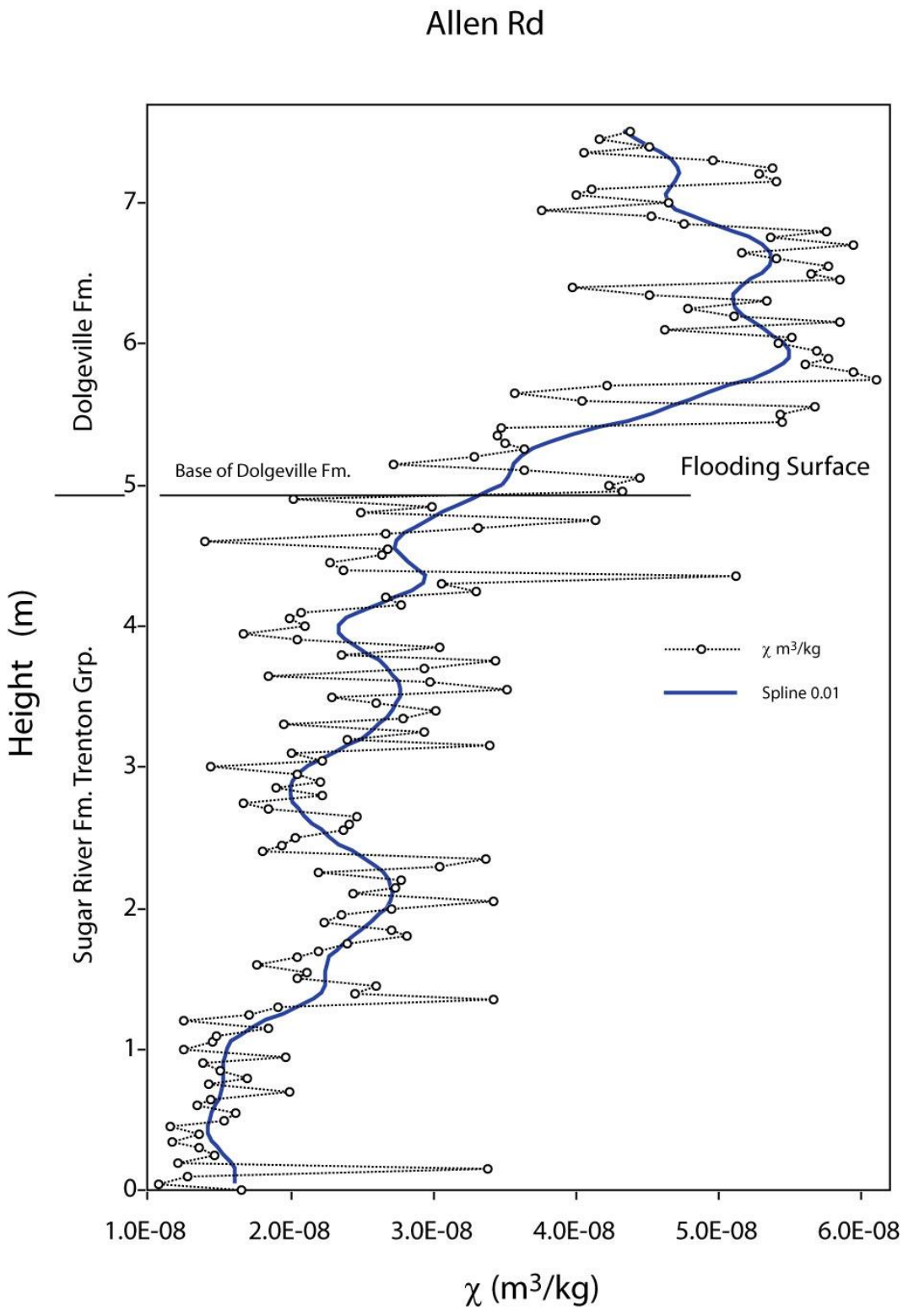

Figure 3.6 Magnetic Susceptibility (χ) profile of Beekmantown Group, Glens Falls Formation, and Utica Formation strata exposed at Canajoharie Creek New York.

Similarly, the Glens Falls Formation at Canajoharie Creek has been suggested to represent the Sugar River Formation (Fisher, 1977). It is suggested here that the lower 2.3-3 meters of the Glens Falls Formation represents Napanee Formation equivalent strata, including a similar facies and preserved gutter casts indicative of the upper portions of this interval. Due to a number of missing Trenton Formation units it is argued that the four similar χ cycles recorded at Canajoharie Creek and Allen Road are the same.

Maximum Flooding Surfaces

Maximum flooding surfaces generally are characterized by sharp shifts to higher χ values. Schramm (2011) recognized a similar pattern at the flooding surface between phosphatic grainstones of the Mt. Auburn formation and overlying dark gray shales of the Sunset formation,. The Curdsville -Logana Member contact on the Cincinnati Arch represents a flooding surface (Brett *et al.*, 2004), marked by a shift to deeper facies and shows a strong single point offset to higher χ values (Figure 2.9). These downlap surfaces represent a change to progradational stacking patterns and this increase in χ values may be associated with increased paramagnetic detrital deposition. Galloway (1989) suggested bounding sequences be placed at flooding surfaces due to their synchronous nature. Recognition of these surfaces has been possible in multiple stratigraphic successions and suggests that this is the most consistently recognizable surface in χ profiles. As demonstrated by the basal Flat Creek-Dolgeville formations this equivalent sequence stratigraphic contact is not isochronous. Thus, while correlations of these large scale shifts at maximum flooding surfaces in χ profiles may be easily possible, they likely represent lithostratigraphic boundaries and are not synchronous surfaces.

Falling Stages (Comments to be tested)

Falling stages have not been widely recognized with the Sandbian-Katian boundary interval. Schramm (2011) and Schramm *et al*. (2012B) recognized well-developed falling stage systems tracts in the Maysvillian, (Katian Stage) Hooke-Gillespie submember of the Fairview Formation. These deposits exhibit three well developed χ cycles, but do not show any other widespread shifts in χ values, other than a sharp shift to lower χ values at the overlying sequence boundary. In general, the widespread shallow carbonate seas spanning the broad Black River-Trenton interval record lowstand, and transgressive deposits. This flooding of epicontinental seas does not generally record high order-low frequency falling stage deposits. Deposits of the upper Katian stage associated with the progradation of the Queenston Delta (New York), Juniata Formation (Virginia), or Saluda Formation (Kentucky) may be better suited to record these conditions.

Transgressive-Regressive Cycles

In their early work using χ Crick *et al*., (1997) suggests a predicable χ response in relation to Transgressive-Regressive cycles. However, it is now clear that changes in sea level are not simply transgressive or regressive, but include aggradational, retrogradational, progradational, normal regressive, and forced regressive stacking patterns (Catunaneu, 2006), and should be included when interpreting χ datasets. Furthermore, truncations of sequences by erosional, or depositional hiatuses are recognized. Basin position throughout a sea-level cycle also dictates the sedimentary response, and distal vs. proximal basin positions are expected to produce a variable response.

Early χ research compared χ successions from the Devonian of North Africa with high biostratigraphic resolution to Devonian sea-level curves of Johnson et al., (1985), which are better suited to North America. While some of these many sea-level cycles may be eustatic, some North American sea-level variations may be localized or a tectonic artifact. Furthermore, these early experiments claim to occur in exclusively pelagic sequences. Most land-based stratigraphic research takes place in shallow shelf settings and epicratonic seas in which such sequences are rare. Hiatuses, storm effects, uplift, and basin rebound may all have an effect on this. It is necessary to evaluate the χ response to base level change in epicratonic seas with a thorough research history.

A compendium of sea-level such as by Johnson et al., (1985), or Brett *et al*., (2011), does not exist for the Ordovician system with adequate temporal resolution amongst multiple continents. Crick *et al.*, (1997 p. 168) recognize that "Increases in MS (χ) magnitude correspond to relative net drops in sea level. Decreasing magnitudes correspond to relative or net rises in sea level in dominantly limestone-rich successions. Lowest magnitudes represent maximum high stands in sea level. Increasing magnitudes correspond to relative or net falls in sea level."

The findings of this study on transgressive-regressive cycles are not entirely consistent with those of Crick *et al*., 1997. This may be largely a factor of this study taking place in epicontinental seas. In these settings siliciclastic sediments are sequestered in estuarine environments during sea level transgression. This results in a siliciclastic sediment starved basin in which autochthonous carbonate sediments may grow. We have generally found low χ values during lowstands and transgressions/early transgressive systems tract. Associated with highstand systems tracts the equilibrium point will shift in a seaward direction and progradation occurs, resulting in siliciclastic deposition in the basin. Here, with the Napanee Formation being

the exception, it is observed that higher χ values occurs during highstands. During tectonic deepenings such as observed at Allen Rd. and Canajoharie Creek we generally find an increase in χ values upwards. Additionally, the thinning of χ cycles is consistent with parasequence stacking patterns found during transgressions (Van Wagoner *et al*., 1988).

Idealized χ sequence stratigraphic model

A simplistic sequence stratigraphic model is presented for mixed carbonate-siliciclastic epicontinental seas (Figure 3.7). Based upon these finding we suggest an idealized depositional cycle consisting of a rapid, or no shift to lower χ values at the sequence boundary. If lowstand systems tract deposits are preserved, a spike to high, and then back to low χ values may be recorded. Values will then generally increase upwards during the transgressive systems tracts displaying four thining upwards χ cycles/parasquences, alternatively, values may remain low. At maximum flooding surfaces χ values are expected to increase rapidly. χ values are expected to remain high during the highstand systems tract, and may be hypothesized to sharply shift to lower χ values at a forced regression surface. Otherwise during late highstands/falling stages, a return to slightly lower χ values may be expected, and are expected to have internal cycles within them.

Shortcomings

A major weakness of this study is that the majority of sections studied are carbonates, or mixed carbonate-siliciclastics in epicontinental seas. It is unclear if this is simply a pattern of epicontinental seas or if the same patterns would be observed within open ocean margins. Furthermore, the temporal duration is limited only to the Sandbian-Katian boundary interval, and

Katian Stage. During this period of time shallow seas cover the North American craton and flood at the onset of the Taconic Orogeny. Thus, falling stage deposits are not readily found in this interval.

Systems Tract or Surface	χ Observations
Sequence Boundary	No shift, or shift to lower χ values
Low Stand Systems Tract	Spike from low to high to low χ values
Transgressive Systems Tract	Low or rising χ values
Maximum Flooding Surface	Shift to higher χ values

Figure 3.7 Matrix showing sequence stratigraphic systems tracts or surfaces observed in this study, and their observed changes in magnetic susceptibility (χ) values.

CONCLUSIONS

An investigation of the utility of analysis of χ profiles for interpreting sequence stratigraphy cannot be determined at this time. While single point shifts in χ values may be present at flooding surfaces, and sequence boundaries, these features are not ubiquitous. Additionally, the trends in increasing or decreasing χ values within systems tracts do not appear uniform. It is suggested that these offsets may be used to confirm the presence of existing stratigraphic surfaces, but their recognition is not entirely possible using this technique alone, and that there is no substitute for precise field investigations. Due to the nature of sequence boundaries, in which various systems tracts may truncated at unconfomities, the χ response may

be variable. This typically results to a shift to slightly lower χ values do to the nature of sedimentary stacking patterns. χ profiles appear better suited to genetic sequence stratigraphic interpretation (Galloway, 1989) as flooding surfaces are generally well preserved, associated with basinward progradational stacking patterns, basinal deposition of argillaceous sediment, and associated sharp offsets in χ values. This method is best used combined with additional methods and traditional sequence stratigraphic analysis.

REFERENCES

Baird, G.C., Brett, C.E., Lehmann, D. 1992. The Trenton-Utica problem revisited; new observations and ideas regarding Middle-Late Ordovician stratigraphy and depositional environments in central New York. *In.* April, R.H., ed. New York Geological Association Fieldtrip Guidebook, 64th annual meeting. No. 64 p. 1-40.

Baird, G.C., Brett, C.E. 2002. Indian Castle Shale: Late synorogenic siliciclastic succession in an evolving Middle to Late Ordovician foreland basin, eastern New York. P 203-230. *In* C.E. Mitchell, Jacobi, R. (eds.), Taconic Convergence: Orogen, Foreland Basin and Craton. Physics and Chemistry of Earth. 27.

Baum, G.R. and Vail, P.R. 1988. Sequence Stratigraphic concepts applied to Paleogene outcrop, gulf and atlantic basins. *In:* Sea Level Changes-and Integrate Approach, C.K. Wilgus, B.S. Hastings, C.G. St.C. Kendall, H.W. Posamentier, C.A.Ross, and J.C. Van Wagoner, Eds., pp. 309-327. SEPM Special Publication 42.

Brett, C.E., McLaughlin, P.I., Cornell, S.R., Baird, G.C., 2004. Comparative sequence stratigraphy of two classic Upper Ordovician successions, Trenton Shelf (New York-Ontario) and Lexington Platform (Kentucky-Ohio): implications for eustasy and local tectonism in eastern Laurentia. Palaeogeography, Palaeoclimatology, Paleoecology 210. 295-329.

Brett, C.E., Baird, G.C., Bartholomew, A.J., DeSantis, M.K. and Ver Straeten, C.A., 2011. Sequence stratigraphy and a revised sea-level curve for the Middle Devonian of eastern North America. Palaeogeography, Palaeoclimatology, Palaeoecology V. 304 p. 21-53.

Brett, C.E., Schramm, T.J., Dattilo, B.F., Marshall, N.T. 2012, Upper Ordovician Strata of Southern Ohio-Indiana: Shales, Shell Beds, Storms, Sediment Starvation, and Cycles. 2012 GSA North-Central Section Meeting Fieldtrip 405 Guidebook. 80 p.

Cameron, G., Mangion, S., Titus, R. 1972. Sedimentary environments and biostratigraphy of the transgressive early Trentonian sea (medial Ordovician) in central and northwestern New

York. *In:* McLelland, J. (ed.) Field Trip Guidebook. New York State Geological Association 44th Annual Meeting. Colgate University. p. H1-H39.

Catuneanu, O. 2006. Principles of Sequence Stratigraphy. Elsevier. 375 p.

Crick, R.E., Ellwood, B.B. 1997. Update on MSEC. Subcommission of Devonian Stratigraphy Newsletter No. 14. p 37-48.

Crick, R.E., Ellwood, B.B., El Hassani, A., Feist, R., and Hladil, J., 1997. MagnetoSusceptibility event and cyclostratigraphy (MSEC) of the Eifelian-Givetian GSSP and associated boundary sequences in North Africa and Europe, Episodes 20, 167-175.

Cushing, H.P. 1909. Geology of the Remsen Quadrangle: including Trenton Falls and vicinity in Oneida and Herkimer Counties. New York State Museum Bulletin, 19: 155-176.

Ellwood, B.B., Crick, R.E., El Hassani, A., 1999. The Magneto-Susceptibility Event and Cyclostratigraphic (MSEC) Method used in Geological Correlation of Devonian Rocks from Anti-Atlas Morocco. AAPG Bulletin, V. 83, No. 7

Ellwood, B.B., Crick, R.E., El Hassani, A., Benoist, S. and Young, R., 2000. MagnetoSusceptibility Event and Cyclostratigraphy (MSEC) in Marine Rocks and the Question of Detrital input versus Carbonate Productivity, Geology, 28, 135-1138.

Ellwood, B.B., Brett, C.E., and MacDonald, W.D., 2007. Magnetostratigraphy susceptibility of the Upper Ordovician Kope Formation, northern Kentucky. Palaeontology, Palaeoclimatology, Palaeoecology 243. 42-54.

Ellwood, B.B., Kafafy, A.M., Kassab, A., Tomkin, J.H., Abdedldayem, A., Obaidalla, N., Randall, K.W., Thompson, D.E., 2010. Magnetostratigraphy Susceptibility used for High-Resolution Correlation among Paleocene-Eocene boundary sequences in Egypt, Spain, and the U.S.A. Application of Modern Stratigraphic Techniques: Theory and Case Histories. SEPM Special Publication No. 94. P. 167-179.

Ellwood, B.B., Wang, W.H., Tomkin, J.H., Ratcliffe, K.T., El Hassani, A., Wright, A.M. 2013. Testing high resolution magnetic susceptibility and gamma radiation methods in the Cenomanian-Turonian (Upper Cretaceous) GSSP and near-by coeval section. Palaeogeography, Paaeoclimatology, Palaeoecology 378. 75-90.

Febo, L.A., 2007. Paleoceanography of the Gulf of Papua using multiple geophysical and micropaleontological proxies: Dissertation, Louisiana State University. P 163.

Fisher, D.W. 1954. Lower Ordovician (Canadian) stratigraphy of the Mohawk Valley. Geological Society of America Bulletin, 65: 71-96.

Fisher, D.W. 1977. Correlation of the Hadrynian, Cambrian, and Ordovician rocks in New York State. New York State Museum Map and Chart Series no. 25, 75 p.

Galloway, W.E. 1989. Genetic stratigraphic sequences in basin analysis, I. Architecture and genesis of flooding-surface bounded depositional units. American Association of Petroleum Geologists Bulletin, V. 73. p. 125-142

Goldman, D., Mitchell, C.E., Berström, S.M., Delano, J.W., Tice, S. 1994. K-bentonites and graptolite biostratigraphy in the Middle Ordovician of New York State and Quebec: A new chronostratigraphic model. Palaios v.9, p. 124-143.

Holland, S.M., Patzkowsky, M.E. 1996. Sequence stratigraphy and long-term paleoceanographic change in the Middle and Upper Ordovician of the eastern United States. Geological Society of America Special Papers. 306. P. 117-129.

Johnson, J.G., Klapper, G., Sandberg, C.A. 1985. Devonian eustatic fluctuation in Eramerica. Geological Society of America Bulletin v. 96 p. 567-587.

Kolata, D.R., Huff, W.M., and Bergström, S.M. 2001. The Ordovician Sebree Trough: An oceanic passage to the Midcontinent United States. GSA Bulletin, V. 113, p. 1067-1078

Plint, A. G., Nummendal, D. 2000. The Falling Stage Systems Tract: recognition and importance in Sequence Stratigraphy analysis. *In* Hunt, D., Gawthorpe, R.L., (eds.) Sedimentary Responses to Forced Regression. Geological Society of London Special Publication. 172.

Posamentier, H.W., Jervery, M.T., Vail, P.R. 1988. Eustatic controls on clastic deposition I – conceptual framework. *In*: Wilgus, C.K., Hastings, B.S., Kendall, C.G. St. C., Posamentier, H.W., Ross, C.A., Van Wagoner, J.C. (eds.) Sea-Level Changes: An integrated approach.Society of Economic Paleontologists and Mineralogists Special Publications. 42. 109-124.

Posamentier, H.W., Vail, P.R. 1988. Eustatic controls on clastic deposition II – sequence and systems tract models. *In*: Wilgus, C.K., Hastings, B.S., Kendall, C.G. St. C., Posamentier, H.W., Ross, C.A., Van Wagoner, J.C. (eds.) Sea-Level Changes: An integrated approach.Society of Economic Paleontologists and Mineralogists Special Publications. 42. 125-154.

Ruedemann, R. 1912. The lower Siluric shales of the Mohawk Valley. New York State Museum Bulletin 162. 151 p.

Schramm, T.J., 2011. Sequence stratigraphy of the Late Ordovician (Katian), Maysvillian Stage of the Cincinnati Arch, Indiana, Kentucky, and Ohio, U.S.A., Department of Geology. University of Cincinnati, Cincinnati, Ohio, p. 215

Schramm, T.J., Brett, C.E., Dattilo, B.F., Ellwood, B.B. 2012. Ordovician Strata of the Type North American Maysvillian Stage. *in* Brett, C.E., Cramer, B.D., and Gerkie, T.L. (*eds*) Middle Paleozoic Sequence Stratigraphy and Paleontology of the Cincinnati Arch: Part 1 Central Kentucky and Southern Ohio. International Geoscience Programme (IGCP) Project 591 Fieldtrip Guidebook. p. 113-119.

Schramm, T.J., Brett, C.E., Dattilo, B.F. 2012B. Stop 1. Rte. 11 Roadcuts, Maysville Kentucky: The Type Maysvillian. *in* Brett, C.E., Cramer, B.D., and Gerkie, T.L. (*eds*) Middle Paleozoic Sequence Stratigraphy and Paleontology of the Cincinnati Arch: Part 1 Central Kentucky and Southern Ohio. International Geoscience Programme (IGCP) Project 591 Fieldtrip Guidebook. p. 126-139.

Schramm, T.J., Brett, C.E., Dattilo, B.F., Marshall, N.T. 2012A. Stop 1. Rte. 48 Roadcut, Lawrenceburg, Indiana. *in* Brett, C.E., Cramer, B.D., and Gerkie, T.L. (*eds*) Middle Paleozoic Sequence Stratigraphy and Paleontology of the Cincinnati Arch: Part 2 Northern Kentucky and SE Indiana. International Geoscience Programme (IGCP) Project 591 Fieldtrip Guidebook. p. 35-48.

Smith, T., Agle, P., Jacobi, R., Nyahay, R., Mithcell, C. 2006. Faulting and Mineralization in the Cambro-Ordovician Section of the Mohawk Valley. NYSGA Annaul Meeting Fieldtrip Guidebook.

Sloss, L.L. (1963). Sequences in the cratonic interior of North America. Geological Society of America Bulletin, Vol. 74, p 93-114.

Ulrich, E.O., Cushing, H.P. 1910. Age and relations of the Little Falls dolomite (calciferous) of the Mohawk Valley. New York State Museum Bulletin no. 140, p. 97-140.

Van Wagoner, J.C., Posamentier, H.W., Mitchum, R.M., Vail, P.R., Sarf, J.F., Loutit, T.S., Hardenbol, J. 1988. An overview of the fundamentals of sequence stratigraphyand key definitions. *In:* Sea Level Changes-and Integrate Approach, C.K. Wilgus, B.S. Hastings, C.G. St.C. Kendall, H.W. Posamentier, C.A.Ross, and J.C. Van Wagoner, Eds., pp. 309-327. SEPM Special Publication 42.

Ver Straeten, C.A., 2007. Basinwide stratigraphic synthesis and sequence stratigraphy, upper Pragian, Emsian, and Eifelian stages (Lower to Middle Devonian), Appalachian Basin. *in*: Becker R.C., and Kirchgasser, W.T. *Eds.* Devonian Events and Correlations. Geological Society Special Publication 278 p. 39- 82.

APPENDIX I
"Z-BED" SECTIONS SAMPLED

1) Lawrenceburg, IN. Rt. 48 (N 39° 5'45.03" W 84°52'32.43")

2) Wesselman Creek OH (N 39°10'55.23" W 84°41'12.91")

3) Rapid Run, OH (N 39° 6'9.78" W 84°38'43.20")

4) Bald Knob, Cincinnati, Ft. Wright OH. (N 39° 7'8.62"W 84°32'53.92")

5) I-275@I-471 (N 39° 2'42.02" W 84°27'57.39")

6) Independence KY. Rt. 17 (N 38°58'48.84" W 84°31'55.43")

7) Reidlin-Mason Road, KY. (N 39° 1'41.48" W 84°30'40.02")

8) AA Highway at Poplar Ridge Rd. (N 38°58'50.16" W 84°22'21.66")

9) AA Highway at Dead Timber (N 38°55'45.30" W 84°18'21.87")

10) AA Highway at Rt. 1019 (N 38°46'24.42" W 84°12'21.00")

11) AA Highway at Rt. 19 (N 38°43'53.52" W 84° 1'36.54")

12) Maysville, KY. Rt. 3056 (New 62-68) (N 38°40'27.54" W 83°47'51.58")

13) Maysville, KY. Old Rt. 62-68 (N 38°38'26.84" W 83°46'0.73")

14) Maysville KY. Rt. 11 (N 38°36'50.93" W 83°45'18.86")

15) Johnson Creek Rt. 68 Just south of Mayslick KY. (Blue Lick Battle Field) (N 38°28'15.90" W 83°54'27.44")

16) Sherburne KY. Rt. 11 (N 38°16'34.83" W 83°48'36.43")

17) Winchester KY. I-64/Mount Sterling (N 38° 3'26.89" W 84° 2'48.14")

18) Caldwell Park Cincinnati OH (N 39°12'15.36" W 84°29'43.40")

19) Sycamore Creek, Indian Hill, OH. (N 39°12'27.13" W 84°20'12.40")

20) 2nd Creek, Morrow, OH. (N 39°20'34.48"W 84° 7'49.27")

21) Cincinnati Nature Center. (N 39° 7'24.42" W 84°14'35.76")

22) Backbone Creek, Batavia, OH.(N 39° 5'31.50"W 84° 9'50.34")

23) Montery KY. Rt. 126 (Brachiopod Heaven) (N 38°27'2.49" W 84°51'10.44")

24) Taylorsville KY. Rt. 44 (N 38° 2'17.47" W 85°19'33.22")

25) Taylorsville KY. Rt. 55 (N 38° 3'6.50"W 85°20'29.43")

26) Blue Grass Pkwy. Mile 39 (N 37°52'33.90" W 85°12'9.24")

27) Boonesborough KY. Rt. 627 (N 37°53'30.75" W 84°16'41.71")

APPENDIX II
"Z-BED" χ VALUES

I275 at I471

Height (m)	Mass (g)	χ m^3/kg	Standard Deviation
0	17.212	1.88E-08	2.57E-10
0.05	20.743	1.51E-08	2.13E-10
0.1	21.045	1.19E-08	1.21E-10
0.15	19.93	1.44E-08	3.39E-10
0.2	17.762	3.55E-08	4.28E-10
0.25	18.595	1.43E-08	3.63E-10
0.3	16.78	1.68E-08	5.49E-10
0.35	13.459	2.32E-08	5.69E-10
0.4	15.991	1.34E-08	2.22E-16
0.45	14.687	1.38E-08	3.48E-10
0.5	14.283	1.39E-08	6.20E-10
0.55	15.78	1.24E-08	5.85E-10
0.6	16.76	1.70E-08	4.57E-10
0.65	14.736	1.61E-08	5.20E-10
0.7	14.561	1.02E-07	3.42E-10
0.75	17.175	9.98E-08	1.50E-10
0.8	16.303	1.28E-07	1.58E-10
0.85	17.072	1.22E-07	4.52E-10
0.9	15.584	1.14E-07	2.87E-10
0.95	18.192	1.09E-07	2.83E-10
1	18.393	1.10E-07	1.40E-10
1.05	16.065	1.21E-07	4.24E-10
1.1	20.401	4.15E-08	3.71E-10
1.15	15.015	1.25E-07	6.19E-10
1.2	13.78	3.08E-08	6.66E-10
1.25	17.468	1.04E-07	1.26E-15
1.3	19.038	1.19E-07	1.35E-10
1.35	16.515	1.07E-07	5.41E-10
1.4	20.056	1.02E-07	1.28E-10
1.45	19.75	9.47E-08	0
1.5	15.144	1.10E-07	6.14E-10
1.55	18.833	1.12E-07	3.62E-10
1.6	15.914	9.36E-08	5.43E-10
1.65	16.67	1.13E-07	2.68E-10

AA Highway at Rt. 19

Height (m)	Mass (g)	χ m^3/kg	Standard Deviation
0	10.006	2.20E-08	7.67E-10

Height (m)	Mass (g)	χ m^3/kg	Standard Deviation
0.05	17.477	2.10E-08	2.53E-10
0.1	16.43	1.97E-08	2.22E-16
0.15	15.373	1.76E-08	4.40E-10
0.2	20.918	3.79E-08	3.63E-10
0.25	18.344	1.11E-07	3.71E-10
0.3	21.245	9.54E-08	3.21E-10
0.35	19.882	2.60E-08	1.28E-10
0.4	18.848	2.53E-08	3.57E-10
0.45	16.519	1.33E-07	0
0.5	21.376	1.04E-07	3.61E-10
0.55	16.948	1.35E-07	5.26E-10
0.6	17.758	1.59E-08	1.44E-10
0.65	13.69	9.60E-08	3.16E-10
0.7	17.48	2.21E-08	3.86E-10
0.75	15.515	1.24E-07	4.39E-10
0.8	16.612	1.21E-07	4.10E-10
0.85	16.339	1.69E-08	4.14E-10
0.9	15.09	1.26E-07	2.96E-10
0.95	17.728	3.19E-08	4.30E-10
1	20.768	1.34E-07	2.47E-10
1.05	18.118	5.08E-08	4.82E-10
1.1	21.451	2.85E-08	3.13E-10
1.15	16.484	2.85E-08	4.63E-10
1.2	17.304	2.32E-08	1.47E-10
1.25	14.25	1.32E-07	4.78E-10
1.3	18.158	1.28E-07	1.42E-10
1.35	19.741	2.50E-08	4.65E-10
1.4	16.089	1.27E-07	3.20E-10
1.45	18.906	1.26E-07	4.90E-10
1.5	20.392	1.22E-07	3.33E-10
1.55	18.026	1.25E-07	5.15E-10
1.6	17.896	1.19E-07	3.81E-10
1.65	15.058	1.28E-07	4.53E-10
1.7	17.172	1.22E-07	4.50E-10
1.75	17.583	1.23E-07	4.39E-10
1.8	14.704	1.23E-07	3.04E-10
1.85	18.667	1.11E-07	3.65E-10
1.9	14.212	1.29E-07	1.81E-10
1.95	23.101	1.07E-07	1.78E-15
2	15.396	1.23E-07	1.67E-10
2.05	15.247	7.96E-08	2.85E-10
2.1	19.792	1.17E-07	1.30E-10
2.15	17.062	1.22E-07	1.51E-10
2.2	12.022	1.15E-07	4.16E-10
2.25	17.644	1.19E-07	4.38E-10

Height (m)	Mass (g)	χ m^3/kg	Standard Deviation
2.3	16.927	8.93E-08	4.42E-10
2.35	13.877	1.15E-07	4.74E-10
2.4	14.92	2.18E-08	4.52E-10
2.45	20.555	1.56E-08	1.24E-10
2.5	15.477	8.14E-08	3.24E-10
2.55	15.047	1.01E-07	0
2.6	14.793	1.26E-07	5.23E-10
2.65	19.373	1.21E-07	1.33E-10
2.7	17.145	1.24E-07	5.41E-10
2.75	19.947	1.16E-07	4.65E-10
2.8	17.864	1.11E-07	5.20E-10
2.85	17.149	1.11E-07	1.50E-10
2.9	22.8	5.71E-08	2.19E-10

AA Highway at Rt. 1019

Height (m)	Mass (g)	χ m^3/kg	Standard Deviation
0	19.859	2.66E-08	2.22E-10
0.05	16.18	2.98E-08	5.67E-10
0.1	18.356	2.17E-08	4.81E-10
0.15	17.417	4.57E-08	2.90E-10
0.2	17.24	1.39E-08	3.92E-10
0.25	15.835	1.43E-08	5.59E-10
0.3	16.501	1.65E-08	5.58E-10
0.35	17.116	9.28E-09	5.98E-10
0.4	20.475	1.83E-08	1.24E-10
0.45	17.463	1.22E-07	3.90E-10
0.5	22.309	1.08E-08	5.25E-10
0.55	19.34	9.74E-08	3.53E-10
0.6	16.645	1.13E-07	2.68E-10
0.65	15.968	1.30E-08	5.77E-10
0.7	16.763	1.86E-08	2.64E-10
0.75	16.645	1.17E-07	4.10E-10
0.8	22.628	1.14E-07	3.93E-10
0.85	20.137	2.95E-08	2.52E-10
0.9	16.735	1.11E-07	4.08E-10
0.95	19.405	1.04E-07	3.51E-10
1	18.995	1.06E-07	5.42E-10
1.05	18.986	1.02E-07	4.89E-10
1.1	17.368	1.10E-07	5.93E-10
1.15	18.623	6.19E-08	1.35E-10
1.2	18.374	1.08E-07	5.05E-10
1.25	19.738	1.17E-07	4.51E-10
1.3	13.872	1.08E-07	1.80E-10
1.35	19.01	1.17E-07	4.88E-10

Height (m)	Mass (g)	χ m^3/kg	Standard Deviation
1.4	19.667	1.13E-07	3.46E-10
1.45	19.731	1.01E-07	3.45E-10
1.5	16.621	1.08E-07	5.59E-10
1.55	23.319	1.01E-07	3.98E-10
1.6	18.454	1.13E-07	4.19E-10
1.65	17.894	1.38E-08	4.95E-10
1.7	15.212	2.35E-08	6.70E-10
1.75	19.216	1.18E-07	5.35E-10
1.8	20.399	1.09E-07	5.05E-10
1.85	16.334	9.69E-08	4.03E-10
1.9	21.554	1.45E-08	3.55E-10
1.95	18.191	1.04E-08	2.81E-10
2	16.016	1.24E-07	4.82E-10
2.05	19.841	1.21E-07	2.24E-10
2.1	19.105	1.29E-07	4.04E-10
2.15	18.212	1.22E-07	2.45E-10
2.2	19.193	1.09E-07	4.02E-10
2.25	18.049	1.10E-07	5.15E-10
2.3	17.524	1.10E-07	3.89E-10
2.35	18.244	1.03E-07	4.24E-10
2.4	19.563	7.79E-08	1.27E-10
2.45	12.856	8.96E-08	3.90E-10
2.5	19.406	1.12E-07	3.51E-10
2.55	13.459	1.07E-08	3.30E-10
2.6	7.033	1.56E-08	1.31E-09

AA Highway at Dead Timber

Height (m)	Mass (g)	χ m^3/kg	Standard Deviation
0	13.869	2.29E-08	5.52E-10
0.05	18.26	1.72E-08	2.80E-10
0.1	18.037	1.71E-08	1.42E-10
0.15	17.885	2.18E-08	3.77E-10
0.2	17.414	1.70E-08	2.54E-10
0.25	19.259	3.56E-08	3.48E-10
0.3	19.968	4.90E-08	6.28E-16
0.35	17.987	1.25E-08	1.42E-10
0.4	19.375	1.67E-08	3.95E-10
0.45	20.603	2.07E-08	2.14E-10
0.5	18.96	1.70E-08	2.69E-10
0.55	17.786	1.22E-07	0
0.6	15.592	1.20E-07	4.37E-10
0.65	16.394	1.24E-07	4.71E-10
0.7	20.322	1.27E-07	2.53E-10
0.75	18.624	1.09E-07	2.40E-10

0.8	16.819	9.94E-08	3.07E-10
0.85	17.433	9.60E-08	2.56E-10
0.9	16.524	2.28E-08	4.63E-10
0.95	20.843	2.04E-08	3.67E-10
1	18.454	1.21E-07	4.18E-10
1.05	14.341	1.19E-07	5.40E-10
1.1	15.522	8.36E-08	1.61E-10
1.15	19.644	1.08E-07	4.54E-10
1.2	18.346	1.06E-07	1.40E-10
1.25	17.391	1.29E-07	1.48E-10
1.3	14.849	1.20E-07	4.59E-10
1.35	17.564	1.10E-07	1.47E-10
1.4	14.886	1.23E-07	3.00E-10
1.45	16.49	1.25E-07	4.68E-10
1.5	18.801	1.21E-07	2.37E-10
1.55	18.38	1.22E-07	3.70E-10

AA Highway at Poplar Ridge

Height (m)	Mass (g)	χ m^3/kg	Standard Deviation
0	16.122	2.06E-08	1.58E-10
0.05	14.988	2.00E-08	6.14E-10
0.1	16.191	1.96E-08	4.73E-10
0.15	19.055	2.02E-08	3.54E-10
0.2	15.263	3.26E-08	3.33E-10
0.25	18.935	1.97E-08	2.69E-10
0.3	15.52	9.18E-08	3.22E-10
0.35	15.406	9.35E-08	5.84E-10
0.4	16.515	1.23E-07	4.13E-10
0.45	15.711	1.23E-07	4.92E-10
0.5	21.315	1.57E-08	4.15E-10
0.55	14.61	1.11E-07	2.95E-10
0.6	16.34	1.64E-08	1.56E-10
0.65	16.862	2.30E-08	0
0.7	18.936	1.22E-07	4.07E-10
0.75	18.685	1.21E-07	4.13E-10
0.8	14.919	1.22E-07	0
0.85	17.04	1.28E-07	2.62E-10
0.9	14.342	1.32E-07	3.11E-10
0.95	18.202	1.17E-07	2.83E-10
1	17.679	1.19E-07	3.85E-10
1.05	16.634	1.23E-07	4.10E-10
1.1	19.054	1.17E-07	2.70E-10
1.15	17.541	1.12E-07	1.47E-10
1.2	15.922	1.29E-07	3.23E-10
1.25	14.071	1.12E-07	6.13E-10

Height (m)	Mass (g)	χ m^3/kg	Standard Deviation
1.3	13.877	1.34E-07	3.22E-10
1.35	18.916	1.27E-07	4.90E-10
1.4	18.392	1.11E-07	1.40E-10
1.45	16.716	9.32E-08	2.58E-10
1.5	13.501	1.12E-07	6.65E-10
1.55	19.442	8.02E-08	2.56E-10
1.6	18.166	1.14E-07	3.75E-10
1.65	16.98	1.01E-07	4.56E-10

Backbone Creek

Height (m)	Mass (g)	χ m^3/kg	Standard Deviation
0	11.439	2.64E-08	6.70E-10
0.05	10.684	2.30E-08	6.33E-10
0.1	12.996	3.36E-08	5.88E-10
0.15	11.996	2.20E-08	6.39E-10
0.2	16.885	2.10E-08	4.00E-10
0.25	13.437	2.03E-08	7.60E-10
0.3	10.668	2.64E-08	8.63E-10
0.35	14.482	2.26E-08	4.66E-10
0.4	9.01	1.29E-07	0
0.45	14.861	1.22E-07	3.47E-10
0.5	12.66	1.25E-07	5.90E-10
0.55	13.578	1.25E-07	5.03E-10
0.6	10.565	1.28E-07	8.20E-10
0.65	14.031	1.24E-07	5.51E-10
0.7	12.326	1.22E-07	7.29E-10
0.75	11.696	1.17E-07	5.65E-10
0.8	12.091	1.05E-07	7.47E-10
0.85	14.139	1.23E-07	3.16E-10
0.9	15.121	1.13E-07	4.51E-10
0.95	13.219	1.14E-07	6.53E-10
1	14.408	1.26E-07	1.79E-10
1.05	14.683	1.06E-07	4.49E-10
1.1	11.314	1.20E-07	4.42E-10

Blue Grass Pkwy Mile 39

Height (m)	Mass (g)	χ m^3/kg	Standard Deviation
0	14.859	1.63E-08	5.96E-10
0.05	12.446	2.83E-08	8.20E-10
0.1	11.781	2.45E-08	4.33E-10
0.15	10.029	2.41E-08	7.64E-10
0.2	10.878	7.71E-08	2.32E-10

Height (m)	Mass (g)	χ m^3/kg	Standard Deviation
0.25	13.176	1.04E-07	6.84E-10
0.3	15.268	3.87E-08	4.40E-10
0.35	12.707	9.85E-08	3.41E-10
0.4	11.258	1.19E-07	8.01E-10
0.45	11.692	5.29E-08	2.17E-10
0.5	9.991	1.22E-07	4.35E-10
0.55	11.904	1.08E-07	6.31E-10
0.6	11.773	9.50E-08	3.70E-10
0.65	11.554	1.05E-07	7.82E-10
0.7	11.943	1.14E-07	4.19E-10
0.75	9.746	1.35E-07	6.79E-10
0.8	14.013	6.30E-08	3.12E-10
0.85	12.114	1.22E-07	2.06E-10
0.9	12.209	9.68E-08	3.56E-10
0.95	13.384	8.75E-08	6.49E-10
1	13.835	9.63E-08	1.81E-10
1.05	11.885	1.10E-07	4.21E-10
1.1	13.655	6.18E-08	4.89E-10

Brachiopod Heaven Montery KY, Rt. 127

Height (m)	Mass (g)	χ m^3/kg	Standard Deviation
0	13.296	1.19E-08	5.09E-10
0.05	13.436	1.05E-08	6.87E-10
0.1	15.031	1.24E-08	1.70E-10
0.15	14.506	8.95E-09	1.77E-10
0.2	15.444	9.70E-09	4.97E-10
0.25	12.507	3.02E-08	3.53E-10
0.3	10.952	1.55E-08	4.67E-10
0.35	9.313	9.46E-08	7.17E-10
0.4	11.636	9.96E-08	4.31E-10
0.45	11.989	8.20E-08	8.40E-10
0.5	13.485	8.42E-09	3.80E-10
0.55	13.069	8.69E-09	3.92E-10
0.6	12.559	9.65E-08	2.00E-10
0.65	12.676	8.96E-09	2.02E-10
0.7	12.954	1.78E-08	6.84E-10
0.75	12.103	4.96E-08	5.55E-10
0.8	13.261	1.07E-07	3.26E-10
0.85	11.81	1.02E-07	7.35E-10
0.9	12.427	8.84E-08	4.04E-10
0.95	11.574	9.91E-08	2.17E-10
1	10.245	1.09E-07	8.84E-10
1.05	10.522	1.12E-07	6.31E-10

Bald Knob Cincinnati Ohio

Height (m)	Mass (g)	χ m^3/kg	Standard Deviation
0	10.372	1.62E-08	6.53E-10
0.1	11.665	1.22E-08	7.91E-10
0.19	9.308	1.67E-08	9.53E-10
0.29	11.855	1.15E-07	7.60E-10
0.39	10.72	1.06E-07	6.20E-10

Boonesborough KY, Rt. 627

Height (m)	Mass (g)	χ m^3/kg	Standard Deviation
0	13.858	1.12E-08	5.54E-10
0.05	11.475	2.05E-08	4.45E-10
0.1	13.815	1.66E-08	4.90E-10
0.15	11.558	1.62E-08	3.83E-10
0.2	15.265	3.33E-08	1.67E-10
0.25	15.221	1.80E-08	2.91E-10
0.3	10.311	9.45E-08	4.23E-10
0.35	13.338	1.05E-07	6.75E-10
0.4	13.757	1.03E-07	4.80E-10
0.45	14.979	7.27E-08	4.44E-10
0.5	11.881	3.34E-08	5.67E-10
0.55	14.279	9.34E-08	4.63E-10
0.6	13.023	8.97E-08	5.10E-10
0.65	12.212	9.74E-08	4.11E-10
0.7	10.161	1.15E-07	4.94E-10
0.75	11.207	8.09E-08	5.95E-10

Cincinnati Nature Center

Height (m)	Mass (g)	χ m^3/kg	Standard Deviation
0	10.477	1.83E-08	9.77E-10
0.05	12.442	1.71E-08	4.11E-10
0.1	11.56	2.87E-08	5.84E-10
0.15	10.681	2.54E-08	6.33E-10
0.2	14.368	2.29E-08	3.08E-10
0.25	12.842	2.60E-08	6.88E-10
0.3	10.428	3.34E-08	4.89E-10
0.35	11.552	2.42E-08	3.83E-10
0.4	11.676	9.82E-08	8.60E-10
0.45	13.982	1.13E-07	3.08E-10
0.5	13.34	1.09E-07	4.95E-10
0.55	10.148	1.14E-07	4.95E-10
0.6	10.309	1.20E-07	7.29E-10

Height (m)	Mass (g)	χ m^3/kg	Standard Deviation
0.65	11.989	1.12E-07	7.52E-10
0.7	10.218	1.25E-07	6.48E-10
0.75	15.12	9.26E-08	5.72E-10
0.8	9.412	1.14E-07	9.63E-10
0.85	11.104	1.22E-07	5.96E-10
0.9	10.382	1.25E-07	9.64E-10
0.95	8.272	1.23E-07	6.08E-10
1	9.86	1.14E-07	7.64E-10
1.05	11.367	9.18E-08	3.83E-10
1.1	11.297	1.12E-07	4.43E-10

Caldwell Park Cincinnati, OH

Height (m)	Mass (g)	χ m^3/kg	Standard Deviation
0	10.807	1.92E-08	6.26E-10
0.05	11.144	1.75E-08	6.07E-10
0.1	14.219	7.33E-08	1.77E-10
0.15	15.106	2.07E-08	2.93E-10
0.2	13.626	1.78E-08	6.50E-10
0.25	12.978	1.66E-08	3.41E-10
0.3	12.141	2.22E-08	3.64E-10
0.35	9.645	2.94E-08	5.30E-10
0.4	15.684	5.53E-08	2.79E-10
0.45	10.128	1.11E-07	8.94E-10
0.5	13.08	3.63E-08	3.37E-10
0.55	10.435	1.02E-07	6.37E-10
0.6	11.604	1.17E-07	2.15E-10
0.65	9.78	7.64E-08	9.33E-10
0.7	11.803	1.15E-07	6.35E-10
0.75	12.484	1.25E-07	5.28E-10
0.8	10.544	1.29E-07	4.74E-10
0.85	11.494	1.26E-07	8.68E-10
0.9	13.042	1.14E-07	6.89E-10
0.95	10.728	2.10E-08	7.15E-10
1	10.15	1.15E-07	8.56E-10
1.05	10.136	2.16E-08	9.09E-10
1.1	9.6	1.22E-07	1.05E-09
1.15	10.595	1.26E-07	6.24E-10
1.2	11.954	2.74E-07	5.67E-10
1.25	11.64	4.28E-08	2.18E-10
1.3	11.795	1.17E-07	4.24E-10
1.35	11.188	2.70E-08	4.44E-16
1.4	12.923	1.61E-08	3.96E-10
1.45	12.073	2.48E-08	2.11E-10
1.5	13.18	2.75E-08	3.87E-10

Height (m)	Mass (g)	χ m^3/kg	Standard Deviation
1.55	11.765	1.00E-07	7.39E-10
1.6	10.407	1.04E-07	8.37E-10
1.65	11.274	1.06E-07	7.71E-10
1.7	9.626	1.05E-07	9.43E-10
1.75	7.879	1.12E-07	3.20E-10
1.8	11.596	1.03E-07	4.33E-10
1.85	9.463	1.04E-07	7.04E-10
1.9	10.317	1.08E-07	8.78E-10
1.95	10.675	9.57E-08	8.17E-10

Independence KY, Rt. 17

Height (m)	Mass (g)	χ m^3/kg	Standard Deviation
0	13.89	1.36E-08	3.68E-10
0.1	10.82	1.33E-08	4.10E-10
0.2	10.492	1.48E-08	7.32E-10
0.3	10.558	1.13E-08	8.75E-10
0.4	13.851	1.11E-07	3.11E-10
0.48	11.748	2.08E-08	5.76E-10
0.58	13.452	1.13E-07	6.68E-10
0.68	12.12	1.20E-07	7.13E-10

Johnson Creek, Mayslick KY.

Height (m)	Mass (g)	χ m^3/kg	Standard Deviation
0	15.083	2.78E-08	4.47E-10
0.05	15.185	2.47E-08	4.44E-10
0.1	19.458	1.10E-07	4.77E-10
0.15	18.726	1.18E-07	1.37E-10
0.2	16.153	1.84E-08	4.18E-10
0.25	17.432	1.15E-07	3.91E-10
0.3	14.666	1.20E-07	3.05E-10
0.35	20.45	1.46E-08	1.25E-10
0.4	16.036	1.43E-08	1.59E-10
0.45	19.141	1.37E-08	1.33E-10
0.5	15.977	4.24E-08	1.59E-10
0.55	20.636	2.19E-08	2.47E-10
0.6	18.678	1.05E-07	1.38E-10
0.65	17.141	1.19E-07	2.60E-10
0.7	17.757	1.13E-07	2.90E-10
0.75	15.699	1.19E-07	2.84E-10
0.8	14.569	1.01E-07	3.42E-10
0.85	13.084	1.89E-08	3.38E-10
0.9	18.043	1.26E-07	4.94E-10

Height (m)	Mass (g)	χ m^3/kg	Standard Deviation
0.95	19.87	1.26E-07	1.29E-10
1	15.754	7.26E-08	4.22E-10
1.05	16.041	1.23E-07	1.61E-10
1.1	19.81	1.19E-07	5.19E-10
1.15	17.247	1.14E-07	2.99E-10
1.2	18.089	1.28E-07	3.76E-10
1.25	18.264	1.23E-07	3.73E-10
1.3	17.023	1.30E-07	3.02E-10
1.35	17.455	2.87E-08	4.37E-10
1.4	16.674	1.34E-07	4.08E-10
1.45	17.82	5.21E-08	3.74E-10
1.5	21.215	9.76E-08	3.21E-10
1.55	18.276	1.14E-07	1.41E-10
1.6	17.97	1.22E-07	3.79E-10
1.65	17.508	1.18E-07	3.89E-10
1.7	19.298	1.23E-07	4.80E-10
1.75	18.16	6.57E-08	0
1.8	13.308	1.36E-07	1.94E-10
1.85	14.388	1.26E-07	3.58E-10
1.9	16.222	7.31E-08	4.09E-10
1.95	14.946	1.01E-07	0
2	17.609	7.14E-08	4.93E-10
2.05	16.502	7.02E-08	3.04E-10
2.1	10.9	6.61E-08	8.37E-10
2.15	17.311	9.00E-08	4.31E-10
2.2	17.293	1.18E-07	5.16E-10
2.25	16.056	1.15E-07	3.21E-10

Lawrenceburg IN, Rt. 48

Height (m)	Mass (g)	χ m^3/kg	Standard Deviation
0	9.981	2.04E-08	4.44E-10
0.1	10.766	1.37E-08	4.76E-10
0.2	10.249	1.13E-08	5.00E-10
0.3	10.19	5.01E-08	8.99E-10
0.4	10.183	9.53E-08	2.47E-10
0.45	10.017	3.68E-08	5.09E-10
0.5	10.555	7.88E-08	8.63E-10
0.6	9.923	9.76E-08	8.79E-10
0.7	10.191	9.33E-08	2.47E-10
0.8	10.483	1.13E-07	8.29E-10
0.9	10.334	1.03E-07	6.44E-10
1	10.432	3.15E-08	7.34E-10
1.1	9.594	5.27E-08	5.30E-10
1.2	10.176	3.97E-08	8.67E-10

2nd Creek, Morrow OH,

Height (m)	Mass (g)	χ m^3/kg	Standard Deviation
0	12.811	3.11E-08	6.89E-10
0.05	12.055	1.65E-08	3.68E-10
0.1	11.085	1.60E-08	4.00E-10
0.15	12.291	1.60E-08	7.50E-10
0.2	10.654	1.92E-08	0
0.25	9.906	2.01E-08	4.47E-10
0.3	8.3	1.67E-08	5.34E-10
0.35	7.996	1.47E-08	0
0.4	15.341	1.55E-08	4.41E-10
0.45	10.645	1.49E-08	6.36E-10
0.5	13.22	1.50E-08	3.35E-10
0.55	11.634	1.68E-08	5.82E-10
0.6	10.537	3.96E-08	6.40E-10
0.65	10.874	1.06E-07	8.32E-10
0.7	13.036	1.06E-07	3.32E-10
0.75	11.66	1.18E-08	4.39E-10
0.8	11.085	1.18E-07	0
0.85	11.013	1.05E-07	6.84E-10
0.9	10.845	1.08E-07	6.12E-10
0.95	8.799	2.38E-08	5.03E-10
1	12.961	1.08E-07	5.10E-10
1.05	11.31	9.68E-08	5.88E-10
1.1	11.29	2.27E-08	8.16E-10
1.15	12.479	9.97E-08	5.31E-10
1.2	13.164	1.01E-07	6.85E-10
1.25	13.3	1.00E-07	3.26E-10

Maysville KY, Rt. 3056

Height (m)	Mass (g)	χ m^3/kg	Standard Deviation
0	12.478	1.35E-08	8.20E-10
0.05	15.343	1.22E-08	1.57E-16
0.1	15.588	1.51E-08	3.28E-10
0.15	11.748	1.66E-08	5.76E-10
0.2	12.267	1.74E-08	7.52E-10
0.25	13.341	1.30E-08	7.67E-10
0.3	9.228	2.07E-08	7.33E-10
0.35	10.215	1.63E-08	0
0.4	13.736	1.27E-08	1.86E-10
0.45	11.206	1.17E-07	3.87E-10
0.5	10.435	1.08E-07	1.78E-15
0.55	12.724	1.46E-08	4.02E-10
0.6	11.875	2.60E-08	7.75E-10

Height (m)	Mass (g)	χ m^3/kg	Standard Deviation
0.65	11.166	1.15E-07	2.24E-10
0.7	11.25	1.19E-07	2.22E-10
0.75	10.9	1.15E-07	3.98E-10
0.8	11.571	1.12E-07	5.72E-10
0.85	10.773	1.18E-07	1.26E-15
0.9	11.081	1.58E-08	4.62E-10
0.95	12.977	2.32E-08	3.41E-10
1	14.406	1.47E-08	4.70E-10
1.05	14.667	1.27E-07	4.65E-10
1.1	10.663	1.12E-07	6.22E-10
1.15	13.368	1.17E-07	6.45E-10
1.2	12.226	1.30E-07	5.38E-10
1.25	12.195	1.20E-07	3.54E-10
1.3	12.608	1.21E-07	1.98E-10
1.35	15.68	1.19E-07	5.93E-10
1.4	11.868	1.19E-07	5.57E-10
1.45	15.496	1.12E-07	4.99E-10
1.5	14.395	1.15E-07	5.38E-10
1.55	13.632	1.09E-07	3.66E-10
1.6	10.835	1.21E-07	8.32E-10
1.65	12.394	1.17E-07	6.97E-10
1.7	13.175	1.20E-07	3.27E-10
1.75	12.852	1.19E-07	5.13E-10
1.8	13.539	3.44E-08	4.97E-10
1.85	11.289	2.85E-08	2.26E-10
1.9	11.596	5.70E-08	2.19E-10
1.95	10.805	1.22E-07	9.26E-10
2	11.468	9.81E-08	2.19E-10

Maysville KY, Old Rt. 62-68

Height (m)	Mass (g)	χ m^3/kg	Standard Deviation
0	11.075	4.29E-08	6.89E-10
0.05	14.812	2.66E-08	2.98E-10
0.1	12.519	1.46E-08	0
0.15	16.472	1.35E-08	4.11E-10
0.2	18.484	1.50E-08	2.76E-10
0.25	16.287	1.87E-08	1.57E-10
0.3	17.162	1.03E-08	2.58E-10
0.35	18.96	1.11E-07	4.70E-10
0.4	19.254	1.01E-07	3.54E-10
0.45	11.9	2.22E-08	6.44E-10
0.5	13.962	1.68E-08	1.83E-10
0.55	16.568	1.06E-07	5.61E-10
0.6	17.291	1.17E-07	5.16E-10

Height (m)	Mass (g)	χ m^3/kg	Standard Deviation
0.65	16.36	1.09E-07	1.58E-10
0.7	17.928	1.06E-07	3.80E-10
0.75	17.588	1.27E-08	5.81E-10
0.8	19.634	1.82E-08	1.30E-10
0.85	12.699	1.44E-08	3.49E-10
0.9	19.15	1.24E-08	2.67E-10
0.95	15.907	1.04E-07	1.62E-10
1	15.255	1.17E-07	3.38E-10
1.05	17.362	3.43E-08	3.87E-10
1.1	17.212	1.04E-07	5.40E-10
1.15	18.639	1.08E-07	1.38E-10
1.2	16.39	2.40E-08	2.69E-10
1.25	10.879	1.03E-07	6.93E-10
1.3	11.975	1.17E-07	4.17E-10
1.35	11.265	9.58E-08	5.90E-10
1.4	19.764	1.07E-07	3.45E-10
1.45	15.71	1.09E-07	4.34E-10
1.5	17.042	1.01E-07	4.00E-10
1.55	13.729	1.21E-07	1.88E-10
1.6	16.805	7.11E-08	3.95E-10
1.65	14.391	9.73E-08	3.01E-10
1.7	16.116	7.97E-08	3.11E-10
1.75	17.736	1.07E-07	4.36E-10
1.8	15.623	6.17E-08	2.79E-10
1.85	16.989	2.10E-08	3.97E-10
1.9	18.926	7.27E-08	4.76E-10
1.95	15.993	1.15E-08	4.23E-10
2	12.575	5.23E-08	6.05E-10
2.05	15.957	1.07E-07	4.28E-10
2.1	13.061	1.04E-07	5.06E-10
2.15	12.106	1.13E-08	5.60E-10
2.2	16.672	1.02E-07	1.55E-10
2.25	16.673	9.52E-08	1.49E-10

Maysville KY, Rt. 11

Height (m)	Mass (g)	χ m^3/kg	Standard Deviation
0	11.159	1.75E-08	4.58E-10
0.05	10.419	1.96E-08	4.25E-10
0.1	12.004	2.11E-08	0
0.15	10.931	1.57E-08	0
0.2	10.378	1.57E-08	6.53E-10
0.25	11.115	1.51E-08	4.61E-10
0.3	12.714	1.02E-08	4.03E-10
0.35	13.735	1.08E-08	4.93E-10

Height (m)	Mass (g)	χ m^3/kg	Standard Deviation
0.4	9.904	1.93E-08	6.83E-10
0.45	16.145	1.13E-08	2.74E-10
0.5	13.442	1.32E-08	3.30E-10
0.55	9.595	1.50E-08	9.24E-10
0.6	13.637	1.70E-08	3.25E-10
0.65	11.892	1.37E-08	5.69E-10
0.7	16.84	1.08E-07	1.53E-10
0.75	13.646	9.99E-08	3.17E-10
0.8	13.228	1.58E-08	3.35E-10
0.85	12.067	1.81E-08	2.12E-10
0.9	11.044	1.04E-07	6.01E-10
0.95	12.112	1.16E-07	4.12E-10
1	11.345	1.30E-07	5.82E-10
1.05	10.3	8.60E-08	4.98E-08
1.1	12.396	1.18E-07	4.02E-10
1.15	13.813	1.04E-07	5.42E-10
1.2	19.136	1.10E-07	2.69E-10
1.25	18.562	1.17E-07	2.77E-10
1.3	11.455	1.13E-07	3.78E-10
1.35	11.931	9.97E-08	2.10E-10
1.4	11.506	1.22E-07	4.34E-10
1.45	14.767	1.17E-07	3.49E-10
1.5	18.482	1.21E-07	3.68E-10
1.55	14.525	1.07E-07	2.97E-10
1.6	13.268	9.28E-08	6.81E-10
1.65	17.354	1.97E-08	3.89E-10
1.7	13.245	2.03E-08	6.68E-10
1.75	12.657	2.25E-08	6.99E-10
1.8	16.619	1.11E-07	1.55E-10
1.85	15.257	6.34E-08	3.30E-10
1.9	11.013	8.20E-08	4.58E-10
1.95	13.361	1.88E-08	1.91E-10
2	14.836	1.44E-08	4.56E-10
2.05	18.56	1.07E-07	1.39E-10
2.1	15.395	1.12E-07	5.03E-10
2.15	12.5	1.42E-08	3.55E-10
2.2	14.928	1.15E-07	5.18E-10
2.25	18.073	1.01E-07	5.71E-10
2.35	16.941	1.12E-07	1.52E-10
2.4	14.671	1.26E-07	3.51E-10
2.45	14.367	1.09E-07	3.00E-10

Rapid Run

Height (m)	Mass (g)	χ m^3/kg	Standard Deviation
0	15.177	1.57E-08	6.07E-10
0.05	19.657	1.56E-08	2.25E-10
0.1	18.685	1.66E-08	2.73E-10
0.15	18.564	1.32E-08	2.75E-10
0.2	18.924	1.28E-08	4.68E-10
0.25	11.854	3.26E-08	5.69E-10
0.3	16.808	2.47E-08	4.55E-10
0.35	19.855	8.17E-08	0
0.4	17.652	1.17E-07	3.86E-10
0.45	18.72	1.11E-07	1.38E-10
0.5	15.86	1.11E-07	6.50E-10
0.55	18.514	1.14E-07	2.41E-10
0.6	12.838	1.23E-07	0
0.65	14.455	1.17E-07	3.09E-10
0.7	15.34	1.13E-07	2.91E-10
0.75	17.843	1.14E-07	5.20E-10
0.8	13.013	1.21E-07	6.89E-10
0.85	15.976	1.00E-07	4.12E-10
0.9	14.467	1.09E-07	3.44E-10
0.95	15.892	9.72E-08	4.15E-10
1	15.435	1.14E-07	1.67E-10

Reidlin Mason Road Fort Wright, KY

Height (m)	Mass (g)	χ m^3/kg	Standard Deviation
0	11.634	1.47E-08	7.62E-10
0.1	9.697	1.71E-08	4.57E-10
0.2	9.36	1.58E-08	7.24E-10
0.3	9.273	2.04E-08	7.30E-10
0.4	8.064	2.24E-08	6.35E-10
0.48	10.197	1.75E-08	1.00E-09
0.58	13.038	1.12E-07	6.90E-10
0.68	8.694	1.16E-07	2.90E-10

Sherburne, KY

Height (m)	Mass (g)	χ m^3/kg	Standard Deviation
0	11.882	2.96E-08	5.68E-10
0.05	13.015	2.40E-08	3.40E-10
0.1	13.942	2.98E-08	3.16E-10
0.15	13.913	2.92E-08	4.84E-10
0.2	12.113	3.25E-08	7.29E-10

Height (m)	Mass (g)	χ m^3/kg	Standard Deviation
0.25	14.316	1.55E-08	4.72E-10
0.3	10.563	2.46E-08	2.42E-10
0.35	14.406	1.07E-07	3.46E-10
0.4	16.72	9.35E-08	2.58E-10
0.45	15.548	9.92E-08	5.55E-10
0.5	13.913	3.98E-08	1.83E-10
0.55	16.4	1.91E-08	0
0.6	12.352	2.02E-08	4.14E-10
0.65	14.579	2.68E-08	1.75E-10
0.7	14.225	1.05E-07	1.75E-10
0.75	15.142	9.30E-08	4.36E-10
0.8	13.492	1.13E-07	4.88E-10
0.85	15.211	1.01E-07	5.90E-10
0.9	16.904	9.21E-08	3.90E-10
0.95	14.905	9.70E-08	4.43E-10
1	15.866	6.98E-08	4.75E-10
1.05	18.936	9.95E-08	1.36E-10
1.1	18.117	3.19E-08	2.43E-10
1.15	14.77	9.38E-08	4.47E-10
1.2	16.101	4.25E-08	2.73E-10
1.25	16.207	1.26E-07	2.75E-10
1.3	15.312	8.09E-08	3.27E-10
1.35	15.971	9.05E-08	3.12E-10
1.4	16.338	7.76E-08	2.65E-10
1.45	18.183	1.17E-07	5.10E-10
1.5	15.675	1.27E-07	4.93E-10

Sycamore Creek Indian Hills Ohio

Height (m)	Mass (g)	χ m^3/kg	Standard Deviation
0	14.816	9.74E-09	5.19E-10
0.05	11.857	1.58E-08	3.74E-10
0.1	12.166	1.93E-08	5.56E-10
0.15	12.458	2.00E-08	7.40E-10
0.2	11.438	1.61E-08	5.92E-10
0.25	11.008	2.03E-08	8.37E-10
0.3	12.439	1.12E-07	2.01E-10
0.35	10.656	1.22E-07	4.70E-10
0.4	10.644	1.24E-07	7.05E-10
0.45	13.49	1.18E-07	3.19E-10
0.5	15.661	1.10E-07	5.94E-10
0.55	15.663	1.11E-07	5.94E-10
0.6	12.688	1.21E-07	7.08E-10
0.65	15.082	1.17E-07	6.16E-10
0.7	10.592	1.14E-07	6.26E-10

Height (m)	Mass (g)	χ m^3/kg	Standard Deviation
0.75	11.469	1.25E-07	7.84E-10
0.8	12.867	1.18E-07	3.35E-10
0.85	13.428	9.37E-08	1.87E-10
0.9	14.474	1.10E-07	4.55E-10
0.95	13.916	1.13E-07	5.36E-10
1	12.366	2.88E-08	7.14E-10
1.05	13.804	1.07E-07	5.42E-10
1.1	14.321	1.06E-07	6.27E-10
1.15	13.578	3.68E-08	3.75E-10
1.2	14.63	1.39E-08	6.06E-10

Taylorsville KY, Rt. 44

Height (m)	Mass (g)	χ m^3/kg	Standard Deviation
0	13.836	1.49E-08	4.89E-10
0.05	10.484	5.01E-08	8.74E-10
0.1	9.956	1.78E-08	8.90E-10
0.15	11.34	1.64E-08	8.13E-10
0.2	12.224	9.87E-08	2.05E-10
0.25	14.958	1.06E-07	1.66E-10
0.3	11.915	1.71E-08	7.44E-10
0.35	11.078	1.35E-08	6.93E-10
0.4	8.75	1.19E-08	7.75E-10
0.45	10.983	2.76E-08	8.38E-10
0.5	10.125	2.10E-08	6.68E-10
0.55	11.51	1.88E-08	4.44E-10
0.6	12.228	2.72E-08	5.52E-10
0.65	11.949	3.44E-08	4.26E-10
0.7	10.409	9.73E-08	2.42E-10
0.75	8.609	1.10E-07	5.85E-10
0.8	11.393	1.03E-07	2.20E-10
0.85	10.631	1.00E-07	8.53E-10

Taylorsville KY, Rt. 55

Height (m)	Mass (g)	χ m^3/kg	Standard Deviation
0	14.529	2.18E-08	1.76E-10
0.05	12.938	3.11E-08	5.21E-10
0.1	11.405	2.04E-08	2.24E-10
0.15	10.188	2.30E-08	2.51E-10
0.2	11.156	1.83E-08	7.94E-10
0.25	9.517	1.55E-08	5.38E-10
0.3	10.352	1.12E-07	8.74E-10
0.35	11.968	1.04E-07	5.54E-10

Height (m)	Mass (g)	χ m^3/kg	Standard Deviation
0.4	9.923	1.11E-07	2.53E-10
0.45	10.705	1.02E-07	6.21E-10
0.5	8.609	1.09E-07	7.75E-10
0.55	9.454	1.13E-07	7.04E-10

Wesselman Creek

Height (m)	Mass (g)	χ m^3/kg	Standard Deviation
0	9.12	1.62E-08	7.43E-10
0.05	9.915	1.86E-08	6.83E-10
0.1	9.859	1.81E-08	5.19E-10
0.15	11.2	3.47E-08	3.94E-10
0.2	9.421	1.14E-07	5.34E-10
0.25	11.692	1.62E-08	5.79E-10
0.3	13.145	2.20E-08	1.94E-10
0.35	11.503	1.16E-07	3.77E-10
0.4	13.721	1.11E-07	5.45E-10
0.45	11.515	1.10E-07	7.53E-10
0.5	10.35	1.04E-07	4.21E-10
0.55	11.461	1.13E-07	7.56E-10
0.6	8.965	1.29E-07	0
0.65	11.778	1.16E-07	4.24E-10
0.7	12.664	1.11E-07	5.22E-10
0.75	12.163	1.12E-07	3.56E-10
0.8	10.175	8.26E-08	4.30E-10
0.85	11.05	1.01E-07	4.55E-10
0.9	12.755	1.06E-07	3.92E-10
0.95	12.734	1.13E-07	3.39E-10
1	11.57	1.05E-07	3.75E-10
1.05	10.091	1.04E-07	8.99E-10
1.1	11.24	1.05E-07	5.90E-10

Winchester KY, I-64

Height (m)	Mass (g)	χ m^3/kg	Standard Deviation
0	13.151	4.48E-08	5.11E-10
0.05	14.638	2.66E-08	6.96E-10
0.1	15.573	4.07E-08	4.31E-10
0.15	13.479	2.39E-08	6.83E-10
0.2	13.013	2.50E-08	3.92E-10
0.25	15.384	1.20E-07	3.35E-10
0.3	12.911	6.77E-08	3.91E-10
0.35	14.097	3.10E-08	5.42E-10
0.4	13.168	4.63E-08	0

Height (m)	Mass (g)	χ m^3/kg	Standard Deviation
0.45	12.215	2.42E-08	3.62E-10
0.5	13.8	1.09E-07	5.42E-10
0.55	13.743	1.00E-07	4.81E-10
0.6	11.402	3.53E-08	8.94E-10
0.65	11.996	5.23E-08	5.59E-10
0.7	14.806	2.84E-08	5.96E-10
0.75	11.315	1.92E-08	8.15E-10
0.8	15.194	2.01E-08	6.06E-10
0.85	12.411	4.50E-08	7.38E-10
0.9	9.98	4.63E-08	9.19E-10
0.95	11.522	6.05E-08	5.82E-10
1	13.473	1.13E-07	1.85E-10
1.05	16.585	2.08E-08	4.61E-10
1.1	13.693	2.02E-08	7.46E-10
1.15	15.767	2.11E-08	5.83E-10
1.2	15.4	1.89E-08	2.87E-10
1.25	11.441	4.09E-08	2.22E-10
1.3	12.79	5.83E-08	1.98E-10
1.35	12.513	8.81E-08	6.96E-10
1.4	13.131	1.03E-07	5.04E-10
1.45	12.77	1.63E-08	5.30E-10
1.5	12.546	1.00E-07	3.99E-10
1.55	13.251	1.08E-07	6.52E-10
1.6	12.305	1.01E-07	6.11E-10
1.65	12.606	8.71E-08	3.99E-10
1.7	11.976	9.16E-08	3.63E-10
1.75	14.371	2.58E-08	4.69E-10
1.8	16.69	2.74E-08	5.50E-10
1.85	10.687	1.05E-07	7.05E-10
1.9	10.932	9.79E-08	3.98E-10

APPENDIX III
"Z-BED" MEASURED SECTIONS

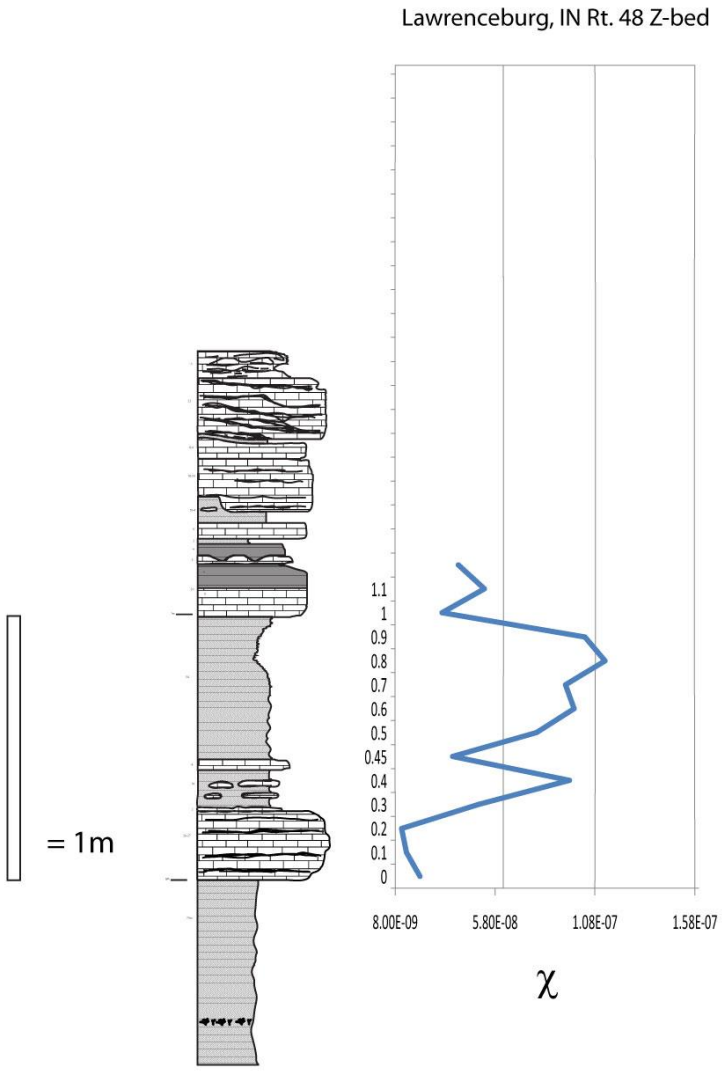

Wesselman Creek OH. Z-bed

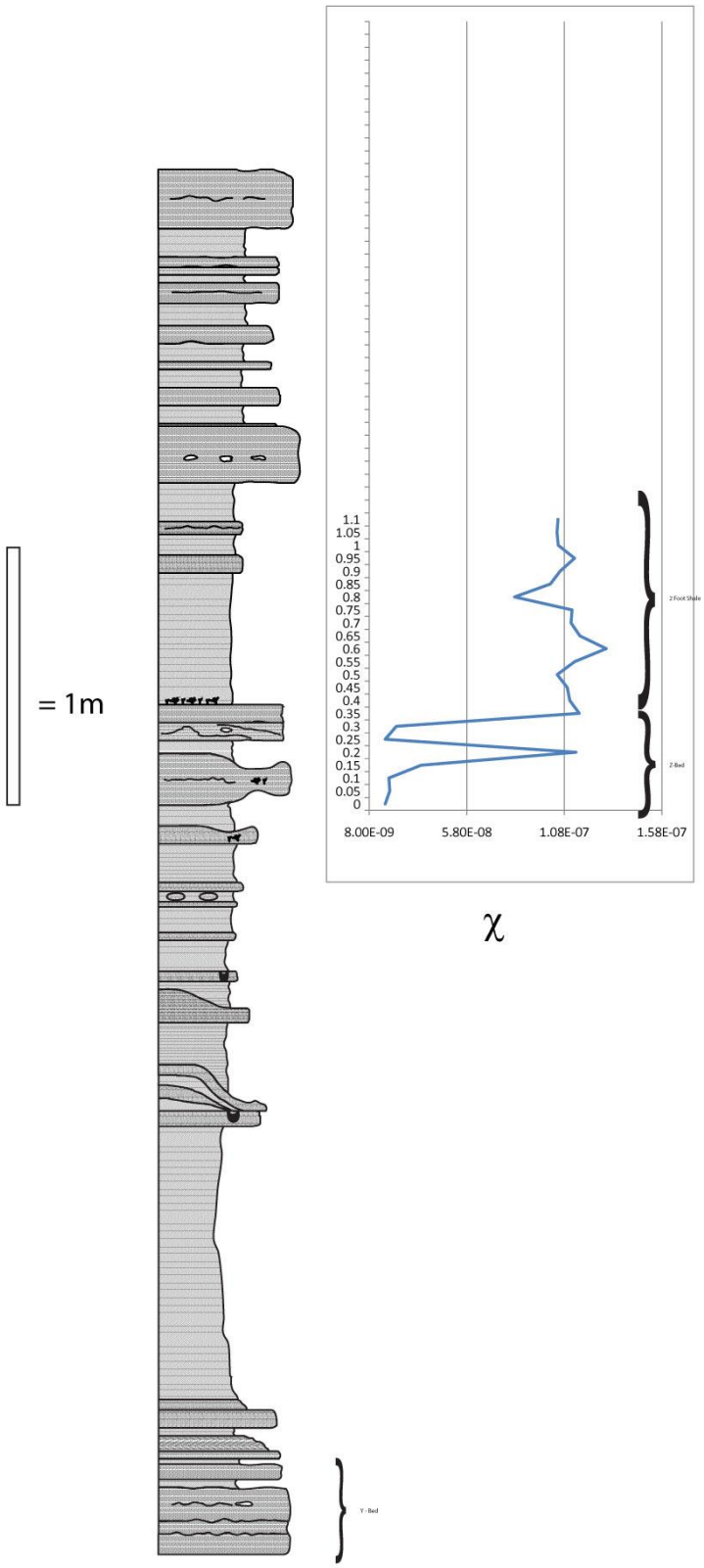

χ

Rapid Run, Z-bed

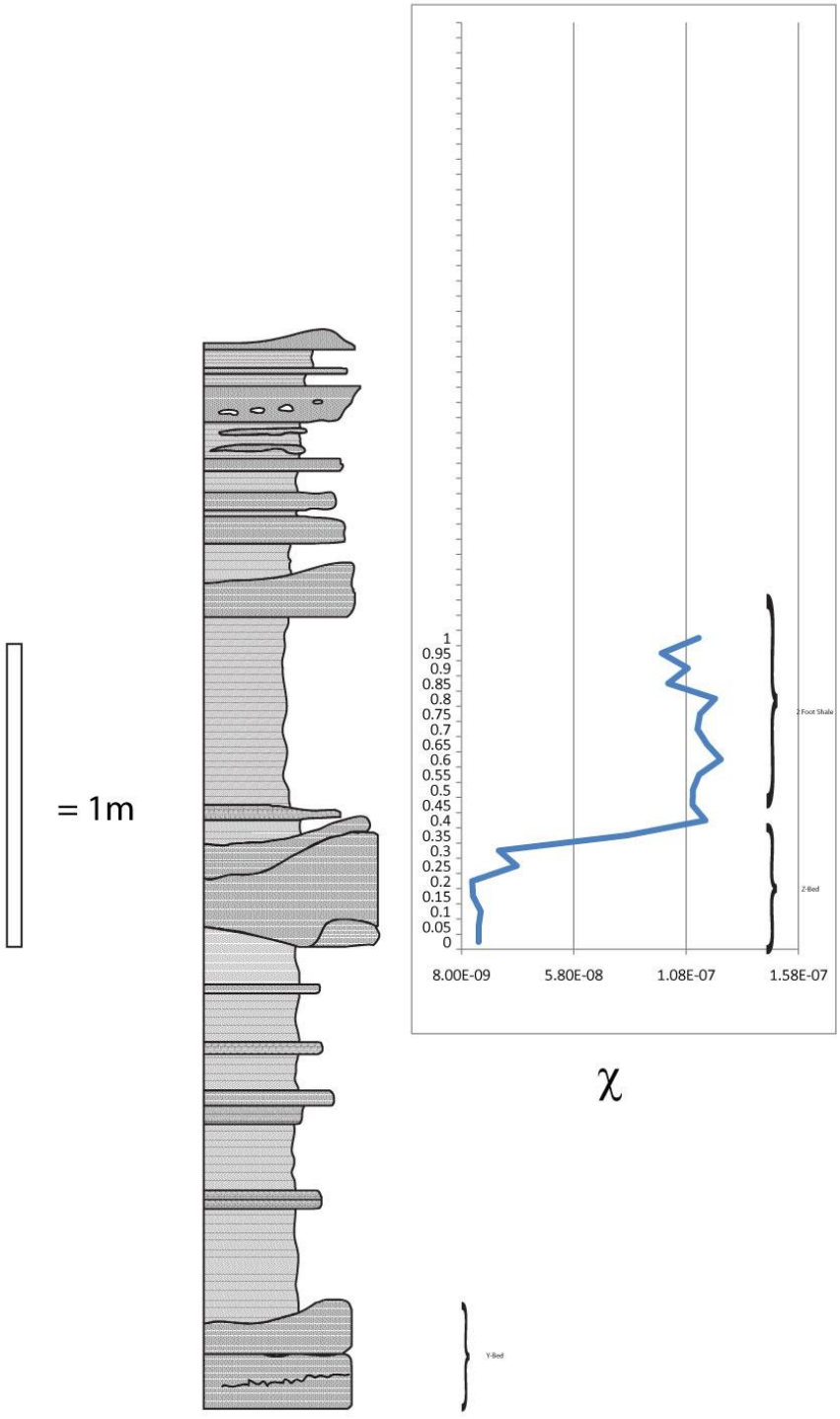

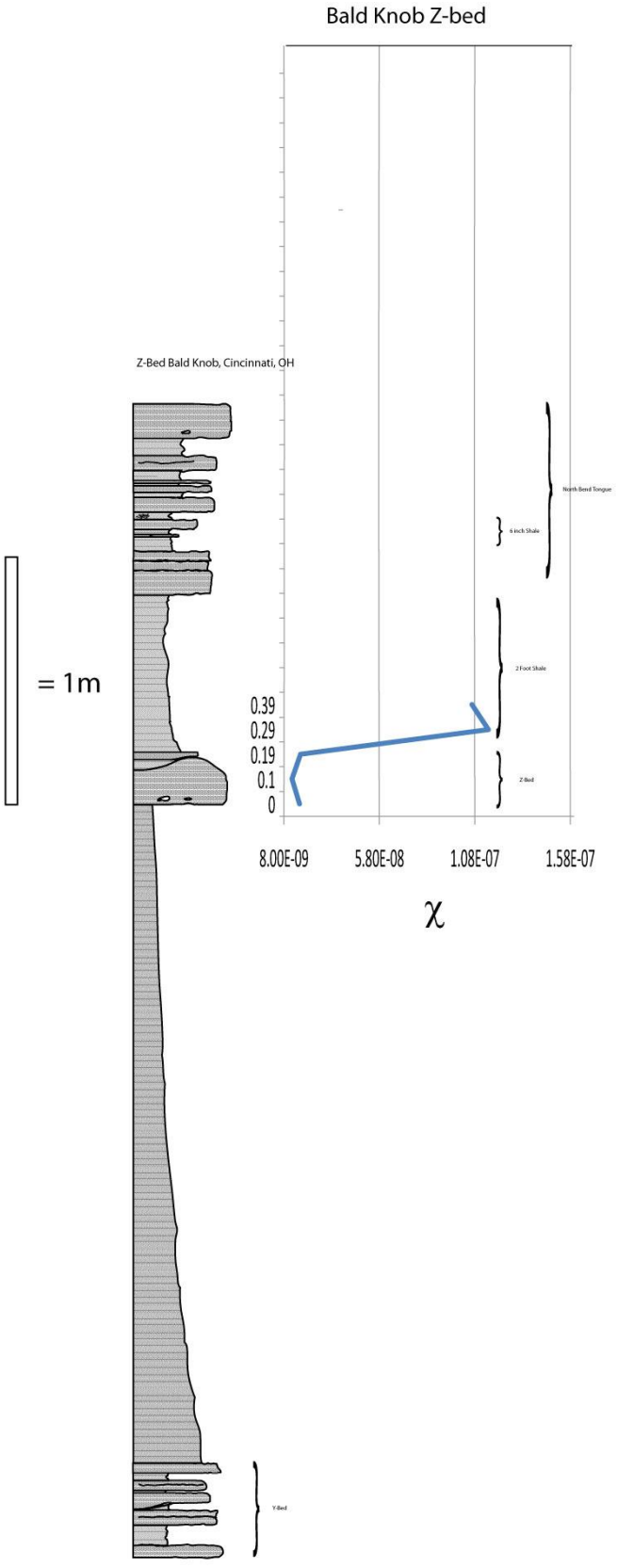
Bald Knob Z-bed
Z-Bed Bald Knob, Cincinnati, OH
= 1m
North Bend Tongue
6 Inch Shale
2 Foot Shale
Z-Bed
Y-Bed
0.39
0.29
0.19
0.1
0
8.00E-09
5.80E-08
1.08E-07
1.58E-07
χ

275@471 Z-bed

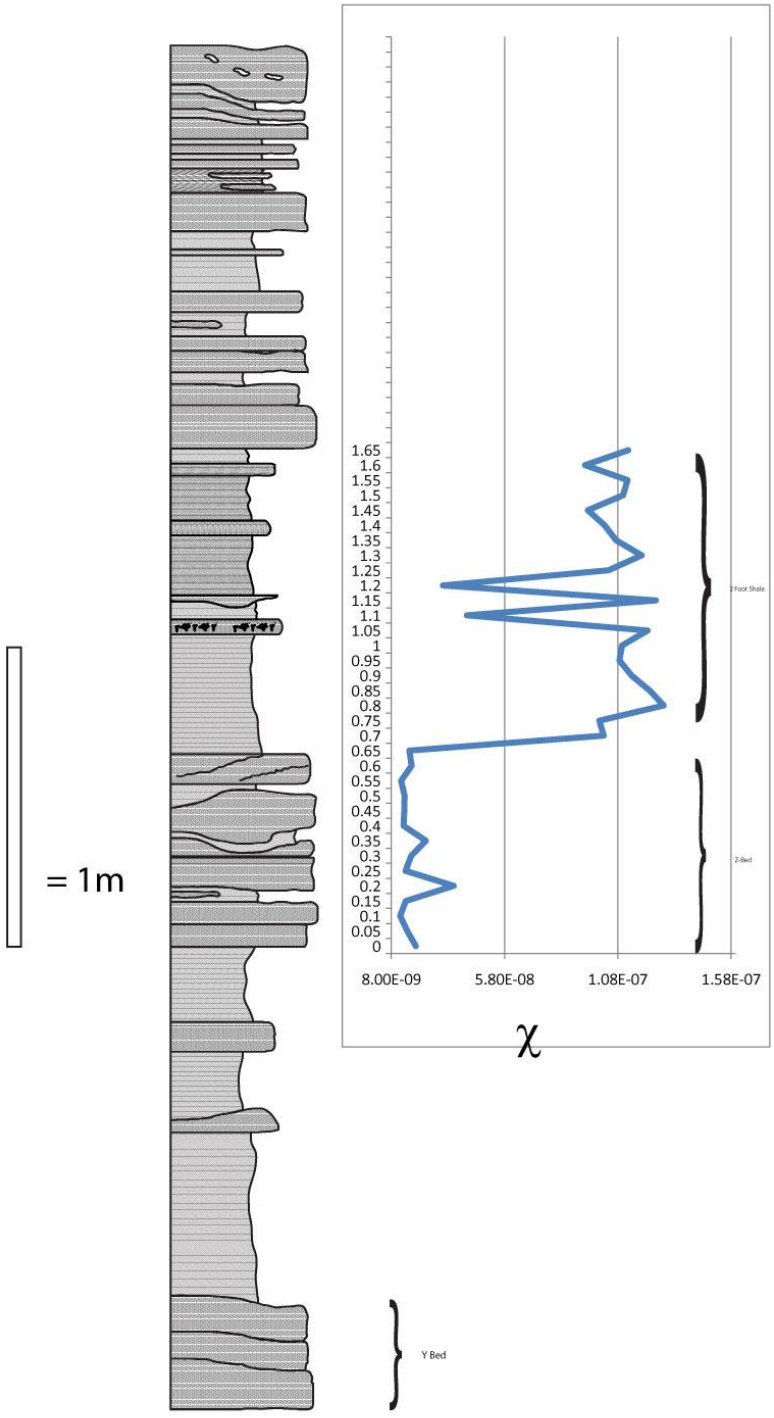
= 1m
1.65
1.6
1.55
1.5
1.45
1.4
1.35
1.3
1.25
1.2
1.15
1.1
1.05
1
0.95
0.9
0.85
0.8
0.75
0.7
0.65
0.6
0.55
0.5
0.45
0.4
0.35
0.3
0.25
0.2
0.15
0.1
0.05
0
8.00E-09
5.80E-08
1.08E-07
1.58E-07
χ
Z-Bed
Y Bed

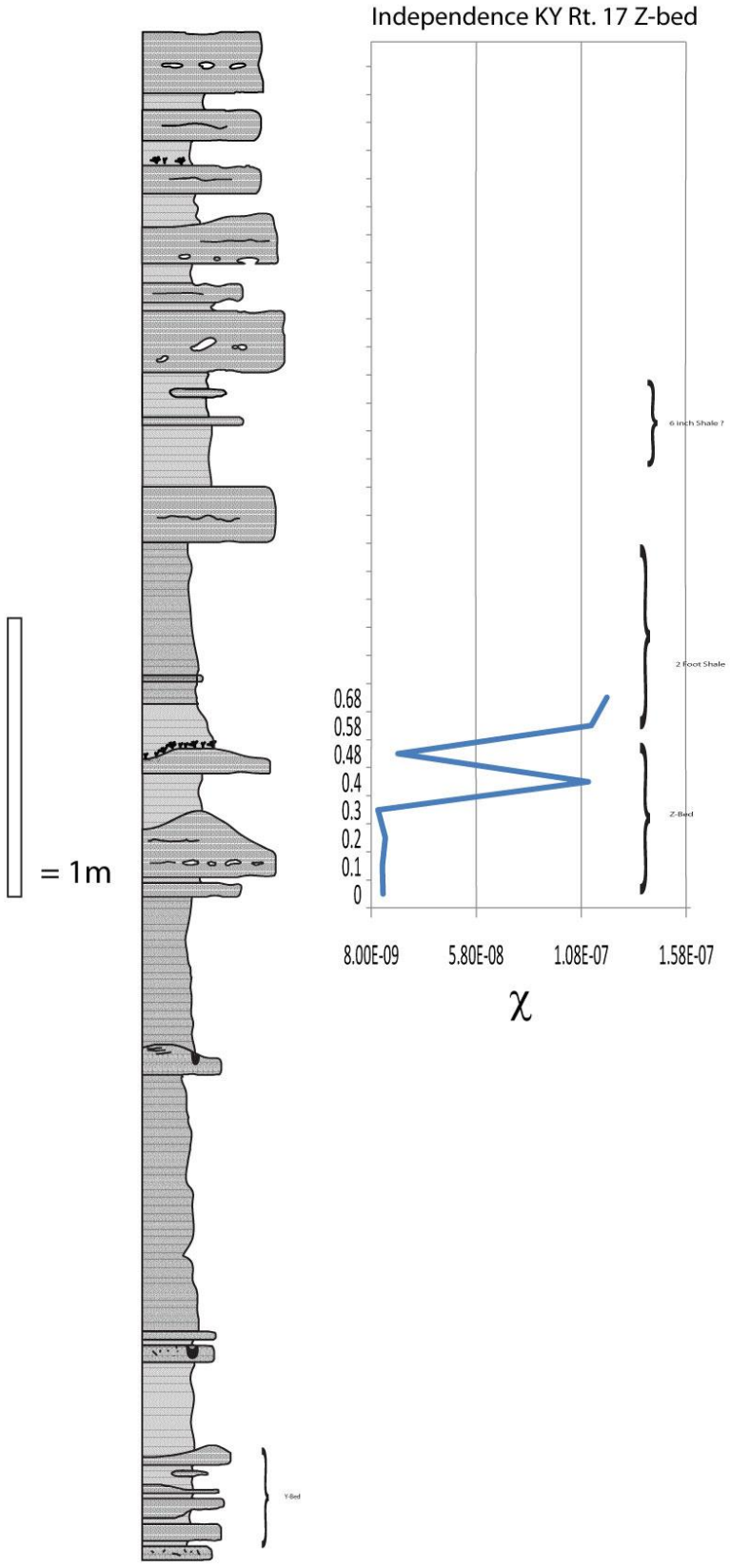
Independence KY Rt. 17 Z-bed
= 1m
6 Inch Shale ?
2 Foot Shale
Z-Bed
Y-Bed
0.68
0.58
0.48
0.4
0.3
0.2
0.1
0
8.00E-09
5.80E-08
1.08E-07
1.58E-07
χ

Reidlin Mason Road Z-bed

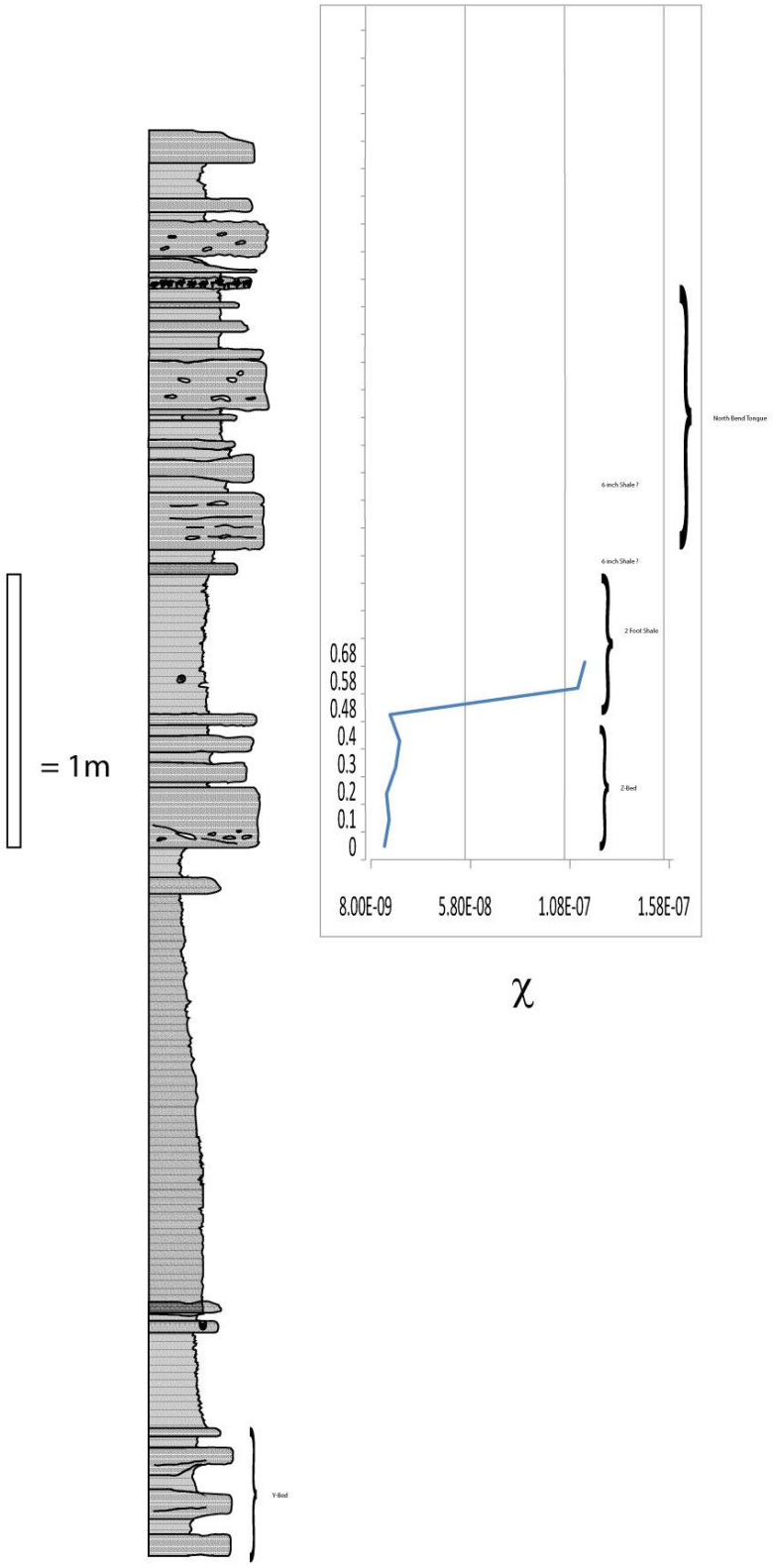

AA Highway @ Poplar Ridge Z-bed

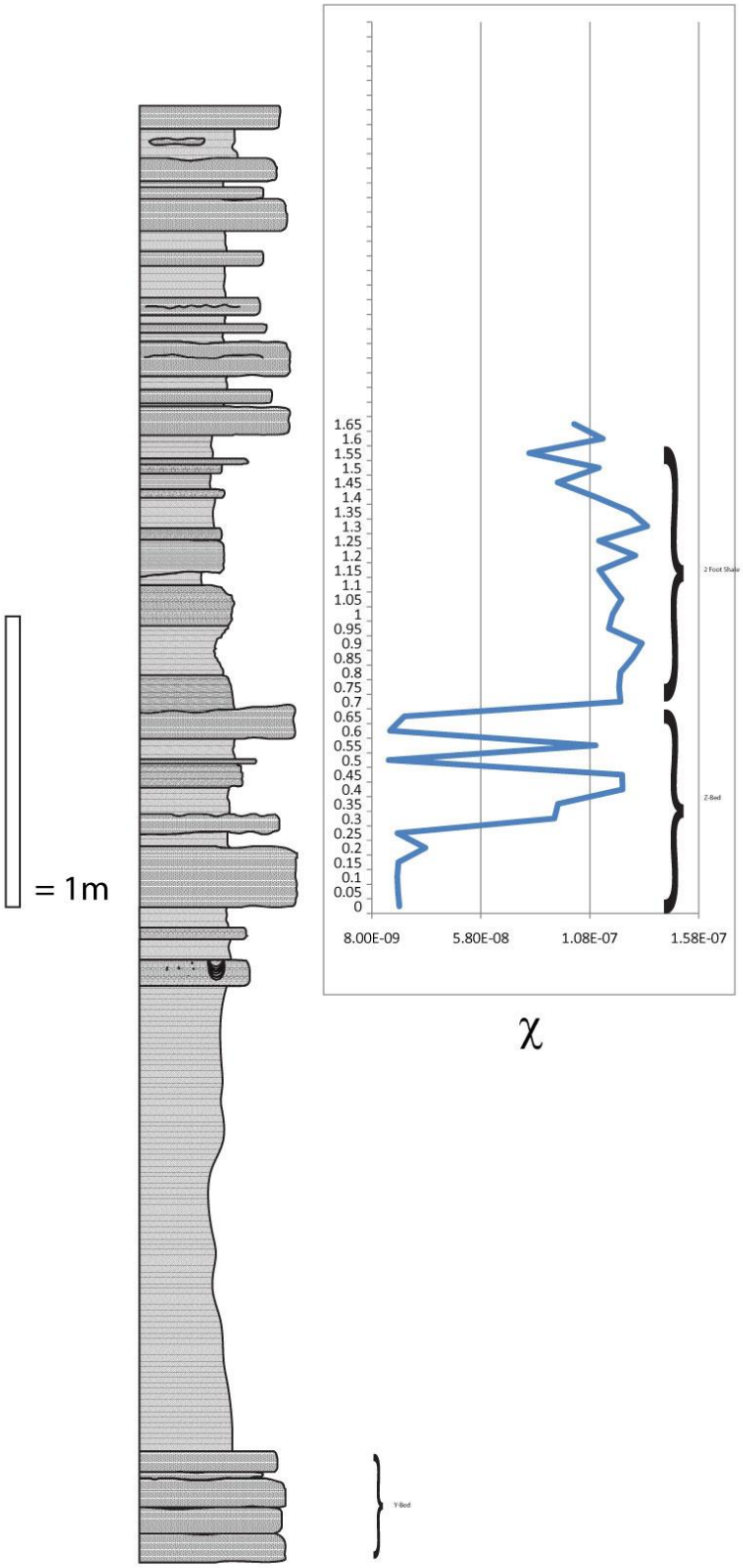

χ

AA Highway @ Dead Timber Z-bed

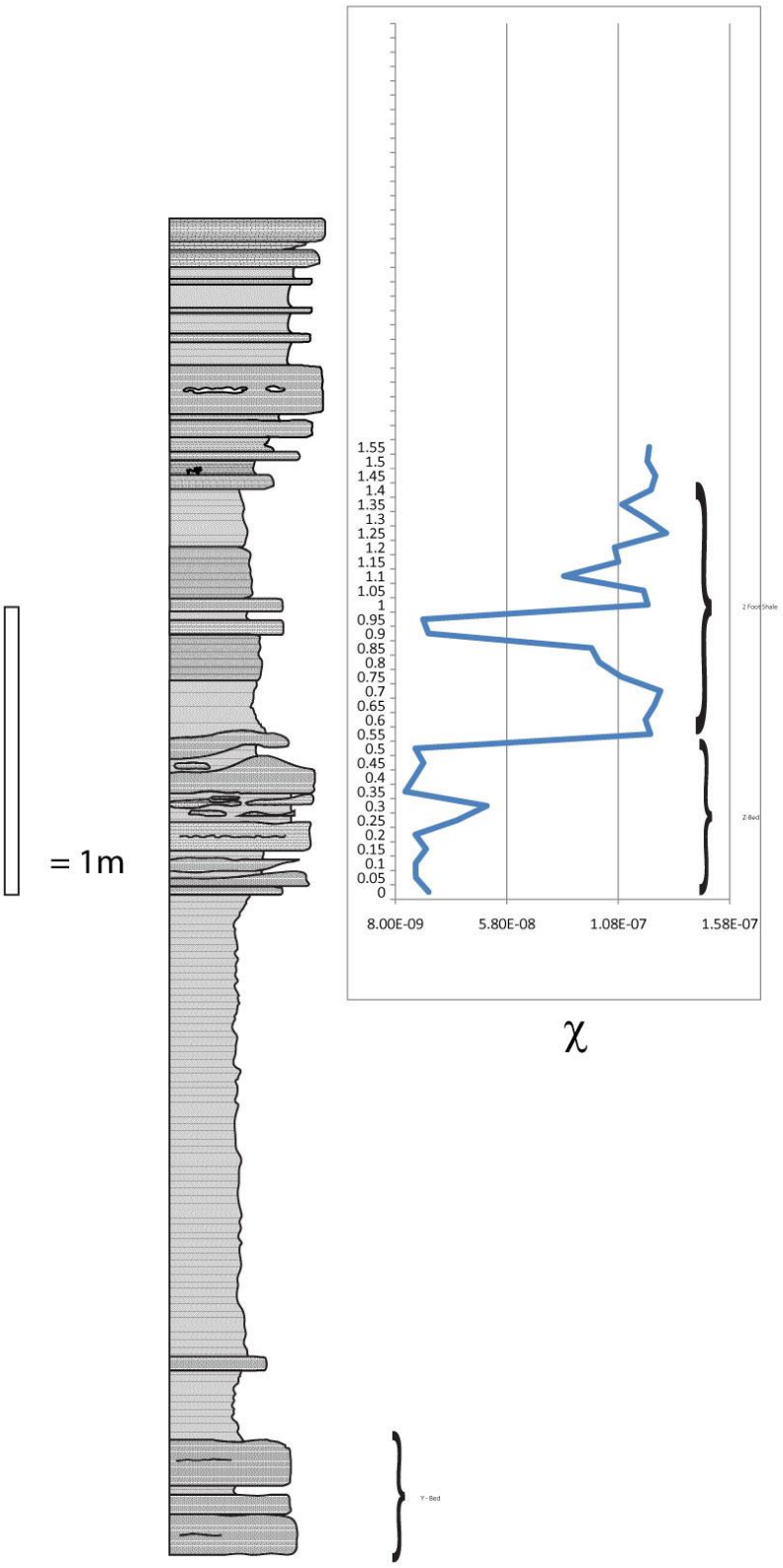

χ

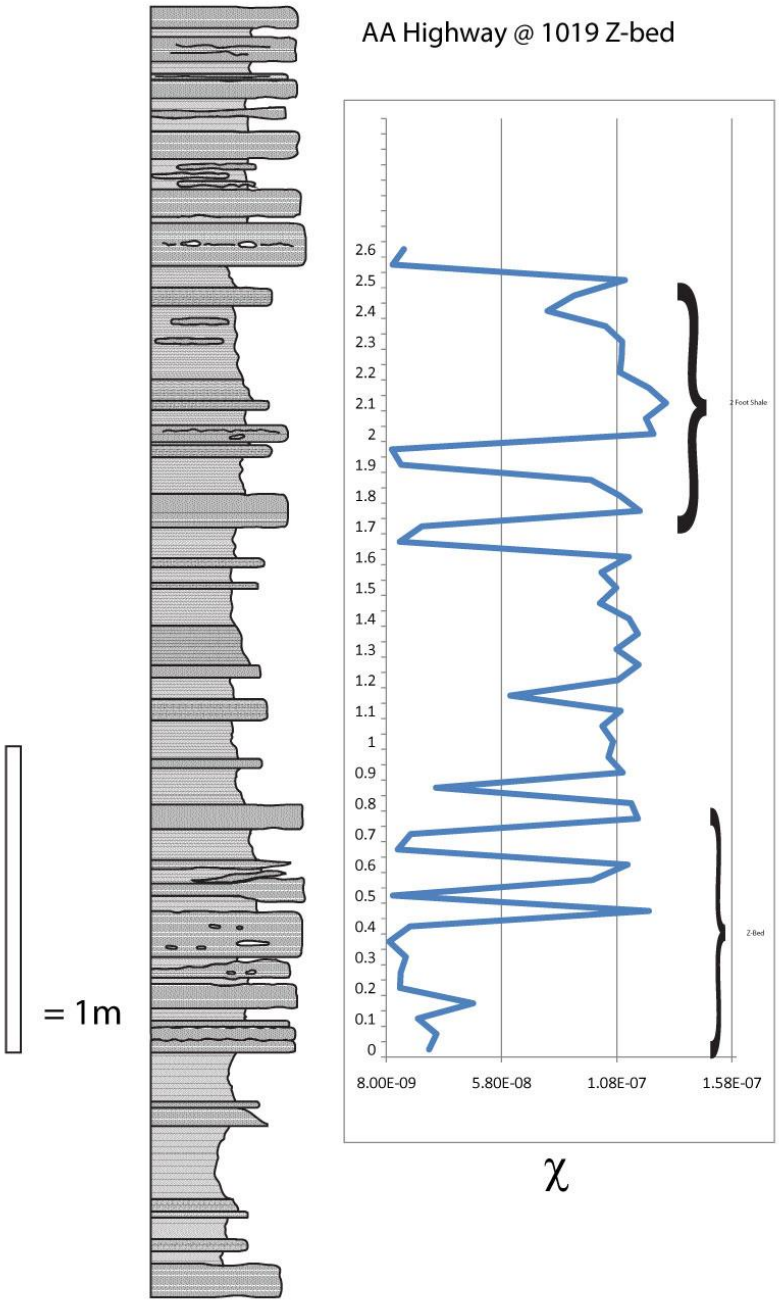
AA Highway @ 1019 Z-bed
= 1m
2.6
2.5
2.4
2.3
2.2
2.1
2
1.9
1.8
1.7
1.6
1.5
1.4
1.3
1.2
1.1
1
0.9
0.8
0.7
0.6
0.5
0.4
0.3
0.2
0.1
0
8.00E-09
5.80E-08
1.08E-07
1.58E-07
2 Foot Shale
Z-Bed
χ

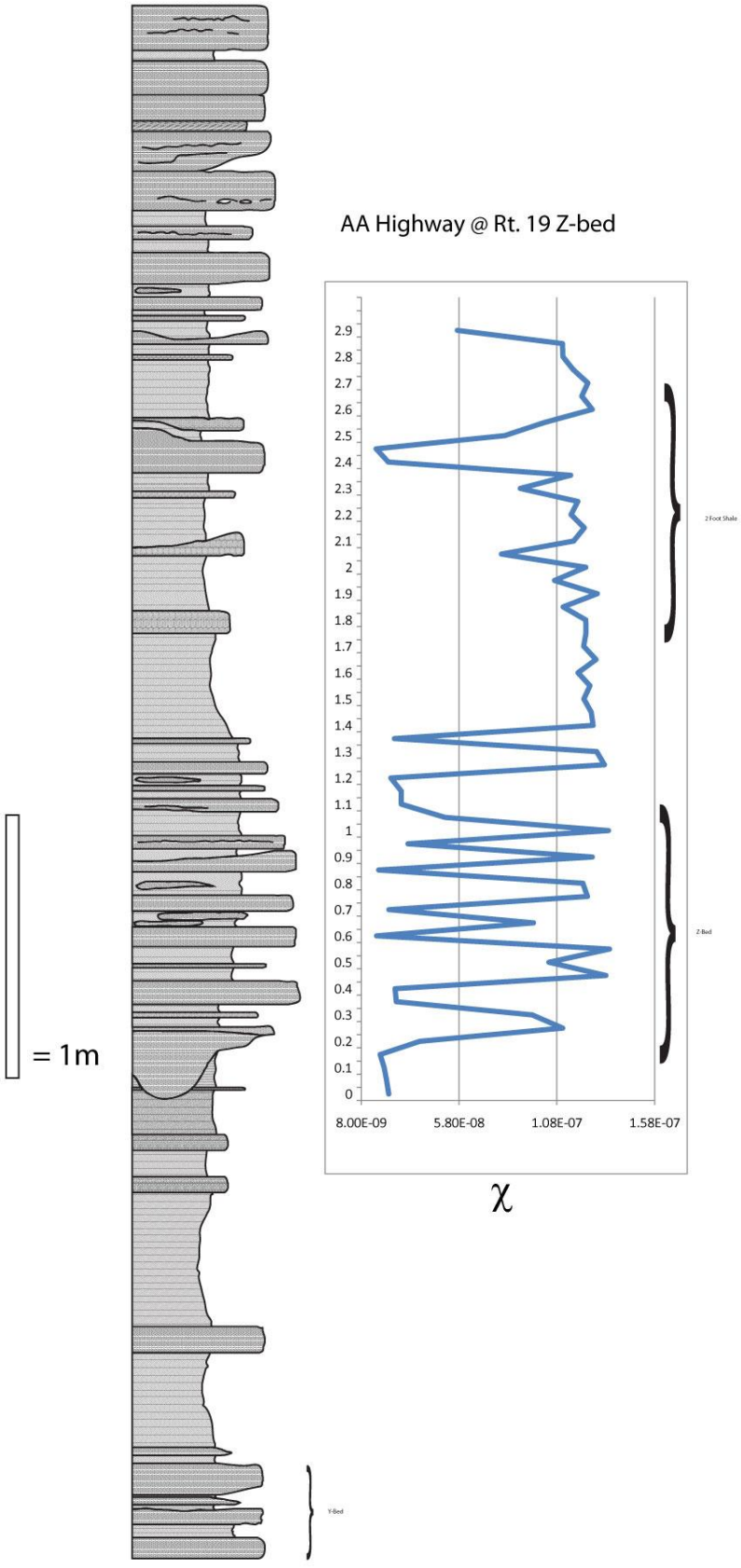
AA Highway @ Rt. 19 Z-bed
= 1m
2.9
2.8
2.7
2.6
2.5
2.4
2.3
2.2
2.1
2
1.9
1.8
1.7
1.6
1.5
1.4
1.3
1.2
1.1
1
0.9
0.8
0.7
0.6
0.5
0.4
0.3
0.2
0.1
0
8.00E-09
5.80E-08
1.08E-07
1.58E-07
χ
Z Bed

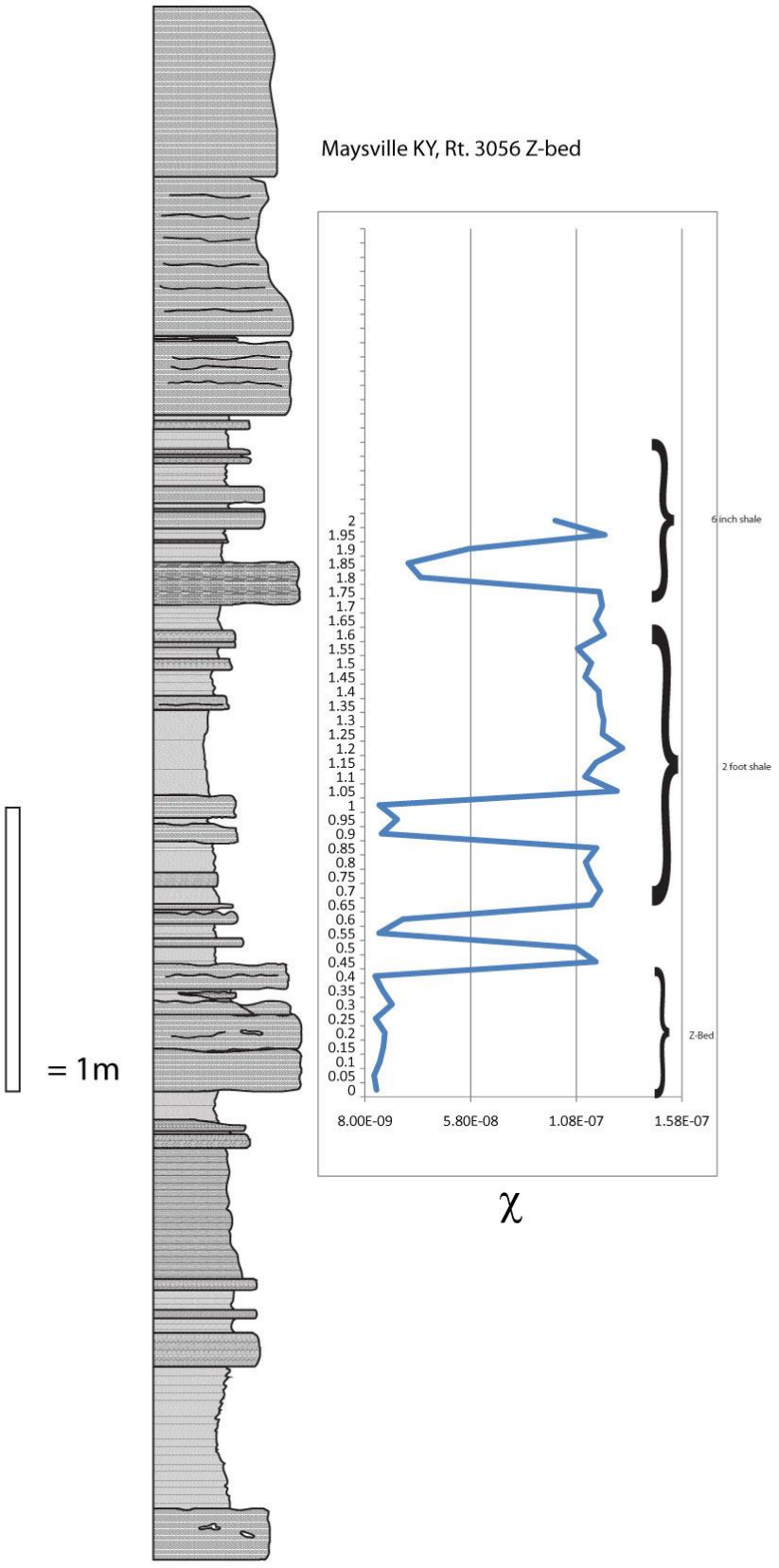
Maysville KY, Rt. 3056 Z-bed
= 1m
2
1.95
1.9
1.85
1.8
1.75
1.7
1.65
1.6
1.55
1.5
1.45
1.4
1.35
1.3
1.25
1.2
1.15
1.1
1.05
1
0.95
0.9
0.85
0.8
0.75
0.7
0.65
0.6
0.55
0.5
0.45
0.4
0.35
0.3
0.25
0.2
0.15
0.1
0.05
0
8.00E-09
5.80E-08
1.08E-07
1.58E-07
6 inch shale
2 foot shale
Z-Bed
χ

Maysville KY, Rt. 6268 Z-bed

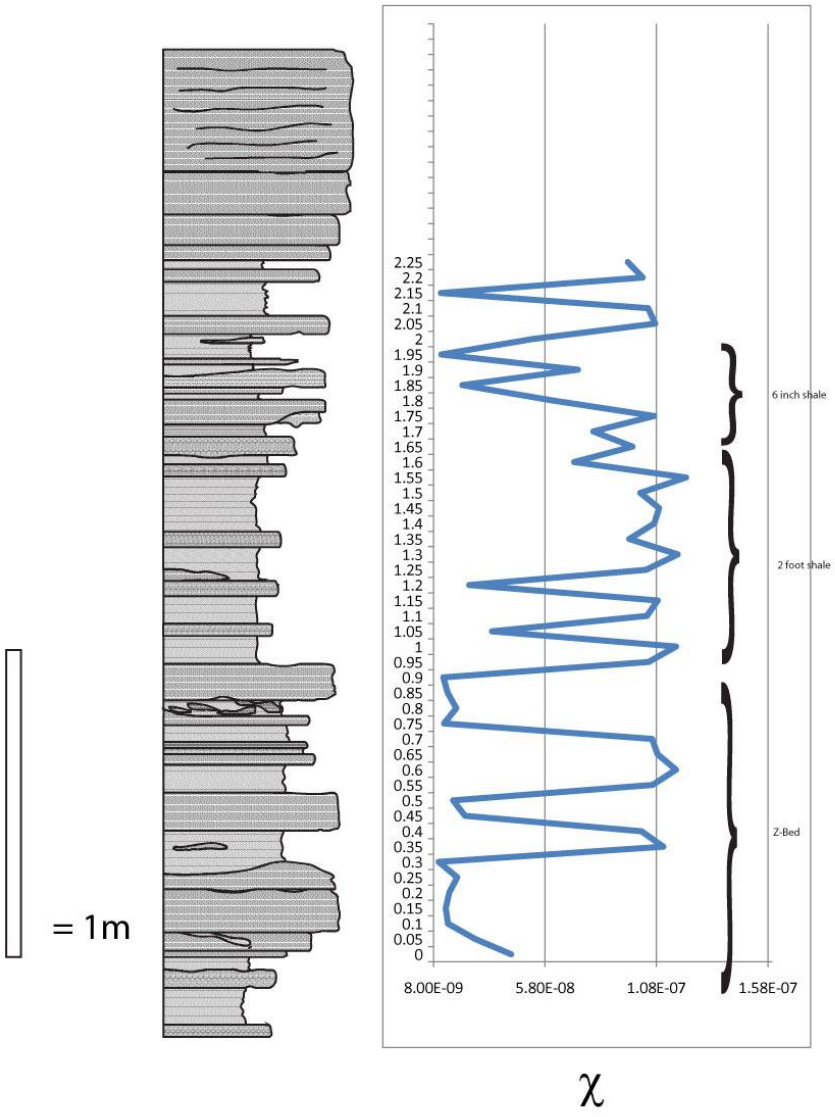

Maysville KY. Rt. 11 Z-bed

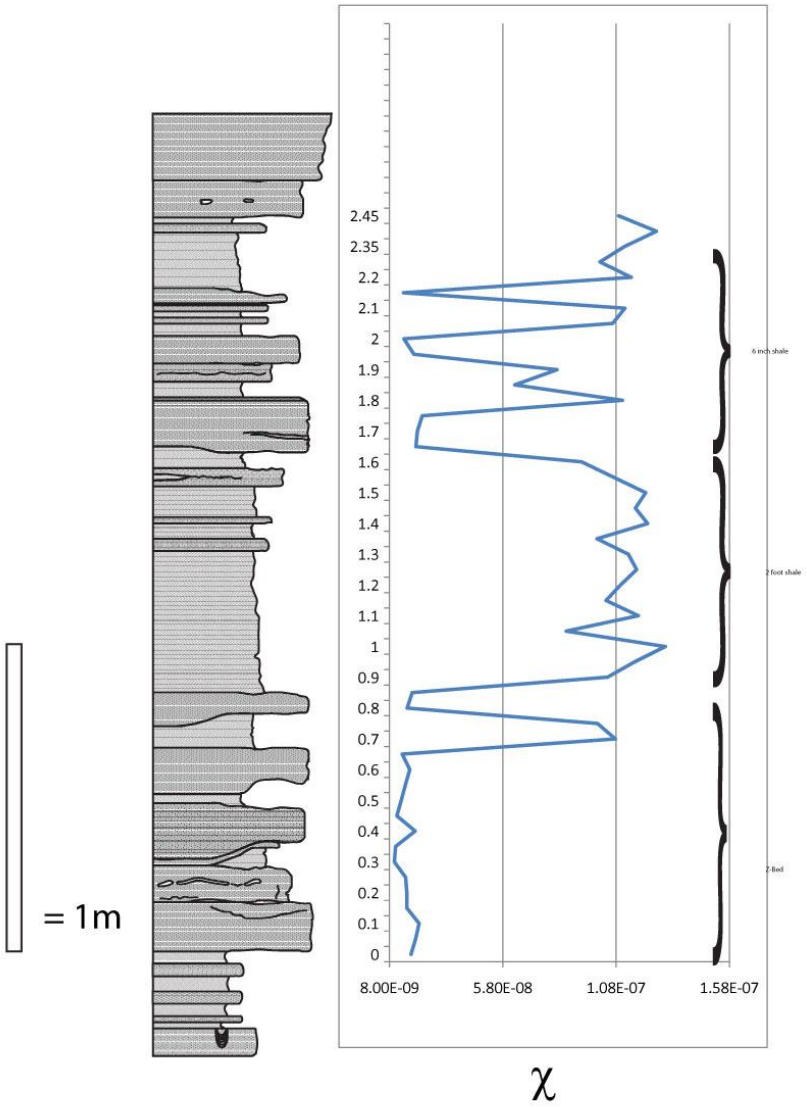

Johnson Creek Rt 68 Z-bed

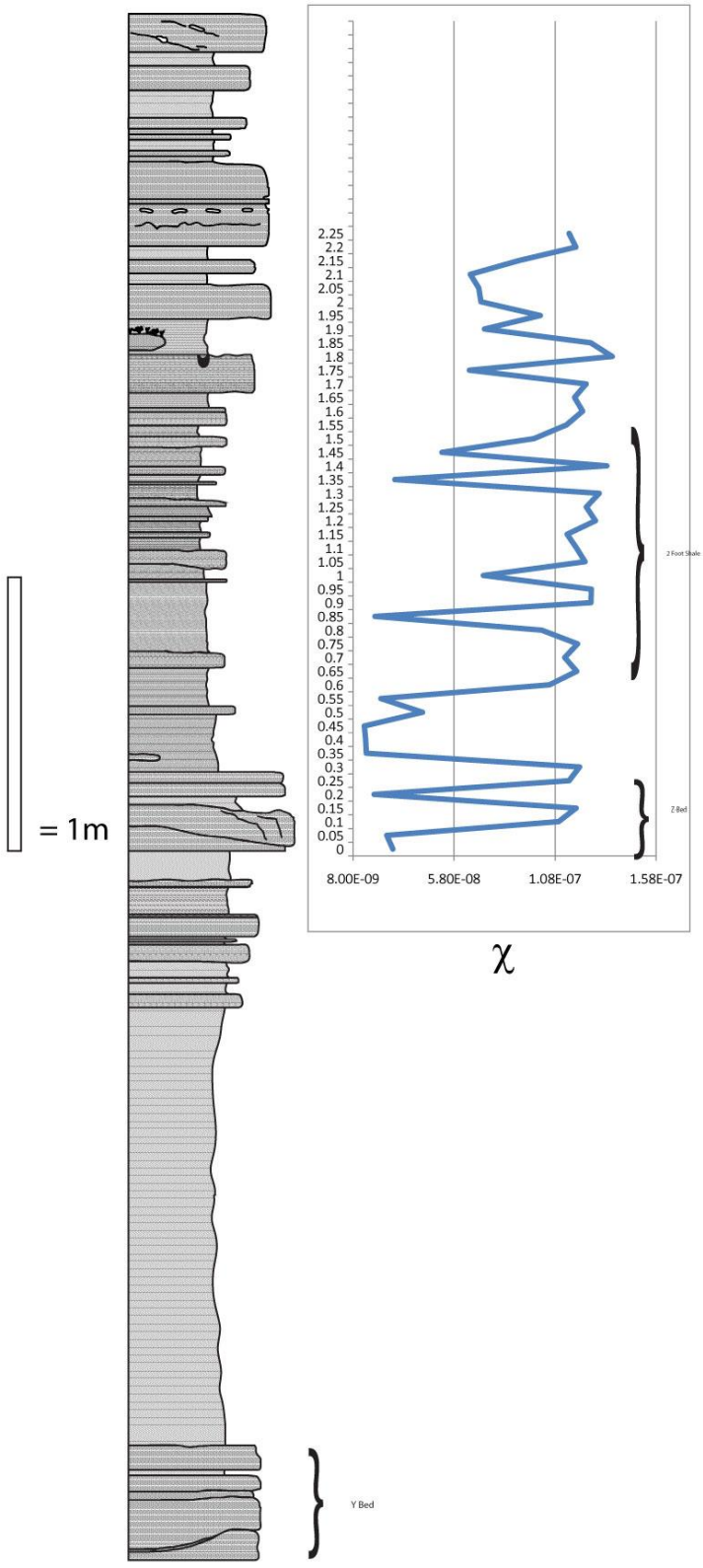

Sherburne KY. Rt. 11 Z-bed

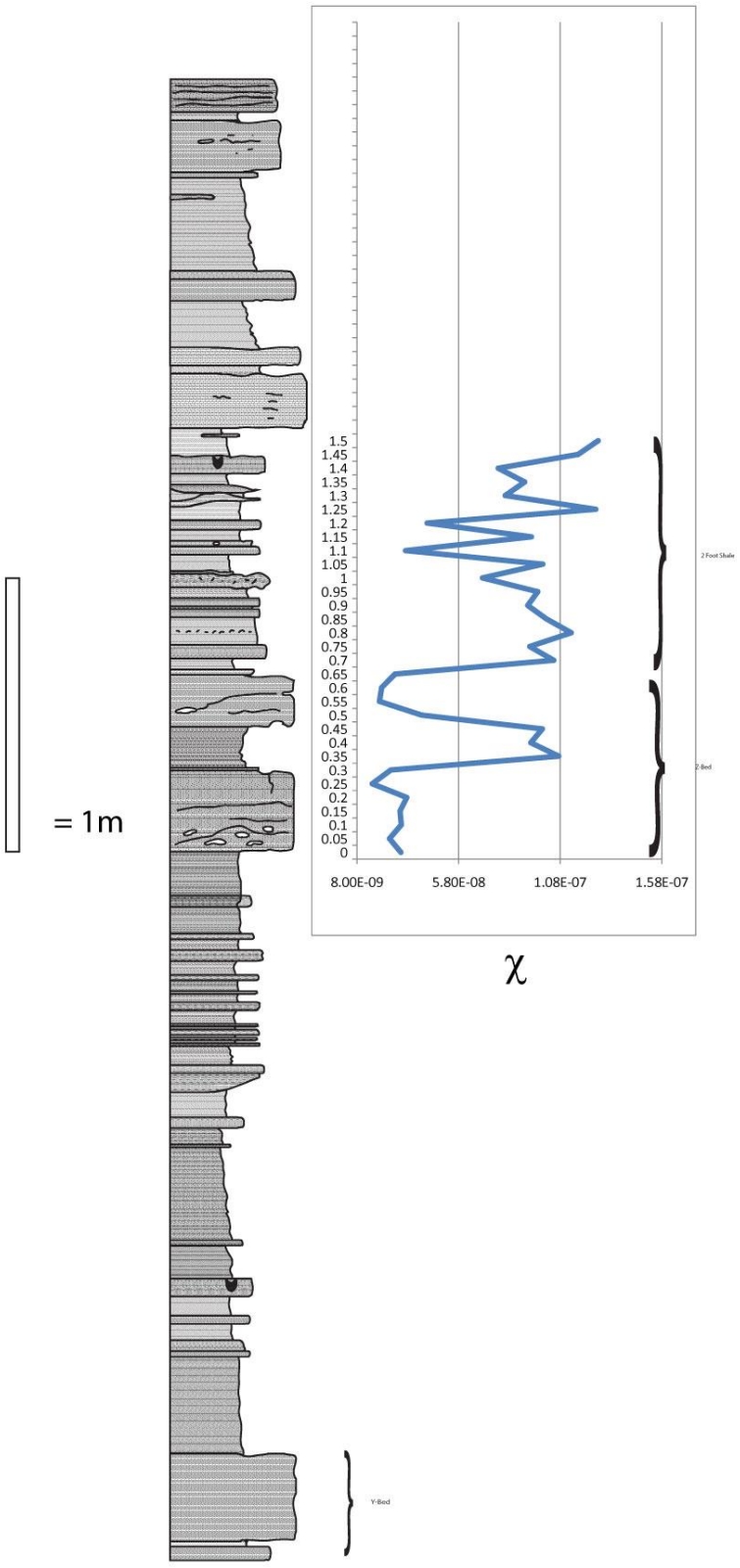

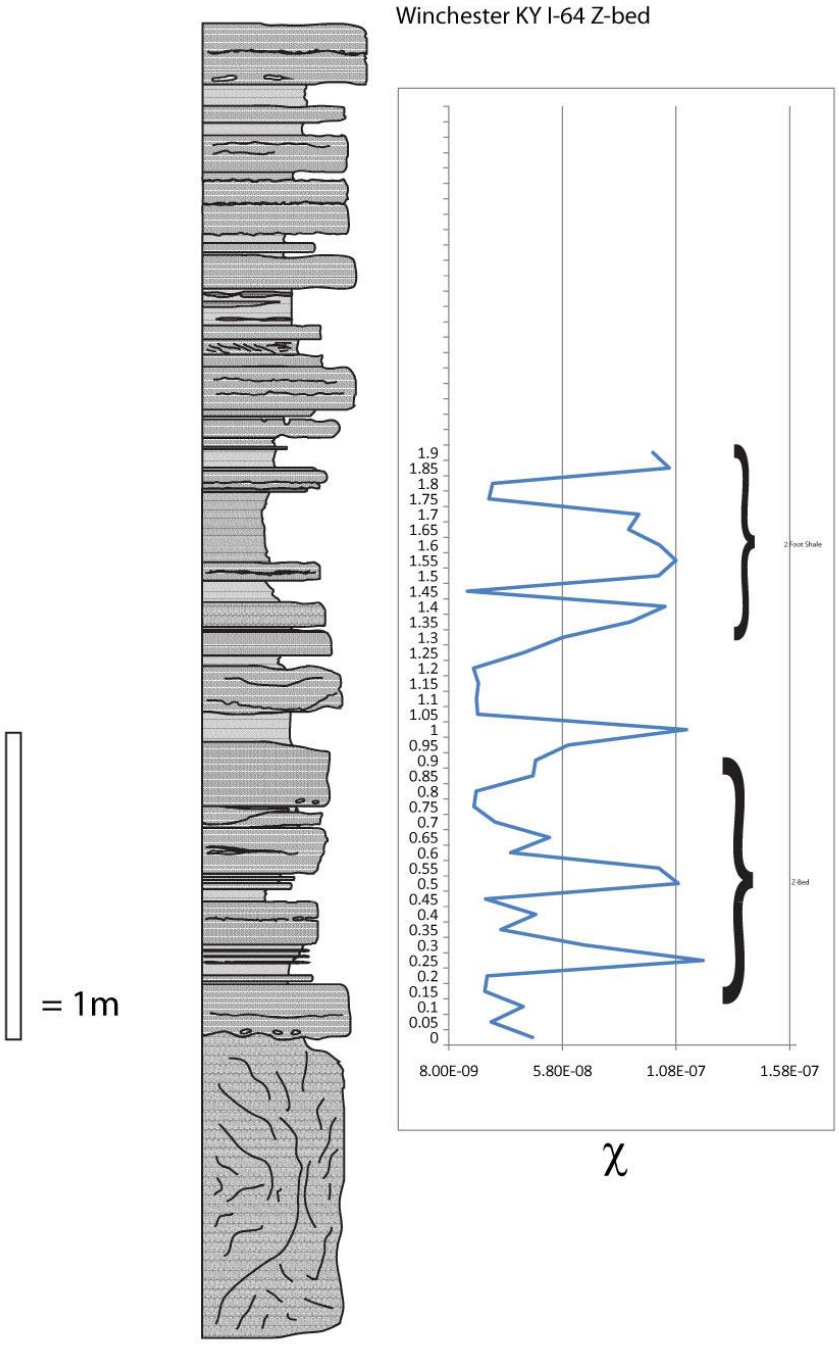
Winchester KY I-64 Z-bed
= 1m
1.9
1.85
1.8
1.75
1.7
1.65
1.6
1.55
1.5
1.45
1.4
1.35
1.3
1.25
1.2
1.15
1.1
1.05
1
0.95
0.9
0.85
0.8
0.75
0.7
0.65
0.6
0.55
0.5
0.45
0.4
0.35
0.3
0.25
0.2
0.15
0.1
0.05
0
8.00E-09
5.80E-08
1.08E-07
1.58E-07
2 Foot Shale
Z-Bed
χ

Caldwell Park, Cincinnati OH Z-bed

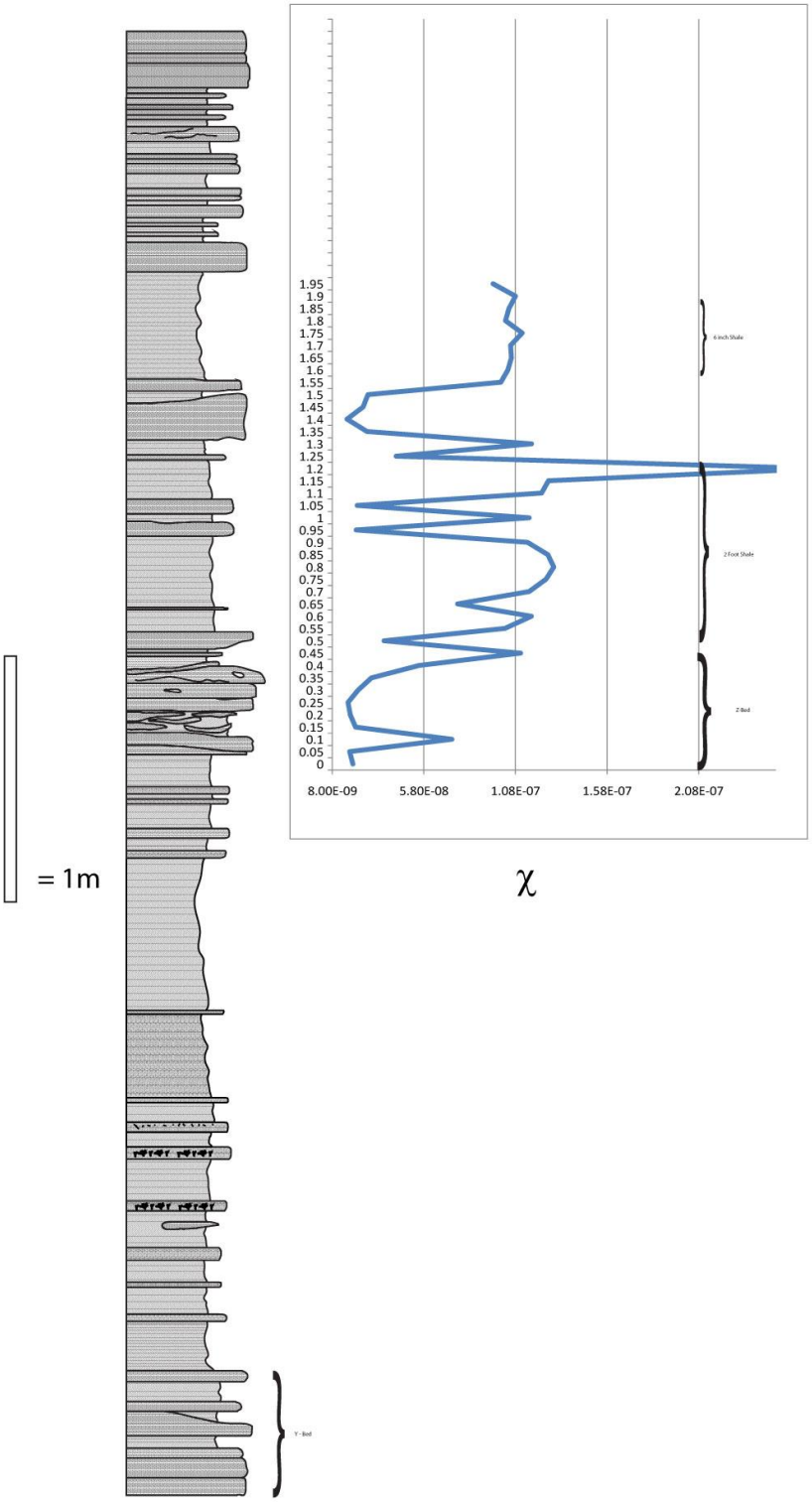

Sycamore Creek Z-bed

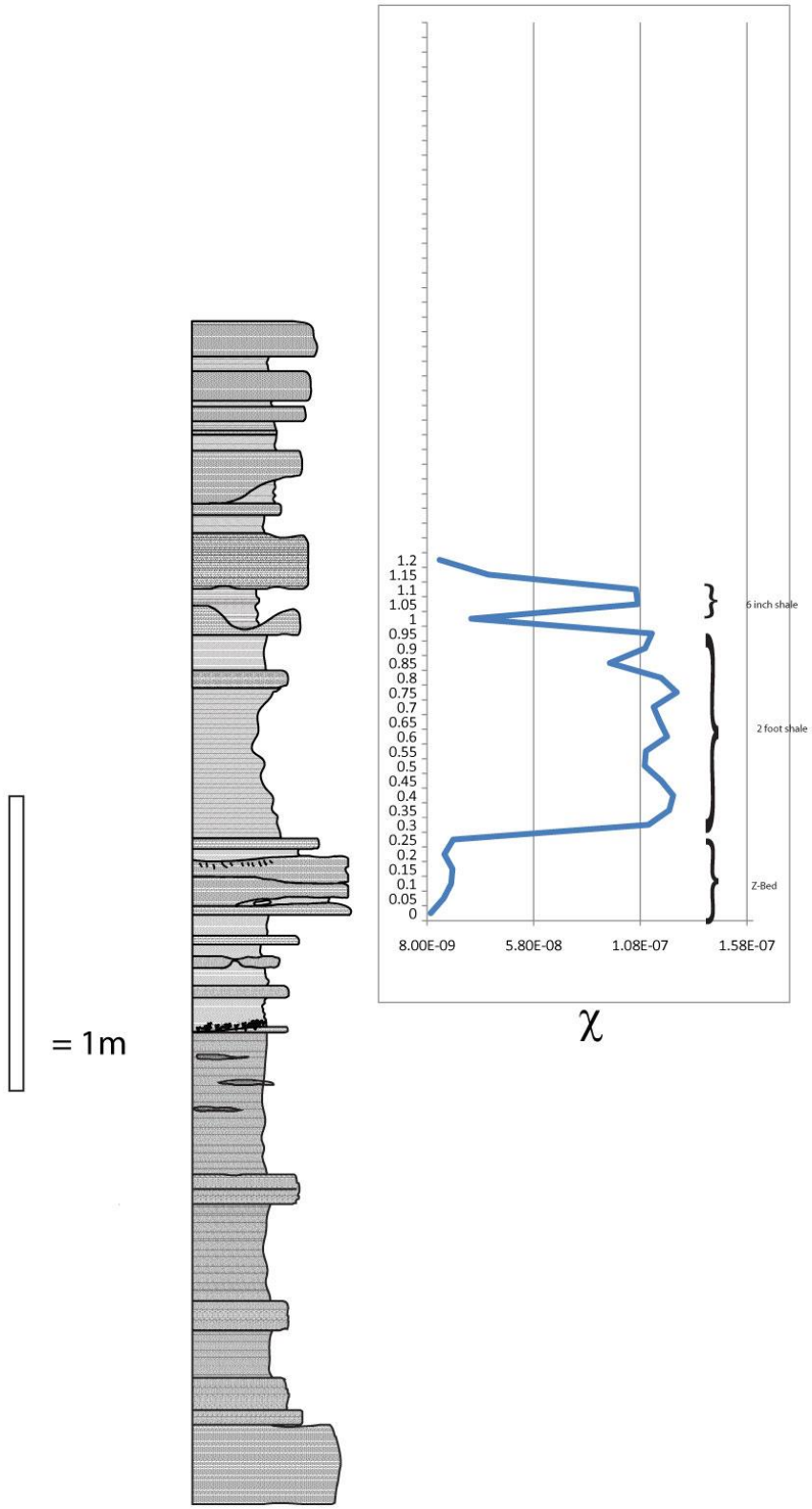

Morrow, OH 2nd Creek Z-bed

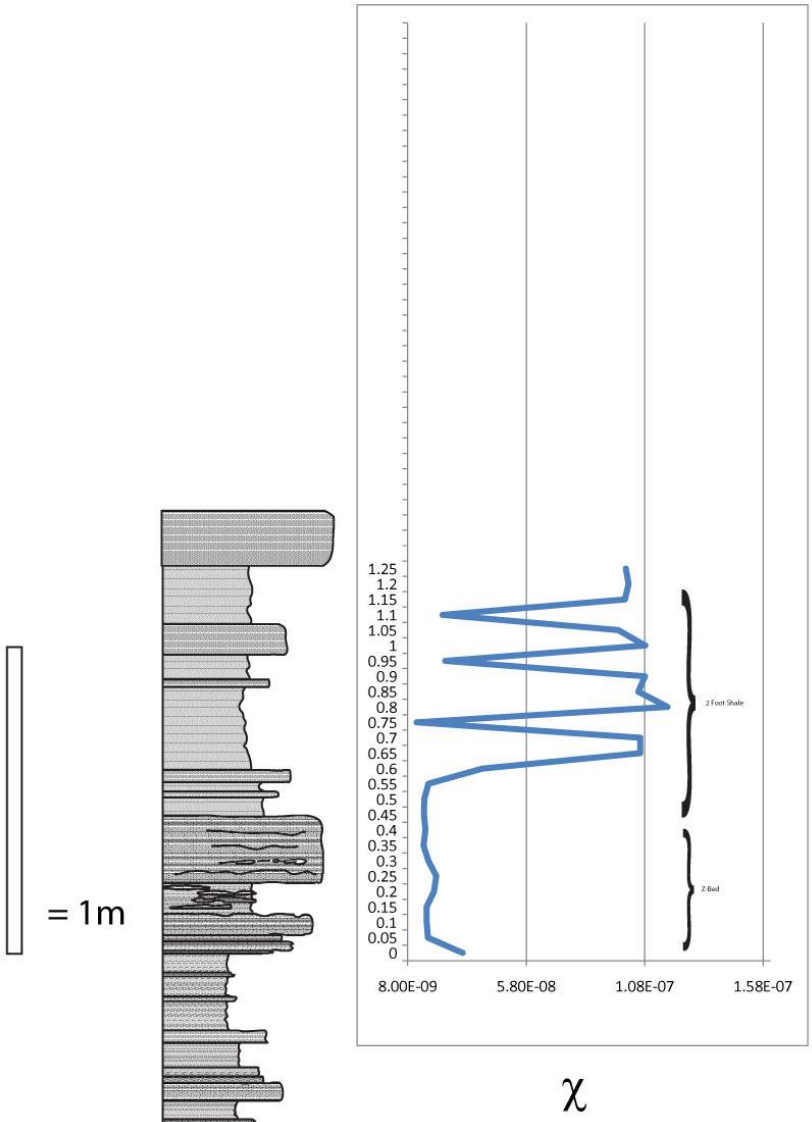

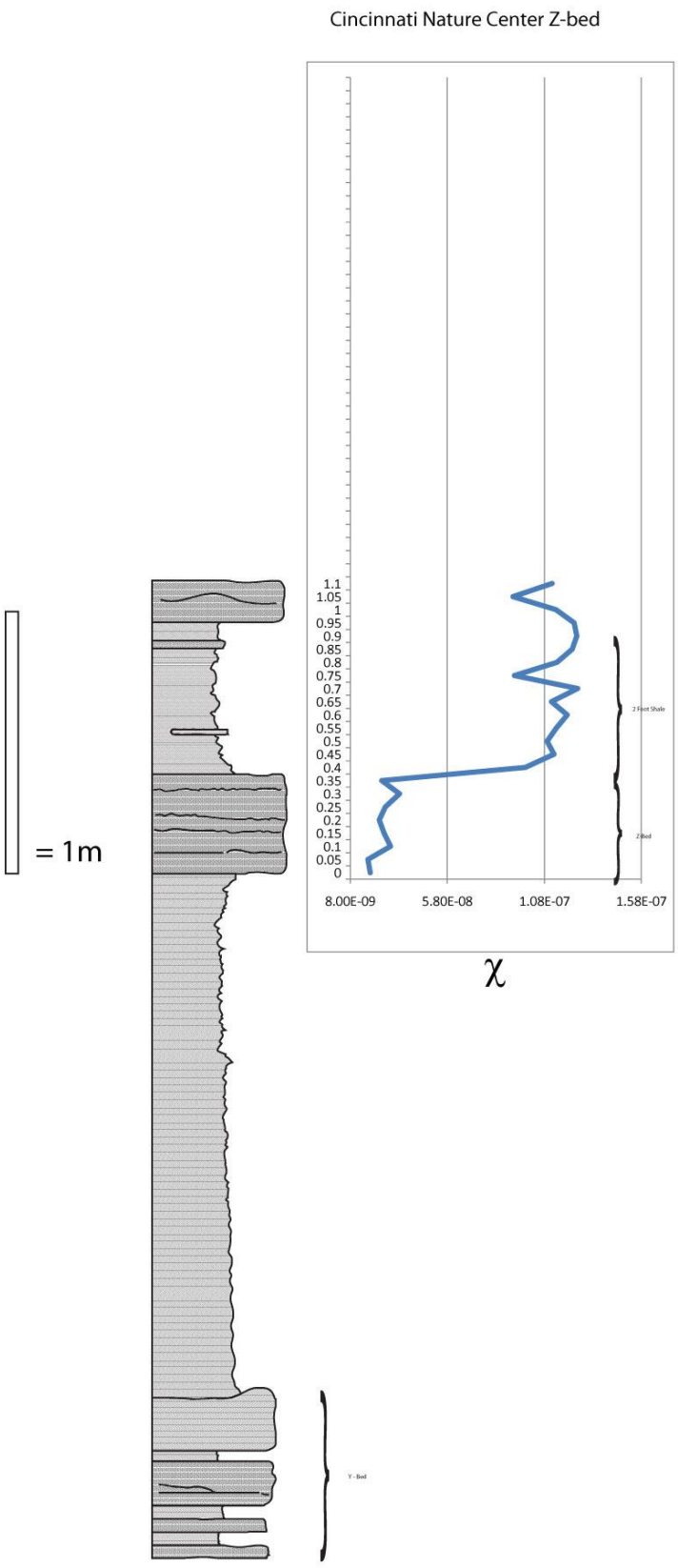
Cincinnati Nature Center Z-bed
= 1m
1.1
1.05
1
0.95
0.9
0.85
0.8
0.75
0.7
0.65
0.6
0.55
0.5
0.45
0.4
0.35
0.3
0.25
0.2
0.15
0.1
0.05
0
8.00E-09
5.80E-08
1.08E-07
1.58E-07
χ
Z Fiest Shale
Z-Bed
Y - Bed

Backbone Creek Z-bed

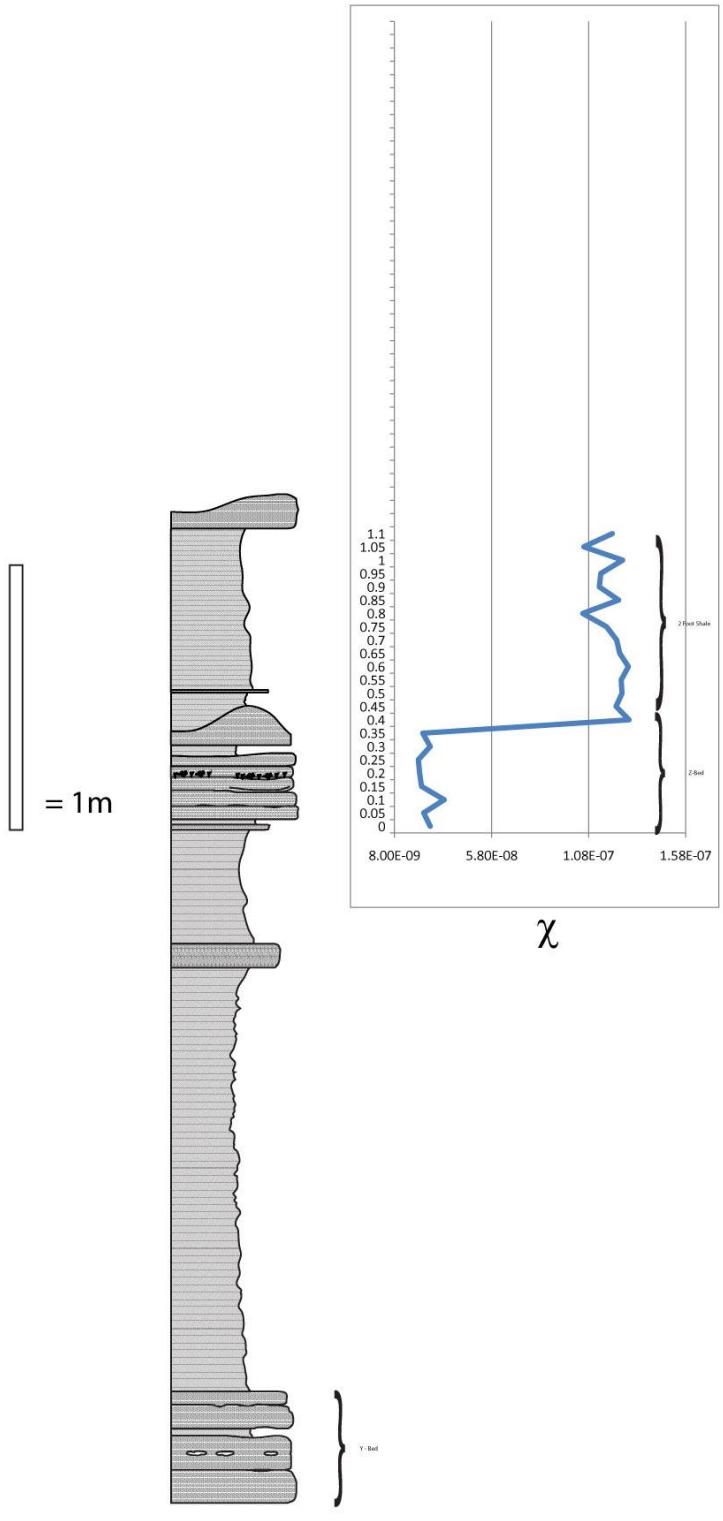

Brachiopod Heaven Montery Ky Rt. 127

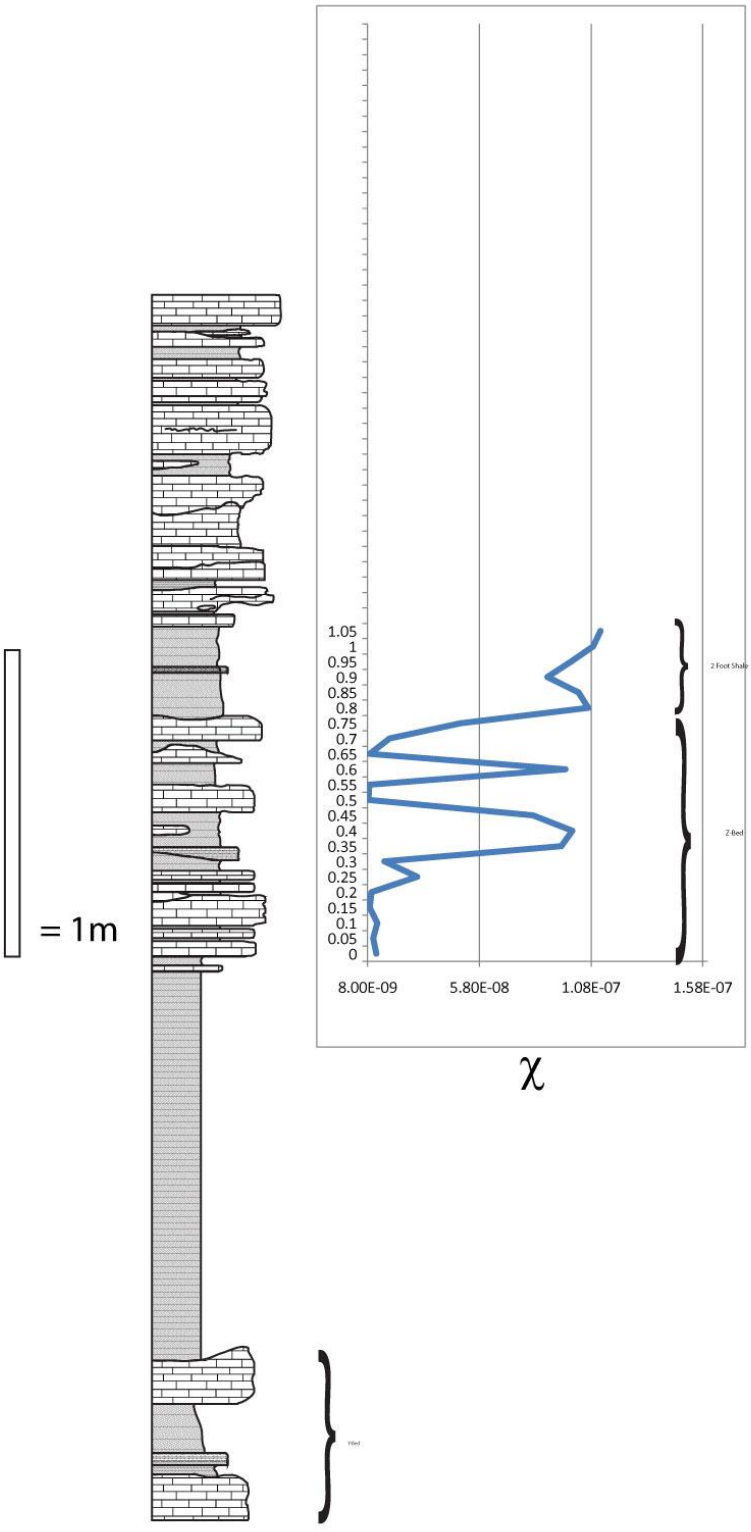

Taylorsville KY Rt. 44 Z-bed

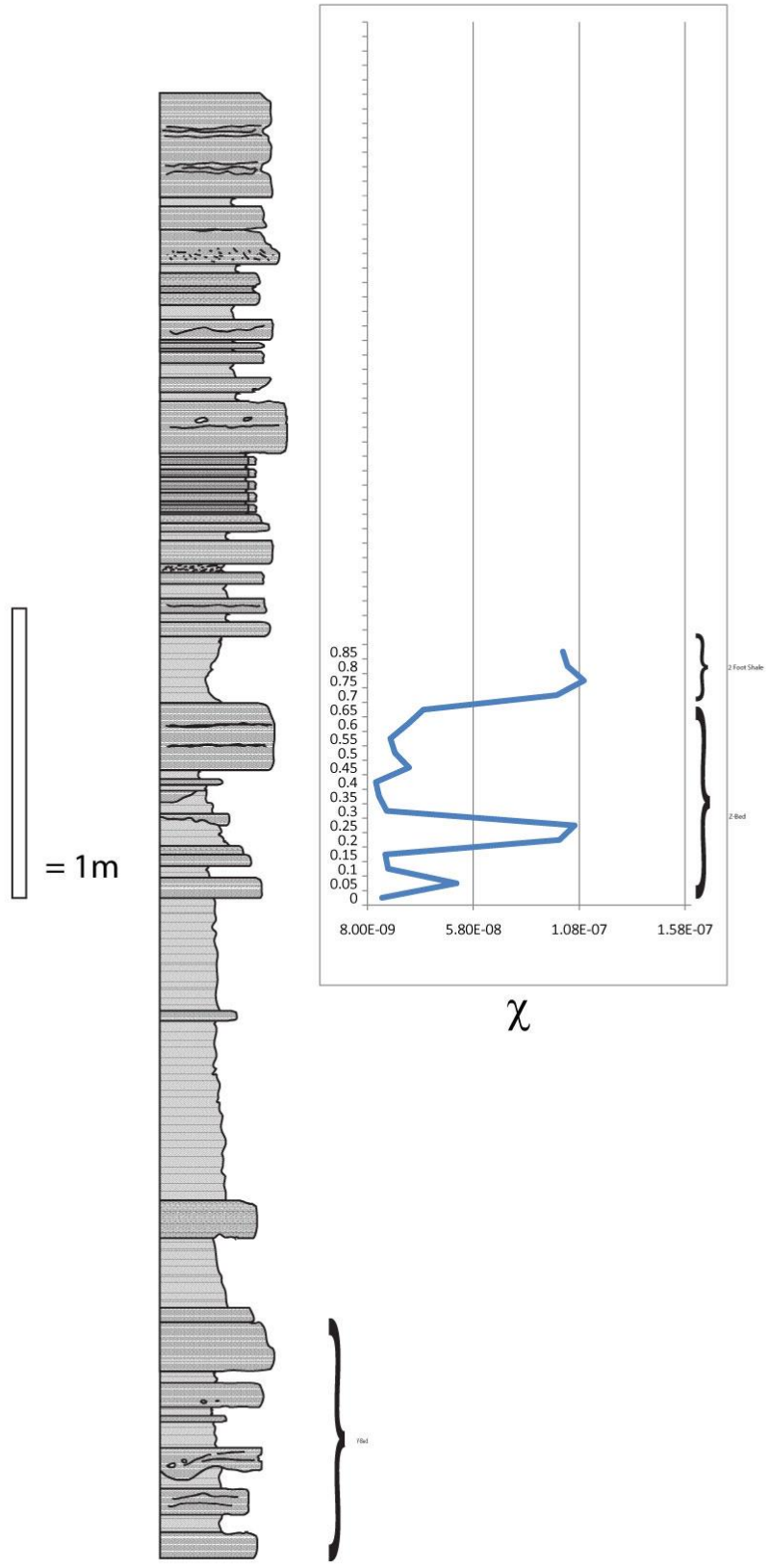

Taylorsville KY Rt. 55 Z-bed

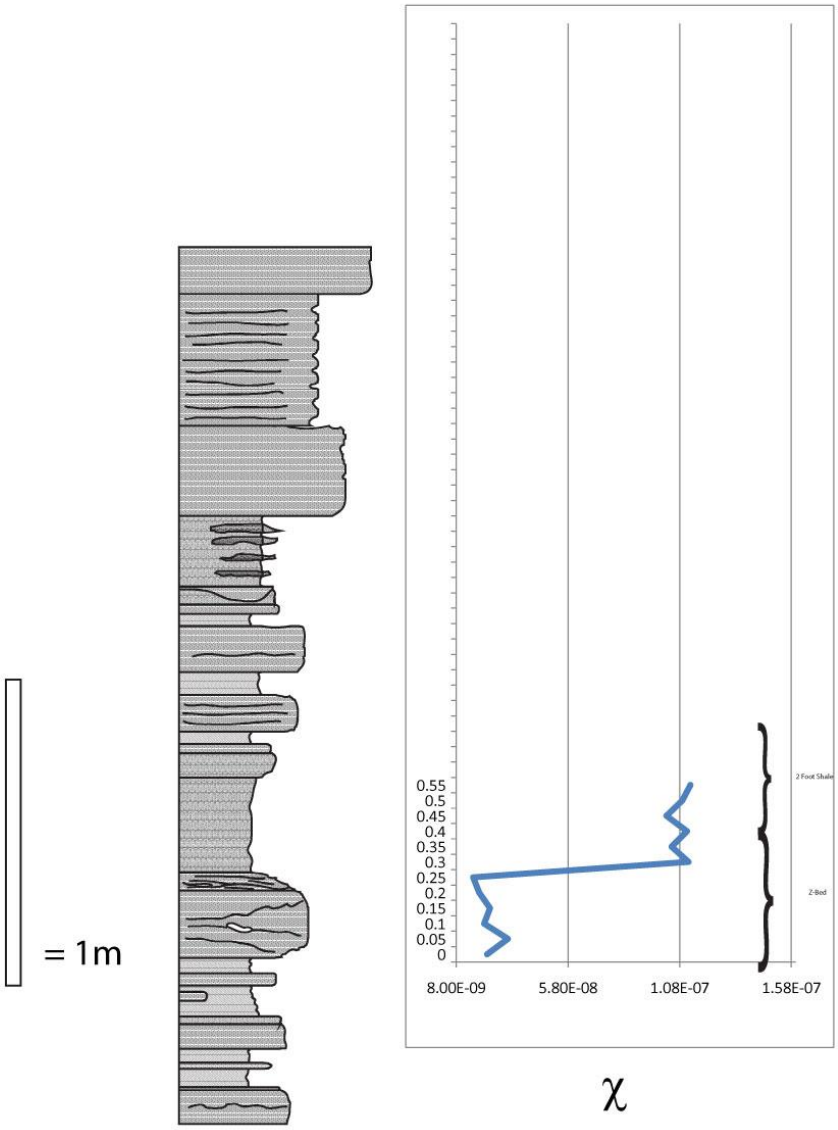

Blue Grass Pkwy Z-bed

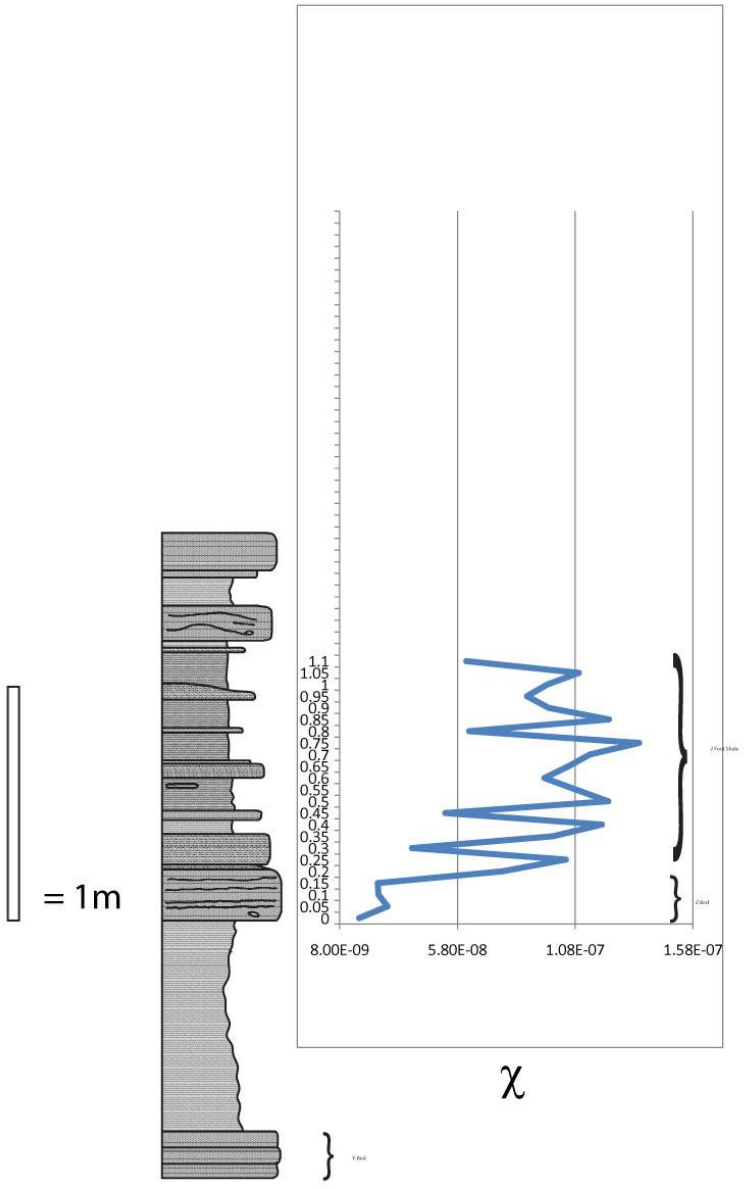

Boonesborough KY. Rt. 627 Z-bed

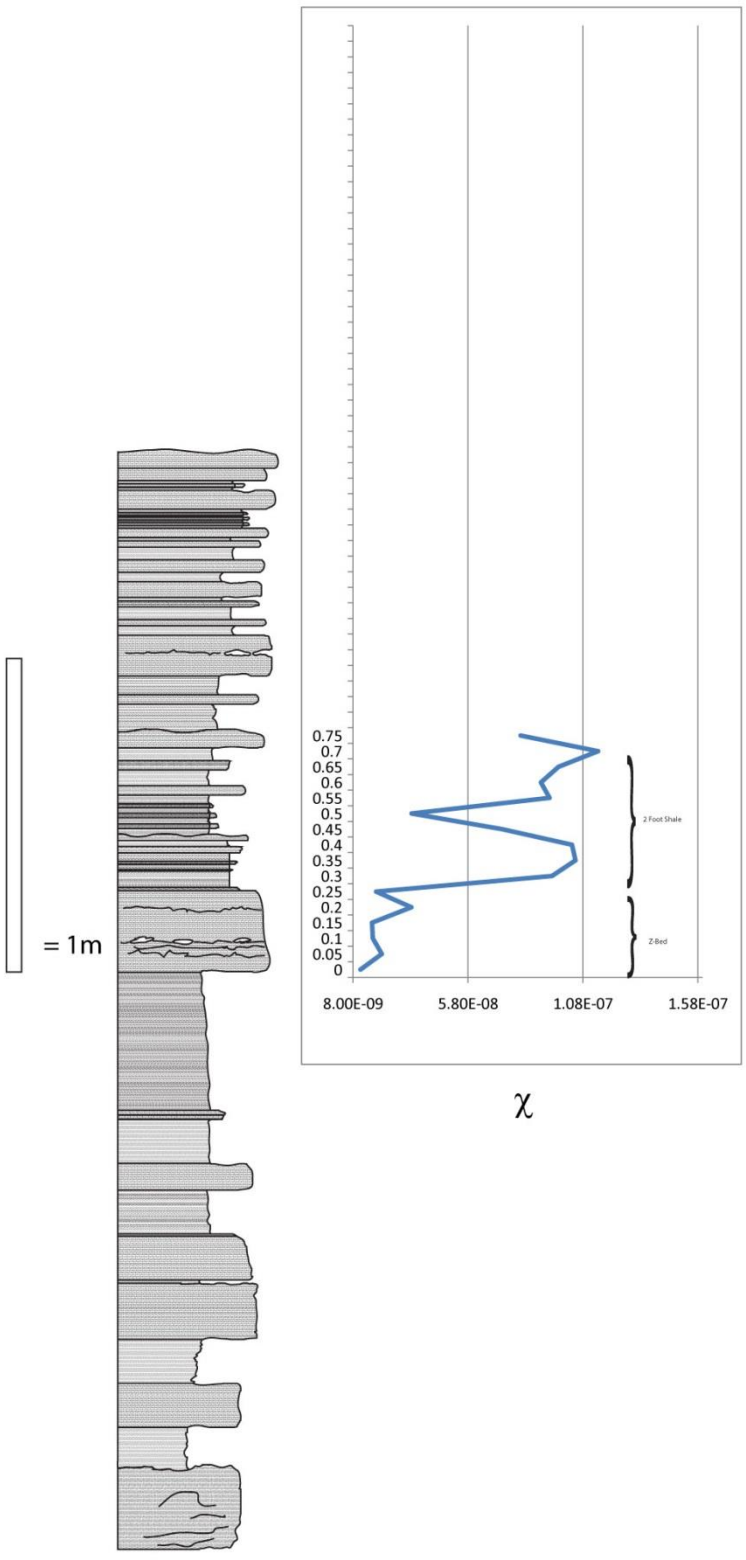

APPENDIX IV
SANDBIAN-KATIAN BOUNDARY SECTIONS SAMPLED

1.) Black Knob Ridge Atoka, OK (N 34°25.845' W 96°04.472')

2.) Fittstown, OK Rt. 99 (N 34°34.155' W 96°37.879')

3.) Frankfort (North), KY Rt. 127/Cove Springs Quarry (N 38°13.158' W 84°51.138')

4.) Hagan, VA (N 36°41.865' W 83°17.237')

5.) Ingham Mills, NY (N 43°03.747' W 74°45.829')

6.) Canajoharie Creek, NY (N 42°53.876' W 74°34.145')

7.) Allen/Schnell Rd. Oppenheimm NY (N 43°02.883' W 74°43.726')

8.) Frankfort (West) Rt. 421 (N 38°12.788' W 84°53.286')

APPENDIX V
SANDBIAN-KATIAN BOUNDARY χ VALUES

Ingham Mills, NY

Sample #	Height (m)	Mass (g)	χ m^3/kg	Standard Deviation
1	0	8.993	3.66E-08	8.51E-10
2	0.05	10.812	3.77E-08	8.49E-10
3	0.1	11.753	3.43E-08	5.74E-10
4	0.15	15.633	2.67E-08	1.63E-10
5	0.2	12.513	3.13E-08	5.39E-10
6	0.25	10.952	3.17E-08	4.66E-10
7	0.3	11.926	3.07E-08	6.41E-10
8	0.35	10.948	3.12E-08	9.32E-10
9	0.4	11.315	2.73E-08	4.51E-10
10	0.45	9.421	2.63E-08	4.70E-10
11	0.5	14.095	2.23E-08	4.79E-10
12	0.55	7.11	3.35E-08	1.30E-09
13	0.6	9.38	3.70E-08	7.19E-10
14	0.65	9.599	3.86E-08	9.58E-10
15	0.7	11.325	4.14E-08	3.89E-10
16	0.75	11.459	4.06E-08	8.01E-10
17	0.8	12.63	3.64E-08	4.03E-10
18	0.85	8.801	4.02E-08	1.04E-09
19	0.9	10.621	4.21E-08	4.15E-10
20	0.95	9.363	3.86E-08	4.72E-10
21	1	9.964	3.52E-08	7.68E-10
22	1.05	10.084	3.33E-08	9.12E-10
23	1.1	8.517	3.65E-08	7.93E-10
24	1.15	8.013	3.47E-08	1.27E-09
25	1.2	9.258	3.32E-08	9.55E-10
26	1.25	10.332	3.27E-08	6.53E-10
27	1.3	8.344	3.10E-08	5.30E-10
28	1.35	10.661	2.54E-08	8.64E-10
29	1.4	7.248	2.97E-08	1.22E-09
30	1.45	8.374	3.13E-08	8.07E-10
31	1.5	9.006	3.09E-08	1.13E-09
32	1.55	9.429	2.64E-08	2.71E-10
33	1.6	7.136	2.71E-08	1.08E-09
34	1.65	10.31	2.42E-08	6.56E-10
35	1.7	8.733	2.56E-08	7.75E-10
36	1.75	12.65	2.76E-08	8.07E-10
37	1.8	11.713	2.98E-08	7.85E-10
38	1.85	10.064	3.00E-08	7.61E-10
39	1.9	12.539	3.28E-08	7.32E-10
40	1.95	10.783	3.05E-08	4.10E-10

Sample #	Height (m)	Mass (g)	χ m^3/kg	Standard Deviation
41	2	8.655	2.96E-08	7.81E-10
42	2.05	10.21	2.37E-08	7.51E-10
43	2.1	12.808	2.72E-08	7.18E-10
44	2.15	11.918	2.82E-08	5.66E-10
45	2.2	7.826	5.01E-08	8.62E-10
46	2.25	11.464	3.04E-08	5.89E-10
47	2.3	10.455	4.04E-08	2.44E-10
48	2.35	11.312	3.45E-08	5.96E-10
49	2.4	11.995	3.28E-08	3.68E-10
50	2.45	11.489	3.85E-08	6.65E-10
51	2.5	13.257	4.43E-08	5.74E-10
52	2.55	10.292	5.14E-08	4.28E-10
53	2.6	8.619	4.86E-08	7.82E-10
54	2.65	11.848	4.70E-08	5.67E-10
55	2.7	8.65	4.70E-08	7.79E-10
56	2.75	15.865	3.84E-08	2.77E-10
57	2.8	7.96	4.76E-08	8.47E-10
58	2.85	10.144	3.88E-08	7.54E-10
59	2.9	12.781	3.07E-08	5.28E-10
60	2.95	12.31	2.58E-08	0
61	3	12.989	2.38E-08	5.20E-10
62	3.05	10.818	2.79E-08	7.08E-10
63	3.1	14.486	2.73E-08	4.65E-10
64	3.15	10.257	3.42E-08	4.31E-10
65	3.2	9.607	2.22E-08	7.04E-10
66	3.25	14.511	1.99E-08	4.66E-10
67	3.3	12.308	2.77E-08	2.07E-10
68	3.35	9.978	2.55E-08	6.77E-10
69	3.4	17.357	2.93E-08	3.88E-10
70	3.45	10.855	3.21E-08	9.40E-10
71	3.5	13.845	2.70E-08	3.68E-10
72	3.55	15.931	1.47E-08	5.78E-10
73	3.6	20.068	1.31E-08	1.27E-10
74	3.65	15.783	1.83E-08	1.62E-10
75	3.7	13.731	2.22E-08	6.70E-10
76	3.75	10.955	1.58E-08	2.34E-10
77	3.8	12.901	1.41E-08	5.95E-10
78	3.85	12.331	2.81E-08	5.47E-10
79	3.9	14.2	2.72E-08	6.47E-10
80	3.95	11.369	1.52E-08	2.25E-10
81	4	11.818	2.75E-08	7.78E-10
82	4.05	12.583	1.62E-08	3.52E-10
83	4.1	17.125	3.02E-08	2.57E-10
84	4.15	15.37	2.76E-08	4.38E-10
85	4.2	10.173	1.31E-08	7.55E-10

Sample #	Height (m)	Mass (g)	χ m^3/kg	Standard Deviation
86	4.25	14.206	4.44E-08	6.18E-10
87	4.3	13.43	1.71E-08	5.04E-10
88	4.35	13.03	1.41E-08	5.20E-10
89	4.4	12.531	2.16E-08	7.35E-10
90	4.45	12.662	2.48E-08	4.03E-10
91	4.5	11.432	1.47E-08	4.48E-10
92	4.55	9.773	2.94E-08	2.61E-10
93	4.6	12.621	2.02E-08	5.36E-10
94	4.65	14.861	1.58E-08	3.44E-10
95	4.7	10.321	1.78E-08	4.96E-10
96	4.75	11.555	1.59E-08	5.86E-10
97	4.8	12.722	1.48E-08	6.03E-10
98	4.85	8.597	3.11E-08	1.19E-09
99	4.9	11.799	3.53E-08	7.78E-10
100	4.95	10.352	1.74E-08	8.91E-10
101	5	13.342	1.41E-08	6.64E-10
102	5.05	10.661	2.07E-08	8.31E-10
103	5.1	13.953	2.25E-08	6.60E-10
104	5.15	10.528	2.61E-08	8.40E-10
105	5.2	10.856	1.60E-08	2.36E-10
106	5.25	16.953	1.46E-08	5.22E-10
107	5.3	16.2	1.42E-08	4.18E-10
108	5.35	15.603	1.50E-08	6.55E-10
109	5.4	15.143	2.24E-08	2.92E-10
110	5.45	15.692	1.63E-08	5.87E-10
111	5.5	10.324	1.57E-08	6.56E-10
112	5.55	11.109	1.76E-08	6.09E-10
113	5.6	15.579	1.69E-08	5.68E-10
114	5.65	12.919	2.07E-08	1.98E-10
115	5.7	17.591	2.38E-08	2.90E-10
116	5.75	14.768	1.12E-08	3.00E-10
117	5.8	14.045	1.48E-08	4.82E-10
118	5.85	14.184	1.80E-08	1.80E-10
119	5.9	13.576	1.58E-08	3.26E-10
120	5.95	14.616	1.30E-08	1.75E-10
121	6	14.328	1.03E-08	4.73E-10
122	6.05	13.525	1.43E-08	5.67E-10
123	6.1	14.438	1.64E-08	3.07E-10
124	6.15	13.656	1.53E-08	3.24E-10
125	6.2	10.725	2.75E-08	6.30E-10
126	6.25	15.661	1.49E-08	1.63E-10
127	6.3	15.04	1.20E-08	3.40E-10
128	6.35	16.256	1.01E-08	4.17E-10
129	6.4	13.479	1.30E-08	1.90E-10
130	6.45	12.444	1.79E-08	2.05E-10

Sample #	Height (m)	Mass (g)	χ m^3/kg	Standard Deviation
131	6.5	9.762	1.76E-08	4.54E-10
132	6.55	13.744	1.51E-08	1.86E-10
133	6.6	16.364	1.28E-08	5.41E-10
134	6.65	12.568	1.77E-08	4.07E-10
135	6.7	13.731	1.72E-08	5.58E-10
136	6.75	11.524	1.63E-08	0
137	6.8	11.125	1.66E-08	2.30E-10
138	6.85	16.108	1.55E-08	5.72E-10
139	6.9	15.81	1.55E-08	5.83E-10
140	6.95	10.935	1.82E-08	7.02E-10
141	7	12.964	1.56E-08	3.95E-10
142	7.05	10.442	2.32E-08	4.24E-10
143	7.1	13.832	2.08E-08	1.85E-10
144	7.15	13.123	1.58E-08	1.95E-10
145	7.2	12.757	2.15E-08	6.94E-10
146	7.25	13.99	2.26E-08	4.83E-10
147	7.3	14.425	1.87E-08	3.07E-10
148	7.35	11.2	1.82E-08	7.91E-10
149	7.4	7.293	2.53E-08	9.28E-10
150	7.45	11.138	1.86E-08	4.59E-10
151	7.5	13.223	1.89E-08	3.87E-10
152	7.55	15.129	2.05E-08	4.46E-10
153	7.6	10.82	2.02E-08	6.25E-10
154	7.65	13.276	1.90E-08	5.77E-10
155	7.7	10.029	1.40E-08	5.11E-10
156	7.75	9.664	1.55E-08	7.95E-10
157	7.8	9.006	1.30E-08	8.53E-10
158	7.85	12.58	1.29E-08	7.34E-10
159	7.9	9.147	1.78E-08	1.01E-09
160	7.95	8.221	1.38E-08	1.12E-09
161	8	10.363	1.65E-08	4.28E-10
162	8.05	9.577	1.41E-08	2.67E-10
163	8.1	10.845	1.13E-08	7.09E-10
164	8.15	11.852	1.37E-08	7.79E-10
165	8.2	9.853	1.26E-08	5.20E-10
166	8.25	11.185	9.83E-09	2.29E-10
167	8.3	11.99	1.75E-08	3.69E-10
168	8.35	12.287	1.34E-08	2.08E-10
169	8.4	10.705	1.99E-08	2.39E-10
170	8.45	15.097	1.34E-08	4.48E-10
171	8.5	14.849	9.84E-09	6.22E-10
172	8.55	12.596	1.22E-08	5.38E-10
173	8.6	15.611	1.20E-08	4.92E-10
174	8.65	10.808	1.12E-08	4.74E-10
175	8.7	12.925	1.07E-08	3.43E-10

Sample #	Height (m)	Mass (g)	χ m^3/kg	Standard Deviation
176	8.75	13.836	1.24E-08	3.20E-10
177	8.8	12.8	1.71E-08	3.99E-10
178	8.85	9.356	3.28E-08	9.45E-10
179	8.9	10.897	1.34E-08	4.70E-10
180	8.95	14.883	1.27E-08	4.55E-10
181	9	9.077	1.31E-08	1.02E-09
182	9.05	12.271	1.60E-08	2.08E-10
183	9.1	10.709	1.36E-08	4.78E-10
184	9.15	9.018	1.10E-08	5.68E-10
185	9.2	11.875	1.31E-08	7.47E-10
186	9.25	8.667	1.73E-08	5.12E-10
187	9.3	12.373	1.34E-08	6.21E-10
188	9.35	15.782	1.21E-08	4.29E-10
189	9.4	10.699	1.23E-08	4.79E-10
190	9.45	9.527	2.20E-08	9.30E-10
191	9.5	10.474	1.12E-08	4.24E-10
192	9.55	11.495	1.59E-08	3.86E-10
193	9.6	11.635	1.37E-08	5.82E-10
194	9.65	11.801	1.99E-08	7.81E-10
195	9.7	10.698	1.55E-08	8.29E-10
196	9.75	12.449	1.78E-08	5.43E-10
197	9.8	12.745	2.00E-08	2.00E-10
198	9.85	15.929	1.42E-08	5.56E-10
199	9.9	13.017	1.47E-08	5.20E-10
200	9.95	10.656	1.17E-08	4.81E-10
201	10	11.178	1.42E-08	6.06E-10
202	10.05	11.513	1.82E-08	6.66E-10
203	10.1	9.282	1.57E-08	2.76E-10
204	10.15	10.677	1.81E-08	8.30E-10
205	10.2	11.578	1.86E-08	3.83E-10
206	10.25	10.328	1.84E-08	6.55E-10
207	10.3	8.152	1.62E-08	3.14E-10
208	10.35	10.431	1.44E-08	7.36E-10
209	10.4	11.594	1.68E-08	4.41E-10
210	10.45	11.613	1.27E-08	5.83E-10
211	10.5	11.661	1.69E-08	2.19E-10
212	10.55	12.542	1.64E-08	7.35E-10
213	10.6	11.983	1.75E-08	3.70E-10
214	10.65	10.571	1.62E-08	4.19E-10
215	10.7	9.959	1.43E-08	6.80E-10
216	10.75	12.062	1.29E-08	6.37E-10
217	10.8	10.442	1.82E-08	8.83E-10
218	10.85	8.954	2.04E-08	8.57E-10
219	10.9	10.21	2.10E-08	4.34E-10
220	10.95	8.398	2.52E-08	1.10E-09

Sample #	Height (m)	Mass (g)	χ m^3/kg	Standard Deviation
221	11	8.725	1.68E-08	5.87E-10
222	11.05	12.15	1.74E-08	5.57E-10
223	11.1	12.205	1.33E-08	5.55E-10
224	11.15	9.856	1.83E-08	6.87E-10
225	11.2	8.164	1.68E-08	1.25E-09
226	11.25	10.48	2.00E-08	4.23E-10
227	11.3	11.812	1.99E-08	2.16E-10
228	11.35	11.129	1.83E-08	6.89E-10
229	11.4	12.809	2.10E-08	3.45E-10
230	11.45	13.702	2.91E-08	3.22E-10
231	11.5	10.516	2.75E-08	8.75E-10
232	11.55	9.505	1.42E-08	5.39E-10
233	11.6	12.645	1.71E-08	5.35E-10
234	11.65	10.095	2.08E-08	2.22E-16
235	11.7	10.225	2.00E-08	7.50E-10
236	11.75	9.962	2.01E-08	6.79E-10
237	11.8	8.72	1.61E-08	5.87E-10
238	11.85	10.18	2.38E-08	7.53E-10
239	11.9	6.917	2.17E-08	1.11E-09
240	11.95	10.659	2.12E-08	4.15E-10
241	12	10.988	2.48E-08	8.38E-10
242	12.05	10.774	1.89E-08	8.22E-10
243	12.1	12.306	1.35E-08	7.20E-10
244	12.15	10.315	1.73E-08	4.96E-10
245	12.2	8.639	1.61E-08	1.03E-09
246	12.25	10.584	1.62E-08	7.25E-10
247	12.3	8.727	2.69E-08	7.75E-10
248	12.35	9.672	1.90E-08	5.29E-10
249	12.4	9.864	2.31E-08	6.86E-10
250	12.45	14.139	2.71E-08	3.12E-10
251	12.5	10.774	1.56E-08	6.28E-10
252	12.55	12.551	3.08E-08	5.37E-10
253	12.6	9.237	1.45E-08	9.60E-10
254	12.65	8.609	1.70E-08	1.07E-09
255	12.7	12.151	1.58E-08	4.21E-10
256	12.75	9.802	1.38E-08	2.61E-10
257	12.8	8.184	2.27E-08	1.13E-09
258	12.85	13.167	2.11E-08	5.13E-10
259	12.9	9.714	1.86E-08	5.27E-10
260	12.95	11.333	1.88E-08	2.26E-10
261	13	17.385	2.43E-08	1.46E-10
262	13.05	12.653	2.14E-08	7.28E-10
263	13.1	11.804	2.31E-08	2.16E-10
264	13.15	13.527	1.78E-08	7.56E-10
265	13.2	12.317	2.54E-08	6.22E-10

Sample #	Height (m)	Mass (g)	χ m^3/kg	Standard Deviation
266	13.25	10.237	1.57E-08	7.50E-10
267	13.3	8.72	3.25E-08	5.86E-10
268	13.35	12.919	2.07E-08	7.13E-10
269	13.4	10.71	1.62E-08	2.39E-10
270	13.45	10.441	2.32E-08	4.24E-10
271	13.5	10.09	1.32E-08	0
272	13.55	12.043	1.38E-08	3.68E-10
273	13.6	12.292	1.97E-08	6.24E-10
274	13.65	12.175	1.74E-08	7.57E-10
275	13.7	10.126	2.23E-08	7.57E-10
276	13.75	10.599	1.57E-08	7.24E-10
277	13.8	13.686	2.59E-08	4.93E-10
278	13.85	13.343	1.20E-08	3.32E-10
279	13.9	13.743	1.43E-08	6.71E-10
280	13.95	12.107	1.46E-08	3.66E-10
281	14	11.737	1.58E-08	7.86E-10
282	14.05	12.492	1.66E-08	5.42E-10
283	14.1	8.64	2.05E-08	5.13E-10
284	14.15	10.344	1.97E-08	8.57E-10
285	14.2	9.919	1.58E-08	6.83E-10
286	14.25	11.524	1.39E-08	7.69E-10

Frankfort, KY

Sample #	Height (m)	Mass (g)	χ m^3/kg	Standard Deviation
1	-6.35	13.441	5.35E-09	3.82E-10
2	-6.3	14.366	3.24E-09	5.36E-10
3	-6.25	12.809	4.76E-09	2.00E-10
4	-6.2	10.255	6.12E-09	4.33E-10
5	-6.15	12.835	9.13E-09	3.46E-10
6	-6.1	9.775	1.03E-08	4.54E-10
7	-6.05	9.808	6.22E-09	5.23E-10
8	-6	9.905	7.99E-09	4.48E-10
9	-5.95	15.016	5.75E-09	3.41E-10
10	-5.9	13.189	4.21E-09	1.94E-10
11	-5.85	11.95	7.38E-09	5.68E-10
12	-5.8	12.794	5.33E-09	6.01E-10
13	-5.75	14.597	6.04E-09	6.33E-10
14	-5.7	9.685	6.86E-09	5.30E-10
15	-5.65	11.52	4.51E-09	3.86E-10
16	-5.6	10.804	1.08E-08	7.11E-10
17	-5.55	14.562	1.57E-09	1.76E-10
18	-5.5	15.449	4.18E-09	5.99E-10
19	-5.45	11.98	4.33E-09	7.42E-10
20	-5.4	12.547	2.55E-09	5.41E-10

Sample #	Height (m)	Mass (g)	χ m^3/kg	Standard Deviation
21	-5.35	11.856	3.92E-09	3.75E-10
22	-5.3	15.473	2.07E-09	4.39E-10
23	-5.25	13.786	2.19E-09	5.58E-10
24	-5.2	10.475	3.05E-09	6.48E-10
25	-5.15	14.276	8.41E-10	6.48E-10
26	-5.1	14.465	7.10E-09	3.54E-10
27	-5.05	11.69	8.32E-09	5.80E-10
28	-5	15.474	1.71E-09	4.39E-10
29	-4.95	14.621	6.97E-10	1.76E-10
30	-4.9	14.883	1.54E-09	6.90E-10
31	-4.85	10.583	2.33E-09	4.20E-10
32	-4.8	15.22	1.03E-09	3.37E-10
33	-4.75	9.278	3.15E-10	9.59E-10
34	-4.7	15.767	1.45E-09	4.31E-10
35	-4.65	14.729	4.51E-09	6.28E-10
36	-4.6	14.934	2.75E-09	2.98E-10
37	-4.55	14.017	1.63E-09	6.60E-10
38	-4.5	14.541	1.57E-09	1.77E-10
39	-4.45	15.483	2.65E-09	4.97E-10
40	-4.4	13.76	1.00E-09	5.60E-10
41	-4.35	13.234	1.18E-09	5.13E-10
42	-4.3	14.52	1.33E-09	5.30E-10
43	-4.25	13.068	1.89E-09	3.40E-10
44	-4.2	12.901	2.34E-09	3.45E-10
45	-4.15	13.132	4.09E-09	3.91E-10
46	-4.1	14.582	2.44E-09	3.05E-10
47	-4.05	13.332	1.85E-09	3.33E-10
48	-4	10.517	4.59E-09	6.45E-10
49	-3.95	12.502	2.34E-10	9.41E-10
50	-3.9	13.874	-5.08E-11	1.85E-10
51	-3.85	10.534	9.67E-10	2.44E-10
52	-3.8	12.751	1.88E-08	7.23E-10
53	-3.75	7.1	2.36E-08	7.21E-10
54	-3.7	12.723	1.66E-08	7.25E-10
55	-3.65	7.89	2.49E-08	3.24E-10
56	-3.6	14.035	7.32E-09	4.83E-10
57	-3.55	12.237	3.65E-09	2.10E-10
58	-3.5	12.849	3.05E-09	2.00E-10
59	-3.45	11.897	4.97E-09	5.70E-10
60	-3.4	14.559	2.20E-09	1.76E-10
61	-3.35	12.778	3.92E-09	2.01E-10
62	-3.3	11.288	3.31E-09	6.01E-10
63	-3.25	11.689	4.60E-09	7.91E-10
64	-3.2	14.621	2.68E-09	1.75E-10
65	-3.15	13.199	3.38E-09	5.14E-10

Sample #	Height (m)	Mass (g)	χ m^3/kg	Standard Deviation
66	-3.05	12.164	3.08E-09	2.11E-10
67	-3.1	14.027	2.28E-09	3.66E-10
68	-3	14.322	4.01E-09	5.37E-10
69	-2.95	13.102	3.55E-09	5.55E-17
70	-2.9	14.339	4.76E-09	5.36E-10
71	-2.85	13.361	4.70E-09	5.76E-10
72	-2.8	16.999	1.65E-08	5.20E-10
73	-2.75	14.173	5.07E-09	3.62E-10
74	-2.7	13.455	6.15E-09	5.04E-10
75	-2.65	13.08	6.46E-09	8.98E-10
76	-2.6	15.662	8.06E-09	4.33E-10
77	-2.55	15.362	6.92E-09	7.64E-10
78	-2.5	12.651	1.41E-08	5.35E-10
79	-2.45	12.534	7.76E-09	4.09E-10
80	-2.4	14.377	4.37E-09	3.09E-10
81	-2.35	11.65	4.46E-09	3.81E-10
82	-2.3	14.599	9.89E-09	3.04E-10
83	-2.25	10.894	3.91E-08	1.07E-09
84	-2.2	16.348	1.06E-08	4.14E-10
85	-2.15	15.881	4.30E-09	5.59E-10
86	-2.1	14.674	4.03E-09	4.62E-10
87	-2.05	13.252	1.99E-08	3.34E-10
88	-2	14.833	5.09E-09	4.57E-10
89	-1.95	14.539	5.44E-09	3.05E-10
90	-1.9	13.904	4.00E-09	4.88E-10
91	-1.85	17.553	4.51E-09	4.38E-10
92	-1.8	15.001	6.12E-09	1.71E-10
93	-1.75	14.343	8.17E-09	5.36E-10
94	-1.7	13.776	3.64E-09	1.86E-10
95	-1.65	12.576	2.54E-09	5.40E-10
96	-1.6	14.67	2.06E-09	5.25E-10
97	-1.55	15.778	3.18E-09	1.63E-10
98	-1.5	14.632	2.06E-09	0
99	-1.45	14.94	1.05E-09	6.20E-10
100	-1.4	13.105	2.30E-09	3.39E-10
101	-1.35	13.107	2.58E-09	5.18E-10
102	-1.3	15.589	2.98E-09	2.85E-10
103	-1.25	15.556	3.22E-09	1.65E-10
104	-1.2	15.195	3.54E-09	6.75E-10
105	-1.15	13.31	2.67E-09	3.34E-10
106	-1.1	12.172	4.12E-09	7.60E-10
107	-1.05	15.744	2.15E-09	4.31E-10
108	-1	17.56	4.09E-09	5.26E-10
109	-0.95	11.564	3.55E-09	3.84E-10
110	-0.9	15.036	2.13E-09	1.71E-10

Sample #	Height (m)	Mass (g)	χ m^3/kg	Standard Deviation
111	-0.85	15.955	1.55E-09	4.83E-10
112	-0.8	13.645	4.07E-09	1.88E-10
113	-0.75	13.444	2.38E-09	5.05E-10
114	-0.7	15.67	1.92E-09	2.84E-10
115	-0.65	15.774	3.18E-09	1.63E-10
116	-0.6	11.774	2.87E-09	2.18E-10
117	-0.55	15.971	2.12E-09	4.25E-10
118	-0.5	15.915	1.89E-09	2.79E-10
119	-0.45	18.138	2.56E-09	4.81E-17
120	-0.4	13.875	1.39E-09	6.41E-10
121	-0.35	13.333	2.13E-09	7.70E-10
122	-0.3	15.199	3.06E-09	2.92E-10
123	-0.25	14.16	2.13E-09	3.14E-10
124	-0.2	14.564	7.00E-10	6.36E-10
125	-0.15	14.692	1.81E-09	1.75E-10
126	-0.1	18.218	1.26E-09	1.41E-10
127	-0.05	18.08	1.17E-09	5.68E-10
128	0	13.39	1.44E-09	6.64E-10
129	0.05	9.456	2.39E-08	4.68E-10
130	0.1	12.575	3.41E-09	2.04E-10
131	0.15	12.062	5.81E-09	2.13E-10
132	0.2	11.322	9.39E-09	1.11E-16
133	0.25	14.06	4.60E-09	4.83E-10
134	0.3	13.009	6.36E-09	7.11E-10
135	0.35	13.019	7.05E-09	5.21E-10
136	0.4	15.849	9.91E-09	4.27E-10
137	0.45	15.479	1.10E-08	5.96E-10
138	0.5	15.648	7.14E-09	4.91E-10
139	0.55	12.69	6.52E-09	2.02E-10
140	0.6	17.008	8.70E-09	1.51E-10
141	0.65	12.682	4.24E-09	7.29E-10
142	0.7	14.446	3.97E-09	5.33E-10
143	0.75	11.212	4.47E-09	2.29E-10
144	0.8	13.829	2.57E-09	0.00E+00
145	0.85	12.429	5.64E-09	7.44E-10
146	0.9	12.558	3.99E-09	4.09E-10
147	0.95	13.69	4.59E-09	0.00E+00
148	1	13.643	4.07E-09	3.76E-10
149	1.05	12.997	1.62E-09	7.12E-10
150	1.1	13.393	1.98E-09	1.92E-10
151	1.15	12.032	2.81E-09	2.13E-10
152	1.2	12.881	3.05E-09	3.98E-10
153	1.25	12.374	3.32E-09	3.59E-10
154	1.3	13.955	3.59E-09	3.68E-10
155	1.35	11.185	5.13E-09	3.97E-10

Sample #	Height (m)	Mass (g)	χ m^3/kg	Standard Deviation
156	1.4	12.877	4.31E-09	3.98E-10
157	1.45	13.824	4.94E-09	3.21E-10
158	1.5	12.269	4.53E-09	2.09E-10
159	1.55	12.878	4.17E-09	1.99E-10
160	1.6	12.807	4.90E-09	6.94E-10
161	1.65	11.865	5.29E-09	6.48E-10
162	1.7	13.72	4.05E-09	1.87E-10
163	1.75	13.61	4.35E-09	1.88E-10
164	1.8	12.186	6.64E-09	2.10E-10
165	1.85	10.637	5.90E-09	0
166	1.9	13.602	4.62E-09	5.66E-10
167	1.95	12.448	5.05E-09	3.57E-10
168	2	12.867	6.43E-09	5.27E-10
169	2.05	10.521	7.00E-09	7.31E-10
170	2.1	11.159	5.95E-09	6.08E-10
171	2.15	10.424	7.07E-09	4.26E-10
172	2.2	12.67	6.39E-09	7.30E-10
173	2.25	13.689	6.44E-09	6.75E-10
174	2.3	11.228	9.95E-09	6.85E-10
175	2.35	12.903	8.38E-09	7.16E-10
176	2.4	11.892	7.87E-09	7.77E-10
177	2.45	13.334	9.06E-09	3.84E-10
178	2.5	12.641	5.69E-09	4.06E-10
179	2.55	13.455	5.88E-09	5.72E-10
180	2.6	12.09	6.39E-09	8.48E-10
181	2.65	14.844	5.09E-09	4.57E-10
182	2.7	8.398	9.21E-09	6.11E-10
183	2.75	11.328	6.98E-09	6.79E-10
184	2.8	12.712	7.94E-09	3.49E-10
185	2.85	10.955	8.55E-09	8.44E-10
186	2.9	12.625	8.42E-09	6.09E-10
187	2.95	12.151	8.60E-09	5.58E-10
188	3	11.381	7.91E-09	3.90E-10
189	3.05	13.78	6.79E-09	4.92E-10
190	3.1	10.101	1.23E-08	6.71E-10
191	3.15	10.464	7.04E-09	4.24E-10
192	3.2	10.752	8.88E-09	8.26E-10
193	3.25	10.977	6.55E-09	9.34E-10
194	3.3	14.024	5.51E-09	6.59E-10
195	3.35	14.545	7.06E-09	4.66E-10
196	3.4	12.885	9.09E-09	5.96E-10
197	3.45	12.154	6.51E-09	6.33E-10
198	3.5	13.557	5.84E-09	0
199	3.55	14.846	7.28E-09	4.57E-10
200	3.6	12.779	9.88E-09	7.23E-10

Sample #	Height (m)	Mass (g)	χ m^3/kg	Standard Deviation
201	3.65	14.674	7.00E-09	6.30E-10
202	3.7	13.039	8.57E-09	6.81E-10
203	3.75	12.388	7.70E-09	7.17E-10
204	3.8	13.832	6.11E-09	3.21E-10
205	3.85	14.885	6.90E-09	4.55E-10
206	3.9	13.024	5.94E-09	3.94E-10
207	3.95	15.005	6.48E-09	4.52E-10
208	4	11.062	9.12E-09	4.01E-10
209	4.05	11.608	1.06E-08	3.82E-10
210	4.1	16.292	1.17E-08	5.66E-10
211	4.11	9.415	1.11E-08	2.72E-10
212	4.15	12.666	1.84E-08	5.34E-10
213	4.151	11.976	9.33E-09	3.71E-10
214	4.2	12.048	7.47E-09	6.38E-10
215	4.25	14.02	6.68E-09	3.66E-10
216	4.3	10.85	1.05E-08	4.72E-10
217	4.35	12.489	9.96E-09	5.43E-10
218	4.4	11.245	1.98E-08	4.55E-10
219	4.45	11.527	1.75E-08	5.87E-10
220	4.5	10.651	1.22E-08	4.81E-10
221	4.55	11.481	1.21E-08	7.73E-10
222	4.6	13.158	1.06E-08	1.57E-16
223	4.65	12.408	8.57E-09	3.58E-10
224	4.7	11.361	1.06E-08	8.13E-10
225	4.75	14.137	6.62E-09	3.63E-10
226	4.8	13.272	4.73E-09	3.35E-10
227	4.85	11.372	4.88E-09	2.26E-10
228	4.9	12.227	4.84E-09	4.20E-10
229	4.95	11.81	5.16E-09	4.34E-10
230	5	11.88	6.05E-09	2.16E-10
231	5.05	15.047	4.05E-09	4.51E-10
232	5.1	13.966	9.82E-09	3.67E-10
233	5.15	12.188	5.00E-09	2.10E-10
234	5.2	12.981	7.07E-09	7.12E-10
235	5.25	12.746	5.92E-09	4.02E-10
236	5.3	12.093	6.09E-09	3.67E-10
237	5.35	12.065	7.16E-09	7.66E-10
238	5.4	12.58	6.00E-09	7.35E-10
239	5.45	11.964	4.04E-09	2.14E-10
240	5.5	14.379	6.01E-09	4.72E-10
241	5.55	13.687	6.71E-09	4.95E-10
242	5.6	13.927	5.16E-09	4.87E-10
243	5.65	13.796	5.21E-09	1.86E-10
244	5.7	13.891	4.78E-09	4.88E-10
245	5.75	11.294	5.08E-09	6.81E-10

Sample #	Height (m)	Mass (g)	χ m^3/kg	Standard Deviation
246	5.8	12.743	1.00E-08	6.03E-10
247	5.85	13.593	4.62E-09	5.66E-10
248	5.9	13.748	4.30E-09	6.73E-10
249	5.95	11.794	1.25E-08	7.83E-10
250	6	15.461	6.29E-09	6.63E-10
251	6.05	11.646	7.11E-09	5.82E-10
252	6.1	15.935	5.19E-09	3.22E-10
253	6.15	13.197	4.62E-09	1.94E-10
254	6.2	10.031	6.26E-09	7.67E-10
255	6.25	13.369	4.02E-09	5.08E-10
256	6.3	14.212	4.67E-09	3.61E-10
257	6.35	12.181	5.60E-09	0
258	6.4	13.142	6.30E-09	3.90E-10
259	6.45	13.805	4.55E-09	3.22E-10
260	6.5	12.502	4.88E-09	7.40E-10
261	6.55	14.212	3.78E-09	4.78E-10
262	6.6	14.388	3.23E-09	6.18E-10
263	6.65	14.022	7.32E-09	7.31E-10
264	6.7	15.028	4.78E-09	4.51E-10
265	6.75	14.859	3.49E-09	2.99E-10
266	6.8	17.031	2.73E-09	2.61E-10
267	6.85	17.241	3.01E-09	5.15E-10
268	6.9	16.924	8.64E-09	3.03E-10
269	6.95	14.062	3.95E-09	4.83E-10
270	7	16.881	2.22E-09	1.52E-10
271	7.05	15.428	1.05E-08	3.32E-10
272	7.1	14.336	2.10E-09	5.37E-10
273	7.15	17.038	3.79E-09	1.51E-10
274	7.2	16.771	3.85E-09	5.51E-10
275	7.25	14.912	4.33E-09	3.44E-10
276	7.3	16.618	3.12E-09	4.63E-10
277	7.35	14.827	8.88E-09	3.45E-10
278	7.4	15.928	7.02E-09	4.83E-10
279	7.45	16.252	1.62E-08	5.45E-10
280	7.5	15.399	9.26E-09	1.66E-10
281	7.55	15.061	6.82E-09	1.70E-10
282	7.6	13.39	3.11E-08	6.86E-10
283	7.65	16.308	1.07E-08	4.15E-10
284	7.7	18.681	1.30E-08	4.10E-10
285	7.75	15.367	3.11E-08	4.38E-10
286	7.8	15.344	1.26E-08	2.89E-10
287	7.85	14.942	1.74E-08	4.52E-10
288	7.9	14.525	1.32E-08	7.05E-10
289	7.95	20.202	2.99E-08	3.77E-10
290	8	14.858	1.39E-08	3.44E-10

Sample #	Height (m)	Mass (g)	χ m^3/kg	Standard Deviation
291	8.05	19.429	2.87E-08	4.71E-10
292	8.1	14.836	2.37E-08	1.72E-10
293	8.15	19.319	8.41E-09	5.30E-10
294	8.2	14.696	6.74E-09	6.29E-10
295	8.25	14.151	1.10E-08	5.43E-10
296	8.3	17.263	1.65E-08	5.12E-10
297	8.35	20.378	2.43E-08	3.30E-10
298	8.4	20.386	1.26E-08	5.01E-10
299	8.45	19.811	3.01E-08	4.62E-10
300	8.5	16.529	1.02E-08	1.55E-10
301	8.55	19.36	1.72E-08	4.75E-10
302	8.6	15.484	3.46E-08	5.92E-10
303	8.65	18.401	2.90E-08	4.78E-10
304	8.7	16.494	3.37E-08	5.33E-10
305	8.75	19.871	1.23E-08	3.40E-10
306	8.8	18.053	2.60E-08	2.44E-10
307	8.85	16.278	1.32E-08	2.72E-10
308	8.9	17.984	1.25E-08	5.13E-10
309	8.95	18.665	1.12E-08	4.11E-10
310	9	16.649	3.15E-08	5.50E-10
311	9.05	17.043	2.99E-08	5.38E-10
312	9.1	17.255	1.24E-08	3.92E-10
313	9.15	17.196	1.67E-08	5.94E-10
314	9.2	16.851	2.13E-08	4.00E-10
315	9.25	18.681	2.44E-08	3.60E-10
316	9.3	18.027	1.42E-08	3.75E-10
317	9.35	19.319	2.44E-08	1.32E-10
318	9.4	16.142	2.71E-08	0
319	9.45	14.056	1.52E-08	6.56E-10
320	9.5	17.649	1.01E-08	1.45E-10
321	9.55	17.009	1.10E-08	4.51E-10
322	9.6	16.132	2.42E-08	5.70E-10
323	9.65	18.901	2.04E-08	3.57E-10
324	9.7	14.107	1.19E-08	4.80E-10
325	9.75	16.534	2.14E-08	5.56E-10
326	9.8	14.218	1.37E-08	1.80E-10
327	9.85	17.169	1.26E-08	1.49E-10
328	9.9	17.05	2.38E-08	2.99E-10
329	9.95	15.974	2.34E-08	6.38E-10
330	10	14.283	2.20E-08	3.57E-10
331	10.05	12.712	2.86E-08	8.02E-10
332	10.1	14.331	1.87E-08	4.72E-10
333	10.15	13.351	1.27E-08	1.92E-10
334	10.2	11.87	1.25E-08	2.16E-10
335	10.25	12.671	1.21E-08	4.04E-10

Sample #	Height (m)	Mass (g)	χ m^3/kg	Standard Deviation
336	10.3	15.742	2.35E-08	5.84E-10
337	10.35	13.66	2.80E-08	6.46E-10
338	10.4	13.006	2.19E-08	5.89E-10
339	10.45	14.968	1.25E-08	5.13E-10
340	10.5	13.967	2.65E-08	4.83E-10
341	10.55	14.056	2.60E-08	4.80E-10
342	10.6	12.303	1.38E-08	8.32E-10
343	10.65	13.443	1.33E-08	1.90E-10
344	10.7	14.765	2.85E-08	5.17E-10
345	10.75	15.451	2.92E-08	1.65E-10
346	10.8	12.371	1.23E-08	2.07E-10
347	10.85	14.634	2.39E-08	3.02E-10
348	10.9	12.694	1.41E-08	4.03E-10
349	10.95	14.972	1.29E-08	5.13E-10
350	11	14.661	1.21E-08	3.02E-10
351	11.05	13.588	1.57E-08	3.76E-10
352	11.1	12.725	2.94E-08	5.30E-10
353	11.15	11.7	2.33E-08	2.18E-10
354	11.2	12.571	1.36E-08	6.11E-10
355	11.25	13.394	2.29E-08	5.72E-10
356	11.3	13.774	2.01E-08	4.91E-10
357	11.35	17.442	1.83E-08	3.87E-10
358	11.4	13.335	1.83E-08	1.92E-10
359	11.45	16.139	2.35E-08	4.18E-10
360	11.5	14.206	5.57E-09	5.41E-10
361	11.55	13.814	5.99E-09	3.71E-10
362	11.6	14.773	5.60E-09	4.59E-10
363	11.65	15.639	3.67E-09	2.84E-10
364	11.7	12.379	3.32E-09	3.59E-10
365	11.75	11.626	2.28E-09	5.84E-10
366	11.8	11.561	2.92E-09	2.22E-10
367	11.85	14.51	4.58E-09	4.68E-10
368	11.9	14.795	5.35E-09	5.20E-10
369	11.95	13.525	5.05E-09	3.28E-10
370	12	14.649	4.41E-09	4.63E-10
371	12.05	13.736	2.99E-09	3.24E-10
372	12.1	13.127	3.40E-09	1.95E-10
373	12.15	14.305	7.12E-10	4.75E-10
374	12.2	11.38	1.53E-09	2.26E-10
375	12.25	11.59	2.45E-09	4.43E-10
376	12.3	14.984	1.29E-09	5.93E-10
377	12.35	13.886	4.52E-09	3.20E-10
378	12.4	13.37	1.44E-09	3.33E-10
379	12.45	13.597	3.95E-09	4.99E-10
380	12.5	10.799	5.48E-09	6.28E-10

Sample #	Height (m)	Mass (g)	χ m^3/kg	Standard Deviation
381	12.55	13.76	2.97E-08	3.70E-10
382	12.6	13.155	1.39E-08	3.37E-10
383	12.65	14.234	1.24E-08	3.11E-10
384	12.7	12.454	1.91E-08	5.43E-10
385	12.75	11.691	8.78E-09	2.19E-10
386	12.8	12.357	1.39E-08	3.59E-10
387	12.85	12.439	2.51E-08	3.55E-10
388	12.9	15.317	8.48E-09	3.34E-10
389	12.95	13.531	7.72E-09	5.01E-10
390	13	12.008	1.17E-08	4.27E-10
391	13.05	13.784	6.92E-09	3.22E-10
392	13.1	13.008	5.53E-09	5.22E-10
393	13.15	13.02	2.29E-08	5.19E-10
394	13.2	11.623	1.37E-08	5.83E-10
395	13.25	16.708	5.50E-09	4.06E-10
396	13.3	13.967	6.05E-09	3.18E-10
397	13.35	12.806	2.23E-08	3.45E-10
398	13.4	14.514	7.20E-09	4.67E-10
399	13.45	14.945	4.93E-09	2.97E-10
400	13.5	13.01	4.41E-09	3.41E-10
401	13.55	15.359	5.86E-09	2.89E-10
402	13.6	14.619	5.04E-09	5.26E-10
403	13.65	13.877	6.49E-09	3.20E-10
404	13.7	14.148	1.63E-08	6.26E-10
405	13.75	11.264	2.44E-08	3.93E-10
406	13.8	14.515	1.97E-08	5.28E-10
407	13.85	13.234	1.15E-08	5.12E-10
408	13.9	13.478	1.38E-08	5.02E-10
409	13.95	12.977	1.66E-08	5.91E-10
410	14	13.077	1.12E-08	5.18E-10
411	14.05	14.673	1.01E-08	4.62E-10
412	14.1	12.413	2.52E-08	3.56E-10
413	14.15	11.905	2.35E-08	7.43E-10
414	14.2	13.053	1.33E-08	7.07E-10
415	14.25	12.359	1.01E-08	5.48E-10
416	14.3	12.292	1.84E-08	6.24E-10
417	14.35	14.694	8.96E-09	6.28E-10
418	14.4	14.472	1.07E-08	3.06E-10
419	14.45	13.507	2.26E-08	3.78E-10
420	14.5	13.626	2.41E-08	0
421	14.55	13.361	1.09E-08	3.83E-10
422	14.6	12.153	1.04E-08	4.22E-10
423	14.65	12.475	9.83E-09	7.11E-10
424	14.7	14.489	1.07E-08	5.30E-10
425	14.75	15.503	2.17E-08	5.93E-10

Sample #	Height (m)	Mass (g)	χ m^3/kg	Standard Deviation
426	14.8	14.577	1.95E-08	1.75E-10
427	14.85	13.212	8.73E-09	1.94E-10
428	14.9	15.953	6.78E-09	1.61E-10
429	14.95	13.506	2.01E-08	1.89E-10
430	15	12.897	1.39E-08	5.25E-10
431	15.05	18.624	1.11E-08	5.49E-10
432	15.1	11.885	1.44E-08	7.46E-10
433	15.15	16.041	2.04E-08	3.18E-10
434	15.2	15.028	2.07E-08	1.70E-10
435	15.25	14.219	1.61E-08	6.48E-10
436	15.3	15.796	1.90E-08	1.62E-10
437	15.35	13.588	1.17E-08	6.79E-10
438	15.4	15.791	9.26E-09	4.29E-10
439	15.45	14.702	1.19E-08	3.48E-10
440	15.5	13.306	1.23E-08	5.09E-10
441	15.55	14.792	2.06E-08	4.57E-10
442	15.6	19.336	5.03E-09	3.51E-10
443	15.65	16.149	1.42E-09	1.59E-10
444	15.7	12.873	3.75E-09	7.19E-10
445	15.75	13.631	2.74E-09	4.98E-10
446	15.8	12.295	2.16E-09	7.53E-10
447	15.85	15.514	4.52E-09	3.31E-10
448	15.9	15.4	4.67E-09	3.33E-10
449	15.95	13.277	4.87E-09	5.11E-10
450	16	17.66	9.88E-10	3.85E-10
451	16.05	13.606	2.75E-09	1.89E-10
452	16.1	13.921	1.91E-09	4.88E-10
453	16.15	15.89	1.43E-08	4.26E-10
454	16.2	13.245	2.59E-08	5.10E-10
455	16.25	14.165	2.41E-08	4.76E-10
456	16.3	13.367	5.65E-09	7.67E-10
457	16.35	14.448	4.97E-09	1.77E-10
458	16.4	15.594	4.61E-09	4.35E-10
459	16.45	12.944	4.29E-09	3.96E-10
460	16.5	14.143	3.54E-09	4.80E-10
461	16.55	15.423	2.54E-09	6.00E-10
462	16.6	14.579	4.68E-09	3.05E-10
463	16.65	16.527	4.79E-09	2.69E-10
464	16.7	13.993	5.53E-09	1.83E-10
465	16.75	13.374	4.29E-09	3.32E-10
466	16.8	13.36	5.38E-09	1.92E-10
467	16.85	15.538	1.71E-09	1.65E-10
468	16.9	15.975	2.80E-09	4.25E-10
469	16.95	12.472	2.42E-09	7.13E-10
470	17	15.859	3.16E-09	1.62E-10

Sample #	Height (m)	Mass (g)	χ m^3/kg	Standard Deviation
471	17.05	15.122	5.95E-09	5.08E-10
472	17.1	14.485	3.08E-09	3.54E-10
473	17.15	12.082	1.04E-08	7.64E-10
474	17.2	14.169	2.64E-09	1.81E-10
475	17.25	15.028	4.06E-09	4.52E-10
476	17.3	15.115	4.16E-09	5.88E-10
477	17.35	16.273	2.41E-09	3.15E-10
478	17.4	14.435	2.84E-09	3.08E-10
479	17.45	15.344	3.62E-09	6.03E-10
480	17.5	15.941	8.37E-09	2.78E-10
481	17.55	12.412	6.23E-09	4.13E-10
482	17.6	12.944	4.71E-09	5.24E-10
483	17.65	13.758	3.91E-09	3.73E-10
484	17.7	15.986	5.06E-09	5.78E-10
485	17.75	16.76	3.12E-08	4.55E-10
486	17.8	14.82	7.66E-09	6.23E-10
487	17.85	14.922	2.14E-09	4.55E-10
488	17.9	17.429	3.92E-09	5.10E-10
489	17.95	13.677	4.59E-09	3.25E-10
490	18	13.717	1.21E-08	5.60E-10
491	18.05	15.806	2.40E-08	4.27E-10
492	18.1	15.825	4.66E-09	5.61E-10
493	18.15	13.676	2.65E-08	6.72E-10
494	18.2	17.076	4.53E-09	3.97E-10
495	18.25	14.381	8.40E-09	6.42E-10
496	18.3	16.258	7.65E-09	4.17E-10
497	18.35	14.932	4.69E-09	6.19E-10
498	18.38	12.328	6.35E-08	4.10E-10
499	18.4	12.058	2.10E-08	6.36E-10
500	18.45	17.636	3.56E-09	5.04E-10
501	18.5	16.492	5.57E-09	3.11E-10
502	18.55	14.935	3.36E-09	1.72E-10
503	18.6	15.357	5.27E-09	3.34E-10
504	18.65	12.336	3.62E-09	2.08E-10
505	18.7	15.279	2.21E-09	3.36E-10
506	18.75	15.439	1.72E-09	4.40E-10
507	18.8	14.082	3.74E-08	7.22E-10
508	18.85	15.855	7.85E-09	3.23E-10
509	18.9	17.315	4.47E-09	1.48E-10
510	18.95	14.449	5.60E-09	3.55E-10
511	19	15.777	3.18E-09	3.25E-10
512	19.05	13.038	1.26E-08	3.93E-10
513	19.1	13.764	7.33E-09	3.22E-10
514	19.15	15.651	4.13E-09	5.91E-10
515	19.2	16.244	5.65E-09	4.17E-10

Sample #	Height (m)	Mass (g)	χ m^3/kg	Standard Deviation
516	19.25	15.957	1.09E-09	5.80E-10
517	19.3	13.155	4.91E-09	3.90E-10
518	19.35	15.905	6.00E-09	7.85E-17
519	19.4	16.104	4.13E-09	4.21E-10
520	19.45	13.77	5.35E-09	5.59E-10
521	19.5	15.608	1.58E-09	2.85E-10
522	19.55	17.849	2.81E-09	1.44E-10
523	19.6	14.727	3.03E-09	1.74E-10
524	19.7	18.316	4.22E-09	3.70E-10
525	19.8	15.035	4.78E-09	1.71E-10
526	19.9	15.992	2.91E-09	4.81E-10
527	20	13.645	4.20E-09	3.26E-10
528	20.1	13.652	5.00E-09	3.25E-10
529	20.2	11.434	2.95E-09	5.94E-10
530	20.3	15.129	5.23E-09	2.94E-10
531	20.4	14.275	3.38E-09	1.80E-10
532	20.5	12.594	8.87E-09	6.10E-10
533	20.6	14.308	5.91E-09	6.21E-10
534	20.7	14.438	6.86E-09	6.40E-10
535	20.8	11.939	6.63E-09	3.72E-10
536	20.9	13.494	4.65E-09	5.70E-10
537	21	13.32	5.40E-09	5.09E-10
538	21.1	13.864	8.06E-09	3.20E-10
539	21.2	12.516	6.61E-09	8.19E-10
540	21.3	13.958	7.49E-09	1.84E-10
541	21.4	15.161	4.86E-09	2.93E-10
542	21.5	11.547	7.95E-09	5.87E-10
543	21.6	14.275	7.07E-09	6.22E-10
544	21.7	14.293	5.03E-09	6.47E-10
545	21.8	12.719	5.65E-09	5.33E-10
546	21.9	15.463	3.71E-09	5.55E-17
547	22	13.861	7.54E-09	4.89E-10
548	22.1	15.231	9.36E-09	4.45E-10
549	22.2	14.238	1.70E-08	5.39E-10
550	22.3	12.826	6.88E-09	7.21E-10
551	22.4	11.905	9.39E-09	3.73E-10
552	22.5	14.486	4.84E-09	1.77E-10
553	22.6	15.152	9.05E-09	4.47E-10
554	22.7	14.511	2.44E-08	6.34E-10
555	22.8	14.851	7.65E-09	3.45E-10
556	22.9	15.186	6.17E-09	1.69E-10
557	23	13.851	3.75E-09	3.21E-10
558	23.1	15.664	2.39E-09	4.33E-10
559	23.2	14.714	4.02E-09	4.61E-10
560	23.3	15.062	3.45E-09	5.11E-10

Sample #	Height (m)	Mass (g)	χ m^3/kg	Standard Deviation
561	23.4	17.583	1.82E-09	1.46E-10
562	23.5	11.972	3.73E-09	4.29E-10
563	23.6	15.541	5.44E-09	4.95E-10
564	23.7	16.071	4.70E-09	5.75E-10
565	23.8	14.821	5.95E-09	1.73E-10
566	23.9	16.552	3.36E-09	6.20E-10
567	24	15.674	3.08E-09	4.33E-10
568	24.1	14.256	2.62E-09	4.76E-10
569	24.2	14.258	3.64E-09	3.12E-10
570	24.3	18.59	3.09E-09	0
571	24.4	17.053	4.96E-09	2.60E-10
572	24.5	14.417	3.98E-09	5.34E-10
573	24.6	15.477	9.79E-09	3.31E-10
574	24.7	14.403	1.37E-08	3.55E-10
575	24.8	15.241	4.83E-09	2.91E-10
576	24.9	14.722	1.68E-09	3.02E-10
577	25	13.915	2.30E-09	4.88E-10
578	25.1	14.321	7.17E-09	4.73E-10
579	25.2	13.569	4.76E-09	1.89E-10
580	25.3	13.691	6.04E-09	3.74E-10
581	25.4	15.839	4.31E-09	2.80E-10
582	25.5	13.124	4.37E-09	3.39E-10
583	25.6	13.044	6.07E-09	3.40E-10
584	25.7	13.463	5.07E-09	5.71E-10
585	25.8	14.489	3.58E-09	3.07E-10
586	25.9	15.737	3.99E-09	2.82E-10
587	26	16.944	5.20E-09	1.51E-10
588	26.1	16.357	3.29E-09	1.57E-10
589	26.2	14.08	5.10E-09	4.82E-10
590	26.3	13.34	3.08E-09	5.77E-10
591	26.4	13.356	1.85E-09	5.77E-10
592	26.5	15.365	4.09E-09	5.01E-10
593	26.6	15.92	4.63E-09	4.83E-10
594	26.7	17.017	5.29E-09	5.22E-10
595	26.8	15.55	3.22E-09	4.36E-10
596	26.9	15.552	4.04E-09	4.95E-10
597	27	15.697	3.77E-09	5.89E-10
598	27.1	14.664	2.43E-09	3.03E-10
599	27.2	9.456	5.68E-09	5.43E-10
600	27.3	14.358	4.75E-09	3.09E-10
601	27.4	14.504	4.08E-09	1.77E-10
602	27.5	13.818	4.15E-09	5.57E-10
603	27.6	11.203	5.12E-09	6.87E-10
604	27.7	14.074	6.01E-09	5.46E-10
605	27.8	14.209	4.16E-09	6.51E-10

Sample #	Height (m)	Mass (g)	χ m^3/kg	Standard Deviation
606	27.9	13.645	1.15E-09	6.78E-10
607	28	14.027	4.99E-09	3.66E-10
608	28.1	15.31	1.26E-09	0
609	28.2	16.314	3.85E-09	2.72E-10
610	28.3	16.118	4.91E-09	0
611	28.4	15.197	5.09E-09	1.69E-10
612	28.5	13.222	5.71E-09	3.88E-10
613	28.5	14.065	4.85E-09	6.32E-10
614	28.7	14.596	2.07E-09	3.05E-10
615	28.8	13.181	5.18E-09	3.37E-10
616	28.9	15.671	3.78E-09	5.90E-10
617	29	14.072	4.08E-09	3.16E-10
618	29.1	14.295	2.87E-09	5.38E-10
619	29.2	15.826	2.82E-09	1.62E-10
620	29.3	15.194	3.06E-09	2.92E-10
621	29.4	13.834	4.80E-09	3.71E-10
622	29.5	13.614	6.48E-09	3.77E-10
623	29.6	14.902	6.77E-09	5.16E-10
624	29.7	14.091	4.59E-09	4.82E-10
625	29.8	15.533	5.56E-09	1.65E-10
626	29.9	13.565	3.03E-09	5.67E-10
627	30	15.499	5.46E-09	2.86E-10
628	30.1	15.563	2.17E-09	1.65E-10
629	30.2	16.673	2.57E-09	1.54E-10
630	30.3	14.398	1.72E-09	5.35E-10
631	30.4	15.698	4.69E-09	4.90E-10
632	30.5	14.556	5.06E-09	6.10E-10
633	30.6	14.973	3.47E-09	5.14E-10
634	30.7	16.316	3.63E-09	1.57E-10
635	30.8	14.742	3.03E-09	1.74E-10
636	30.9	12.365	1.85E-09	7.48E-10
637	31	13.706	4.19E-09	5.61E-10
638	31.1	15.32	2.68E-09	5.80E-10
639	31.2	15.926	6.40E-10	1.61E-10
640	31.3	16.758	2.56E-09	4.05E-10
641	31.4	13.93	2.82E-09	3.68E-10
642	31.5	13.843	3.75E-09	5.56E-10
643	31.6	14.883	3.00E-09	6.21E-10
644	31.7	14.122	3.29E-09	3.15E-10
645	31.8	14.586	3.06E-09	1.76E-10
646	31.9	16.401	3.39E-09	1.56E-10
647	32	14.689	5.14E-09	4.62E-10
648	32.1	15.902	3.49E-09	4.27E-10
649	32.2	15.387	4.91E-09	4.41E-10
650	32.3	12.446	4.03E-09	7.43E-10

Sample #	Height (m)	Mass (g)	χ m^3/kg	Standard Deviation
651	32.4	13.976	3.33E-09	5.51E-10
652	32.5	14.513	2.70E-09	1.77E-10
653	32.6	13.263	2.68E-09	5.80E-10
654	32.7	16.266	4.08E-09	3.15E-10
655	32.8	13.18	3.80E-09	5.15E-10
656	32.9	15.6	4.84E-09	4.35E-10
657	33	14.301	3.12E-09	3.59E-10
658	33.1	13.362	5.11E-09	5.76E-10
659	33.2	15.107	4.64E-09	6.79E-10
660	33.3	16.05	3.12E-09	4.23E-10
661	33.4	16.862	3.08E-09	5.27E-10
662	33.5	12.227	6.17E-09	2.10E-10
663	33.6	11.928	4.81E-09	6.45E-10
664	33.7	9.307	4.80E-09	5.51E-10
665	33.8	15.938	4.74E-09	4.26E-10
666	33.9	12.686	4.24E-09	4.04E-10
667	34	11.015	4.22E-09	4.03E-10
668	34.1	13.392	4.28E-09	3.32E-10
669	34.2	13.656	2.61E-09	3.25E-10
670	34.3	12.142	3.38E-09	3.66E-10
671	34.4	14.478	1.63E-08	3.06E-10
672	34.5	13.011	5.52E-09	3.94E-10
673	34.6	9.778	4.75E-09	7.87E-10
674	34.7	10.491	5.11E-08	4.84E-10
675	34.8	14.989	1.04E-08	5.92E-10
676	34.9	13.409	3.86E-08	3.28E-10
677	35	12.808	6.46E-09	8.01E-10
678	35.1	9.628	4.45E-09	5.33E-10
679	35.2	13.34	1.99E-09	1.92E-10
680	35.3	12.035	1.08E-08	4.26E-10
681	35.4	14.412	3.04E-08	1.77E-10
682	35.5	15.83	3.74E-09	3.24E-10
683	35.6	14.841	5.33E-09	1.11E-16
684	35.7	12.98	3.72E-09	3.95E-10
685	35.8	10.798	1.67E-08	4.74E-10
686	35.9	11.711	9.54E-09	7.58E-10
687	36	10.239	3.33E-08	4.98E-10
688	36.1	10.915	1.36E-08	4.69E-10
689	36.2	9.603	3.33E-08	2.66E-10
690	36.3	9.953	5.03E-09	5.15E-10
691	36.4	11.638	6.02E-09	2.20E-10
692	36.5	12.685	9.95E-09	2.02E-10
693	36.6	12.191	3.05E-08	3.62E-10
694	36.7	14.572	1.94E-09	4.66E-10
695	36.8	12.534	4.29E-09	7.38E-10

Sample #	Height (m)	Mass (g)	χ m^3/kg	Standard Deviation
696	36.9	12.056	5.06E-09	4.25E-10
697	37	11.164	2.05E-09	8.29E-10
698	37.1	12.157	5.17E-09	0
699	37.2	13.175	4.08E-09	3.89E-10
700	37.3	12.523	4.00E-09	2.05E-10
701	37.4	14.409	4.34E-08	0
702	37.5	9.783	1.48E-08	9.07E-10
703	37.6	12.085	1.22E-08	5.61E-10
704	37.7	12.038	1.24E-08	3.68E-10
705	37.8	12.278	1.32E-08	5.52E-10
706	37.9	13.837	4.18E-08	1.83E-10
707	38	13.259	1.77E-08	5.10E-10
708	38.1	14.414	4.46E-08	6.34E-10
709	38.2	12.624	3.97E-08	6.98E-10
710	38.3	14.947	3.62E-08	3.40E-10
711	38.4	14.902	3.29E-08	2.96E-10
712	38.5	11.916	1.67E-08	7.44E-10
713	38.6	12.28	4.04E-08	3.59E-10
714	38.7	11.339	1.54E-08	5.97E-10
715	38.8	12.097	3.58E-08	2.10E-10
716	38.85	12.371	2.44E-08	6.19E-10
717	38.9	14.637	1.56E-09	1.75E-10
718	39	12.794	3.35E-09	2.01E-10
719	39.1	13.719	2.20E-09	3.24E-10
720	39.2	12.784	1.65E-09	2.01E-10
721	39.3	11.963	2.52E-09	6.44E-10
722	39.4	13.963	2.10E-10	5.52E-10
723	39.5	15.092	4.52E-09	2.94E-10
724	39.6	13.651	6.73E-09	3.76E-10
725	39.7	14.519	3.95E-09	5.30E-10
726	39.8	15.24	1.22E-08	4.44E-10
727	39.9	14.649	4.41E-09	1.75E-10
728	40	13.443	2.18E-10	6.62E-10
729	40.1	16.137	5.35E-09	3.18E-10
730	40.2	14.621	2.31E-09	1.76E-10
731	40.3	14.944	9.17E-09	4.53E-10
732	40.4	13.945	1.27E-08	3.18E-10
733	40.5	11.395	1.79E-08	3.89E-10
734	40.6	16.059	8.42E-09	4.22E-10
735	40.7	15.241	7.93E-09	3.36E-10
736	40.8	14.604	8.52E-09	1.75E-10
737	40.9	15.255	2.81E-09	1.68E-10
738	41	14.046	5.50E-09	1.83E-10
739	41.1	13.138	1.60E-09	5.17E-10
740	41.2	13.52	2.23E-09	3.29E-10

Sample #	Height (m)	Mass (g)	χ m^3/kg	Standard Deviation
741	41.3	11.858	4.38E-09	6.49E-10
742	41.4	14.569	1.82E-09	3.52E-10
743	41.5	10.045	3.90E-09	6.76E-10
744	41.6	12.507	1.24E-08	7.09E-10
745	41.7	14.485	4.09E-09	3.54E-10
746	41.8	13.936	7.76E-09	1.84E-10
747	41.9	14.944	5.66E-09	2.97E-10
748	42	12.44	8.11E-09	0
749	42.1	13.427	4.95E-09	5.05E-10
750	42.2	13.801	4.42E-09	1.86E-10
751	42.3	14.04	1.76E-09	3.17E-10
752	42.4	14.877	1.05E-09	1.73E-10
753	42.5	14.867	1.54E-09	3.45E-10
754	42.6	11.8	6.09E-09	4.35E-10
755	42.7	16.96	6.55E-11	4.01E-10
756	42.8	16.818	1.58E-09	3.05E-10
757	42.9	13.099	1.89E-09	5.88E-10
758	43	15.21	3.06E-09	5.06E-10
759	43.1	14.129	2.39E-09	4.81E-10
760	43.2	13.856	1.78E-09	3.21E-10
761	43.3	13.253	2.28E-09	6.71E-10
762	43.4	13.892	4.91E-09	0
763	43.5	15.601	5.65E-09	1.64E-10
764	43.6	16.123	1.39E-08	5.72E-10
765	43.7	13.735	9.98E-09	1.86E-10
766	43.8	11.37	4.25E-09	2.26E-10
767	43.9	12.318	1.88E-08	6.23E-10
768	44	15.276	6.13E-09	4.44E-10
769	44.1	13.86	1.25E-08	1.85E-10
770	44.2	14.984	1.89E-09	4.53E-10
771	44.3	15.192	5.57E-09	5.06E-10
772	44.4	15.391	2.55E-09	1.67E-10
773	44.5	13.683	4.32E-09	4.96E-10
774	44.6	13.649	3.41E-09	3.26E-10
775	44.7	14.438	5.73E-09	1.78E-10
776	44.8	14.133	3.80E-09	1.81E-10
777	44.9	14.368	4.25E-09	1.79E-10
778	45	15.589	1.02E-08	4.34E-10
779	45.1	15.919	6.00E-09	4.83E-10
780	45.2	11.596	9.48E-09	5.85E-10
781	45.3	15.417	5.72E-09	4.40E-10
782	45.4	12.209	7.52E-09	4.20E-10
783	45.5	13.875	7.14E-09	3.69E-10
784	45.6	13.976	6.05E-09	6.35E-10
785	45.7	12.071	8.36E-09	3.68E-10

Sample #	Height (m)	Mass (g)	χ m^3/kg	Standard Deviation
786	45.8	14.809	5.22E-09	3.46E-10
787	45.9	12.269	7.04E-09	8.36E-10
788	46	16.934	5.96E-09	5.24E-10
789	46.1	12.794	7.46E-09	6.01E-10
790	46.2	14.9	5.55E-09	6.20E-10
791	46.3	15.453	6.18E-09	2.87E-10
792	46.4	14.696	3.29E-09	6.98E-10
793	46.5	14.38	7.08E-10	3.57E-10
794	46.6	16.839	4.81E-09	3.05E-10
795	46.7	15.622	2.51E-09	3.28E-10
796	46.8	16.149	5.57E-09	4.76E-10
797	46.9	15.788	7.77E-09	5.62E-10
798	47	16.12	4.12E-09	1.59E-10
799	47.1	14.085	6.26E-09	1.82E-10
800	47.2	14.062	1.97E-08	3.63E-10
801	47.3	18.269	1.16E-08	3.70E-10
802	47.4	17.49	1.03E-08	1.46E-10
803	47.5	16.707	5.39E-09	4.60E-10
804	47.6	14.987	1.12E-08	4.52E-10
805	47.7	10.278	1.09E-08	7.48E-10
806	47.8	14.638	1.41E-08	3.49E-10
807	47.9	15.381	1.46E-08	1.66E-10
808	48	14.274	7.57E-09	7.18E-10
809	48.1	12.909	1.37E-08	0
810	48.2	15.152	1.02E-08	5.07E-10
811	48.3	13.363	5.51E-09	3.32E-10
812	48.4	15.945	3.26E-09	3.93E-17
813	48.5	16.776	2.34E-09	3.06E-10
814	48.6	13.18	3.11E-09	6.74E-10
815	48.7	15.754	6.17E-09	5.87E-10
816	48.8	13.763	1.11E-08	4.92E-10
817	48.9	15.034	9.72E-09	6.14E-10
818	49	13.139	5.88E-09	1.95E-10
819	49.1	14.744	4.01E-09	4.60E-10
820	49.2	16.796	1.80E-09	4.58E-10
821	49.3	13.852	6.89E-09	3.20E-10
822	49.4	16.246	4.65E-09	4.18E-10
823	49.5	16.177	3.43E-09	5.72E-10
824	49.6	16.493	1.61E-09	1.56E-10
825	49.7	15.103	5.72E-09	4.49E-10
826	49.8	16.4	2.83E-09	2.71E-10
827	49.9	14.337	6.02E-09	3.58E-10
828	50	15.16	2.35E-09	2.93E-10
829	50.1	13.56	4.50E-09	1.89E-10
830	50.2	15.21	8.30E-09	6.07E-10

Sample #	Height (m)	Mass (g)	χ m^3/kg	Standard Deviation
831	50.3	15.481	2.25E-08	3.29E-10
832	50.4	11.948	1.87E-08	5.66E-10
833	50.5	16.681	5.40E-09	4.61E-10
834	50.6	15.751	1.07E-08	3.25E-10
835	50.7	14.966	1.04E-08	0
836	50.8	14.205	1.87E-08	3.60E-10
837	50.9	16.577	1.95E-08	2.67E-10
838	51	17.002	1.88E-08	3.97E-10
839	51.1	16.713	1.61E-08	2.65E-10
840	51.2	18.574	1.17E-08	1.38E-10
841	51.3	17.53	1.83E-08	5.82E-10
842	51.4	15.715	2.06E-08	4.87E-10
843	51.5	15.195	1.57E-08	3.36E-10
844	51.6	16.394	1.18E-08	5.41E-10
845	51.7	15.333	1.00E-08	6.02E-10
846	51.8	15.982	1.66E-09	3.21E-10
847	51.9	15.746	5.37E-09	2.82E-10
848	52	15.912	1.44E-09	5.82E-10
849	52.1	16.064	8.08E-09	5.75E-10
850	52.2	16.675	2.13E-09	4.62E-10
851	52.3	13.214	5.03E-09	1.94E-10
852	52.4	14.718	1.68E-09	3.02E-10
853	52.5	14.506	2.45E-09	3.06E-10
854	52.6	15.337	5.63E-09	3.34E-10
855	52.7	16.461	4.81E-09	2.70E-10
856	52.8	14.608	1.66E-08	3.03E-10
857	52.9	16.279	1.01E-08	4.16E-10
858	53	18.278	1.69E-08	2.79E-10
859	53.1	15.798	1.43E-08	5.61E-10
860	53.2	11.604	1.18E-08	5.84E-10
861	53.3	15.188	6.76E-09	3.37E-10
862	53.4	15.636	9.00E-09	3.28E-10
863	53.5	13.296	7.86E-09	6.95E-10
864	53.6	15.778	8.57E-09	1.62E-10
865	53.7	13.326	7.98E-09	5.77E-10
866	53.8	17.208	1.21E-08	3.93E-10
867	53.9	17.38	1.62E-08	3.89E-10
868	54	13.031	1.91E-08	5.19E-10
869	54.1	13.399	1.19E-08	6.89E-10
870	54.2	14.625	1.70E-08	4.62E-10
871	54.3	15.193	1.01E-08	1.69E-10
872	54.4	15.224	5.79E-09	6.74E-10
873	54.5	14.088	3.17E-09	4.82E-10
874	54.6	14.095	7.80E-09	4.81E-10
875	54.7	13.598	3.95E-09	4.99E-10

Sample #	Height (m)	Mass (g)	χ m^3/kg	Standard Deviation
876	54.8	14.99	2.01E-09	5.14E-10
877	54.9	13.806	5.60E-09	4.91E-10
878	55	13.796	3.63E-09	6.70E-10
879	55.1	15.334	4.57E-09	3.34E-10
880	55.2	14.504	4.58E-09	7.07E-10
881	55.3	13.683	1.83E-08	7.47E-10
882	55.4	17.549	9.98E-09	2.92E-10
883	55.5	14.594	6.42E-09	6.33E-10
884	55.6	16.045	1.27E-08	4.78E-10
885	55.7	14.005	4.87E-09	3.17E-10
886	55.8	14.07	3.17E-09	3.65E-10
887	55.9	17.657	3.35E-09	1.45E-10
888	56	16.146	-1.56E-10	2.75E-10
889	56.1	15.786	3.63E-09	4.87E-10
890	56.2	15.909	3.38E-09	4.27E-10
891	56.3	13.802	9.41E-09	4.91E-10
892	56.4	17.404	1.94E-09	3.90E-10
893	56.5	14.046	4.60E-09	1.83E-10
894	56.6	15.328	2.09E-09	4.43E-10
895	56.7	15.281	6.25E-09	5.03E-10
896	56.8	15.24	1.38E-09	3.37E-10
897	56.9	18.495	2.02E-09	3.67E-10
898	57	14.227	4.80E-09	6.24E-10
899	57.1	17.749	2.11E-09	1.45E-10
900	57.2	15.141	3.55E-09	3.39E-10
901	57.3	15.206	1.15E-09	3.38E-10
902	57.4	14.625	4.29E-09	6.07E-10
903	57.5	15.232	4.48E-09	2.92E-10
904	57.6	16.082	2.55E-09	2.76E-10
905	57.7	16.163	3.66E-09	4.20E-10
906	57.8	16.085	4.69E-09	3.19E-10
907	57.9	20.049	3.95E-09	4.43E-10
908	58	15.118	2.95E-09	4.49E-10
909	58.1	17.478	3.80E-09	3.88E-10
910	58.2	12.667	5.10E-09	2.02E-10
911	58.3	14.575	6.30E-09	3.52E-10
912	58.4	13.241	6.11E-09	3.87E-10
913	58.5	16.089	7.51E-09	1.59E-10
914	58.6	15.658	5.98E-09	1.64E-10
915	58.7	15.166	6.77E-09	1.69E-10
916	58.8	13.868	4.40E-09	4.89E-10
917	58.9	17.704	3.24E-09	2.51E-10
918	59	14.381	6.01E-09	3.57E-10
919	59.1	17.571	6.46E-09	5.26E-10
920	59.2	16.237	5.10E-09	4.18E-10

Sample #	Height (m)	Mass (g)	χ m^3/kg	Standard Deviation
921	59.3	17.161	4.40E-09	3.95E-10
922	59.4	16.03	5.73E-09	4.23E-10
923	59.5	17.222	5.33E-09	3.94E-10
924	59.6	13.557	7.98E-09	1.89E-10
925	59.7	15.987	7.90E-09	4.24E-10
926	59.8	12.676	6.67E-09	6.07E-10
927	59.9	15.781	5.36E-09	2.81E-10
928	60	13.569	4.49E-09	3.78E-10
929	60.1	14.393	4.87E-09	3.56E-10
930	60.2	14.268	5.80E-09	4.75E-10
931	60.3	17.126	5.78E-09	1.50E-10
932	60.4	16.798	5.14E-09	3.05E-10
933	60.5	16.667	1.92E-09	1.54E-10
934	60.6	17.912	3.51E-09	2.48E-10
935	60.7	15.198	7.31E-11	4.47E-10
936	60.8	15.837	1.10E-09	4.29E-10
937	60.9	14.52	5.95E-09	6.37E-10
938	61	18.456	3.80E-09	3.68E-10
939	61.1	18.968	3.50E-09	3.58E-10
940	61.2	17.045	5.39E-09	5.42E-10
941	61.3	16.259	1.13E-08	6.29E-10
942	61.4	19	4.93E-09	2.70E-10
943	61.5	18.143	3.66E-09	3.74E-10
944	61.6	16.725	4.84E-09	5.53E-10
945	61.7	16.39	4.05E-09	5.64E-10
946	61.8	19.577	5.52E-09	2.62E-10
947	61.9	15.83	5.46E-09	3.24E-10
948	62	17.636	5.82E-09	2.91E-10
949	62.1	18.361	5.20E-09	2.42E-10
950	62.2	14.15	6.74E-09	5.43E-10
951	62.3	18.432	4.19E-09	3.68E-10
952	62.4	16.89	6.08E-09	4.01E-10
953	62.5	16.944	7.98E-09	6.05E-10
954	62.6	14.616	5.17E-09	6.33E-10
955	62.7	16.066	8.20E-09	1.59E-10
956	62.8	16.446	8.78E-09	2.70E-10
957	62.9	17.364	4.87E-09	4.43E-10
958	63	17.849	3.62E-09	1.44E-10

Hagan, VA Eggleston Formation

Sample #	Height (m)	Mass (g)	χ m^3/kg	Standard Deviation
1	0	7.256	5.18E-08	7.03E-10
2	0.05	8.496	4.97E-08	6.00E-10
3	0.1	8.687	2.74E-08	5.88E-10

Sample #	Height (m)	Mass (g)	χ m^3/kg	Standard Deviation
4	0.15	9.964	2.47E-08	5.13E-10
5	0.2	11.604	4.71E-08	5.79E-10
6	0.25	10.3	2.93E-08	8.59E-10
7	0.3	12.185	3.10E-08	3.62E-10
8	0.35	9.691	1.56E-08	6.99E-10
9	0.4	11.949	2.98E-08	7.39E-10
10	0.5	10.723	2.71E-08	7.14E-10
11	0.55	9.774	3.34E-08	5.22E-10
12	0.6	9.997	2.71E-08	9.21E-10
13	0.65	10.425	4.09E-08	8.46E-10
14	0.7	8.84	3.33E-08	2.89E-10
15	0.75	7.756	3.63E-08	1.32E-09
16	0.8	10.083	3.55E-08	5.06E-10
17	0.85	8.42	3.39E-08	9.10E-10
18	0.9	11.885	3.52E-08	4.29E-10
19	0.95	11.507	5.06E-08	6.62E-10
20	1	11.741	3.60E-08	7.82E-10
21	1.05	10.873	3.11E-08	8.46E-10
22	1.1	10.841	2.55E-08	2.36E-10
23	1.15	10.064	5.70E-09	0
24	1.2	14.161	5.20E-09	3.14E-10
25	1.25	11.079	9.88E-08	6.00E-10
26	1.3	12.661	7.54E-09	3.51E-10
27	1.35	10.404	2.97E-08	4.91E-10
28	1.4	9.544	2.48E-08	4.64E-10
29	1.45	11.444	4.54E-09	3.88E-10
30	1.5	12.322	2.42E-08	5.48E-10
31	1.55	10.438	5.84E-09	2.46E-10
32	1.6	11.136	5.64E-09	6.91E-10
33	1.65	12.297	7.32E-09	3.61E-10
34	1.7	10.761	6.00E-09	6.31E-10
35	1.75	9.21	5.05E-09	4.82E-10
36	1.8	9.466	1.31E-08	2.71E-10
37	1.85	9.852	6.01E-09	1.04E-09
38	1.9	8.846	8.74E-09	5.80E-10
39	1.95	9.409	1.32E-08	7.20E-10
40	2	8.604	1.07E-08	5.96E-10
41	2.05	9.871	8.38E-09	5.19E-10
42	2.1	10.769	9.37E-09	0
43	2.15	8.063	5.99E-09	3.18E-10
44	2.2	11.049	4.21E-09	8.04E-10
45	2.25	10.063	6.60E-09	2.55E-10
46	2.3	11.092	6.64E-09	4.00E-10
47	2.35	8.657	1.12E-08	7.83E-10
48	2.4	10.055	8.05E-09	2.55E-10

Sample #	Height (m)	Mass (g)	χ m^3/kg	Standard Deviation
49	2.45	9.922	1.07E-08	8.95E-10
50	2.5	9.469	3.57E-08	1.08E-09
51	2.55	9.934	1.27E-08	9.30E-10
52	2.6	10.171	1.42E-08	8.72E-10
53	2.65	8.555	1.94E-08	1.04E-09
54	2.7	11.813	1.28E-08	5.73E-10
55	2.75	11.778	2.81E-08	5.73E-10
56	2.8	11.979	2.62E-08	7.68E-10
57	2.85	8.416	2.36E-08	5.26E-10
58	2.9	10.729	2.19E-08	4.76E-10
59	2.95	10.684	6.56E-09	9.60E-10
60	3	11.406	1.85E-08	8.08E-10
61	3.05	10.253	1.83E-08	4.32E-10
62	3.1	12.015	1.41E-08	4.26E-10
63	3.15	11.441	2.59E-08	6.69E-10
64	3.2	9.235	3.01E-08	9.97E-10
65	3.25	9.779	3.25E-08	4.52E-10
66	3.3	9.549	5.63E-08	1.06E-09
67	3.35	10.579	3.70E-08	6.37E-10
68	3.4	12.278	3.24E-08	4.15E-10
69	3.45	8.897	3.33E-08	9.94E-10
70	3.5	12.358	3.00E-08	7.44E-10
71	3.55	9.916	2.57E-08	5.15E-10
72	3.6	10.224	3.46E-08	9.98E-10
73	3.65	9.951	5.31E-08	4.42E-10
74	3.7	10.613	4.17E-08	7.20E-10
75	3.75	9.352	3.09E-08	7.22E-10
76	3.8	9.502	3.38E-08	9.68E-10
77	3.85	10.492	3.10E-08	6.43E-10
78	3.9	8.981	3.90E-08	8.52E-10
79	3.95	12.691	3.73E-08	7.23E-10
80	4	8.668	3.75E-08	1.18E-09
81	4.05	11.998	4.67E-08	6.35E-10
82	4.1	11.012	1.33E-08	6.15E-10
83	4.15	10.637	3.73E-08	4.79E-10
84	4.2	10.124	2.02E-08	4.38E-10
85	4.25	13.107	2.33E-08	3.89E-10
86	4.3	10.601	2.08E-08	4.18E-10
87	4.35	10.483	4.30E-08	2.43E-10
88	4.4	10.998	2.68E-08	6.14E-10
89	4.45	11.34	3.73E-08	5.94E-10
90	4.5	8.5	3.08E-08	7.95E-10
91	4.55	10.61	5.69E-08	8.29E-10
92	4.6	11.228	1.74E-08	6.03E-10
93	4.65	9.122	4.24E-08	7.39E-10

Sample #	Height (m)	Mass (g)	χ m^3/kg	Standard Deviation
94	4.7	9.653	2.36E-08	5.30E-10
95	4.75	10.29	4.46E-08	7.42E-10
96	4.8	11.534	3.60E-08	3.82E-10
97	4.85	8.98	4.66E-08	7.50E-10
98	4.9	10.651	3.05E-08	8.64E-10
99	4.95	10.661	2.30E-08	6.34E-10
100	5	11.204	3.09E-08	2.28E-10
101	5.05	10.556	4.33E-08	6.38E-10
102	5.1	9.444	6.68E-08	4.65E-10
103	5.15	8.764	5.13E-08	1.16E-09
104	5.2	10.532	3.19E-08	9.69E-10
105	5.25	12.195	6.27E-08	7.19E-10
106	5.3	11.237	3.12E-08	3.93E-10
107	5.35	9.823	2.34E-08	2.60E-10
108	5.4	8.351	2.47E-08	1.10E-09
109	5.45	9.325	4.45E-08	9.46E-10
110	5.5	10.79	3.60E-08	4.09E-10
111	5.55	9.753	3.61E-08	5.23E-10
112	5.6	9.281	3.68E-08	1.10E-09
113	5.65	9.171	3.09E-08	1.00E-09
114	5.7	9.166	4.06E-08	8.34E-10
115	5.75	10.682	3.47E-08	8.60E-10
116	5.8	10.266	3.69E-08	6.57E-10
117	5.85	11.137	3.32E-08	6.06E-10
118	5.9	8.471	4.09E-08	7.97E-10
119	5.95	11.09	3.47E-08	8.29E-10
120	6	10.992	3.86E-08	6.13E-10
121	6.05	9.277	3.29E-08	2.75E-10
122	6.1	10.903	3.58E-08	4.67E-10
123	6.15	10.544	2.28E-08	2.42E-10
124	6.2	8.969	3.52E-08	5.69E-10
125	6.25	9.37	2.78E-08	9.83E-10
126	6.3	11.219	2.37E-08	6.02E-10
127	6.35	7.452	4.05E-08	5.93E-10
128	6.4	10.268	3.31E-08	7.45E-10
129	6.45	10.551	2.43E-08	6.41E-10
130	6.5	9.322	3.47E-08	8.21E-10
131	6.55	10.512	2.42E-08	8.76E-10
132	6.6	9.829	3.07E-08	4.50E-10
133	6.65	10.331	3.11E-08	2.47E-10
134	6.7	11.123	2.84E-08	4.59E-10
135	6.75	8.648	2.07E-08	2.96E-10
136	6.8	9.425	3.83E-08	4.69E-10
137	6.85	10.182	3.07E-08	4.34E-10
138	6.9	10.802	3.03E-08	6.25E-10

Sample #	Height (m)	Mass (g)	χ m^3/kg	Standard Deviation
139	6.95	12.132	2.78E-08	5.56E-10
140	7	11.651	2.87E-08	6.57E-10
141	7.05	10.05	3.22E-08	7.62E-10
142	7.1	8.221	3.16E-08	1.12E-09
143	7.15	9.995	1.79E-08	5.12E-10
144	7.2	8.767	2.76E-08	5.05E-10
145	7.25	9.848	2.92E-08	9.35E-10
146	7.3	10.849	2.16E-08	4.71E-10
147	7.35	10.238	2.73E-08	3.14E-16
148	7.4	8.242	2.87E-08	9.30E-10
149	7.45	8.214	3.28E-08	9.33E-10
150	7.5	11.061	3.02E-08	6.92E-10
151	7.55	8.239	3.29E-08	8.20E-10
152	7.6	8.303	2.91E-08	5.33E-10
153	7.65	9.262	2.98E-08	9.94E-10
154	7.7	10.971	3.34E-08	8.05E-10
155	7.75	9.93	3.84E-08	2.57E-10
156	7.8	10.022	4.65E-08	2.54E-10
157	7.85	10.284	3.21E-08	6.56E-10
158	7.9	10.105	3.57E-08	4.37E-10
159	7.95	7.809	4.86E-08	1.18E-09
160	8	10.016	4.54E-08	6.72E-10
161	8.05	11.201	3.45E-08	8.20E-10
162	8.1	10.14	3.67E-08	4.35E-10
163	8.15	7.368	3.78E-08	1.25E-09
164	8.2	10.202	3.17E-08	4.33E-10
165	8.25	9.223	3.92E-08	8.29E-10
166	8.3	8.649	3.15E-08	2.95E-10
167	8.35	8.66	4.63E-08	1.18E-09
168	8.4	9.315	3.61E-08	2.74E-10
169	8.45	10.082	4.35E-08	1.01E-09
170	8.5	9.58	2.92E-08	8.00E-10
171	8.55	9.989	2.19E-08	2.56E-10
172	8.6	8.935	4.77E-08	4.94E-10
173	8.65	10.056	5.58E-08	8.75E-10
174	8.7	10.047	5.31E-08	8.76E-10
175	8.75	9.795	5.32E-08	9.36E-10
176	8.8	10.717	4.46E-08	2.37E-10
177	8.85	10.926	3.57E-08	6.17E-10
178	8.9	8.681	3.35E-08	1.02E-09
179	8.95	9.256	4.68E-08	5.50E-10
180	9	9.389	4.46E-08	7.18E-10
181	9.05	9.855	3.90E-08	5.17E-10
182	9.1	8.476	3.96E-08	3.01E-10
183	9.15	9.052	4.31E-08	2.82E-10

Sample #	Height (m)	Mass (g)	χ m^3/kg	Standard Deviation
184	9.2	8.562	4.39E-08	7.88E-10
185	9.25	11.021	3.62E-08	0
186	9.3	9.104	4.15E-08	4.85E-10
187	9.35	9.657	4.45E-08	6.98E-10
188	9.4	10.718	3.54E-08	2.38E-10
189	9.45	8.415	4.33E-08	1.09E-09
190	9.5	9.229	4.01E-08	5.52E-10
191	9.55	8.987	3.96E-08	4.91E-10
192	9.6	8.835	6.27E-08	2.88E-10
193	9.65	9.749	3.00E-08	6.93E-10
194	9.7	10.989	2.47E-08	9.30E-10
195	9.75	12.766	4.10E-08	3.45E-10
196	9.8	8.588	1.62E-08	8.95E-10
197	9.85	9.755	4.00E-08	2.61E-10
198	9.9	9.753	3.94E-08	5.23E-10
199	9.95	9.682	4.08E-08	2.63E-10
200	10	9.825	4.76E-08	6.85E-10
201	10.05	8.123	4.89E-08	3.14E-10
202	10.1	9.563	4.17E-08	9.23E-10
203	10.15	10.232	4.88E-08	6.58E-10
204	10.2	10.5	4.04E-08	4.85E-10
205	10.25	7.798	5.07E-08	1.31E-09
206	10.3	10.591	4.91E-08	8.65E-10
207	10.35	10.015	4.16E-08	2.54E-10
208	10.4	10.712	4.11E-08	2.38E-10
209	10.45	10.659	4.03E-08	6.32E-10
210	10.5	10.58	3.65E-08	2.41E-10
211	10.55	8.933	3.90E-08	7.55E-10
212	10.6	10.188	3.54E-08	4.33E-10
213	10.65	9.005	3.81E-08	1.02E-09
214	10.7	10.695	3.98E-08	4.12E-10
215	10.75	9.724	3.21E-08	9.09E-10
216	10.8	9.157	4.28E-08	1.11E-09
217	10.85	9.494	4.05E-08	2.68E-10
218	10.9	10.608	2.11E-08	8.69E-10
219	10.95	10.797	2.73E-08	4.73E-10
220	11	10.329	2.45E-08	7.42E-10
221	11.05	8.904	2.52E-08	7.60E-10
222	11.1	9.346	2.43E-08	7.24E-10
223	11.15	9.851	2.55E-08	6.86E-10
224	11.2	8.507	1.76E-08	1.04E-09
225	11.25	10.528	1.22E-08	7.30E-10
226	11.3	8.001	6.49E-09	5.55E-10
227	11.35	11.778	2.22E-08	2.17E-10
228	11.4	8.285	2.24E-08	8.17E-10

Sample #	Height (m)	Mass (g)	χ m^3/kg	Standard Deviation
229	11.45	10.772	1.88E-08	6.28E-10
230	11.5	9.937	1.94E-08	4.46E-10
231	11.55	10.895	1.08E-08	4.07E-10
232	11.6	10.915	5.92E-09	2.35E-10
233	11.65	10.497	2.08E-08	6.44E-10
234	11.7	9.744	1.98E-08	4.55E-10
235	11.75	8.943	1.96E-08	2.86E-10
236	11.8	10.67	1.83E-08	4.80E-10
237	11.85	11.482	1.98E-08	8.03E-10
238	11.9	9.921	1.56E-08	8.94E-10
239	11.95	9.354	6.52E-09	7.25E-10
240	12	9.324	8.10E-09	5.50E-10
241	12.05	9.986	1.28E-08	7.69E-10
242	12.1	11.015	7.84E-09	6.16E-10
243	12.15	10.651	7.26E-09	8.68E-10
244	12.2	9.112	5.10E-09	5.55E-17
245	12.25	12.099	8.34E-09	7.34E-10
246	12.3	10.191	3.49E-09	4.36E-10
247	12.35	7.521	4.25E-09	9.03E-10
248	12.4	9.933	5.04E-09	6.83E-10
249	12.45	9.609	6.16E-09	7.06E-10
250	12.5	8.516	3.54E-09	1.04E-09
251	12.55	12.074	6.40E-09	5.62E-10
252	12.6	9.708	7.96E-09	9.52E-10
253	12.65	8.145	8.38E-09	9.44E-10
254	12.7	9.092	8.10E-09	0
255	12.75	6.781	1.03E-08	3.78E-10
256	12.8	10.064	9.12E-09	6.74E-10
257	12.85	9.307	7.14E-09	5.51E-10
258	12.9	8.508	7.17E-09	3.01E-10
259	12.95	7.261	1.04E-08	1.41E-09
260	13	9.054	1.31E-08	5.66E-10
261	13.05	7.426	5.93E-08	6.86E-10
262	13.1	8.481	3.34E-08	1.09E-09
263	13.15	9.109	2.18E-08	8.42E-10
264	13.2	9.907	3.15E-08	4.46E-10
265	13.25	6.805	3.05E-08	3.76E-10
266	13.3	8.687	3.56E-08	2.94E-10
267	13.35	10.744	4.35E-08	9.47E-10
268	13.4	8.951	4.08E-08	2.85E-10
269	13.45	8.176	5.03E-08	1.12E-09
270	13.5	11.532	3.35E-08	7.97E-10
271	13.55	8.723	3.38E-08	7.74E-10
272	13.6	12.569	3.92E-08	5.35E-10
273	13.65	8.327	4.12E-08	8.10E-10

Sample #	Height (m)	Mass (g)	χ m^3/kg	Standard Deviation
274	13.7	8.672	3.54E-08	5.10E-10
275	13.75	8.95	2.87E-08	1.03E-09
276	13.8	8.425	2.44E-08	3.04E-10
277	13.85	8.658	2.25E-08	5.91E-10
278	13.9	10.14	2.96E-08	5.03E-10
279	13.95	10.803	1.03E-08	4.11E-10
280	14	9.437	1.51E-08	7.18E-10
281	14.05	8.124	7.28E-09	6.31E-10
282	14.1	9.294	4.82E-08	4.74E-10
283	14.15	9.411	2.96E-08	7.18E-10
284	14.2	8.525	5.06E-08	1.03E-09
285	14.25	9.84	4.04E-08	5.18E-10
286	14.3	8.788	5.81E-08	1.04E-09
287	14.35	7.873	1.53E-08	6.51E-10
288	14.4	8.236	2.32E-08	6.21E-10
289	14.45	8.411	1.11E-08	1.22E-09
290	14.5	8.516	1.25E-08	5.21E-10
291	14.55	8.794	1.06E-08	7.71E-10
292	14.6	9.208	1.08E-08	7.36E-10
293	14.65	8.14	1.04E-08	5.45E-10
294	14.7	8.564	1.50E-08	5.18E-10
295	14.75	10.528	1.51E-08	2.43E-10
296	14.8	8.11	1.89E-08	6.31E-10
297	14.85	8.572	1.90E-08	7.90E-10
298	14.9	8.976	2.17E-08	2.85E-10
299	14.95	9.041	1.54E-08	0
300	15	8.9	9.09E-09	2.88E-10
301	15.05	10.195	5.09E-09	4.36E-10
302	15.1	10.389	1.23E-08	4.27E-10
303	15.15	9.316	1.08E-08	4.76E-10
304	15.2	11.923	6.48E-09	5.69E-10
305	15.25	10.651	1.13E-08	9.62E-10
306	15.3	9.153	9.04E-09	2.80E-10
307	15.35	10.744	1.31E-08	8.59E-10
308	15.4	11.377	9.66E-09	5.96E-10
309	15.45	9.274	8.53E-09	9.58E-10
310	15.5	11.727	1.82E-08	7.86E-10
311	15.55	10.209	1.91E-08	5.01E-10
312	15.6	10.995	1.53E-08	9.31E-10
313	15.65	7.123	5.65E-08	1.29E-09
314	15.7	9.606	1.84E-08	7.99E-10
315	15.75	11.509	1.84E-08	4.44E-10
316	15.8	10.439	2.11E-08	8.48E-10
317	15.85	11.273	2.13E-08	6.00E-10
318	15.9	12.732	1.55E-08	4.02E-10

Sample #	Height (m)	Mass (g)	χ m^3/kg	Standard Deviation
319	15.95	11.7	1.43E-08	7.89E-10
320	16	9.739	1.82E-08	4.55E-10
321	16.05	9.49	5.15E-08	1.07E-09
322	16.1	10.832	1.78E-08	8.18E-10
323	16.15	10.762	4.01E-08	8.20E-10
324	16.2	10.669	3.86E-08	8.61E-10
325	16.25	11.955	3.65E-08	6.39E-10
326	16.3	10.714	3.83E-08	4.12E-10
327	16.35	11.243	2.14E-08	6.01E-10
328	16.4	11.528	1.06E-08	3.85E-10
329	16.45	9.254	4.55E-08	8.26E-10
330	16.5	10.281	2.21E-08	2.49E-10
331	16.55	11.414	1.53E-08	5.93E-10
332	16.6	10.296	1.37E-08	6.58E-10
333	16.65	11.308	3.46E-08	4.51E-10
334	16.7	10.598	5.93E-09	7.26E-10

Black Knob Ridge, Atoka OK Katian GSSP

Sample #	Height (m)	Mass (g)	χ m^3/kg	Stadard Deviation
1	0	11.699	1.13E-08	8.76E-10
2	0.05	12.933	7.66E-09	5.24E-10
3	0.1	12.829	4.75E-09	2.00E-10
4	0.15	15.032	8.88E-09	7.81E-10
5	0.2	8.739	1.18E-08	2.93E-10
6	0.25	8.984	2.51E-08	8.54E-10
7	0.3	10.613	2.76E-08	1.05E-09
8	0.35	12.29	2.09E-08	7.50E-10
9	0.4	11.081	2.75E-08	2.30E-10
10	0.5	10.849	2.11E-08	6.23E-10
11	0.55	10.148	2.67E-08	5.03E-10
12	0.6	12.214	1.72E-08	9.60E-10
13	0.65	8.882	2.36E-08	1.32E-09
14	0.7	12.734	1.93E-08	4.01E-10
15	0.75	10.105	2.65E-08	9.11E-10
16	0.8	11.423	2.37E-08	5.92E-10
17	0.85	11.709	3.68E-08	3.77E-10
18	0.9	12.043	2.08E-08	5.61E-10
19	0.95	12.034	2.51E-08	6.36E-10
20	1	11.057	2.12E-08	6.12E-10
21	1.05	8.918	2.49E-08	1.03E-09
22	1.1	10.938	3.20E-08	1.07E-09
23	1.15	12.939	2.93E-08	5.21E-10
24	1.2	9.16	3.39E-08	2.79E-10
25	1.25	12.744	3.85E-08	3.46E-10

Sample #	Height (m)	Mass (g)	χ m^3/kg	Stadard Deviation
26	1.3	15.236	3.76E-08	1.67E-10
27	1.35	14.647	3.96E-08	6.93E-10
28	1.4	15.374	3.71E-08	7.20E-10
29	1.45	15.312	3.83E-08	5.98E-10
30	1.5	11.744	4.00E-08	4.44E-16
31	1.55	11.062	4.29E-08	7.97E-10
32	1.6	11.048	3.91E-08	6.91E-10
33	1.65	13.094	4.11E-08	7.00E-10
34	1.7	10.084	4.24E-08	5.05E-10
35	1.75	9.659	4.52E-08	7.91E-10
36	1.8	12.042	4.48E-08	6.33E-10
37	1.85	9.408	4.05E-08	1.18E-09
38	1.9	11.21	4.52E-08	3.93E-10
39	1.95	10.21	4.38E-08	7.48E-10
40	2	7.88	4.86E-08	1.12E-09
41	2.05	8.719	4.97E-08	7.73E-10
42	2.1	7.8	5.35E-08	8.64E-10
43	2.15	11.964	4.34E-08	9.26E-10
44	2.2	9.449	4.74E-08	9.33E-10
45	2.25	12.579	4.32E-08	4.04E-10
46	2.3	8.742	4.46E-08	1.17E-09
47	2.35	10.827	4.52E-08	4.70E-10
48	2.4	12.15	4.00E-08	7.25E-10
49	2.45	11.483	4.26E-08	4.43E-10
50	2.5	11.252	4.19E-08	9.86E-10
51	2.55	10.249	4.16E-08	1.14E-09
52	2.6	10.44	4.30E-08	6.45E-10
53	2.65	13.26	4.34E-08	3.83E-10
54	2.7	11.62	3.84E-08	9.55E-10
55	2.75	14.944	3.78E-08	1.70E-10
56	2.8	12.009	3.76E-08	5.61E-10
57	2.85	9.599	3.29E-08	9.59E-10
58	2.9	14.015	2.99E-08	4.81E-10
59	2.95	9.105	2.86E-08	7.42E-10
60	3	10.973	3.18E-08	8.38E-10
61	3.05	13.689	3.05E-08	4.92E-10
62	3.1	10.155	3.49E-08	2.51E-10
63	3.15	14.696	2.49E-08	0
64	3.2	13.798	2.41E-08	6.67E-10
65	3.25	14.514	2.71E-08	5.27E-10
66	3.3	10.653	2.27E-08	4.16E-10
67	3.35	8.922	1.80E-08	9.94E-10
68	3.4	14.183	1.66E-08	4.77E-10
69	3.45	13.362	1.49E-08	0
70	3.5	13.143	1.17E-08	8.49E-10

Sample #	Height (m)	Mass (g)	χ m^3/kg	Stadard Deviation
71	3.55	12.3	1.39E-08	3.60E-10
72	3.6	11.341	1.32E-08	3.91E-10
73	3.65	11.649	1.44E-08	4.39E-10
74	3.7	10.65	1.53E-08	2.40E-10
75	3.75	10.098	1.25E-08	1.11E-09
76	3.8	13.067	1.62E-08	5.18E-10
77	3.85	11.501	1.63E-08	3.85E-10
78	3.9	10.453	1.22E-08	7.35E-10
79	3.95	9.563	1.55E-08	7.08E-10
80	4	9.381	1.09E-08	2.73E-10
81	4.05	12.347	1.33E-08	5.48E-10
82	4.1	7.81	1.41E-08	1.43E-09
83	4.15	10.031	1.46E-08	6.75E-10
84	4.2	12.132	1.20E-08	7.61E-10
85	4.25	7.722	1.82E-08	6.63E-10
86	4.3	6.347	1.13E-08	1.46E-09
87	4.35	5.18	1.81E-08	9.90E-10
88	4.4	5.598	2.32E-08	1.21E-09
89	4.45	7.897	1.51E-08	1.17E-09
90	4.5	7.012	1.44E-08	1.27E-09
91	4.55	9.349	6.91E-09	9.89E-10
92	4.6	6.079	9.44E-09	7.31E-10
93	4.65	9.986	7.02E-09	1.28E-09
94	4.7	8.455	5.93E-09	3.03E-10
95	4.75	9.223	6.02E-09	1.00E-09
96	4.8	8.841	9.15E-09	7.67E-10
97	4.85	7.795	2.36E-08	8.68E-10
98	4.9	8.813	2.62E-08	1.00E-09
99	4.95	7.23	2.32E-08	9.37E-10
100	5	8.43	2.03E-08	1.39E-09
101	5.05	8.934	1.41E-08	7.59E-10
102	5.1	9.191	9.20E-09	8.37E-10
103	5.15	9.964	9.40E-09	5.14E-10
104	5.2	8.341	1.95E-08	1.11E-09
105	5.25	10.494	1.38E-08	1.12E-09
106	5.3	15.446	4.15E-08	2.84E-10
107	5.35	5.452	1.55E-08	8.14E-10
108	5.4	7.681	1.38E-08	5.78E-10
109	5.45	9.384	1.54E-08	4.73E-10
110	5.5	10.995	2.53E-08	1.01E-09
111	5.55	5.101	3.29E-08	5.02E-10
112	5.6	4.782	2.19E-08	1.42E-09
113	5.65	7.363	2.01E-08	3.48E-10
114	5.7	7.792	5.03E-08	8.65E-10
115	5.75	11.24	5.39E-08	9.84E-10

Sample #	Height (m)	Mass (g)	χ m^3/kg	Stadard Deviation
116	5.8	11.396	2.04E-08	5.93E-10
117	5.85	10.878	2.34E-08	9.39E-10
118	5.9	12.706	9.37E-09	5.33E-10
119	5.95	8.676	1.96E-08	1.18E-09
120	6	10.347	6.60E-09	4.29E-10
121	6.05	9.018	3.50E-08	1.41E-09
122	6.1	12.359	2.97E-08	6.19E-10
123	6.15	9.806	3.08E-08	4.51E-10
124	6.2	8.544	1.69E-08	1.04E-09
125	6.25	7.364	1.25E-08	1.26E-09
126	6.3	8.529	1.18E-08	9.01E-10
127	6.35	11.883	1.18E-08	2.15E-10
128	6.4	6.806	9.23E-09	1.31E-09
129	6.45	9.662	1.76E-08	7.01E-10
130	6.5	9.869	7.83E-09	1.04E-09
131	6.55	11.721	5.51E-09	5.79E-10
132	6.6	12.769	4.78E-09	5.31E-10
133	6.65	10.061	3.36E-09	5.10E-10
134	6.7	9.401	1.54E-08	8.17E-10
135	6.75	9.123	1.01E-08	1.01E-09
136	6.8	9.844	6.75E-09	1.04E-09
137	6.85	7.5	9.58E-09	6.84E-10
138	6.9	9.758	9.59E-09	1.14E-09
139	6.95	10.243	1.00E-08	1.25E-09
140	7	9.593	1.32E-08	1.07E-09
141	7.05	8.36	1.29E-08	1.11E-09
142	7.1	9.019	7.16E-09	1.14E-09
143	7.15	10.489	9.79E-09	1.22E-09
144	7.2	9.333	2.03E-08	7.25E-10
145	7.25	8.021	1.64E-08	3.19E-10
146	7.3	8.141	1.39E-08	8.33E-10
147	7.35	8.574	2.02E-08	1.08E-09
148	7.4	10.476	1.05E-08	6.47E-10
149	7.45	10.955	9.87E-09	9.36E-10
150	7.5	8.413	9.62E-09	3.05E-10
151	7.55	9.276	1.56E-08	9.56E-10
152	7.6	10.767	6.84E-09	7.14E-10
153	7.65	13.054	1.96E-08	7.06E-10
154	7.7	11.237	3.92E-08	8.17E-10
155	7.75	12.203	1.00E-08	9.62E-10
156	7.8	9.513	5.65E-09	7.13E-10
157	7.85	11.681	7.39E-09	4.39E-10
158	7.9	9.569	3.10E-08	8.00E-10
159	7.95	8.932	9.87E-09	1.03E-09
160	8	9.613	1.56E-08	9.23E-10

Sample #	Height (m)	Mass (g)	χ m^3/kg	Stadard Deviation
161	8.05	11.318	9.07E-09	1.13E-09
162	8.1	8.254	1.07E-08	8.22E-10
163	8.15	8.951	7.62E-09	4.96E-10
164	8.2	11.406	1.01E-08	5.94E-10
165	8.25	8.394	9.86E-09	1.10E-09
166	8.3	12.019	1.11E-08	3.69E-10
167	8.35	10.155	9.58E-09	6.68E-10
168	8.4	10.512	3.21E-09	2.44E-10
169	8.45	9.122	3.31E-09	8.44E-10
170	8.5	10.922	4.42E-09	6.21E-10
171	8.55	9.147	7.46E-09	4.86E-10
172	8.6	12.041	2.81E-09	2.13E-10
173	8.65	10.836	1.78E-09	7.11E-10
174	8.7	10.746	6.35E-09	1.09E-09
175	8.75	10.467	4.96E-09	1.12E-09
176	8.8	12.454	2.28E-09	8.24E-10
177	8.85	12.366	6.69E-09	8.29E-10
178	8.9	10.66	7.08E-09	1.20E-09
179	8.95	9.651	4.25E-09	4.60E-10
180	9	10.286	5.22E-09	2.49E-10
181	9.05	11.015	1.59E-08	4.65E-10
182	9.1	10.219	3.31E-09	1.00E-09
183	9.15	9.945	5.95E-09	6.82E-10
184	9.2	8.918	1.09E-08	7.60E-10
185	9.25	14.355	4.12E-09	7.79E-10
186	9.3	13.223	7.63E-09	3.36E-10
187	9.35	10.556	1.33E-07	8.19E-10
188	9.4	11.344	8.41E-09	6.78E-10
189	9.45	8.146	8.16E-09	8.33E-10
190	9.5	13.914	1.17E-08	6.63E-10
191	9.55	12.257	1.24E-08	5.53E-10
192	9.6	12.705	4.80E-09	5.34E-10
193	9.65	9.375	3.60E-09	5.47E-10
194	9.7	10.591	8.50E-09	8.38E-10
195	9.75	11.893	2.38E-09	8.63E-10
196	9.8	9.623	2.76E-09	7.06E-10
197	9.85	10.03	7.35E-09	8.86E-10
198	9.9	10.282	8.22E-09	1.14E-09
199	9.95	10.472	7.04E-09	8.48E-10
200	10	10.466	1.14E-08	6.48E-10
201	10.05	8.344	2.31E-09	1.07E-09
202	10.1	11.515	1.75E-07	1.03E-09
203	10.15	8.517	6.95E-09	3.01E-10
204	10.2	9.783	6.70E-10	1.05E-09
205	10.25	8.37	2.08E-09	6.13E-10

Sample #	Height (m)	Mass (g)	χ m^3/kg	Stadard Deviation
206	10.3	13.627	7.48E-10	6.79E-10
207	10.35	11.293	6.52E-09	1.04E-09
208	10.4	10.185	2.43E-09	1.15E-09
209	10.45	8.032	8.72E-09	3.19E-10
210	10.5	11.408	3.92E-09	8.11E-10
211	10.55	8.38	6.63E-09	3.06E-10
212	10.6	7.65	7.26E-09	1.34E-09
213	10.65	11.664	1.22E-08	5.81E-10
214	10.7	7.783	2.23E-08	6.58E-10
215	10.75	7.756	2.28E-08	5.71E-10
216	10.8	9.342	1.45E-08	1.10E-09
217	10.85	6.682	6.41E-09	3.84E-10
218	10.9	10.521	2.16E-08	1.06E-09
219	10.95	7.887	1.14E-08	1.13E-09
220	11	9.239	7.19E-09	1.39E-09
221	11.05	9.361	6.13E-09	0
222	11.1	10.246	3.65E-09	6.63E-10
223	11.15	9.686	5.36E-09	4.59E-10
224	11.2	11.259	8.32E-09	6.02E-10
225	11.25	8.275	5.84E-09	3.10E-10
226	11.3	7.979	1.22E-08	1.16E-09
227	11.35	10.461	6.18E-09	4.90E-10
228	11.4	10.502	1.01E-08	7.32E-10
229	11.45	9.275	1.19E-08	7.31E-10
230	11.5	9.585	2.58E-09	4.64E-10
231	11.55	11.086	4.03E-09	8.34E-10
232	11.6	8.607	3.08E-09	5.96E-10
233	11.65	8.986	5.98E-09	2.85E-10
234	11.7	6.371	2.27E-08	1.21E-09
235	11.75	10.394	6.91E-09	4.93E-10
236	11.8	10.78	9.36E-09	8.24E-10
237	11.85	10.245	8.78E-09	4.33E-10
238	11.9	9.135	6.48E-09	1.01E-09
239	11.95	10.285	2.41E-08	0
240	12	8.463	1.36E-08	8.01E-10
241	12.05	8.573	6.48E-09	7.92E-10
242	12.1	5.521	4.71E-08	1.22E-09
243	12.15	8.75	2.41E-09	5.87E-10
244	12.2	8.876	1.22E-08	7.64E-10
245	12.25	9.165	5.07E-09	8.40E-10
246	12.3	9.234	8.96E-09	7.35E-10
247	12.35	10.51	7.70E-09	4.88E-10
248	12.4	10.804	9.00E-09	8.55E-10
249	12.45	10.429	7.07E-09	7.38E-10
250	12.5	9.308	1.40E-08	7.28E-10

Sample #	Height (m)	Mass (g)	χ m^3/kg	Stadard Deviation
251	12.55	8.845	1.37E-08	1.26E-09
252	12.6	9.647	3.13E-09	9.22E-10
253	12.65	11.416	7.72E-09	2.25E-10
254	12.7	13.15	1.04E-08	7.02E-10
255	12.75	9.524	7.36E-09	2.69E-10
256	12.8	10.622	1.63E-08	8.69E-10
257	12.85	10.77	1.54E-08	4.12E-10
258	12.9	11.339	2.04E-08	6.76E-10
259	12.95	12.286	1.81E-08	2.08E-10
260	13	11.472	1.08E-08	8.05E-10
261	13.05	5.531	3.07E-08	4.63E-10
262	13.1	11.622	4.94E-09	3.82E-10
263	13.15	7.721	2.17E-08	1.33E-09
264	13.2	13.033	6.91E-09	3.41E-10
265	13.25	13.02	1.07E-08	3.41E-10
266	13.3	13.112	5.48E-09	3.91E-10
267	13.35	10.31	2.10E-08	1.08E-09
268	13.4	11.746	1.20E-08	5.77E-10
269	13.45	11.768	5.95E-09	8.72E-10
270	13.5	10.483	8.24E-09	2.45E-10

Highway 99 Fittstown, OK Alternate Katian Stratotype

Sample #	Height (m)	Mass (g)	χ m^3/kg	Standard Deviation
-36	-5	12.359	-7.92E-10	7.49E-10
-35	-4.95	11.724	-2.23E-09	2.19E-10
-34	-4.9	12.634	8.79E-11	7.33E-10
-33	-4.85	14.546	-2.98E-10	1.77E-10
-32	-4.8	14.392	-6.80E-10	1.78E-10
-31	-4.75	12.637	-2.07E-09	5.38E-10
-30	-4.7	12.016	-9.65E-10	2.14E-10
-29	-4.65	10.956	4.33E-10	2.34E-10
-28	-4.6	10.265	1.51E-08	0
-27	-4.55	10.64	1.02E-08	4.82E-10
-26	-4.5	12.649	7.55E-09	6.08E-10
-25	-4.45	11.875	5.44E-09	4.32E-10
-24	-4.4	10.378	2.91E-09	7.42E-10
-23	-4.35	10.956	2.26E-09	8.11E-10
-22	-4.3	11.948	1.46E-09	5.68E-10
-21	-4.25	13.836	2.57E-09	3.21E-10
-20	-4.2	12.932	1.05E-08	5.24E-10
-19	-4.15	13.469	-9.96E-10	0
-18	-4.1	11.597	1.35E-09	4.43E-10
-17	-4.05	15.236	1.50E-09	6.74E-10
-16	-4	12.49	-5.65E-11	5.44E-10
-15	-3.95	12.783	1.58E-08	7.21E-10

Sample #	Height (m)	Mass (g)	χ m^3/kg	Standard Deviation
-14	-3.9	14.59	2.32E-09	1.76E-10
-13	-3.85	12.159	5.61E-09	6.33E-10
-12	-3.8	14.137	4.06E-09	5.44E-10
-11	-3.75	12.62	1.53E-09	7.05E-10
-10	-3.7	13.834	1.79E-09	6.43E-10
-9	-3.65	12.769	1.51E-09	3.48E-10
-8	-3.6	15.19	5.69E-09	3.38E-10
-7	-3.55	15.137	6.19E-09	1.69E-10
-6	-3.5	14.309	4.14E-09	6.46E-10
-5	-3.45	14.809	1.55E-09	1.73E-10
-4	-3.4	13.998	7.93E-11	6.61E-10
-3	-3.35	14.207	-6.89E-10	6.52E-10
-2	-3.3	13.029	1.20E-09	7.10E-10
-1	-3.25	11.099	2.23E-09	6.94E-10
0	-3.2	11.973	1.31E-09	8.58E-10
1	-3.15	11.787	1.48E-09	4.36E-10
2	-3.05	14.81	4.73E-09	3.46E-10
3	-3.1	10.204	3.84E-09	6.65E-10
4	-3	11.096	1.25E-09	8.01E-10
5	-2.95	10.837	1.44E-09	2.37E-10
6	-2.9	12.285	1.42E-09	2.09E-10
7	-2.85	11.012	3.89E-09	2.33E-10
8	-2.8	11.42	3.75E-09	2.25E-10
9	-2.75	13.119	2.02E-09	7.05E-10
10	-2.7	10.839	1.44E-09	4.74E-10
11	-2.65	10.921	3.92E-09	8.47E-10
12	-2.6	12.491	1.45E-08	4.10E-10
13	-2.55	10.643	2.66E-09	8.69E-10
14	-2.5	10.699	5.53E-09	2.40E-10
15	-2.45	10.177	3.14E-09	9.09E-10
16	-2.4	10.27	2.23E-09	1.00E-09
17	-2.35	11.413	2.04E-08	4.48E-10
18	-2.3	9.644	1.55E-08	4.60E-10
19	-2.25	8.697	2.35E-08	1.02E-09
20	-2.2	10.655	2.24E-08	2.40E-10
21	-2.15	11.919	8.46E-09	7.45E-10
22	-2.1	11.633	3.84E-09	4.41E-10
23	-2.05	11.527	2.62E-09	5.55E-17
24	-2	10.46	1.60E-08	2.45E-10
25	-1.95	11.778	2.10E-09	7.55E-10
26	-1.9	11.81	-5.21E-10	2.17E-10
27	-1.85	11.677	-5.27E-10	4.40E-10
28	-1.8	9.557	-1.97E-09	4.66E-10
29	-1.75	10.885	7.69E-10	8.17E-10
30	-1.7	9.566	4.10E-09	2.68E-10

Sample #	Height (m)	Mass (g)	χ m^3/kg	Standard Deviation
31	-1.65	10.057	3.18E-09	9.20E-10
32	-1.6	9.82	2.33E-09	6.92E-10
33	-1.55	10.387	8.66E-09	4.27E-10
34	-1.5	11.972	4.94E-09	7.72E-10
35	-1.45	10.145	6.01E-09	9.11E-10
36	-1.4	9.956	6.31E-09	8.92E-10
37	-1.35	9.743	3.65E-09	7.90E-10
38	-1.3	12.177	3.82E-09	6.32E-10
39	-1.25	9.061	6.13E-09	2.83E-10
40	-1.2	12.408	1.70E-09	7.46E-10
41	-1.15	11.397	1.85E-09	9.01E-10
42	-1.1	10.138	4.76E-09	1.01E-09
43	-1.05	11.9	3.45E-09	3.73E-10
44	-1	11.333	6.02E-09	7.84E-10
45	-0.95	13.32	3.35E-09	3.85E-10
46	-0.9	9.871	2.14E-09	9.38E-10
47	-0.85	12.203	1.15E-08	7.57E-10
48	-0.8	12.291	9.04E-11	2.09E-10
49	-0.75	8.461	-1.16E-09	6.07E-10
50	-0.7	10.854	4.28E-09	7.09E-10
51	-0.65	10.912	6.09E-09	8.47E-10
52	-0.6	14.391	6.00E-09	4.71E-10
53	-0.55	11.319	5.39E-09	9.06E-10
54	-0.5	10.99	3.01E-08	8.37E-10
55	-0.45	11.398	4.87E-09	4.50E-10
56	-0.4	11.74	2.41E-09	8.74E-10
57	-0.35	11.151	3.35E-09	2.30E-10
58	-0.3	6.684	2.34E-09	1.38E-09
59	-0.25	7.894	2.90E-09	8.60E-10
60	-0.2	12.16	5.02E-09	4.22E-10
61	-0.15	12.672	2.81E-09	6.08E-10
62	-0.1	11.219	4.95E-09	2.29E-10
63	-0.05	12.828	4.05E-09	6.93E-10
64	0	9.908	1.58E-09	5.18E-10
65	0.05	7.922	3.03E-08	8.54E-10
66	0.1	10.753	-5.72E-10	2.39E-10
67	0.15	11.303	2.35E-09	4.54E-10
68	0.2	10.256	1.04E-08	7.50E-10
69	0.25	12.217	3.21E-09	2.10E-10
70	0.3	9.216	1.89E-09	5.57E-10
71	0.35	11.357	1.19E-08	4.51E-10
72	0.4	10.717	1.57E-08	6.32E-10
73	0.5	13.104	9.91E-09	3.91E-10
74	0.55	11.382	9.66E-09	2.25E-10
75	0.6	10.959	8.38E-09	8.43E-10

Sample #	Height (m)	Mass (g)	χ m^3/kg	Standard Deviation
76	0.65	10.447	7.57E-09	4.25E-10
77	0.7	9.801	3.26E-09	5.24E-10
78	0.75	11.343	7.14E-09	5.98E-10
79	0.8	11.218	9.32E-09	6.04E-10
80	0.85	10.934	5.08E-09	2.35E-10
81	0.9	10.062	7.14E-09	5.10E-10
82	0.95	10.272	4.53E-09	4.33E-10
83	1	12.809	8.58E-09	4.00E-10
84	1.05	11.573	7.78E-09	3.84E-10
85	1.1	11.309	1.69E-08	2.26E-10
86	1.15	11.378	6.79E-09	4.51E-10
87	1.2	10.277	6.64E-09	7.49E-10
88	1.25	11.396	6.78E-09	2.25E-10
89	1.3	12.279	4.97E-09	8.36E-10
90	1.35	11.649	6.01E-09	7.94E-10
91	1.4	11.724	1.64E-09	3.79E-10
92	1.45	11.203	6.42E-09	9.16E-10
93	1.5	9.252	1.01E-08	7.33E-10
94	1.55	11.881	9.10E-09	7.78E-10
95	1.6	10.487	1.01E-08	7.33E-10
96	1.65	11.513	7.35E-09	0
97	1.7	10.068	7.86E-09	4.41E-10
98	1.75	12.13	6.07E-09	1.11E-16
99	1.8	11.636	6.18E-09	2.20E-10
100	1.85	10.161	7.97E-09	5.05E-10
101	1.9	10.151	7.44E-09	5.05E-10
102	1.95	9.28	5.99E-09	5.53E-10
103	2	10.284	5.23E-09	9.98E-10
104	2.05	10.423	6.55E-09	8.52E-10
105	2.1	10.663	7.08E-09	6.36E-10
106	2.15	10.522	7.00E-09	8.44E-10
107	2.2	9.091	7.91E-09	1.13E-09
108	2.25	11.027	3.39E-09	6.16E-10
109	2.3	10.885	5.94E-09	9.42E-10
110	2.35	11.43	7.08E-09	4.49E-10
111	2.4	10.11	5.67E-09	4.39E-10
112	2.45	10.186	6.34E-09	6.66E-10
113	2.5	11.271	6.70E-09	2.27E-10
114	2.55	9.552	1.83E-09	9.69E-10
115	2.6	10.545	4.92E-09	7.30E-10
116	2.65	10.697	5.53E-09	4.80E-10
117	2.7	10.643	6.07E-09	8.69E-10
118	2.75	9.001	6.17E-09	7.54E-10
119	2.8	9.98	7.93E-09	8.90E-10
120	2.85	10.035	4.81E-09	5.11E-10

Sample #	Height (m)	Mass (g)	χ m^3/kg	Standard Deviation
121	2.9	11.142	5.96E-09	8.30E-10
122	2.95	7.781	1.31E-09	3.30E-10
123	3	11.611	7.28E-09	3.82E-10
124	3.05	10.549	7.50E-09	7.29E-10
125	3.1	11.133	7.76E-09	4.61E-10
126	3.15	9.951	5.95E-09	6.82E-10
127	3.2	9.356	6.71E-09	8.22E-10
128	3.25	7.594	7.08E-09	3.38E-10
129	3.3	8.089	6.19E-09	3.17E-10
130	3.35	8.196	8.11E-09	3.13E-10
131	3.4	9.36	7.48E-09	2.74E-10
132	3.45	8.637	9.69E-10	5.15E-10
133	3.5	10.836	6.47E-09	8.53E-10
134	3.55	10.392	6.39E-09	6.53E-10
135	3.6	10.189	6.70E-09	4.36E-10
136	3.65	10.824	5.97E-09	8.54E-10
137	3.7	10.876	6.61E-09	9.43E-10
138	3.75	9.575	7.88E-09	5.36E-10
139	3.8	8.834	8.34E-09	8.71E-10
140	3.85	11.299	7.16E-09	6.00E-10
141	3.9	10.473	7.04E-09	4.24E-10
142	3.95	9.173	6.65E-09	1.01E-09
143	4	12.666	5.10E-09	4.05E-10
144	4.05	9.534	4.30E-09	8.07E-10
145	4.1	10.384	6.75E-09	8.90E-10
146	4.15	13.217	5.85E-09	5.13E-10
147	4.2	9.258	6.59E-09	2.77E-10
148	4.25	8.155	6.37E-09	5.45E-10
149	4.3	10.775	8.86E-09	4.12E-10
150	4.35	10.349	7.47E-09	2.48E-10
151	4.4	8.128	5.94E-09	3.16E-10
152	4.45	13.95	5.80E-09	3.68E-10
153	4.5	9.89	3.97E-09	6.86E-10
154	4.55	11.985	5.54E-09	7.71E-10
155	4.6	8.83	7.11E-09	0
156	4.65	9.346	7.30E-09	4.75E-10
157	4.7	8.492	7.61E-09	7.99E-10
158	4.75	9.229	8.97E-09	1.11E-09
159	4.8	8.577	9.01E-09	1.08E-09
160	4.85	9.903	9.09E-09	4.48E-10
161	4.9	7.834	5.70E-09	8.66E-10
162	4.95	8.485	8.68E-09	1.05E-09
163	5	8.46	9.35E-09	5.25E-10
164	5.05	9.02	6.76E-09	5.69E-10
165	5.1	9.57	7.51E-09	7.09E-10

Sample #	Height (m)	Mass (g)	χ m^3/kg	Standard Deviation
166	5.15	10.435	5.50E-09	4.26E-10
167	5.2	8.441	6.58E-09	8.04E-10
168	5.25	9.485	7.58E-09	5.41E-10
169	5.3	8.927	6.83E-09	1.04E-09
170	5.35	8.22	6.98E-09	9.36E-10
171	5.4	9.301	7.53E-09	5.51E-10
172	5.45	9.508	6.61E-09	8.09E-10
173	5.5	8.046	8.48E-09	9.56E-10
174	5.55	8.365	8.16E-09	9.20E-10
175	5.6	8.673	5.57E-09	1.07E-09
176	5.65	8.007	8.07E-09	3.20E-10
177	5.7	8.481	6.55E-09	8.00E-10
178	5.75	8.796	5.49E-09	1.17E-09
179	5.8	7.575	9.73E-09	5.86E-10
180	5.85	9.375	7.09E-09	5.47E-10
181	5.9	9.159	6.46E-09	5.60E-10
182	5.95	8.76	5.93E-09	0
183	6	7.324	-3.82E-09	9.28E-10
184	6.05	9.152	5.08E-09	4.86E-10
185	6.1	8.208	6.10E-09	1.13E-09
186	6.15	9.878	7.83E-09	6.87E-10
187	6.2	8.17	3.91E-09	8.31E-10
188	6.25	8.28	7.80E-09	8.19E-10
189	6.3	8.892	8.08E-09	2.88E-10
190	6.35	9.279	6.18E-09	7.85E-17
191	6.4	7.765	8.32E-09	6.61E-10
192	6.45	8.484	7.40E-09	5.24E-10
193	6.5	9.076	7.12E-09	1.02E-09
194	6.55	10.542	8.54E-09	4.21E-10
195	6.6	9.108	5.90E-09	5.63E-10
196	6.65	7.549	6.16E-09	5.89E-10
197	6.7	10.743	7.87E-09	4.13E-10
198	6.75	10.608	7.46E-09	7.25E-10
199	6.8	9.528	7.16E-09	8.07E-10
200	6.85	8.284	1.26E-08	1.24E-09
201	6.9	8.941	7.23E-09	1.15E-09
202	6.95	9.036	8.56E-09	7.51E-10
203	7	10.155	6.54E-09	6.68E-10
204	7.05	8.054	8.02E-09	6.37E-10
205	7.1	9.463	6.83E-09	5.42E-10
206	7.15	8.441	5.62E-10	6.08E-10
207	7.2	9.047	1.03E-08	1.02E-09
208	7.25	10.367	8.68E-09	8.57E-10
209	7.3	8.444	9.37E-09	5.26E-10
210	7.35	9.34	8.08E-09	2.75E-10

Sample #	Height (m)	Mass (g)	χ m^3/kg	Standard Deviation
211	7.4	10.275	8.76E-09	8.64E-10
212	7.45	9.434	7.23E-09	4.71E-10
213	7.5	10.265	7.18E-09	0
214	7.55	7.4	1.02E-08	3.46E-10
215	7.6	8.927	8.25E-09	4.97E-10
216	7.65	9.236	6.41E-09	7.35E-10
217	7.7	11.056	7.65E-09	4.02E-10
218	7.75	9.568	7.89E-09	2.68E-10
219	7.8	12.05	7.02E-09	6.38E-10
220	7.85	7.848	3.61E-09	6.54E-10
221	7.9	9.402	8.03E-09	9.83E-10
222	7.95	9.398	9.00E-09	9.45E-10
223	8	9.507	7.94E-09	9.72E-10
224	8.05	8.993	1.04E-08	7.54E-10
225	8.1	9.719	6.84E-09	5.28E-10
226	8.15	7.762	3.42E-09	8.75E-10
227	8.2	11.955	6.77E-09	5.67E-10
228	8.25	10.608	7.63E-09	4.83E-10
229	8.3	8.952	8.23E-09	9.92E-10
230	8.35	9.141	1.06E-08	7.42E-10
231	8.4	8.119	8.18E-09	8.36E-10
232	8.45	7.156	9.03E-09	9.48E-10
233	8.5	8.808	7.75E-09	8.73E-10
234	8.55	10.503	8.05E-09	8.46E-10
235	8.6	11.686	6.62E-09	2.19E-10
236	8.65	10.774	7.34E-09	8.24E-10
237	8.7	9.604	8.80E-09	8.01E-10
238	8.75	9.922	9.44E-09	2.58E-10
239	8.8	8.909	9.70E-09	7.61E-10
240	8.85	11.013	1.15E-08	2.33E-10
241	8.9	8.472	8.06E-09	5.24E-10
242	8.95	6.946	9.83E-09	6.39E-10
243	9	10.772	8.02E-09	6.30E-10
244	9.05	9.438	1.03E-08	7.18E-10
245	9.1	9.638	8.77E-09	4.61E-10
246	9.15	7.953	1.02E-08	6.45E-10
247	9.2	9.282	1.03E-08	0
248	9.25	10.103	8.19E-09	2.54E-10
249	9.3	8.4	9.42E-09	9.16E-10
250	9.35	9.655	1.10E-08	0
251	9.4	9.029	9.57E-09	5.68E-10
252	9.45	8.426	7.45E-09	9.13E-10
253	9.5	8.211	7.65E-09	9.37E-10
254	9.55	8.86	8.32E-09	8.68E-10
255	9.6	9.049	8.74E-09	8.50E-10

Sample #	Height (m)	Mass (g)	χ m^3/kg	Standard Deviation
256	9.65	9.282	1.01E-08	1.10E-09
257	9.7	8.97	1.00E-08	9.90E-10
258	9.75	8.625	9.80E-09	1.03E-09
259	9.8	9.387	1.23E-08	2.73E-10
260	9.85	10.352	1.39E-08	7.42E-10
261	9.9	9.99	1.32E-08	6.78E-10
262	9.95	9.341	1.16E-08	2.74E-10
263	10	10.06	1.24E-08	6.74E-10
264	10.05	7.462	1.40E-08	9.09E-10
265	10.1	8.483	1.47E-08	1.21E-09
266	10.15	9.84	1.19E-08	9.02E-10
267	10.2	9.379	1.37E-08	4.73E-10
268	10.25	10.161	1.37E-08	7.56E-10
269	10.3	9.024	1.32E-08	1.02E-09
270	10.35	9.903	1.29E-08	7.76E-10
271	10.4	9.234	1.39E-08	9.61E-10
272	10.45	9.145	1.16E-08	8.41E-10
273	10.5	12.749	1.19E-08	2.01E-10
274	10.55	9.528	1.08E-08	5.38E-10
275	10.6	10.692	1.23E-08	8.64E-10
276	10.65	11.153	1.25E-08	3.98E-10
277	10.7	9.477	1.18E-08	4.68E-10
278	10.75	10.545	1.42E-08	7.28E-10
279	10.8	10.498	1.41E-08	8.79E-10
280	10.85	10.519	1.25E-08	6.44E-10
281	10.9	9.424	1.05E-08	5.44E-10
282	10.95	8.916	1.40E-08	7.60E-10
283	11	9.758	1.15E-08	7.88E-10
284	11.05	11.209	1.32E-08	4.57E-10
285	11.1	9.292	1.22E-08	2.76E-10
286	11.15	9.58	1.58E-08	2.67E-10
287	11.2	10.479	1.34E-08	6.47E-10
288	11.25	11.377	1.36E-08	7.79E-10
289	11.3	12.071	1.27E-08	7.65E-10
290	11.35	9.508	1.29E-08	0
291	11.4	9.55	1.34E-08	9.29E-10
292	11.45	9.19	1.26E-08	1.12E-09
293	11.5	10.591	1.48E-08	4.83E-10
294	11.55	9.45	1.30E-08	9.39E-10
295	11.6	11.412	1.14E-08	8.98E-10
296	11.65	9.354	1.16E-08	2.74E-10
297	11.7	10.534	1.23E-08	8.77E-10
298	11.75	9.549	1.23E-08	8.05E-10
299	11.8	9.701	1.23E-08	6.99E-10
300	11.85	10.072	1.07E-08	1.02E-09

Sample #	Height (m)	Mass (g)	χ m^3/kg	Standard Deviation
301	11.9	8.235	1.11E-08	1.12E-09
302	11.95	9.163	1.24E-08	2.80E-10
303	12	9.127	1.34E-08	0
304	12.05	8.107	1.18E-08	9.48E-10
305	12.1	8.166	1.21E-08	3.14E-10
306	12.15	8.339	1.30E-08	1.11E-09
307	12.2	7.472	1.11E-08	3.43E-10
308	12.25	7.819	1.22E-08	9.83E-10
309	12.3	7.687	9.35E-09	1.20E-09
310	12.35	7.728	9.77E-09	8.78E-10
311	12.4	8.529	9.49E-09	6.01E-10
312	12.45	8.353	9.04E-09	6.14E-10
313	12.5	7.112	1.01E-08	7.21E-10
314	12.55	7.933	7.46E-09	6.47E-10
315	12.6	6.585	1.26E-08	3.89E-10
316	12.65	9.24	8.96E-09	5.55E-10
317	12.7	10.528	9.58E-09	8.43E-10
318	12.75	8.261	1.02E-08	0
319	12.8	7.662	8.91E-09	1.00E-09
320	12.85	8.982	8.41E-09	5.71E-10
321	12.9	9.571	8.84E-09	8.03E-10
322	12.95	10.53	9.24E-09	8.78E-10
323	13	10.184	9.19E-09	2.52E-10
324	13.05	8.019	1.03E-08	3.20E-10
325	13.1	8.941	1.07E-08	8.60E-10
326	13.15	8.027	1.21E-08	6.39E-10
327	13.2	6.755	1.28E-08	1.00E-09
328	13.25	10.599	1.14E-08	4.83E-10
329	13.3	8.061	9.82E-09	1.11E-16
330	13.35	8.29	1.06E-08	1.24E-09
331	13.4	8.981	9.21E-09	1.14E-09
332	13.45	8.861	9.95E-09	2.89E-10
333	13.5	8.377	1.38E-08	1.10E-09
334	13.55	8.111	1.04E-08	9.48E-10
335	13.6	9.347	9.05E-09	4.75E-10
336	13.65	8.596	9.63E-09	1.08E-09
337	13.7	7.632	1.06E-08	1.34E-09
338	13.75	9.702	1.04E-08	7.92E-10
339	13.8	8.897	9.30E-09	5.76E-10
340	13.85	9.882	8.56E-09	7.78E-10
341	13.9	8.221	1.12E-08	1.12E-09
342	13.95	8.707	1.26E-08	2.94E-10
343	14	9.227	9.36E-09	7.35E-10
344	14.05	10.195	1.04E-08	8.71E-10
345	14.1	9.54	8.29E-09	9.31E-10

Sample #	Height (m)	Mass (g)	χ m^3/kg	Standard Deviation
346	14.15	10.317	7.85E-09	2.48E-10
347	14.2	10.226	5.61E-09	4.34E-10
348	14.25	10.014	6.81E-09	8.87E-10
349	14.3	8.824	7.32E-09	1.16E-09
350	14.35	8.955	7.62E-09	0
351	14.4	11.517	7.34E-09	3.86E-10
352	14.45	9.682	9.30E-09	7.94E-10
353	14.5	8.94	9.66E-09	7.59E-10
354	14.55	9.654	9.70E-09	2.66E-10
355	14.6	9.874	7.65E-09	1.04E-09
356	14.65	8.863	5.04E-09	1.16E-09
357	14.7	6.095	6.14E-09	8.42E-10
358	14.75	8.363	-1.82E-09	6.14E-10
359	14.8	7.826	1.53E-09	8.68E-10
360	14.85	9.167	8.63E-09	9.69E-10
361	14.9	6.901	2.53E-09	1.34E-09
362	14.95	9.936	8.51E-09	7.74E-10
363	15	10.946	8.39E-09	6.20E-10

APPENDIX VI
FRANKFORT, KY χ COMPOSITE SECTION

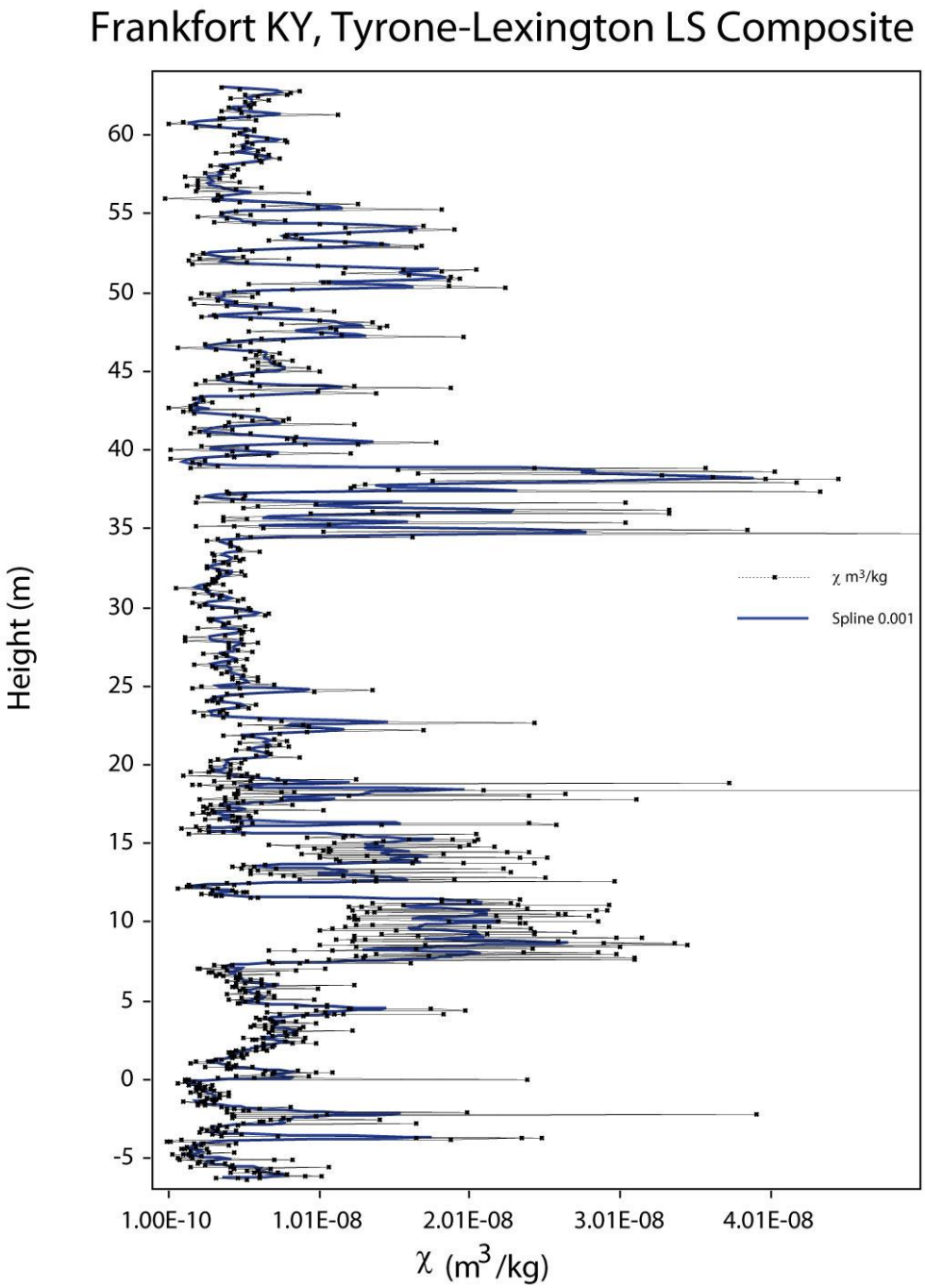

APPENDIX VII
ADDITIONAL χ SEQUENCE STRATIGRAPHY SECTIONS SAMPLED

1) Moorehead, KY I-64. Silurian Crab Orchard Fm; Devonian Olentangy Shale; Devonian Huron Shale. Sequence Boundaries 120 Samples Collected
2) Crestwood, KY Rt 329. Ordovician Saluda Formation; Silurian Brasfield Formation Sequence Boundary 62 Sample Collected
3) Chestnut Street, Cherry Valley NY. Devonian Bakoven Member Union Springs Fm, Cherry Valley Limestone, East Berne Member Falling Stage, Sequence Boundary, Lowstand, TST, and MFS 64 samples collected
4) City View Terrace, Kingston NY Devonian Bakoven-Stony Hollow Mbrs. Of Union Springs Formation contact. Forced Regression Surface, Falling Stage 81 samples collected
5) Katterskill Creek, Catskill NY. Devonian Moorehouse Member Onondaga Formation-Bakoven Member Union Springs Fm contact. Flooding Surface. 88 samples collected
6) Rt 23A Catskill NY. Devonian Port Ewen Limestone, Glen Erie Limestone, Esopus Shale. Wallbridge Unconformity, Maximum Flooding Surface. 113 samples collected
7) Catskill, NY Rt 23. Ordovician Austin Glen Formation, Silurian Roundout Formation Angular Taconic Unconformity. 106 samples collected
8) I-88 Cobleskill NY. Devonian Alsen Formation, Oriskany Sandstone, and Esopus Shale. Wallbridge Unconformity Sequence Boundary and Flooding Surface. 116 samples collected
9) Rt. 20 Cherry Valley NY. Devonian Kalkberg Formation, Oriskany Sandstone, Esopus Shale. Wallbridge Unconformity Sequence Boundary and Flooding Surface. 73 samples collected.

10) Kennedy Rd. Nedrow NY. Seneca Member Onondaga Limestone-Bakoven Member Union Springs Formation contact. Flooding Surface Bakoven-Cherry Valley Limestone contact. Sequence Boundary. 76 samples collected

11) Stony Creek, Little Falls NY. Ordovician Little Falls Dolostone, Black River Group, Knox Unconformity Sequence Boundary 92 samples collected.

12) Nine Mile Creek So. Trenton NY. Stueben-Indian Castle Shale Contact. Maximum Flooding Surface. 50 samples collected.

13) Cape Rock Park. Cape Girardeau, Mo. Ordovician Girardeau Fm.-Silurian Sexton Creek Fm. Sequence Boundary. 180 samples collected.

APPENDIX VIII
χ SEQUENCE STRATIGRAPHY VALUES

Allen Rd. Oppenheim, NY. (5cm sample interval)

Sample #	Mass (g)	χ m^3/kg	Standard Deviation
-29	7.106	1.65E-08	6.24E-10
-28	8.104	1.07E-08	1.14E-09
-27	6.604	1.28E-08	6.72E-10
-26	8.016	3.38E-08	8.43E-10
-25	8.512	1.21E-08	7.97E-10
-24	7.454	1.47E-08	1.38E-09
-23	8.193	1.36E-08	5.42E-10
-22	8.597	1.17E-08	1.03E-09
-21	7.288	1.36E-08	1.53E-09
-20	7.744	1.16E-08	1.15E-09
-19	6.809	1.53E-08	1.51E-09
-18	6.885	1.62E-08	1.71E-09
-17	9.466	1.35E-08	2.22E-16
-16	8.029	1.44E-08	3.19E-10
-15	7.339	1.99E-08	1.52E-09
-14	7.874	1.42E-08	9.76E-10
-13	7.843	1.70E-08	5.66E-10
-12	8.812	1.51E-08	5.03E-10
-11	9.269	1.38E-08	9.57E-10
-10	6.08	1.96E-08	1.11E-09
-9	9.093	1.25E-08	2.82E-10
-8	8.376	1.46E-08	1.57E-16
-7	7.31	1.48E-08	1.26E-09
-6	7.153	1.84E-08	9.47E-10
-5	8.081	1.25E-08	5.49E-10
-4	9.39	1.71E-08	8.18E-10
-3	8.329	1.91E-08	1.34E-09
-2	8.967	3.42E-08	9.86E-10
-1	8.419	2.45E-08	8.04E-10
0	9.438	2.60E-08	1.18E-09
1	9.338	2.05E-08	9.88E-10
2	8.51	2.12E-08	3.01E-10
3	6.868	1.76E-08	1.63E-09
4	7.256	2.04E-08	1.54E-09
5	8.29	2.20E-08	1.07E-09
6	7.949	2.39E-08	8.51E-10
7	7.914	2.81E-08	1.16E-09
8	8.948	2.70E-08	9.89E-10
9	7.439	2.23E-08	1.58E-09
10	8.237	2.35E-08	5.38E-10

Sample #	Mass (g)	χ m^3/kg	Standard Deviation
11	7.464	2.71E-08	6.85E-10
12	6.549	3.42E-08	3.90E-10
13	9.017	2.44E-08	1.30E-09
14	7.746	2.73E-08	3.30E-10
15	6.653	2.77E-08	1.92E-09
16	7.5	2.19E-08	1.23E-09
17	7.634	3.05E-08	3.35E-10
18	7.885	3.37E-08	6.48E-10
19	7.704	1.80E-08	9.97E-10
20	7.441	1.94E-08	1.58E-09
21	6.13	2.03E-08	1.67E-09
22	6.843	2.37E-08	1.87E-09
23	6.895	2.41E-08	1.70E-09
24	7.869	2.46E-08	9.75E-10
25	8.957	1.85E-08	0
26	8.737	1.67E-08	1.28E-09
27	6.739	2.22E-08	0
28	6.559	1.90E-08	3.91E-10
29	6.366	2.21E-08	1.06E-09
30	8.065	2.04E-08	8.40E-10
31	9.424	1.44E-08	9.80E-10
32	9.204	2.22E-08	9.63E-10
33	9.022	2.00E-08	1.02E-09
34	7.653	3.40E-08	1.20E-09
35	7.853	2.39E-08	5.64E-10
36	6.898	2.93E-08	3.71E-10
37	7.854	1.95E-08	8.62E-10
38	8.151	2.79E-08	3.14E-10
39	8.097	3.01E-08	8.35E-10
40	8.068	2.60E-08	1.45E-09
41	7.259	2.29E-08	6.11E-10
42	5.764	3.51E-08	1.17E-09
43	8.781	2.98E-08	1.16E-09
44	9.301	1.84E-08	4.77E-10
45	8.331	2.93E-08	1.34E-09
46	7.625	3.43E-08	8.86E-10
47	7.961	2.36E-08	5.57E-10
48	7.955	3.04E-08	1.11E-09
49	7.146	2.05E-08	9.48E-10
50	8.218	1.67E-08	1.12E-09
51	8.08	2.10E-08	1.14E-09
52	9.626	1.99E-08	7.03E-10
53	8.149	2.08E-08	1.37E-09
54	8.125	2.78E-08	1.44E-09

Sample #	Mass (g)	χ m^3/kg	Standard Deviation
55	9.287	2.66E-08	4.77E-10
56	7.333	3.30E-08	1.60E-09
57	8.801	3.06E-08	5.03E-10
58	7.786	5.12E-08	5.67E-10
59	8.694	2.37E-08	7.78E-10
60	8.318	2.28E-08	1.34E-09
61	7.263	2.64E-08	7.04E-10
62	8.42	2.68E-08	1.39E-09
63	9.126	1.40E-08	1.29E-09
64	7.204	2.66E-08	3.55E-10
65	8.184	3.31E-08	8.26E-10
66	7.085	4.13E-08	1.30E-09
67	9.058	2.49E-08	4.89E-10
68	8.816	2.99E-08	5.02E-10
69	9.218	2.02E-08	7.34E-10
70	6.885	4.33E-08	9.81E-10
71	9.398	4.23E-08	7.17E-10
72	8.983	4.44E-08	0
73	8.689	3.64E-08	5.87E-10
74	8.436	2.72E-08	3.03E-10
75	10.036	3.28E-08	4.40E-10
76	8.068	3.63E-08	6.33E-10
77	9.122	3.50E-08	7.40E-10
78	8.805	3.45E-08	1.16E-09
79	9.023	3.48E-08	7.48E-10
80	7.636	5.44E-08	0
81	8.571	5.43E-08	2.97E-10
82	6.841	5.67E-08	1.12E-09
83	8.311	4.04E-08	1.53E-09
84	9.456	3.57E-08	5.40E-10
85	7.739	4.22E-08	1.32E-09
86	9.37	6.10E-08	0
87	8.633	5.94E-08	1.35E-09
88	8.4	5.61E-08	3.03E-10
89	8.544	5.77E-08	2.98E-10
90	7.648	5.69E-08	3.33E-10
91	6.1	5.42E-08	1.51E-09
92	7.207	5.51E-08	1.77E-09
93	8.528	4.62E-08	8.96E-10
94	8.754	5.85E-08	1.01E-09
95	7.932	5.10E-08	9.63E-10
96	9.627	4.78E-08	9.53E-10
97	9.98	5.33E-08	6.74E-10
98	7.721	4.51E-08	1.19E-09
99	6.778	3.97E-08	6.53E-10

100	8.438	5.84E-08	1.09E-09
Sample #	Mass (g)	χ m^3/kg	Standard Deviation
101	6.84	5.65E-08	1.62E-09
102	8.269	5.76E-08	6.15E-10
103	7.517	5.40E-08	1.22E-09
104	6.166	5.16E-08	6.28E-16
105	7.621	5.94E-08	1.53E-09
106	6.533	5.36E-08	6.76E-10
107	6.629	5.75E-08	1.68E-09
108	7.873	4.75E-08	8.57E-10
109	6.336	4.53E-08	2.02E-09
110	7.066	3.76E-08	7.23E-10
111	7.533	4.65E-08	1.02E-09
112	8.407	4.00E-08	3.03E-10
113	6.729	4.11E-08	1.52E-09
114	9.017	5.40E-08	1.13E-09
115	7.108	5.28E-08	3.59E-10
116	9	5.37E-08	7.48E-10
117	6.598	4.95E-08	1.69E-09
118	7.332	4.06E-08	1.52E-09
119	8.815	4.51E-08	7.65E-10
120	8.895	4.16E-08	2.87E-10
121	8.245	4.38E-08	1.42E-09

Canajoharie Creek, Canjoharie New York (5 cm sample interval)

Sample (#)	Mass (g)	χ m^3/kg	Standard Deviation
1	8.659	2.11E-08	5.12E-10
2	6.088	2.43E-08	1.11E-09
3	6.285	1.60E-08	1.87E-09
4	7.769	1.81E-08	1.65E-09
5	7.178	2.41E-08	1.55E-09
6	7.476	1.40E-08	3.43E-10
7	7.789	2.50E-08	3.28E-10
8	7.951	2.13E-08	8.52E-10
9	6.746	2.22E-08	0
10	9.536	2.23E-08	9.67E-10
11	8.919	2.31E-08	7.59E-10
12	7.909	2.42E-08	1.41E-09
13	8.706	2.16E-08	3.14E-16
14	6.852	2.19E-08	6.47E-10
15	7.649	1.93E-08	8.86E-10
16	7.173	1.99E-08	9.45E-10
17	8.862	2.08E-08	2.89E-10
18	9.73	2.65E-08	7.88E-10
19	9.041	2.24E-08	7.48E-10

Sample (#)	Mass (g)	χ m^3/kg	Standard Deviation
20	10.105	2.73E-08	5.06E-10
21	6.716	2.82E-08	1.37E-09
22	7.784	2.74E-08	6.57E-10
23	7.136	3.21E-08	1.43E-09
24	6.388	2.83E-08	1.75E-09
25	7.15	3.13E-08	7.15E-10
26	7.325	2.98E-08	1.40E-09
27	6.56	3.11E-08	1.35E-09
28	7.802	2.71E-08	8.67E-10
29	8.781	2.69E-08	1.01E-09
30	7.506	2.86E-08	5.90E-10
31	7.557	2.63E-08	1.55E-09
32	6.595	2.82E-08	1.94E-09
33	8.638	2.15E-08	2.96E-10
34	6.302	2.69E-08	4.06E-10
35	5.723	3.06E-08	1.61E-09
36	6.096	1.18E-08	1.11E-09
37	7.909	1.09E-08	1.41E-09
38	11.089	8.93E-09	6.11E-10
39	7.778	1.02E-08	1.14E-09
40	7.38	1.15E-08	6.02E-10
41	9.388	8.62E-09	7.23E-10
42	7.285	7.38E-09	7.04E-10
43	6.753	1.49E-08	1.74E-09
44	9.034	1.26E-08	5.67E-10
45	8.025	8.73E-09	8.45E-10
46	8.36	9.46E-09	1.41E-09
47	9.066	1.17E-08	4.90E-10
48	9.034	1.54E-08	9.82E-10
49	8.155	1.44E-08	5.44E-10
50	7.856	2.53E-08	3.14E-16
51	9.719	1.19E-08	2.64E-10
52	9.168	8.43E-09	1.22E-09
53	8.015	1.73E-08	0
54	7.819	3.12E-08	1.42E-09
55	9.855	1.48E-08	5.20E-10
56	7.836	1.63E-08	5.66E-10
57	8.028	1.55E-08	1.15E-09
58	9.728	2.45E-08	9.47E-10
59	6.892	1.62E-08	1.70E-09
60	9.679	1.44E-08	4.58E-10
61	10.061	2.08E-08	1.16E-09
62	8.134	1.53E-08	1.37E-09
63	8.108	2.38E-08	1.09E-09
64	9.074	2.57E-08	1.02E-09

Sample (#)	Mass (g)	χ m^3/kg	Standard Deviation
65	7.309	1.73E-08	1.40E-09
66	8.693	2.04E-08	8.83E-10
67	8.57	1.98E-08	1.30E-09
68	7.403	2.12E-08	9.15E-10
69	8.034	2.38E-08	1.39E-09
70	8.837	1.37E-08	1.05E-09
71	6.034	2.27E-08	1.70E-09
72	6.273	3.40E-08	4.08E-10
73	10.159	1.81E-08	5.04E-10
74	8.1	1.96E-08	6.32E-10
75	7.658	2.38E-08	1.00E-09
76	8.204	1.74E-08	1.36E-09
77	7.707	2.23E-08	1.15E-09
78	7.617	2.01E-08	1.21E-09
79	8.017	1.71E-08	3.19E-10
80	9.255	2.17E-08	9.97E-10
81	9.196	2.20E-08	5.56E-10
82	7.5	1.92E-08	1.56E-09
83	9.034	1.02E-08	1.24E-09
84	9.026	1.50E-08	7.51E-10
85	7.229	8.69E-09	1.23E-09
86	7.819	1.57E-08	5.67E-10
87	8.51	3.31E-08	1.08E-09
88	7.885	2.06E-08	6.49E-10
89	8.554	1.24E-08	1.37E-09
90	9.046	1.54E-08	8.49E-10
91	6.229	5.65E-08	1.78E-09
92	7.71	1.59E-08	5.75E-10
93	7.985	1.56E-08	6.42E-10
94	7.11	1.65E-08	6.24E-10
95	7.225	2.07E-08	1.62E-09
96	7.11	4.14E-08	1.29E-09
97	8.931	2.00E-08	5.73E-10
98	9.899	1.64E-08	1.29E-09
99	8.499	1.85E-08	1.31E-09
100	9.13	2.18E-08	8.41E-10
101	7.769	1.93E-08	1.51E-09
102	8.617	1.63E-08	5.94E-10
103	8.734	1.80E-08	5.86E-10
104	8.122	9.74E-09	9.47E-10
105	8.25	1.68E-08	1.42E-09
106	8.191	3.29E-08	1.08E-09
107	7.959	1.86E-08	1.29E-09
108	8.773	1.95E-08	1.01E-09
109	7.832	2.14E-08	6.54E-10

Sample (#)	Mass (g)	χ m^3/kg	Standard Deviation
110	7.591	2.04E-08	1.17E-09
111	8.356	3.70E-08	8.08E-10
112	8.136	3.73E-08	8.30E-10
113	8.976	1.27E-08	2.85E-10
114	7.458	1.47E-08	1.37E-09
115	7.619	2.16E-08	1.34E-09
116	8.496	2.68E-08	1.50E-09
117	8.247	1.90E-08	1.12E-09
118	7.123	2.00E-08	7.19E-10
119	6.149	3.17E-08	8.32E-10
120	6.615	2.78E-08	3.87E-10
121	6.244	2.80E-08	1.08E-09
122	7.358	2.63E-08	1.20E-09
123	6.402	1.58E-08	6.93E-10
124	7.614	2.61E-08	1.16E-09
125	7.34	3.12E-08	1.39E-09
126	6.081	1.21E-08	1.27E-09
127	6.977	1.45E-08	1.27E-09
128	7.499	1.47E-08	1.37E-09
129	7.372	2.42E-08	6.94E-10
130	6.384	2.37E-08	1.06E-09
131	7.083	1.86E-08	3.62E-10
132	7.379	2.03E-08	1.04E-09
133	7.005	1.91E-08	1.10E-09
134	8.23	2.59E-08	3.11E-10
135	7.895	1.94E-08	6.49E-10
136	7.338	2.56E-08	1.05E-09
137	7.447	2.16E-08	0
138	6.664	2.79E-08	3.84E-10
139	8.131	2.29E-08	1.13E-09
140	7.896	2.79E-08	1.12E-09
141	6.492	3.28E-08	1.04E-09
142	5.636	3.27E-08	1.20E-09
143	7.291	3.42E-08	3.50E-10
144	7.765	3.23E-08	6.58E-10
145	7.581	3.45E-08	1.21E-09
146	6.857	3.50E-08	7.45E-10
147	6.754	3.32E-08	1.65E-09
148	7.448	3.30E-08	1.24E-09
149	6.854	3.40E-08	1.86E-09
150	8.488	3.51E-08	1.31E-09
151	6.65	3.56E-08	1.76E-09
152	7.633	3.48E-08	6.69E-10
153	6.606	3.66E-08	1.16E-09
154	8.112	3.56E-08	8.33E-10

155	8.276	3.38E-08	5.34E-10
Sample (#)	Mass (g)	χ m^3/kg	Standard Deviation
156	5.946	3.43E-08	1.29E-09
157	8.452	3.31E-08	1.05E-09
158	9.17	3.39E-08	1.00E-09
159	9.266	3.29E-08	2.75E-10
160	9.849	3.19E-08	6.86E-10
161	9.638	3.34E-08	1.15E-09
162	8.337	3.29E-08	5.31E-10
163	8.022	2.84E-08	6.37E-10
164	7.179	3.04E-08	1.55E-09
165	7.664	3.54E-08	1.20E-09
166	8.228	3.18E-08	1.12E-09
167	6.509	3.39E-08	6.80E-10
168	7.416	3.09E-08	1.24E-09
169	7.679	3.15E-08	1.53E-09
170	8.425	3.37E-08	8.02E-10
171	7.965	3.13E-08	6.42E-10
172	7.685	3.10E-08	1.45E-09
173	8.63	3.39E-08	7.83E-10
174	8.788	3.21E-08	5.81E-10
175	7.071	3.37E-08	1.81E-09

VITA

Originally from Smithtown, New York, Thomas Schramm has always had an interest in the outdoors. His hobbies include hiking, hunting, fishing, and cooking. As a boy he wanted to become a paleontologist and even had a rock hammer at a young age. Tom attended S.U.N.Y New Paltz where he became passionate about the study of stratigraphy and completed an undergraduate research project on Marcellus Shale paleoecology. There he later earned a Bachelor of Science Degree, majoring in geology in 2009. Upon graduation he attended the Indiana University field-camp in the Tobacco Root Mountains and enrolled in a master's program at the University of Cincinnati. At the University of Cincinnati Tom studied the sequence stratigraphy of the Ordovician, Maysvillian Stage on the Cincinnati Arch. There he served as a teaching assistant and graduated with a Master of Science Degree in 2011. Tom is currently pursuing a Doctorate in geology at Louisiana State University studying Ordovician stratigraphy and the stratigraphic applications of magnetic susceptibility.